Creation of smart polymeric systems using cyclobis(paraquat-p-phenylene) & cyclobis(paraquat-4,4'-biphenylene)

Lieselot de Smet

Université de Lille
Ecole Doctorale Sciences de la Matière, du Rayonnement et de l'Environnement

THESE
Pour l'obtention du grade de Docteur de l'Université de Lille : Spécialité Chimie Organique et Macromoléculaire

Création de systèmes polymères intelligents utilisant le cyclobis(paraquat-p-phénylène) et le cyclobis(paraquat-4,4'-biphénylène)

Creation of smart polymeric systems using cyclobis(paraquat-p-phenylene) & cyclobis(paraquat-4,4'-biphenylene)

Présentée et soutenue par

Lieselot De Smet

Le 7 Janvier 2020

Prof. Dr. Sandra Van Vlierberghe	Ghent University, Président
Prof. Dr. Filip Du Prez	Ghent University, Examinateur
Prof. Dr. Rachel Auzely	University Grenobles Alpes, Rapporteur
Prof. Dr. Loïc Jierry	University Strassbourg, Rapporteur
Prof. Dr. Pol Besenius	Johannes Gutenberg-University Mainz, Rapporteur
Prof. Dr. Oren Scherman	University of Cambridge, Examinateur
Prof. Dr. Richard Hoogenboom	Ghent University, CoDirecteur de thèse
Prof. Dr. Patrice Woisel	ENSCL Université de Lille, Directeur de thèse

Creation of smart polymeric systems using cyclobis(paraquat-*p*-phenylene) & cyclobis(paraquat-4,4'-biphenylene)

Members of the examination committee in alphabetical order:

Prof. Dr. Rachel Auzely (University Grenobles Alpes, FR)

Prof. Dr. Pol Besenius (Johannes Gutenberg-University Mainz, DE)

Prof. Dr. Filip Du Prez (Ghent University, BE)

Prof. Dr. Loïc Jierry (University Strassbourg, FR)

Prof. Dr. Oren Scherman (University of Cambridge, UK)

Prof. Dr. Sandra Van Vlierberghe (Ghent University, BE)

Table of Contents

Chapter 3. Supramolecular hydrogels with time memory function

Chapter 4. Expansion of the Plasma Dye Coating (PDC) procedure towards the fabrication of smart supramolecular surfaces

Outline and aims of this thesis

The main research focus of this PhD thesis is the development of "smart" stimuli-responsive polymers and polymeric materials that are mediated by supramolecular host-guest complexation. The dynamic and selective character of these complexes allows the synthesis of highly adaptable materials in which their macroscopic properties can be altered by subtle external stimuli like temperature, pH or the presence of specific molecules. Nowadays, the creation of these smart materials through host-guest chemistry is mostly done by using cyclodextrins, curcurbit[n]urils and pillar[n]arenes as macrocyclic host molecules. In this thesis, the potential use of cyclobis(paraquat-*p*-phenylene), also called blue box (BB) and cyclobis(paraquat-4,4'-biphenylene), also called big blue box (BBB) is investigated for the creation of intelligent polymers and polymeric materials. These electron deficient cyclophane box like structures can form multi-sensitive, colored donor-accceptor charge transfer complexes with different electron-rich guest molecules including naphthalene (Napht), tetrathiafulvalene (TTF) and hydroquinone making them the perfect candidate for sensing purposes as the unambiguous output signal is immediately visible to the naked eye.

Chapter 1 will provide a broad introduction on the two major chemistry fields used in this thesis, namely supramolecular and polymer chemistry, complemented with recent developments reported in literature combining both fields to create smart polymeric systems mediated by host-guest molecules.

The rather unexplored macrocyclic host BBB, is discussed in **Chapter 2** focusing on the formation of 1:2 complexes with electron rich guest molecules Napht and TTF in water to allow the creation of smart hydrogels and aqueous nanostructures. To investigate the complexation of the hydrophobic guest molecules with BBB in water, reversible addition–fragmentation chain transfer (RAFT) polymerization was employed to synthesize short, water-soluble poly(dimethylacrylamide) (PDMAc) chains end-functionalized with either the hydrophobic Napht or TTF guest moiety through the modification of the CTA agent. Afterwards, the complexation of both these Napht and TTF polymer chains with BBB was studied in aqueous media using UV-VIS and ^{1}H-NMR spectroscopic titrations, isothermal calorimetry titration (ITC) and diffusion ordered NMR spectroscopy (DOSY). In a final step the potential thermo-responsiveness of the Napht-PDMAc complex with BBB was highlighted allowing the creation of highly adaptable and sophisticated smart materials with an inherent visual output signal.

Hydrogels are 3D polymeric networks which have the ability to retain and a maintain substantial amount of water within their complex structure. The structural integrity of the hydrogels upon swelling is preserved using either chemical cross-links or reversible physical junctions. By incorporating host-guest complexes into such 3D polymeric structure the sol-gel transition or expansion-contraction

process can be regulated via different external stimuli which can be used in wide range of applications including catalysis, sensor systems and biomedical materials. **Chapter 3** will focus on the creation of intelligent hydrogels by incorporating BB-Napht host-guest complexes into the complex 3D-structure of covalent hydrogels in order to control its water uptake. The hydrogels were synthesized using free radical co-polymerization of *N*-isopropylacrylamide (NIPAm), dialkoxynaphthalene functionalized with an acrylamide (Napht.Ac) and *N,N'*-methylenebisacrylamide as cross-linker. It was observed that the dynamic character of the BB-Napht assembly introduces a large hysteresis window in the thermo-responsive volume phase transition of the PNIPAm-based system which was thoroughly investigated via differential scanning microscopy (DSC) and ^{1}H-NMR spectroscopy. When heated above its volume phase transition temperature in aqueous solution, the collapse of the hydrogels causes disassembly of the complex, expelling the BB from the hydrogel through contraction. The rate of releasing the BB was found to be dependent on both the solution temperature and heating time. This difference in BB release influences the hydrophobicity of the remaining hydrogel inducing size changes upon subsequent cooling and reswelling in fresh aqueous medium. By careful monitoring of these variations, the system can report how long it was heated at a known temperature. To the best of our knowledge, this is the first reported polymeric sensor device that contains a time memory function.

Finally in **Chapter 4**, the Plasma Dye Coating (PDC) procedure was explored as a less time-consuming fabrication method for host-guest complexation based stimuli-responsive materials and surfaces. The PDC procedure was initially developed by the university of Ghent for the creation of colored material with significantly reduced dye leaching through covalent immobilization of the desired dye onto the material surface using plasma-generated surface radicals. A pre-adsorbed layer of polymerizable dye on the surface is immobilized through radical addition caused by a short plasma treatment step. The non-specific nature of the plasma-generated surface radicals allows surface modification for a wide variety of complex dyes including azobenzenes, functionalized with radical sensitive groups to avoid significant dye degradation, to be combined with various polymeric materials including polypropylene (PP), polyethylene (PE), polyamide6 (PA6), cellulose and Teflon (PTFE). As part of this thesis, the work originally done in our group was firstly extended by the further characterization of the material surface after PDC using scanning electron microscope (SEM), contact angle measurements and X-ray photoelectron spectroscopy (XPS). Secondly, the dye application step was further optimized by using a liquid spray technique to coat the materials with the desired dye prior to plasma treatment in order to allow lower dye consumption, the application of a specific design onto the surface and the use of more complex material geometries. Finally, the applicability of this PDC technique was expanded towards the incorporation of naphthalene moieties as representative electron-rich guest molecule

allowing the incorporation of host-guest assemblies, on the surface of a variety of materials including more inert Teflon, PP and PE.

Chapter 1. Introduction

1 Supramolecular chemistry

Supramolecular chemistry can be defined as the 'chemistry beyond the covalent bond' and aims for the creation of complex, adaptive and functional chemical systems through the assembly of different molecular components and subunits. This branch of chemistry focusses on the formation of weak and dynamic non-covalent interactions rather than the stronger and irreversible covalent bonds used in more traditional chemistry and was firstly introduced by Jean-Marie Lehn, who received the Nobel Prize in Chemistry 1987 together with Charles Pederson and Donald Cram for their seminal work on 'the development and use of molecules with structure-specific interactions of high selectivity' (Figure 1.1).[1–5]

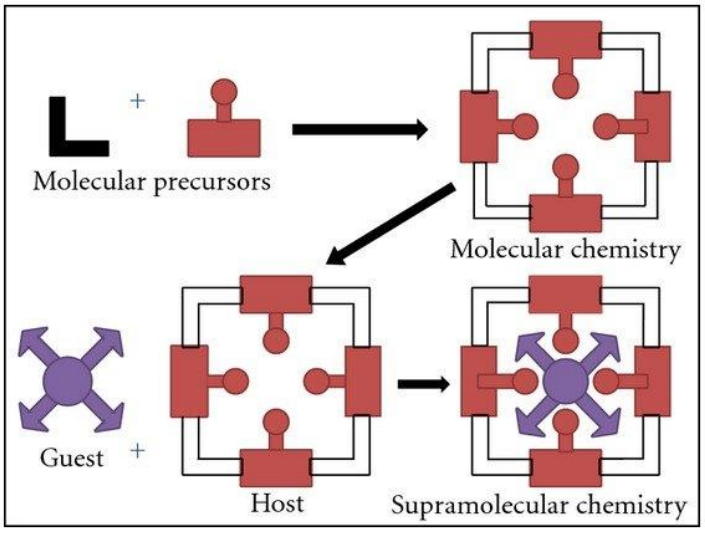

Figure 1.1. Comparison between molecular chemistry and supramolecular chemistry.[3]

In the last 25 years, this highly interdisciplinary field of supramolecular chemistry covering chemical, biological and physical features has gained more interest by scientists to form well-defined functional nanostructures used in various applications, including smart materials[6–8], drug delivery systems[9–11] and molecular machines.[12–16] Especially the latter topic has been gaining interest recently with attempts to take macroscopic machines down to the molecular level resulting in the Nobel Prize in chemistry awarded to Jean-Pierre Sauvage, J.Fraser Stoddart and Bernard L. Ferringa in 2016. Most of these assemblies are inspired by different biological processes found in nature relying on similar physical intermolecular forces for their functionality, such as the enzyme-substrate recognition, metal-ligand coordination, phospholipid bilayer formation and the helical assembly of the DNA complementary strains (Figure 1.2).

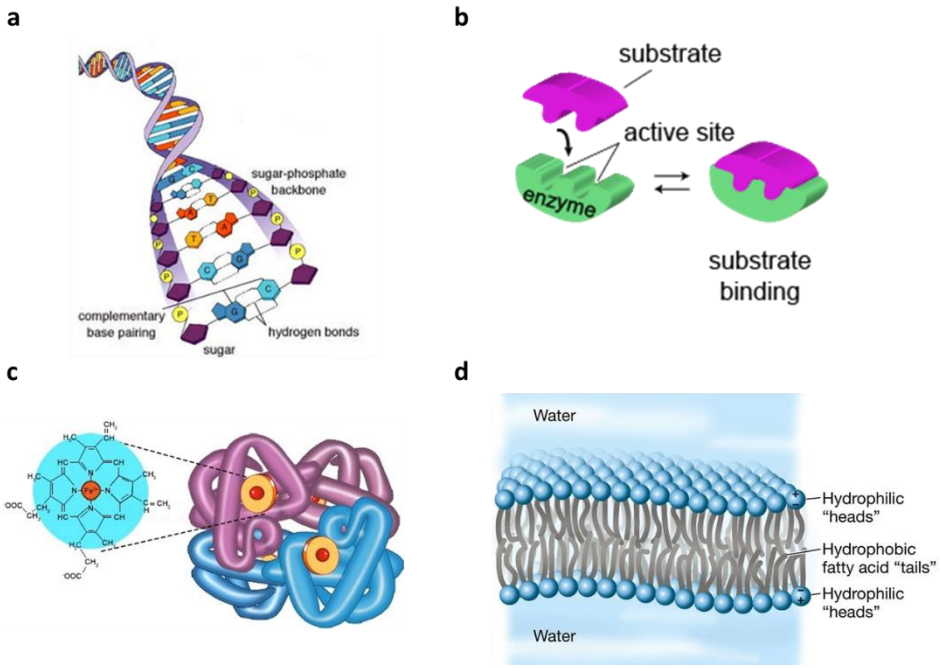

Figure 1.2. Examples of biological processes driven by non-covalent bonds: a) hydrogen bond formation of the complementary DNA strains forming a double helical structure, b) recognition of enzyme-substrate[17], c) metal-ligand coordination with Fe^{2+} present in the hemoglobin protein[18] and d) formation of a phospholipid bilayer membrane via the hydrophobic effect of the phospholipids in water.[19]

These different weak and reversible non-covalent interactions mainly consist of van der Waals forces, electrostatic interaction, hydrophobic interaction, hydrogen bonding, metal- ligand coordination and π-π interaction (Figure 1.3).[20] Although these bonds are significantly weaker than covalent bonds (200-1000 kJ/mol), most of the supramolecular assemblies that are common in nature and used in supramolecular chemistry do not rely on a single bond(type) between molecule A and B, but allow for a complex binding pattern containing multiple binding types reinforcing the assembly.

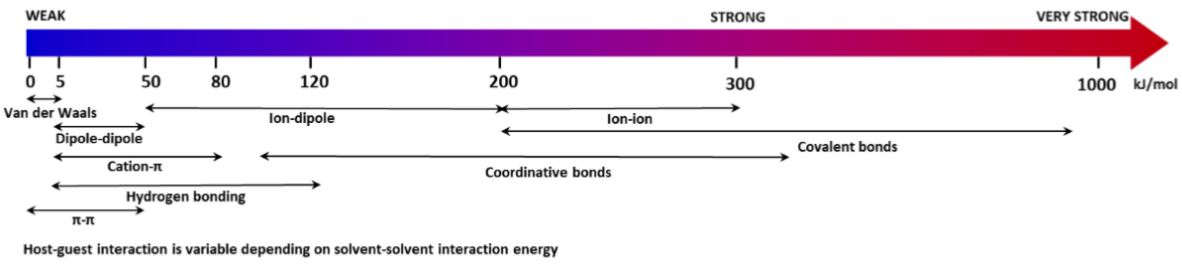

Figure 1.3. Schematic overview of the non- and covalent interactions together with their respective association strengths.

Supramolecular chemistry can be organized in two main categories: self-assembly and host-guest chemistry. Self-assembly is the process where individual molecules assemble spontaneously to form an organized structure via reversible, selective physical interactions. Although host-guest chemistry can be considered as a specific case of self-assembly, it is generally associated with the enclosure of one or more guest molecules inside an 'artificial' receptor called a host molecule, containing a

complementary structural cavity using non-covalent interactions. The difference between both is illustrated in Figure 1.4.[21] Because the work described in this thesis deals with the use of host-guest complexes, we will focus our attention on these specific supramolecular interactions for the remainder of this introduction.

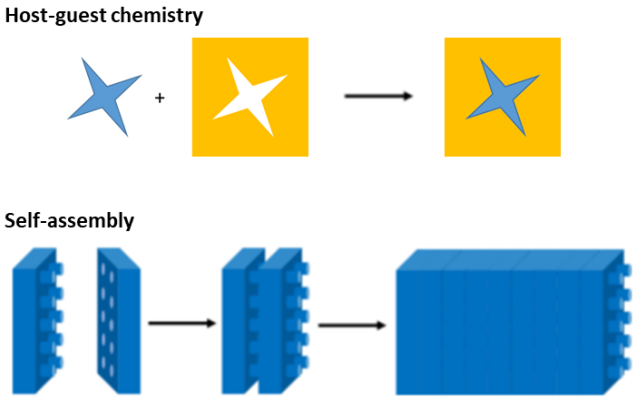

Figure 1.4. Simplified illustration showing the difference between host-guest chemistry and self-assembly.

Host-guest chemistry relies on the reversible supramolecular interactions between the host (H) and the guest (G) molecule(s) upon complexation. Because of this, host-guest complexes are in a constant dynamic equilibrium with their free components in solution, which can be described by the following equation:

Equation 1.1
$$mH + nG \underset{k_d}{\overset{k_a}{\rightleftharpoons}} H_mG_n$$

with m and n defining the stoichiometry of the assembly. This equilibrium is determined by the rate of the association (k_a) and dissociation (k_d) of the host and guest substrates and is characterized by the thermodynamic binding constant or association constant K_a:

Equation 1.2
$$K_a = \frac{k_a}{k_d} = \frac{[H_mG_n]}{[H]^m[G]^n}$$

Where [H], [G] and $[H_mG_n]$ represent the concentration of free host, the concentration of free guest and the concentration of host-guest complexes in solution. This binding constant K_a is the most important value when describing supramolecular chemistry as it indicates the affinity of the host-guest complex, i.e. a high K_a above 10^6 M^{-1} is generally considered an indication of a strong supramolecular assembly while below a K_a of 10^2 there is practically no association (equation 1.2). The K_a is specific for each host-guest complex and is strongly dependent on the solvent and temperature. This binding constant can be experimentally determined by monitoring physical changes in the system during titration experiments which will be explained in more detail in Chapter 2 of this thesis.

1.1 Examples of host molecules

Nowadays, a wide range of artificial receptors or "hosts" have been discovered and evaluated displaying exceptionally affinity and selectivity towards different organic, inorganic and biological molecules. In the following section the most well-known host molecules, namely cyclodextrin, curcurbit[n]uril, pillar[n]arene and cyclobis(paraquat-*p*-phenylene), will be briefly discussed.

1.1.1 Cyclodextrins

Cyclodextrins (CD) are the most widely studied host molecules. One of the earliest papers describing the interaction between CD and D/L-alanine β-naphthylamide was published in 1990 by T. Shono *et al*.[22] Nowadays CD is commonly used for the microencapsulation of different sensitive flavours, oils and dyes to prolong their shelf-life, which is important in various applications ranging from textiles[23–25] to cosmetics and food-industry favored by its negligible cytotoxic effects, high solubility in water and wide variation in guest molecules.[26–29] The most common CDs are composed of six, seven and eight glucopyranose units joined together by α-(1-4)-glycosidic linkages in a ring and are named α-, β- and γ-CD, respectively. These cyclic oligosaccharides form a toroidal 3D-structure where both the primary and the secondary hydroxyl groups are orientated to the surrounding environment making the CDs soluble in water (Figure 1.5). Due to this design, the interior cavity of the CDs is hydrophobic enabling the encapsulation of molecules that are otherwise insoluble in water. The main driving force for complexation is the hydrophobic effect causing the displacement of the high-energy water molecules from the apolar cavity into the surrounding water. The size of the interior cavity also plays an important role in the host-guest complexation as it will only allow guest molecules with a complementary size to enter the cavity, facilitating in the use of CD in molecular recognition (Figure 1.5).[30–33] The smallest CD (α-CD) is characterized by a cavity volume of roughly 174 Å³ and can encapsulate linear organic alkyl chains and smaller aromatic compounds, such as dodecyl groups and azobenzene, the latter only in trans-configuration.[33–35] Increasing the cavity volume up to 262 Å³ (β-CD) allows for the complexation with more branched alkyl chains or more bulky aromatic molecules, including ferrocene and adamantyl groups.[36–39] Finally, the cavity of the γ-CD (427 Å³) is large enough to even complex two guest molecules simultaneously yielding ternary assemblies, e.g. with anthracene.[40,41]

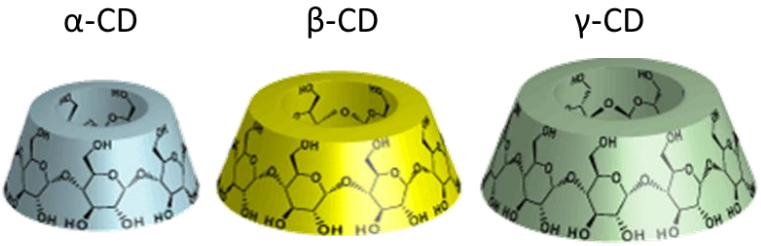

	α-CD	β-CD	γ-CD
glucopryranose units	6	7	8
cavity diameter (Å)	4.7-5.3	6.0-6.5	7.5-8.3
cavity volume (Å³)	174	262	427
outer diameter (Å)	14.6	15.4	17.5
height (Å)	7.9	7.9	7.9

Figure 1.5. Schematic illustrations of the cone shaped and the structural dimensions of α-, β- and γ-CD. Adapted with permission from ref. [33] Copyright 2019 American Chemical Society.

1.1.2 Cucurbit[n]urils

Cucurbit[n]uril (CB[n]) is a cyclic oligomer consisting of n glycoluril units and is commonly prepared by the condensation reaction of glycoluril and formaldehyde under acidic conditions (Figure 1.6). The first macrocyclic compound of this CB[n] family was published in 1905 by Behrend *et al.* and was named CB[6] highlighting the six glycoluril compounds incorporated in the host molecule.[42] Later, more CB[n] molecules were synthesized and purified with various cavity sizes as depicted in Figure 1.6.[43–45]

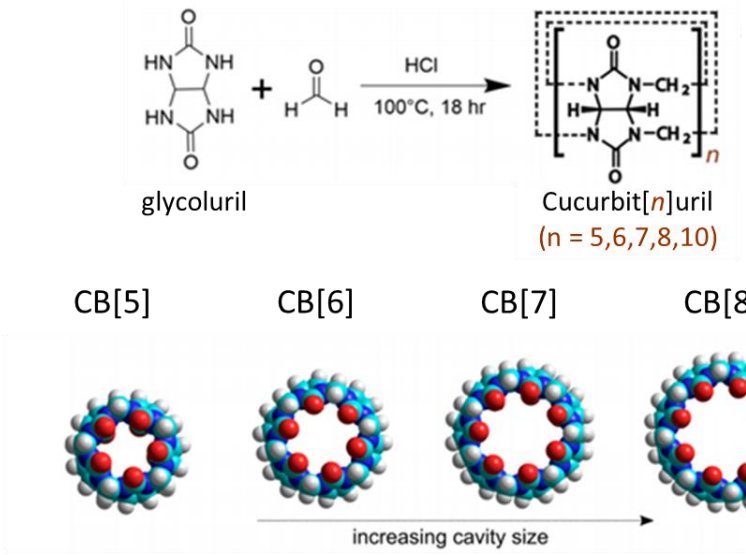

	CB[5]	CB[6]	CB[7]	CB[8]	CB[10]
Portal diameter (Å)	2.4	3.9	5.4	6.9	9.5-10.6
cavity diameter (Å)	4.4	5.8	7.3	8.8	11.3-12.4
cavity volume (Å³)	82	164	279	479	870
outer diameter (Å)	13.1	14.4	16.0	17.5	20.0
height (Å)	9.1	9.1	9.1	9.1	9.1

Figure 1.6. Top: Reaction scheme for the synthesis of CB[n]. Center: Schematic representation of the difference in size for the hydrophobic cavity of CB[5], CB[6], CB[7] and CB[8]. Bottom: Dimensions of CB[n]. Adapted with permission from ref.[44] Copyright 2019 American Chemical Society.

These pumpkin shaped molecules show two carbonyl-lined rims at the top and bottom of the cavity that act as portals with an electronegative nature making it possible for the outside of the CB[n] to interact with cations via ion-dipole interactions. The inner cavities of these macrocyclic molecules are relatively hydrophobic as the alignment of the glycoluril units prohibits the presence of any functional groups or electron pairs inside the cavity. This interesting duality of a hydrophobic cavity with an electron rich rim allows for strong host-guest complexes with dicationic species separated via an alkyl spacer, such as alkylated ammonium and imidazolium ions. While the cation of the guest interacts with the hydrophilic portals on either side of the hydrophobic cavity, the alky chain becomes encapsulated in the cavity resulting in exceptionally strong complexes.[46–48] Similarly to cyclodextrins, the size and volume of the hydrophobic cavity play an important role in the molecular recognition of the guest with the CB[n]-host. By tailoring its cavity volume, CB[n] can encapsulate different guest molecules ranging from gaseous molecules for the smaller CB[5] to linear alkyl chains in CB[6] and aromatic compounds in CB[7]. The bigger CB[8] and CB[10] can simultaneously accommodate two guest molecules.[49–51]

A nice example of the use of CB[8] for the simultaneous complexation of two guest molecules has been reported by the group of Scherman who formed ternary complexes in a host:guestA:guestB ratio of 1:1:1 by the encapsulation of both an electron-poor and an electron rich aromatic guest molecule by

CB[8] in water.[52,53] In this stepwise binding process a charge transfer complex is formed inside the CB[8] whereby first an electron-deficient guest molecule, such as methyl viologen, enters the cavity followed by the corresponding electron-rich guest molecule, such as dihydroxynaphthalene (Figure 1.7). These charge transfer interactions are easily detected by the unique features in their electronic spectra resulting in colored complexes which can be visualized and followed upon complexation. The synergistic event of supramolecular interactions results in the formation of an assembly with an overall high binding constant of up to 10^{14} M^{-2}.[54,55] This highly stabilized complex can be used in different applications, such as protein conjugates[56–58] as well as supramolecular polymers and networks.[54,55,59–62]

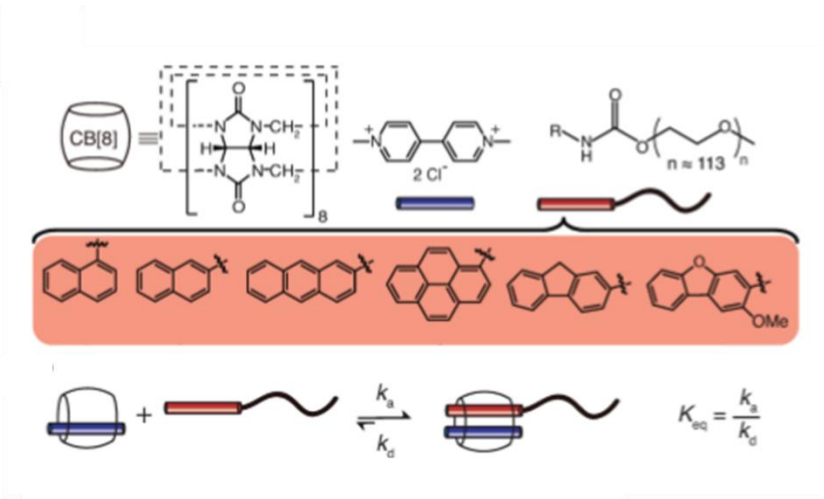

Figure 1.7. Top: The chemical structures of CB[8], the auxiliary first electron-deficient guest molecules and the second guest labelled polymer. Bottom: Schematic illustration of the ternary complex formation. Reprinted with permission from ref.[53] Copyright 2019 American Chemical Society.

1.1.3 Pillar[n]arenes

This more recently developed class of macrocyclic host molecules consisting of 1.4-dialkoxybenzene units linked by methylene bridges, was first reported by the group of Ogoshi in 2008.[63] Ever since, this pillar[n]arene chemistry has been extensively studied for their ability to self-assemble and to form host-guest complexations. Pillar[n]arene is a highly symmetrical cylindrical-shaped molecule composed of 5-15 aligned electron-donating hydroquinone units where the alkoxy groups are gathered at both outer rims of the cylinder as depicted in Figure 1.8 for pillar[5]arene and pillar[6]arene as examples. The most common synthesis route for pillar[n]arenes is the Lewis acid catalysed condensation reaction of hydroquinone monomers with paraformaldehyde (Figure 1.8). By fine-tuning the reaction conditions, a desired cavity size can be selected either kinetically by carefully controlling the reaction temperature and time or thermodynamically by adding specific templates, like cyclohexane and adamantane promoting the synthesis of pillar[6]arene by arranging the 1,4-dialkoxybenzene building blocks in a specific confirmation prior to condensation.[64] Besides the cavity

size, pillar[n]arenes can also easily be functionalized via two simple approaches: i) Co-cyclooligomerization with two or more differently functionalized dialkoxybenzene monomers resulting in a final pillar[n]arene consisting of different repeating units (Figure 1.8). ii) Post-functionalization of a simple pillar[n]arene mostly performed by dealkyloxylation and oxidation of the alkoxy group present in the rims of the molecule.[65] These chemical alterations have a huge impact on both the host-guest complexation and the chemical properties of the host-molecule including the solubility in different solvents ranging from water to dichloromethane and acetone.[64–67]

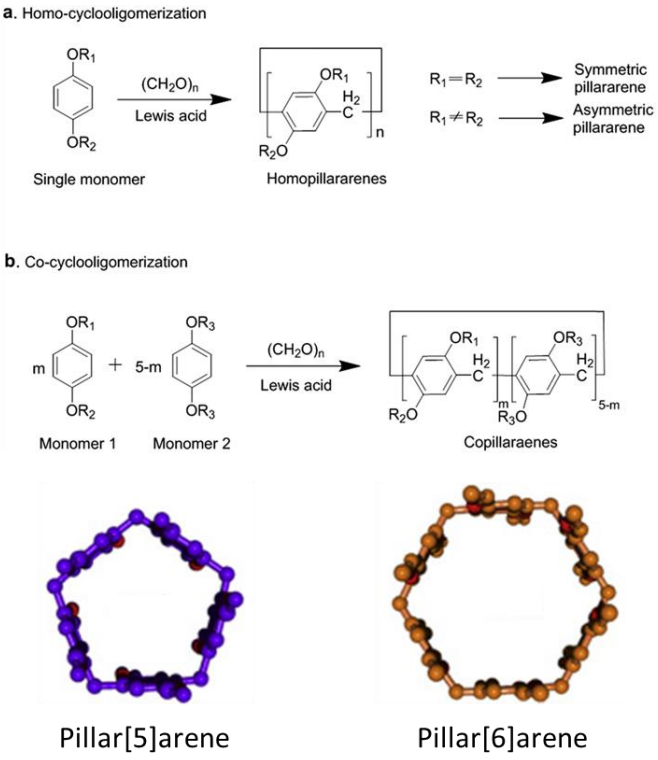

Pillar[5]arene Pillar[6]arene

	Pillar[5]arene	Pillar[6]arene
Dialkoxybenzene units	5	6
cavity diameter (Å)	4.7	6.7
cavity volume (Å³)	225	400
outer diameter (Å)	13.0	14.5
height (Å)*	7.8	7.8

Figure 1.8. Top: The schematic synthesis route of homopillararenes (a) and copillararenes (b). Center: Schematic representation of the difference in size for pillar[5]arene and pillar[6]arene. Bottom: Dimensions of pillar[5]arene and pillar[6]arene. *based on the distance between the two oxygen atoms present in the dialkoxybenze units.[65,66,68,69] Reprinted from ref.[70] Copyright 2019 with permission from Elsevier.

The symmetrical architecture of pillar[n]arenes, together with the electron-rich benzene units and the alkoxy rims allows them to encapsulate many different cationic, neutral and, to a lesser extent, anionic organic guest molecules driven by electrostatic, hydrophobic and charge-transfer interactions similarly to cucurbit[n]uril. For example, Ogoshi et al reported that pillar[5]arene can both encapsulate cationic

viologen and pyridinium groups while pillar[6]arene are reported to accommodate larger guest molecules including the ferrocenium cation and adamantane derivatives.[65] Pillar[n]arenes are used in various applications ranging from biology to materials science and environmental sciences, mostly due to their easy preparation and functionalization, allowing their incorporation into larger structures.[71–77]

1.1.4 Cyclobis(paraquat-*p*-phenylene) and derivatives

A final interesting host molecule that will be discussed here is cyclobis(paraquat-*p*-phenylene), which is commonly referred to as Blue Box (BB). BB is a tetracationic rectangular shaped molecule consisting of two electron-poor paraquat or dimethyl viologens units linked by para-phenylene spacers. This particular cyclophane host was first reported in 1988 by J. Fraser Stoddart's group reporting the ability to form strong inclusion complexes with electron-rich aromatic guest molecules due to the unique design features of the BB structure.[78] Nowadays a plethora of different tetracationic cyclophanes, containing two electron-poor bipyridinium units have been synthesized capable of interacting with one or two electron-rich aromatic guests depending on the cavity sizes.[79–83] A common method to increase the cavity size of these tetracationic cyclophanes is to incorporate additional phenyl moieties along the cyclic structure with the most prominent examples being cyclobis(paraquat-4,4'-biphenylene) also called big blue box (BBB) and the semi-rigid ExBox comprised of bipyridinium units extended with 1,4-phenylene bridges which are illustrated in Figure 1.9.[82,84,85]

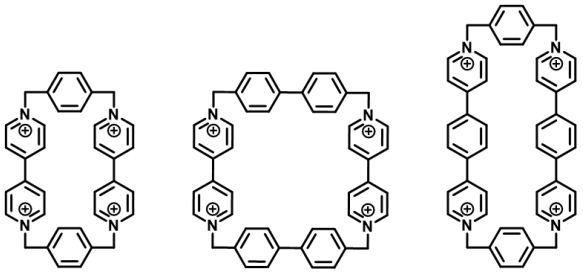

BB BBB ExBox

	BB	BBB	ExBox
Width (Å)	6.90	10.87	6.90
Length (Å)	10.30	10.96	14.60
K_a (10^3 M^{-1})	2.6[a]	3.8[a]	0.3[b]

Figure 1.9. Top: The structures of the BB (left), BBB (middle) and ExBox (right). Bottom: Structural dimensions of BB, BBB and ExBox together with the association constants of their complexes with [a]TTF or [b]azulene in CH_3CN at 298 K.[80,82,84,85]

The number of compatible guest molecules for the BB hosts has expanded since the initial report to include dialkoxybenzene (DB), tetrathiafulvalene (TTF) and 1.5-dialkoxynaphthalene (DNP). The interesting complexation properties can firstly be attributed to the distance between the two paraquat moieties which is ideal to encapsulate an electron-rich aromatic ring structure while maximizing the π-π stacking and the charge transfer (CT) interactions with the two paraquat units. Due to these CT-

interactions, an absorption wavelength characteristic to a specific guest molecule will be present in their UV-VIS spectra resulting in strong colored complexes which can be easily visualized and followed upon complexation. Secondly, the tetracationic character of the cyclophane makes it possible to gain control over the solubility of both the host and the eventual complex by careful selection of the counterions allowing the use of BB in various solvent. For example, the solubility of BB can easily be switched from water to acetonitrile by exchanging the counterions from chloride to hexafluorophosphate.[78,86–88] A final interesting feature of the BB unit is its ability to manipulate the host-guest interaction via the redox potential of its two bipyridinium units. By using oxidation/reduction reactions, the BB molecule can be switched between its tetracationic, dicationic and neutral form, drastically altering the electronegativity of the host-molecule. These different redox states cause drastic changes in its binding mode, as reducing the electron deficiency of the tetracationic BB form, will result in less affinity towards electron rich quest molecules like DNP, TTF and DB due to the decreasing dominance of the CT interaction between the host and the guest. Instead the dicationic BB selectively forms stronger assemblies with guest like methyl viologen radical cations ($MV^{+\bullet}$) with radical pairing interactions being the dominant interaction while the neutral BB encapsulate electron-poor aromatic units like terephthalonitrile via van der Waals interactions (Figure 1.9).[89]

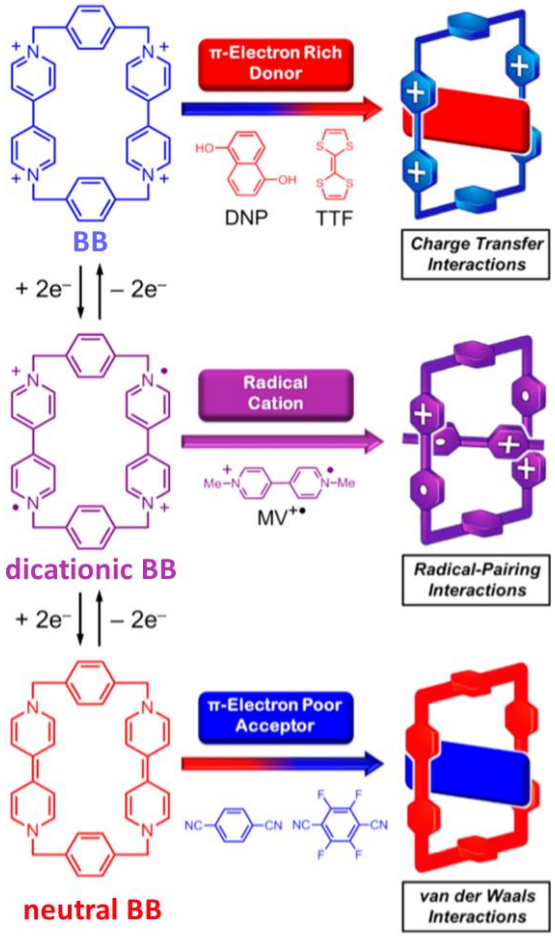

Figure 1.9. Structural and graphical representation of the different redox states of the cyclophane involving (tetracationic) BB (top), dicationic BB (center) and neutral BB (bottom). Depending on the redox state of BB, different supramolecular interactions will be involved in the selective complexation of electron-rich, radical or electron-poor substrates respectively. Reprinted with permission from ref.[89] Copyright 2019 American Chemical Society.

These cyclophane hosts have been widely used for the synthesis of mechanically interlocked molecules, such as rotaxanes and catenanes.[90–98] For example, Stoddart *et al.* reported the synthesis of palindromical [3]rotaxane consisting of both a Napht – and TTF unit which can interact with the threaded BB ring via donor-acceptor interactions. The location of the BB along the rotaxane is electrochemically controlled by the oxidation/reduction of the TTF unit allowing the directional motion of the BB rings between both guest units. Via this alternating switching of the inter-ring distance from 4.2 to 1.4 nm, an artificial molecular machinery was created which mimics the contraction and extension of skeletal muscle (Figure 1.10).[95]

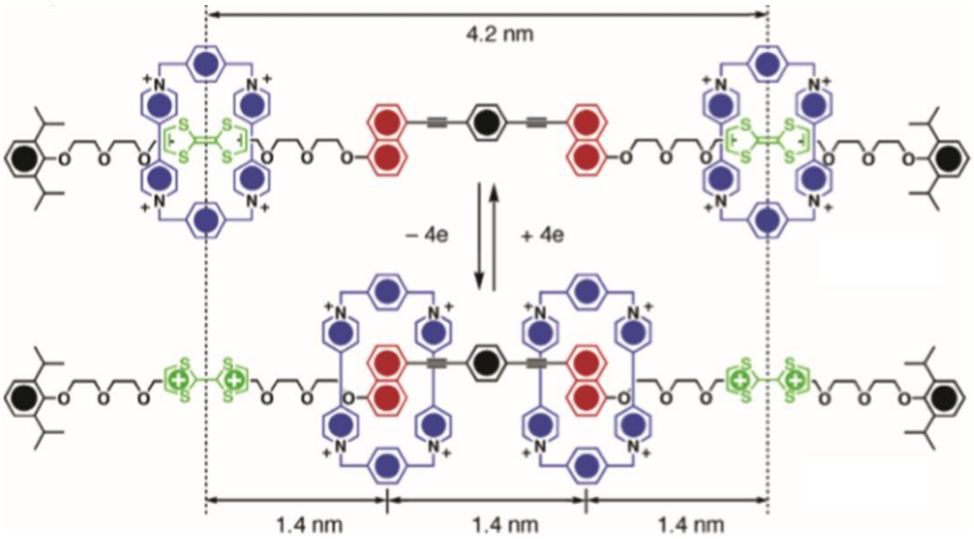

Figure 1.10. The structural illustration of the extended (top) and contracted (bottom) state of the [3]rotaxane. Reprinted with permission from ref.[95] Copyright 2019 American Chemical Society.

2 Polymers

A Polymer chain is a macromolecule composed of small repeating subunits, called monomers typically consisting of hydrocarbons, and are defined by the international Union of Pure and Applied Chemistry (IUPAC) as: *"A molecule of high relative molecular mass, the structure of which essentially comprises the multiple repetition of units derived, actually or conceptually, from molecules of low relative molecular mass called monomers, typically consisting of hydrocarbons besides other hetero-atoms"*.[99] A large number of natural polymers have already been discovered and many play an important key role in essential biological processes. Proteins for example consist of highly ordered monomers called amino acids, which participate in various metabolic pathways including cell communication, catalysing metabolic reactions and immune responses. Another example is the DNA double helix that consists of polynucleotide chains carrying the genetic information on development, growth, functioning and reproduction of every organism and virus.

Over the past 50 years, the production of synthetic polymers has exponentially grown due to their light weight, cheap production cost and large variation on the eventual properties. Originally, the term "plastics" was used to describe the cheap synthetic polymer materials that were used as alternative material in food packaging, clothes and lightweight transportation vehicles reducing the fuel consumption. However, polymer research in the last few decades has pushed the properties of polymers far beyond simple plastics, resulting in the use of these versatile macromolecules in high added-value, high-end applications in the biomedical fields, clean energy and complex composite materials.[100,101]

The most important parameter that influences the polymer properties is the chemical composition. Depending on the chemical structure of the used monomer(s), the material can possess different thermal properties and heat/chemical resistance for example. The incorporation of two or more monomers into the polymer chain allows for different polymer compositions including block copolymers, random copolymers and gradient copolymers determined by the arrangement of de co-monomers in the polymer chain (Figure 1.9). The selection of the composition depends on multiple parameters such as the used co-monomers, their relative reactivity and their molar ratios in the feedstock. Another parameter that has a profound impact on properties of the polymeric material is the architecture or topology of the polymer chains. This is basically how the monomers will be linked and arranged on a macromolecular level which can range from simple linear polymers to more complexed structures like crosslinked networks and hyperbranched polymers (Figure 1.9).[100,101] Finally, the incorporation of functional groups along the polymer chain, on the side chains or at the end-chains of the polymer structure can have an additional influence on the polymer properties such as its solubility by changing the hydrophobicity of the polymer chain. The functional groups can be introduced on the polymer chain by either the use of monomers containing a desired functional group, via a post polymerization modification reaction or via the use of functional initiators or terminators.[102] Nowadays, a vast range of different polymers can be synthesized for a wide range of different applications. There is a lot of research focused on the fine tuning of polymer materials on a structural and chemical level and, recently, the investigation towards bio-based resources has gained a lot of importance in an attempt to decrease the dependence on the mostly petroleum-based monomers and look for monomers created from renewable sources.[100]

Another important parameter which has an enormous influence on the physical properties, including crystallinity, viscosity and the glass transition temperature is the molecular weight of the polymer. This molecular weight, which is defined by the monomer unit and the number of incorporated monomer units, is an average value due to the lack of uniformity in chain length of a polymer material. As a result, polymer materials are described via an average molecular weight, e.g. number averaged (M_n) or mass averaged (M_w), and the dispersity (Đ) which is a measure for the broadness of the molecular weight distribution. The latter value is characterized by the ratio of M_w/M_n and approaches 1 when all the polymer chains have the same length.[103,104]

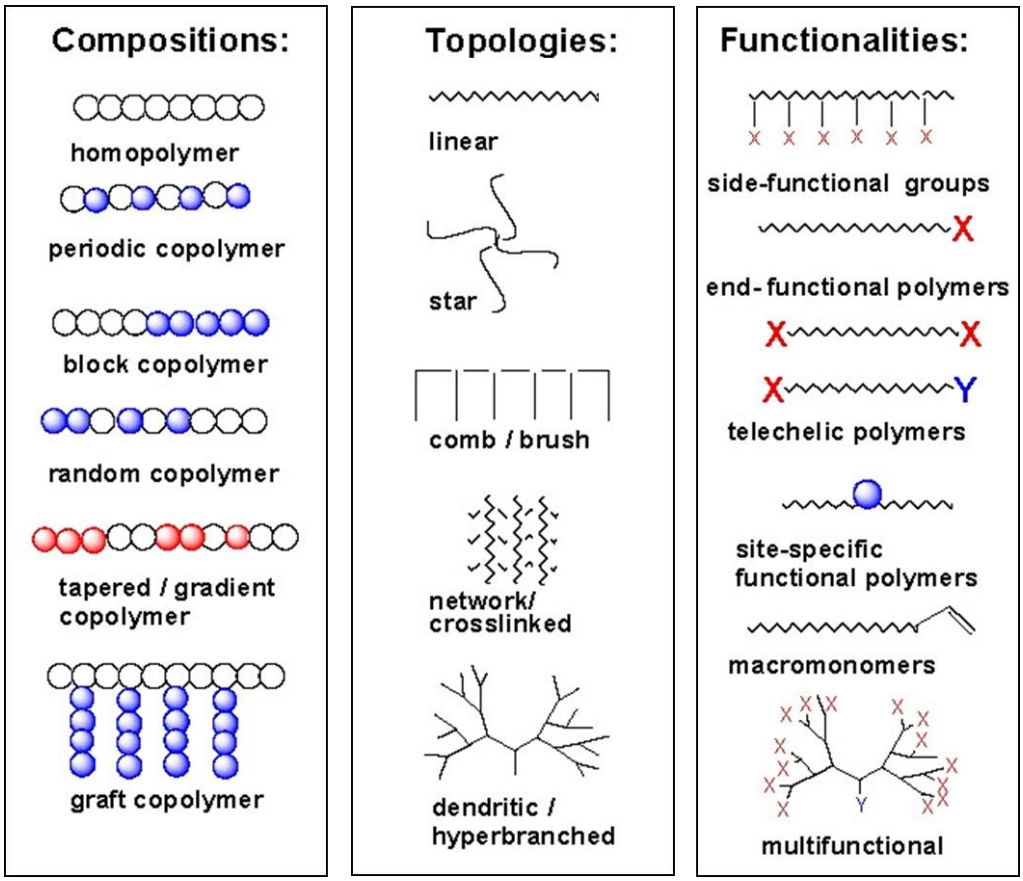

Figure 1.9. Schematic illustration of the possible polymer architectures with different compositions, topologies and functionalities.[105]

Polymers are synthesized via two general polymerization methods: 1) step-growth polymerization and 2) chain-growth polymerization (Figure 1.10). The first human-made polymer was Bakelite which was formed via the step-growth polymerization of phenol and formaldehyde in 1909. In such a process, at least two different bifunctional or multifunctional monomers with complementary functional groups undergo addition or condensation reactions with each other forming alternating co-polymers. The mechanism of this polymerization type is as follows: Firstly, the highly abundant monomers will react with each other forming dimers, trimers and oligomers. Subsequent reaction of these structures will lead to the formation of long chain polymers. This means that only high molecular weight polymers are obtained at high conversions.[106]

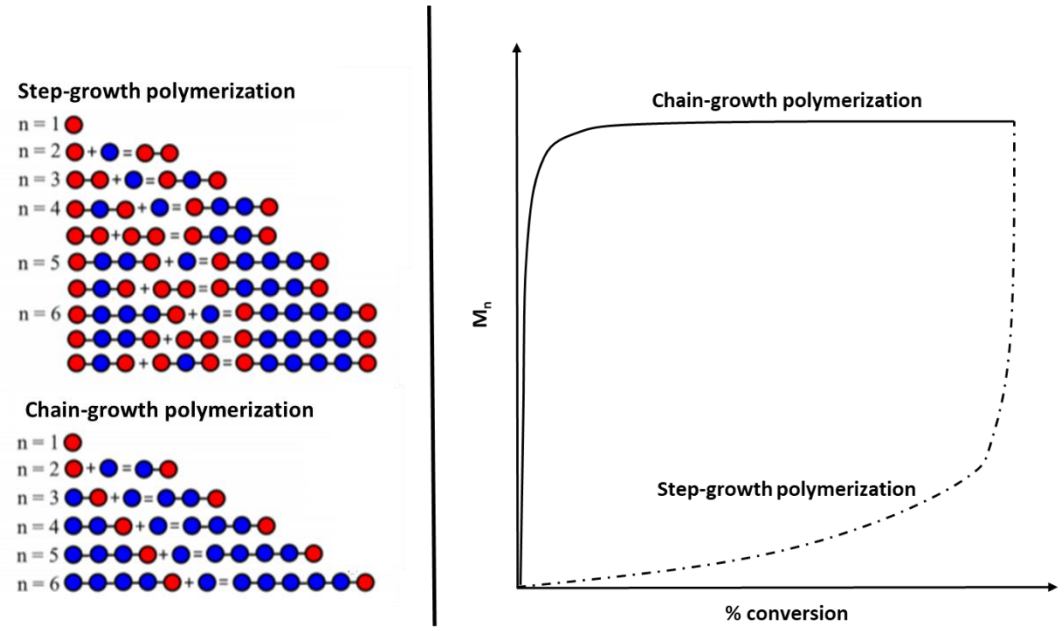

Figure 1.10. Right: Schematic illustration of the step-growth and chain-growth polymerization process. Left: The difference in the evolution of the molecular weight (M_n) during chain-growth polymerizations and step-growth polymerizations.[107] Aadapted with permission from ref.[108] Copyright 2019 American Chemical Society.

The second type of polymerization process, called chain-growth polymerizations, involves the repetitive inclusion of monomers to an active site, which can be of radical or ionic nature, on the growing polymer chain re-establishing the active site after every monomer addition. As a result, high molecular weight chains can be formed already at the start of the polymerization as only monomer addition is possible at the reactive end of the polymer chain.[108,109]

The mechanism of the step-growth polymerization is characterized by four distinct reactions that happen continuously during the polymerization: initiation, propagation, transfer and termination, which are explained below for a subset of the chain-growth polymerizations, called radical polymerizations (Figure 1.11):

- **Initiation**: During this step, radicals are introduced into the reaction mixture mostly via thermal decomposition or photolysis of initiator molecules. These formed radicals can then react with a monomer creating a growing polymer chain with an active radical center.
- **Propagation**: The polymer chain is growing (propagating) during this step by the repetitive addition of monomers to the radical active site of the polymer chain, regeneration the radical center at the chain end after every chemical reaction with a monomer unit.
- **Transfer**: The growth of a polymer chain is terminated by transferring the radical site to another molecule (transfer agent, monomer, solvent molecule) or an already existing polymer chain starting the growth of a new chain or side chain, respectively.

- **Termination**: the growth of the polymerization is terminated by the disappearance of active radical centers on polymer chains via recombination or disproportionation reactions between two radicals.

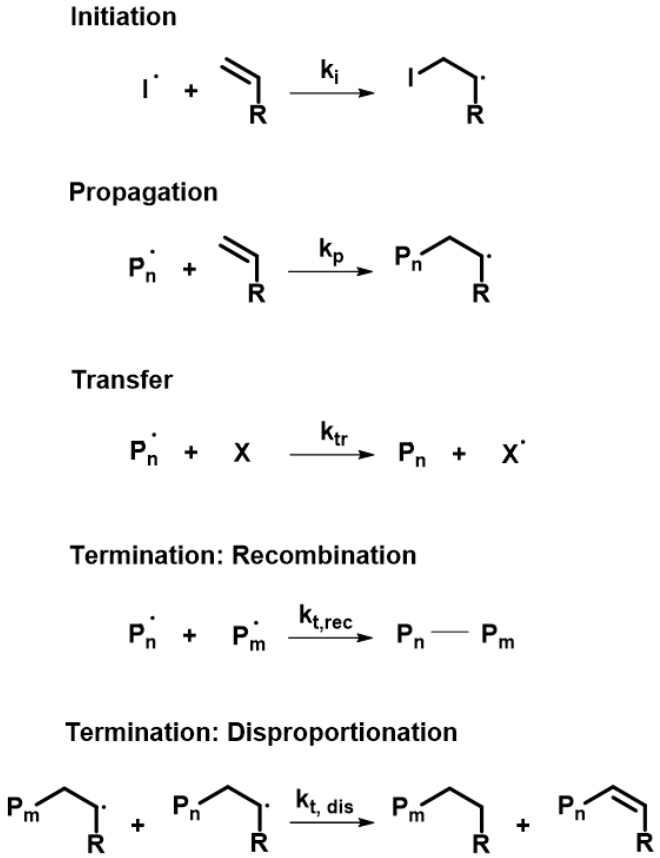

Figure 1.11. Schematic reaction mechanism of a radical polymerization.

The simplest and mostly used method to produce synthetic high-molecular-weight polymers worldwide is free radical polymerization (FRP) due to its robustness and simplicity allowing the production of a wide range of materials with unique properties. Furthermore, this FRP process is compatible with a lot of different monomers including (metha)acrylates, styrene and (meth)acrylamides. Secondly, it is tolerant to a lot of different functional groups, such as alcohols, acids, amides. Finally, it is easy to implement in different reaction conditions, eg. emulsion-, solution- and bulk polymerizations. However, due to the high reactivity and concentration of radicals, especially at high conversions, very little control over the molecular weight (M_n), molecular weight distribution (Đ) and the architecture of the synthesized polymer chains is possible. To overcome these restrictions a new class called living/controlled polymerizations was invented allowing the synthesis of more tailor-made polymers while retaining the versatility of the radical polymerization process.[110–112]

2.1 Living/controlled polymerizations

Living polymerization was first reported by Szwarc for the anionic polymerization of non-polar vinyl monomers by performing the polymerization under high vacuum to minimize the traces of oxygen and moisture, eliminating termination and transfer reactions. Under these conditions the active site will not be deactivated and therefore the polymer chain will propagate for an unlimited time even if the initial monomer feed is exhausted and will theoretically keep on growing as long as fresh monomer is added into the reaction mixture.[113] This discovery in polymer science made it possible to synthesize tailor-made polymers with predetermined molecular weights, low dispersity and precise control over the chain architecture and end-group functionality. Unlike in anionic and cationic polymerization, where termination through recombination is impossible due to electrostatic repulsion, the active sites of radical polymerization has the propensity to undergo bimolecular recombination and disproportionation reactions making a true "living"-polymerization impossible. However, these irreversible deactivation processes can be limited by keeping the concentration of active radicals low, significantly reducing the contribution of termination reactions during the polymerization, allowing for a "living"-like polymerization called "controlled" radical polymerizations (CRP). From the kinetics of general radical polymerizations listed below, it can be determined that with a low concentration of the propagating species $[P^{\cdot}]$ (~10^{-7} M) termination will be limited as a result of its second order kinetic dependence on the concentration of active propagating centres without quenching the propagation.[102,114]

Equation 1.3 Propagation $R_p = k_p\,[M]\,[P^{\cdot}]$

Equation 1.4 Termination $R_t = 2k_t[P^{\cdot}]^2$

With R_p and R_t, the rates of the propagation – and termination step, respectively. The real-time concentration of the monomer is represented by [M], the concentration of the propagating polymer chain by $[P^{\cdot}]$ and the propagation – and termination rate constant by k_p and k_t, respectively.

Different controlled radical polymerizations have been reported since early 1980, such as nitroxide-mediated polymerization (NMP), atom transfer radical polymerization (ATRP) and reversible addition-fragmentation chain transfer (RAFT) polymerization. All mechanisms have one common key aspect, namely establishing a dynamic equilibrium between the propagating radicals and dormant non-propagating species resulting in a low concentration of the propagating species. In NMP and ATRP this equilibrium is achieved by deactivating the propagating polymer chains via the reversible reaction with a stable radical deactivator X, such as a nitroxide for NMP or a halogen for ATRP (Figure 1.12). The reactivation of these dormant species can either be accomplished via heat (NMP) or via the addition

of an appropriate catalyst, such as copper(I) (ATRP), reforming the growing chains and allowing them to react with a number of monomer units before going back to their dormant state.[102,115,116]

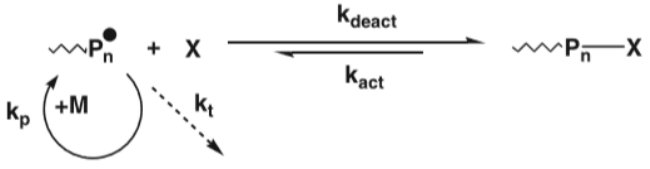

Figure 1.12. Deactivation/activation process of the growing polymer chain controlled via stable radicals. Reprinted from ref.[102] Copyright 2019, with permission from Elsevier.

In RAFT polymerization, however, this equilibrium is achieved by a degenerative exchange reaction based on the addition of a transfer agent. Here, the transfer agent plays the role of the dormant species and can be transferred between growing chains (Figure 1.13). This CRP technique will also be used in this thesis and will therefore be further explained in the next section.

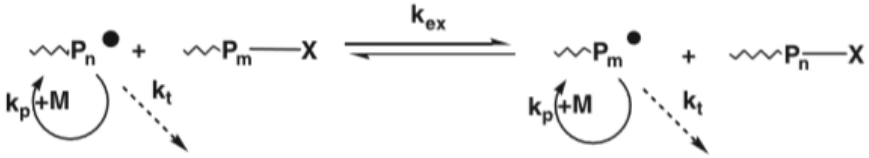

Figure 1.13. degenerative exchange process. Reprinted from ref.[102] Copyright 2019, with permission from Elsevier.

To accomplish high control over molecular weight, topology and dispersity, it is necessary that the CRP processes have a fast initiation rate compared to the rate of propagation as this will allow the simultaneous growth of all polymers and therefore a low dispersity. Furthermore, the equilibrium between dormant and active species should be shifted towards the dormant species ensuring the necessary low concentration of radicals but the exchange should also be very fast compared to the propagation rate to ensure that all active chain termini are equally susceptible to reaction with the monomer and grow evenly.[102,117]

To analyze whether the radical polymerization is controlled, both the kinetics of the polymerization and the progression of the molecular weight M_n with conversion should be analyzed. Controlled radical polymerizations follow first order kinetics if both fast initiation compared to propagation rate occurs and a constant number of growing chains are maintained throughout the polymerization by suppressing the termination reactions.

Equation 1.5 $$R_p = -\frac{d[M]}{dt} = k_P[P^{\cdot}][M]$$

Integration of this equation leads to the following equation:

Equation 1.6 $$\ln\frac{[M]_0}{[M]} = k_P[P^{\cdot}]t$$

By plotting the value of $\ln\frac{[M]_0}{[M]}$ against the reaction time (t) a linear relationship should be obtained considering a constant $[P^{\cdot}]$ is established by both a swift initiation and limited termination reactions. A deviation in this linearity is caused by either slow initiation or the occurrence of irreversible termination reactions and indicates a lack of control of the polymerization (Figure 1.14).

The number average molecular weight (M_n) or the degree of polymerization (DP) also should show a linear relationship in function of the monomer conversion in a CRP, assuming fast initiation and the negligible transfer or termination reactions. This can be derived from the following equation:

Equation 1.7 $$DP_n = \frac{M_n}{M_0} = \frac{[M]_0}{[I]_0} \times conversion$$

Equation 1.8 $$M_n = M_0\frac{[M]_0}{[I]_0} \times conversion$$

A shift from this linear trend implies that all the polymer chains are not growing at the same rate indicating that one of the above mentioned requirements for CRP is not fulfilled (Figure 1.14). Finally, the dispersity (Đ), calculated as Mw/Mn, is used as a measure for the control during CRP reaction and indicates the MW distribution of the obtained polymeric species. It is generally considered for CRP that Đ < 1.2 is acceptable, although this value is dependent on the specific polymerization conditions, conversion and CRP-technique.

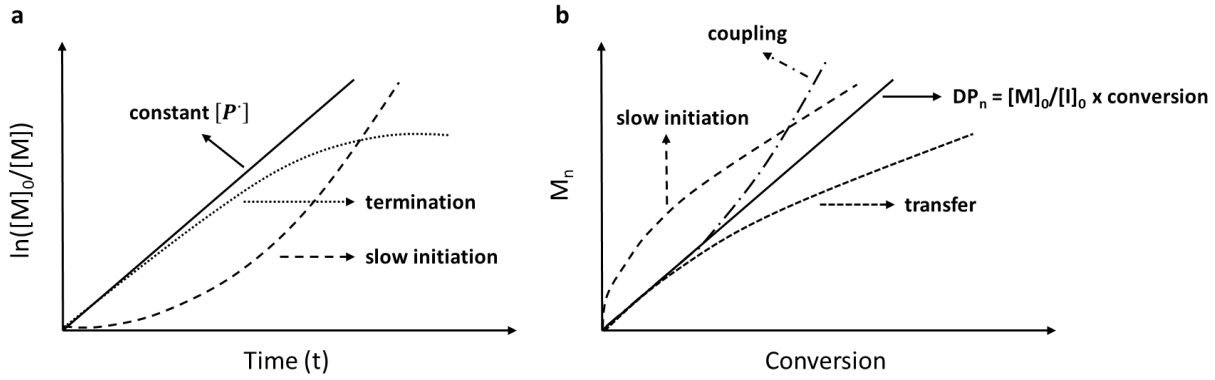

Figure 1.14. a) Kinetic plot showing the linear dependence of $\ln([M]_0/[M])$ versus time during an ideal CRP, a slow initiated CRP and CRP where termination is occurring. b) The molecular weight evolution showing of the linear dependence of M_n on the conversion during an ideal CRP, slow initiated CRP and a CRP interfered by coupling and transfer.[118]

2.1.1 Reversible addition-fragmentation chain transfer (RAFT) polymerization

RAFT polymerization was first described in 1988 by Moad, Thang and Rizzardo at the Commonwealth Scientific and Industrial Research Organization (CSIRO) in Australia[104] and has mainly been used for the creation of functional and complex polymeric topologies including dendrimers, star- or brush-like polymers and even cross-linked materials. Among the existing CRP techniques, RAFT has some advantages as it is compatible with a lot of different reaction conditions like solvents and is tolerant to unprotected functionalities including OH, COOH and $CONR_2$ groups.[119,120]

In the RAFT polymerization process a degenerative exchange process is achieved by using thiocarbonyl compounds (RAFT agents), such as trithiocarbonates, xanthates or dithioesters as a chain transfer agent to regulate the equilibrium between the propagating radicals and the dormant polymer chains. In this thesis, mostly acrylamide-based monomers will be used for the synthesis of end-functionalized polymers bearing the guest molecules TTF or DNP. To do this, a trithiocarbonate is used as RAFT-agent modified with an activating group (Z) and a homolytic leaving group (R) to control the polymerization, which will be explained using the mechanism in Figure 1.15. After the initiation step with a separate thermal or photo-initiator, the growing oligomeric radical chain ($P_m^{\cdot}$) will react with the reactive carbon center of the C=S bond of the RAFT agent (i), favoring the radical addition to the RAFT agent over the radical initiation with the vinyl moieties present in the monomers. The formed radical intermediate (ii) can subsequently fragment to generate an oligomeric RAFT agent and the homolytic cleaved radical R$^{\cdot}$ (iii). Ideally, this R-group should not only be a better leaving group than the propagating species ($P_m^{\cdot}$) but also possess a higher reaction rate with the monomer (k_i) compared to the propagation rate k_p to ensure a fast reinitiation step (iii) leading to a second growing polymer chain ($P_n^{\cdot}$). During the main equilibrium step (iv) the nature of the Z group controls the life-time and thus the stability of the radical intermediate. Mostly a rapid exchange between the growing polymer chains is necessary to ensure the uniform growth of the polymer chains resulting in low Đ-values. Although, most recombination and disproportionation mechanisms are mainly suppressed by limiting the concentration of active radicals through the formation of an intermediate species, still some minor termination reactions (v) will inevitably occur.[110,121]

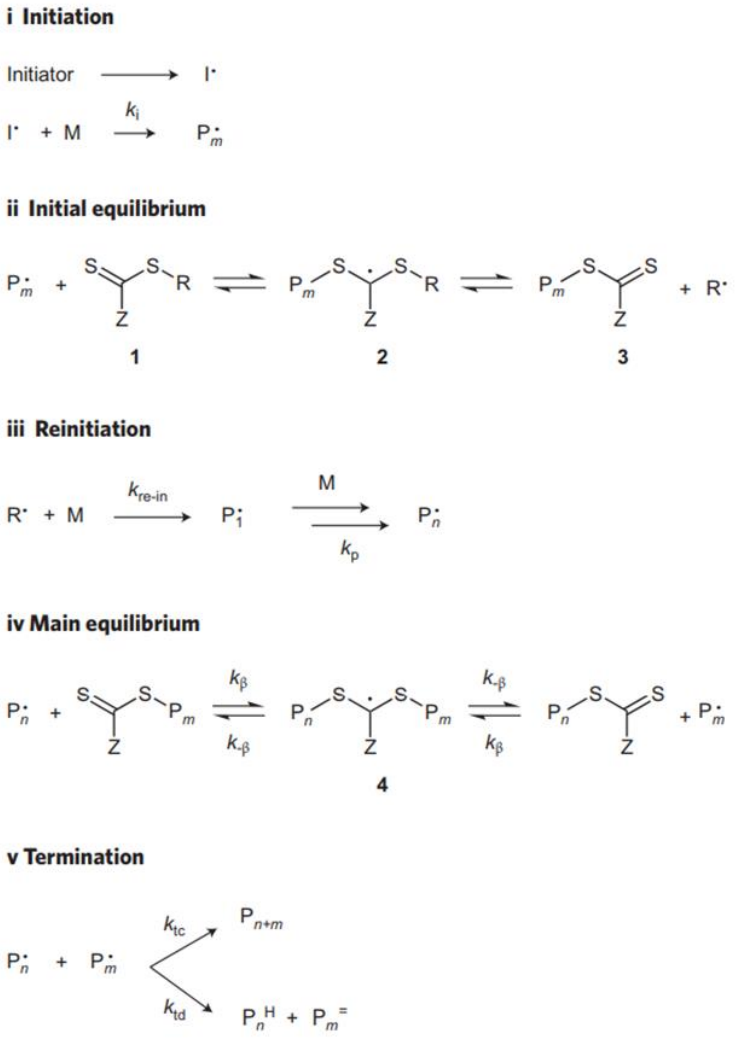

Figure 1.15. Mechanism of RAFT-polymerization based on M. Semsarilar *et al*. Reprinted by permission from ref.[110] Copyright 2019, Springer Nature.

2.2 Stimuli-responsive polymers induced by host-guest chemistry

Living organisms are adaptive as they possess the ability to sense and respond to small changes in the environment, for example carnivorous plants that rapidly close when an insect crawls into its trap or the growth direction of plants that is regulated by the external stimuli gravity (gravitropism) and light (phototropism). Also in our human body many examples of stimuli responsive mechanisms exist, such as muscle contraction upon the release of calcium ions from the nerve terminals and the change in the size of our pupils by the brightness of the light in the environment.[122–124] Inspired by these naturally occurring responsive mechanisms, scientists have created a new class of materials that can alter their properties in response to changes in external stimuli, called smart or intelligent materials. By careful design, these materials can reversibly change their shape, solubility properties, their interaction with light, surface properties or its permeability induced by the occurrence of one or more of the physical or chemical stimuli enlisted in Figure 1.16..[125,126]

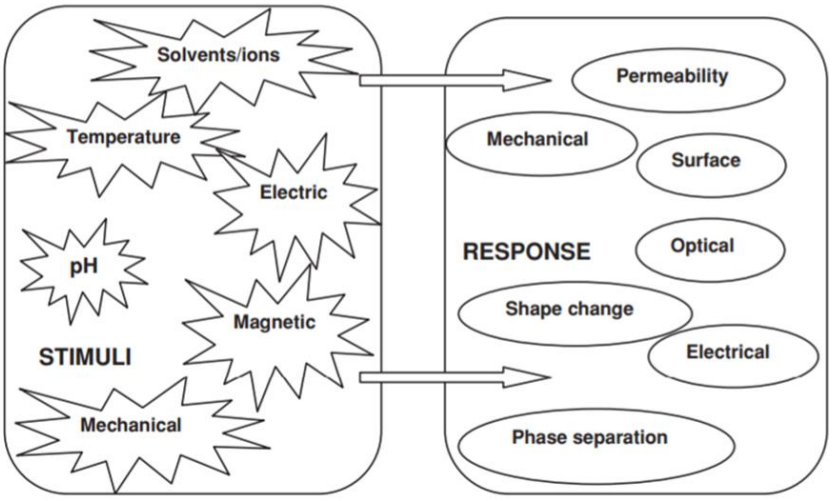

Figure 1.16. Examples of potential stimuli and responses.[126]

The discovery of the CRP played an important role in the further development of more complex stimuli responsive materials including hydrogels, micelles and porous membranes. It allowed for the full control over the polymer microstructure on various levels including the identity of the side chains/monomer, the composition of the polymer to allow block-co-polymers and gradient copolymers and finally the topology of the polymer chain to create star and cyclic polymers. This has enabled the design of more controlled smart materials with tailor-made responses through careful alteration of the polymer properties, for instance the hydrophilic/hydrophobic balance in thermo-responsive polymers to fine-tune their transition temperature.[127–130] A final mechanism to alter the properties of (stimuli-responsive) polymers that has been made available through the use of CRP-techniques is the incorporation of host-guest assemblies into the polymeric chains. The latter involves the incorporation of either the host or guest as polymeric side chain or end-functionality allowing significant changes in the polymer properties upon assembly/disassembly of the host-guest complex. The reversible, non-covalent interactions involved in the host-guest assembly can influence the molecular interactions and/or the hydrophilic/hydrophobic balance of the polymer microstructure, allowing for the design of more controlled smart materials with tailor-made responses.[1] Indeed, the use of these artificial supramolecular assemblies not only provides an additional level of control over the properties in stimuli-responsive polymers but also allows for the on demand switching as the molecular recognition is governed by subtle external changes in the environment like the presence of a stronger guest or oxidation/reduction reaction to change the charge on the guest/host molecule. For example, rotaxanes and catenanes consisting of redox-active π-electron-rich TTF units encircled by a π-electron-poor tetracationic cyclophanes allows the fabrication of electrochemically induced molecular switching devices which is applicable for information storage and microscale mechanical actuation processes.[93] The most extensively studied smart materials are thermo-responsive polymers

as they can be used in many different applications, especially biomedical applications and their stimulus can be easily controlled and fine-tuned.

2.2.1 Thermo-responsive polymers

Most thermo-responsive polymers exhibit a unique solubility transition in aqueous solutions at a desired temperature. These polymers can be mainly divided into two categories: 1) polymers that exhibit a lower critical solution temperature (LCST) in which the polymer becomes insoluble upon heating and 2) an upper critical solution temperature (UCST) where it becomes insoluble upon cooling.[131]

The most studied thermo-responsive polymer exhibiting a LCST behavior is poly(*N*-isopropylacrylamide) (PNIPAm), especially as its phase transition occurs around the human body temperature making it possible to implement them in various biomedical applications varying from drug delivery systems, tissue engineering to biosensors.[132] At lower temperatures this polymer will be hydrated, forming hydrogen bond interactions with the water molecules. These favorable enthalpic interactions will overcome the entropic loss resulting from the coordinated water molecules surrounding the polymer chain promoting the solubility of the polymer. With rising temperature however, this entropic value will become more important until at a certain temperature, called the cloud point temperature (T_{cp}), this entropic loss can no longer be compensated by the enthalpic gain of the polymer-water interactions. At this state the hydrophobic polymer-polymer interactions becomes favorable causing the polymer chains to phase separate in high polymer concentration mesoglobules by expelling the coordinated water into the low polymer concentration environment (Figure 1.17).

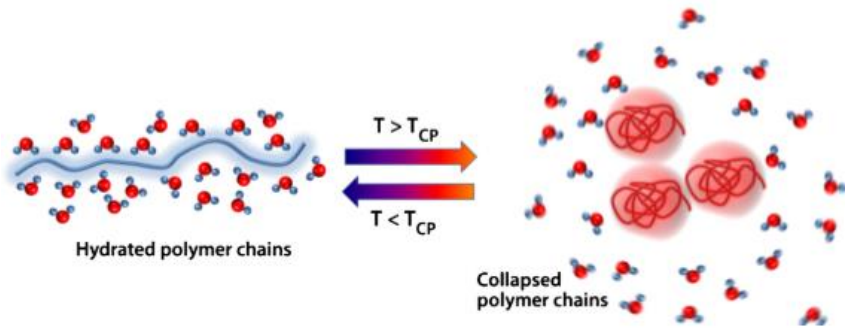

Figure 1.17. The schematic illustration of an thermo-responsive polymer displaying a LCST behavior. Reprinted from ref.[123]

This T_{cp} can be finely tuned by careful selection of the identity of the incorporated monomers/side-chains that control the hydrophobic/hydrophilic balance in the polymer.[125] Recently, scientist have shown increasing interest to modify this thermo-responsive behavior via supramolecular approaches based on host-guest assemblies. For example, Yu G., et al. were able to tune the LCST behavior of a

random co-polymer of PNIPAm and styrene modified with a paraquat derivative. Upon the addition of an excess of the carboxylic acid functionalized pillar[10]arene to an aqueous solution of this PNIPAm-co-paraquat polymer, it was noticed that the T_{cp} was increased with approximately 15°C (from 40.7°C to 56.1°C). This complexation-induced increase in T_{cp} was not only caused by the enhanced hydrophilicity upon complexation but also results from the extra steric hindrance and electrostatic repulsion introduced by the pillar[10]arene host molecules preventing the formation of intra- and interpolymer aggregates. The reversibility of the complexation was highlighted by showing the decrease in T_{cp} upon gradual addition of a competitive guest molecule, e.g. 1,10-phenanthrolinium, which possesses a higher binding affinity towards pillar[10]arene compared to the paraquat derivatives (Figure 1.18).[133]

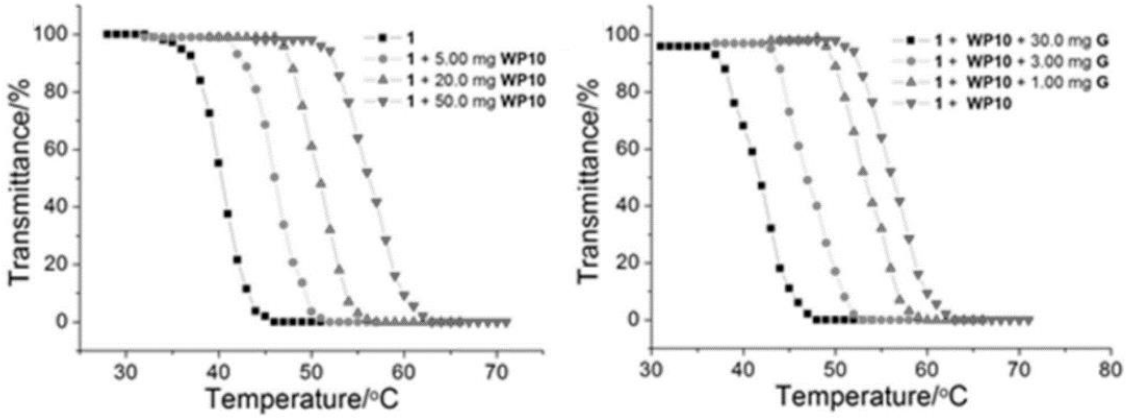

Figure 1.18. Left: The result of turbidity measurements showing the transmittance in function of the temperature for a solution containing the PNIPAm-co-paraquat polymer (30 mg, 1.5 mL) upon the addition of 5.00 mg, 20.00 mg and 50.00 mg of Pillar[10]arene. Right: The result of turbidity measurements showing the transmittance in function of the temperature for a solution containing the PNIPAm-co-paraquat polymer (30 mg, 1.5 mL) complexed with pillar[10]arene polymer (50 mg, 1.5 mL) upon the addition of 1.00 mg, 3.00 mg and 30.0 mg of the competitive guest 1,10-phenanthrolinium. Reprinted from ref.[133] Copyright 2019 John Wiley and Sons.

In a second example reported by our group, the LCST behavior of PNIPAm was tuned by the incorporation of hydrophobic naphthalene units, which can form donor-acceptor complexes with BB. It was noticed that the T_{cp} of the PNIPAm-co-naphtalene polymer could be altered from approx. 20°C to approx. 32°C upon the addition of stoichiometric amounts of BB. It was found that this PNIPAm-co-naphtalene complexed with BB polymeric system showed a large hysteresis in its thermal transition, which could be employed as a thermal sensor with memory function as depicted in Figure 1.19. Heating this system above its T_{cp} (32°C) leads to the aggregation of the polymer and disruption of the BB-naphthalene (BB-Napht) complex accompanied by the disappearance of the characteristic purple color of the BB-Napht complex. Rehydration of the more hydrophobic non-complexed collapsed PNIPAm-co-naphthalene polymer and the subsequent reformation of the BB-Napht complex, is only possible after cooling the system below 20°C. This means that at room temperature the systems still remembers if it was heated above its T_{cp}, which can be evaluated via a direct visible read-out.[134] These

two examples are just a glimpse of the many possible strategies which can be used to finely tune the transition temperature in a reversible and adaptive manner by the incorporation of the appropriate host –guest complexes into thermo-responsive polymers.[135–143]

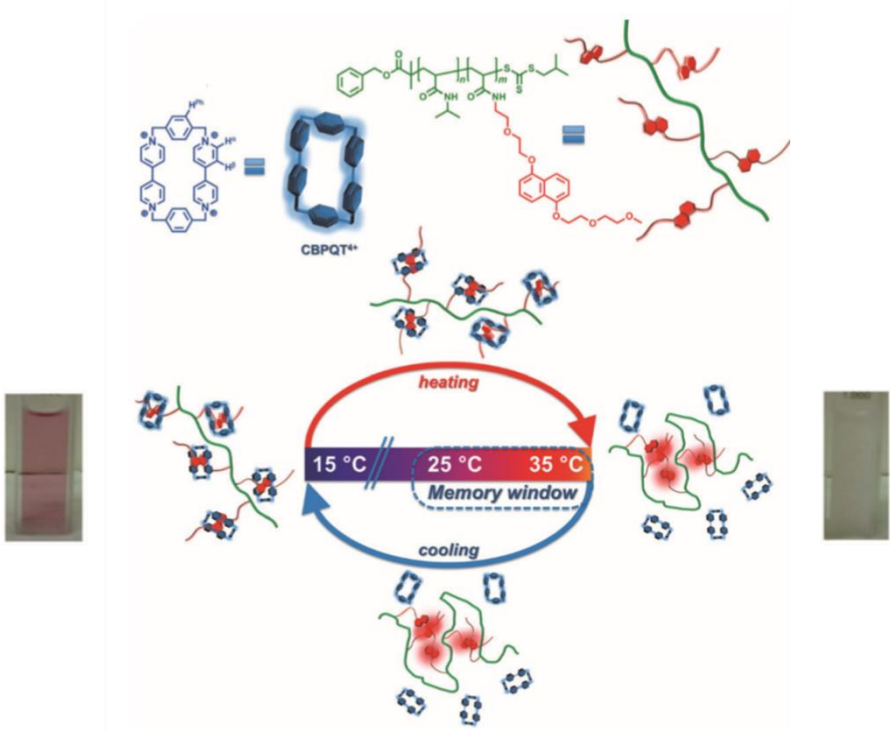

Figure 1.19. Top: The structure of the host molecule BB and the PNIPAm-co-naphthalene polymer. Bottom: Schematic representation of the thermal memory function provided by the difference in T_{cp} and clearance point temperature of the PNIPAm-co-naphthalene polymer with BB. Reprinted from ref.[134] Copyright 2019 John Wiley and Sons.

A final example highlights the possibility of using supramolecular interactions to change the self-assembly of the polymer under influence of a certain stimuli. Higher degree of complexity in the polymer architectures can easily be achieved with the use of supramolecular recognition, including the formation of block co-polymers via the synthesis of end-functionalized polymers or the formation of graft co-polymers by modifying the side chains with the molecular recognition units. Mostly these noncovalent interactions will link a hydrophilic and hydrophobic oligomer or polymer chain creating macromolecular supra-amphiphiles which can further assemble into nanostructures ranging from micelles to vesicles and nanotubes. Furthermore, due to the dynamic nature of these interactions, these macromolecular supra-amphiphiles can also display on demand switching regulated by multiple stimuli as highlighted in Figure 1.20.

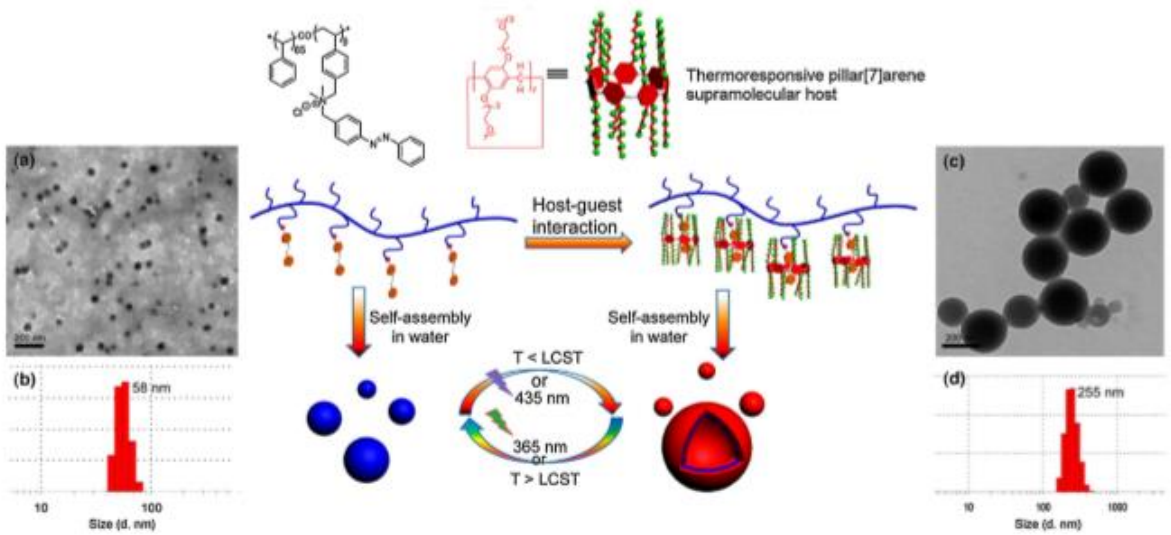

Figure 1.20. Schematic overview of a) the TEM image of an aqueous solution containing 7.00 mM WP7 and 1.00 mM styrene-co-azobenzene polymer heated above the Tcp (60°C), b) DLS results of the solid nanospheres formed at T = 60°C, c) TEM image of the vesicles formed by the assembly of the pillararene-based supra-amphiphilic polypseudorotaxane at room termperature, d) DLS results of the vesicles formed at room temperature. Adapted with permission from ref.[144] Copyright 2019 American Chemical Society.

In this example reported by Huang *et al.*, a pillararene-based supra-amphiphilic polypseudorotaxane was synthesized which can undergo thermo- and photo-responsive switching between solid nanospheres and vesicular structures. Therefore, a co-polymer of polystyrene containing 12 mol% azobenzene moieties was prepared which can form host-guest complexes with water-soluble pillar[7]arene (WP7) that was decorated with methoxy-(tri(ethylene glycol) chains. Due to the amphiphilic character of this polypseudorotaxane, the polymer chains will assemble into a vesicular nanostructure in aqueous solutions with a hydrophobic inner layer of styrene-based copolymer (blue) solubilized by the hydrophilic WP7 layers on both sides (red) as seen in Figure 1.20. The tri(ethylene glycol) chains on WP7 exhibit LCST behavior and when heated above their T_{cp} (> 50 °C), these oligomeric chains can no longer solubilize the hydrophobic WP7 cavities. This means that upon heating the pillararene-based supra-amphiphilic polypseudorotaxane above this T_{cp}, the dethreading process of WP7 occurs, releasing the hydrophobic styrene-co-azobenzene polymers which will assemble into smaller solid nanospheres. Upon cooling the inverse effect was observed and the original vesicle was reformed. A similar reversible phenomenon was achieved by the irradiation of UV light (365 nm) by switching the conformation of the azobenzene from trans to cis promoting the disruption of the WP7 – azobenzene complex.[144] Nowadays, different macrocyclic host molecules have been used for the creation of such macromolecular supra-amphiphiles including, cyclodextrins[145–149], pillar[n]arenes[150–155] and cucurbit[n]urils[156–158].

3 Smart hydrogels

As shown before, supramolecular chemistry, and more particularly host-guest interactions, has profoundly altered the field of polymer chemistry, especially how these interactions can be used to control the properties of complex 3D polymeric networks, such as hydrogels. Hydrogels consisting of hydrophilic polymers can take up and retain large amounts of water within their 3D structure. Upon swelling, their structural integrity can either be maintained via covalent crosslinks, called chemical hydrogels, or via reversible physical junctions including metal ligand coordination or ionic interactions, called physical hydrogels.[159–162] By incorporating host-guest molecules into the hydrogels, the water uptake can be regulated reversibly via either a sol-gel transition of a physical hydrogel or via an expansion-contraction process of a covalent hydrogel.

Sol-gel transitions can be achieved in hydrogels where the polymeric 3D structure is held together by reversible physical crosslinks. Whereby, the hydrogel formation is driven by the molecular recognition process of the binding motifs incorporated along the polymer chain. These stimuli-responsive supramolecular hydrogels are mostly used in biomedical applications including tissue engineering, biosensors and wound healing.[159,163–167] In Figure 1.21, an example of a physical hydrogel used for biomedical applications is depicted. Chen, L et al. tried to mimic the extracellular matrix by mixing β-CD modified filamentous bacteriophage M13 with azobenzene guest molecules functionalized on hyaluronan disaccharide polymer chains creating a physical hydrogel dynamically interlocked by the β-CD-azobenzene host-guest interactions. The hydrogel exhibits an in situ sol-gel transition induced by either the photo-irradiation of the azobenzene guest molecule or by the presence of competitive host or guest (adamantine) molecules which has the potential to be used as 3D cell culture systems and controlled delivery systems for therapeutic proteins and cells.[168]

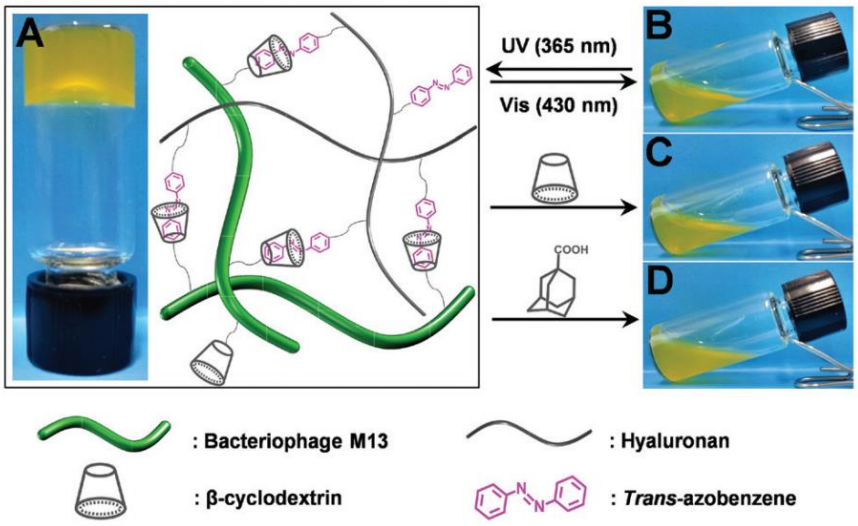

Figure 1.21. (A) The schematic illustration of the formation of the physical hydrogel created upon the mixing of 0.5 wt% M13-β-CD with 0.5 wt% HA-Azo. Pictures proving the sol-gel transition of the β-CD-azobenzene physical hydrogel by using the simple vial inversion method upon a change in photo-irradiation (B), the addition of the competitive host molecule β-CD (C) and the addition of a competitive guest molecule adamantane (D).Reprinted from ref.[168] Copyright 2019 Royal Society of Chemistry.

In the second class, host-guest assemblies can be used to control the water uptake of covalent hydrogels while leaving the structural integrity unchanged, e.g. contraction or expansion of the hydrogel, by responding to subtle environmental changes. These chemical hydrogels mediated by host-guest chemistry are mostly applicable in shape memory engineering, artificial muscle formation, creation of actuators and in drug delivery systems.[164,165,169] An example of such a drug delivery hydrogel system is shown in Figure 1.22. Wuang *et al.* reported the synthesis of a polymeric network functionalized with ferrocene moieties which upon complexation with water-soluble carboxylic acid functionalized pillar[6]arene (WP6) can drastically promote its swelling ratio through increased hydrophilicity and the electrostatic repulsion between the polymer chains due to the negatively charged carboxylates of the now embedded WP6. The reversibility of the host-guest interaction allows for the expansion and contraction of the WP6-ferrocene mediated hydrogel which can be controlled via many stimuli such as temperature, pH, redox potential and by the addition of competitive guest molecules. It was demonstrated that this system can be used for controlled release of a pre-absorbed drug through minor variations in the environmental pH. This stimulus can regulate the disassembly of the WP6-ferrocene complex leading to the shrinkage of the hydrogel and expulsion of the pre-absorbed drug through contraction of the hydrogel matrix (Figure 1.22).[170]

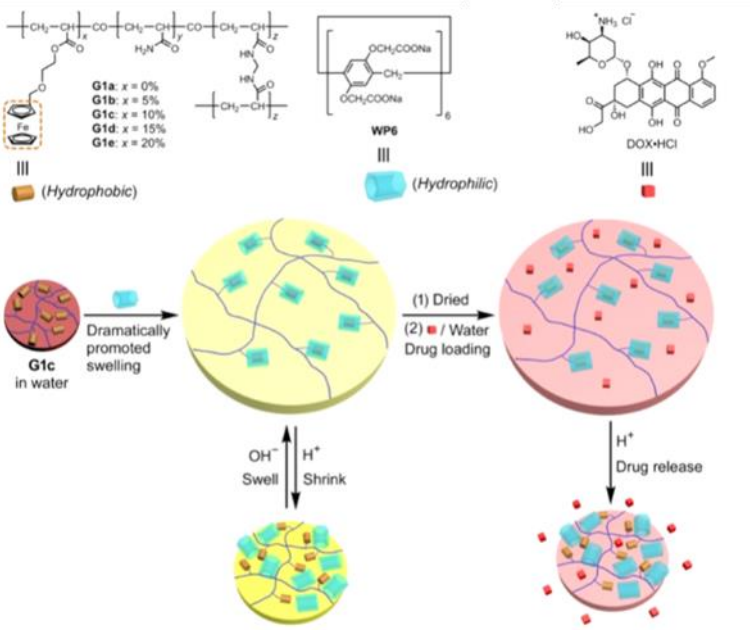

Figure 1.22. Top: Schematic illustration of the hydrogel modified with ferrocene moieties, WP6 and doxorubicin hydrochloride. Bottom: Illustration of the promoted swelling upon the addition of WP6 to the hydrogel together with the pH-responsive release of the doxorubicin. Reprinted with permission from ref.[170] Copyright 2019 American Chemical Society.

Another feature that these host-guest assemblies can implement into a hydrogel is their ability to both enhance the mechanical strength or toughness and also the stretchability of the gel by forming a double-network where the host-guest complexes can act as energy dissipation components.[171] Via this approach, Scherman and coworkers were able to create a polymeric network that could be stretched 100 x its initial length and can lift objects of 2000 x their weight by implementing dynamic CB[8] mediated host-guest assemblies into a chemically crosslinked polyacrylamide hydrogel.[172]

Different smart hydrogels have already been developed with a wide variety of tailor-made responses depending on the used host molecule, including cyclodextrins[173–177], curcurbit[n]urils[51,172,178–182] and pilar[n]arenes[183–187] showing diverse dynamic properties and bindings strengths. In this thesis we will focuss on thermoresponsive, chemically-crosslinked materials in which the volume changes are modulated by the association and dissociation of host-guest complexes.

3.1 Thermo-responsive hydrogels mediated via host-guest chemistry

In the remainder of this chapter a selection of interesting examples of thermo-responsive hydrogels based on host-guest chemistry will be discussed. The remarkable responses that these materials show towards changes in temperature can be used in different fields ranging from biomedicine to smart advanced materials such as self-healing materials and shape-memory materials.

A first example will focus on the use of host-guest chemistry for the modulation of macroscopic assemblies composed of hydrogels. Harada *et al.* used radical polymerization to synthesize

polyacrylamide hydrogels containing 15 mol% benzyl moieties (Bz-gel) which can interact and adhere to hydrogels functionalized either with α-CD, β-CD or γ-CD as depicted in Figure 1.23. Depending on the environmental temperature, different macroscopic self-assemblies were formed in which the strength of adhesion of the CD-gels to the Bz-gel is increasing in the order of γ-CD-gel < α-CD-gel < β-CD-gel which is in line with the strength of the K_a values of their respective complex. The temperature sensitive macroscopic self-assembly is shown in Figure 1.23 where each gel was stained with a color, namely the γ-CD-gel (green), α-CD-gel (blue), β-CD-gel (red) and Bz-gel (yellow), for better visualization of the formed macroscopic assemblies. It can be noticed that at lower temperatures all the CD-hydrogel pieces are participating in the macromolecular assembly (α-CD, β-CD or γ-CD). The dissociation of the green colored γ-CD-gels and the blue colored α-CD-gels from the macromolecular assembly occurs when the temperature was increased to respectively 15 °C and 23 °C. This indicates that at room temperature the interactions between the Bz-gel and the respective γ-CD and α-CD are too weak favoring the dissociation of this host-guest complex. Finally, the remaining gel assembly of Bz-gel and β-CD-gel will eventually dissociate at 90°C. This high dissociation temperature is not only indicative for the high K_a of the Bz-CD complexes, but also for the synergetic event that multiple host-guest assemblies are formed at the interface of both gels. Upon cooling the reverse effect is established and the macroscopic assemblies can stepwise be reformed.

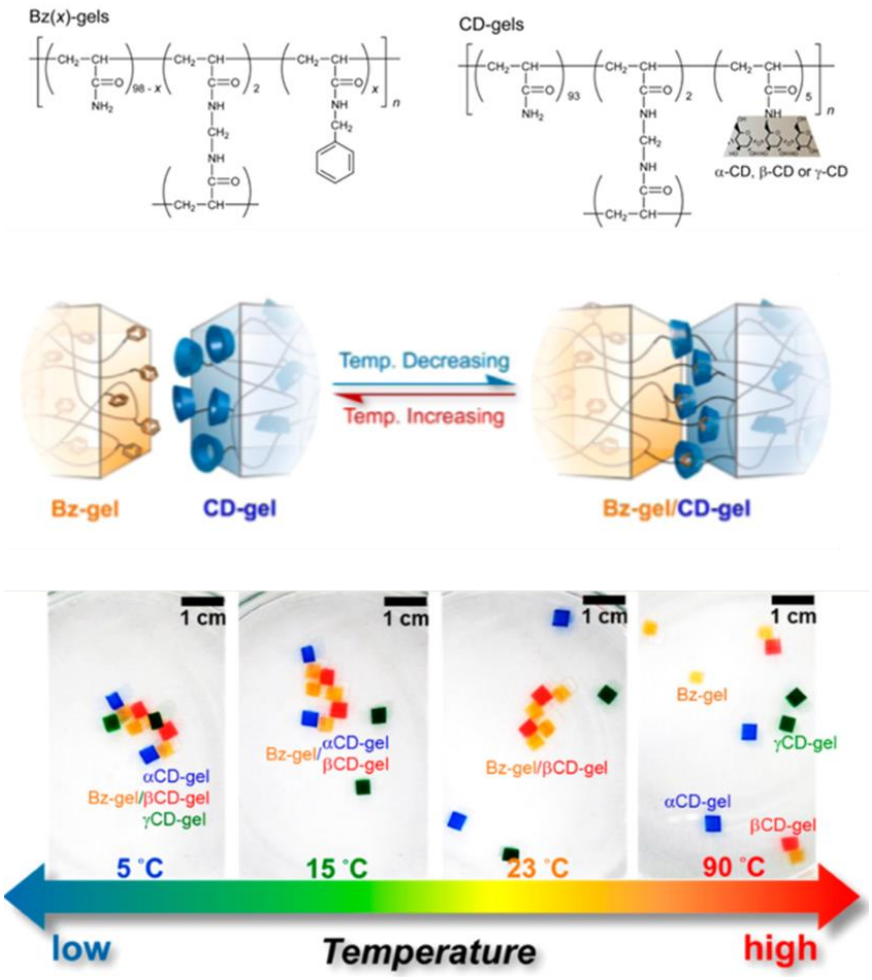

Figure 1.23. Top: Structural composition of the hydrogels modified with benzyl moieties and CD. Middle: Illustrative representation of thermo-responsive complex assembly and disassembly at the interface of a benzyl modified hydrogel and a hydrogel functionalized with CD. Bottom: Pictures showing the interaction of the Bz-gel with the γ-CD-gel (green), α-CD-gel (blue), β-CD-gel (red) at different temperatures. The different host hydrogels were stained with dyes to better visualize the temperature dependent supramolecular assemblies. Adapted with permission from ref.[188] Copyright 2019 American Chemical Society.

In a second example, Wang *et al.* reported a smart window that is able to autonomously change color, allowing to e.g. control the input of solar panels and, or so they claim, boost the emotions of the inhabitants by regulating the color of the window (Figure 1.24). This was realized by using pillar[6]arene modified with multiple triethylene glycol groups (EGP6), which exhibits LCST behavior. EGP6 is able to from inclusion complexes with ferrocene groups embedded in a polyacrylamide based polymer network masking the hydrophobic character of the ferrocene units (Fc) and resulting in an induced swelling upon complexation. The higher water absorption of the EGP6-Fc-gel enhances the transparency of the Fc-gel, which is necessary for the smart window application. This transmittance of light can be drastically altered by increasing the temperature above the T_{cp} of EGP6 which disrupts the EGP6- Fc complex followed by the formation of insoluble EGP6 aggregates in the water entrapped within the hydrogel. By lowering the temperature from 40°C to 25°C the now opaque EGP6.Fc-gel turns back to its originally transparent state as the EGP6 re-dissolves and subsequently assembles back with

the embedded ferrocene moieties. An additional feature of these incorporated ferrocene moieties is that via oxidation to the ferrocenium cation, the smart window can change from a warm tone color (yellow) to a cool tone color (green) and vice versa making the homes of the inhabitants more comfortable by improving their feelings and emotions, as claimed by the authors.[189]

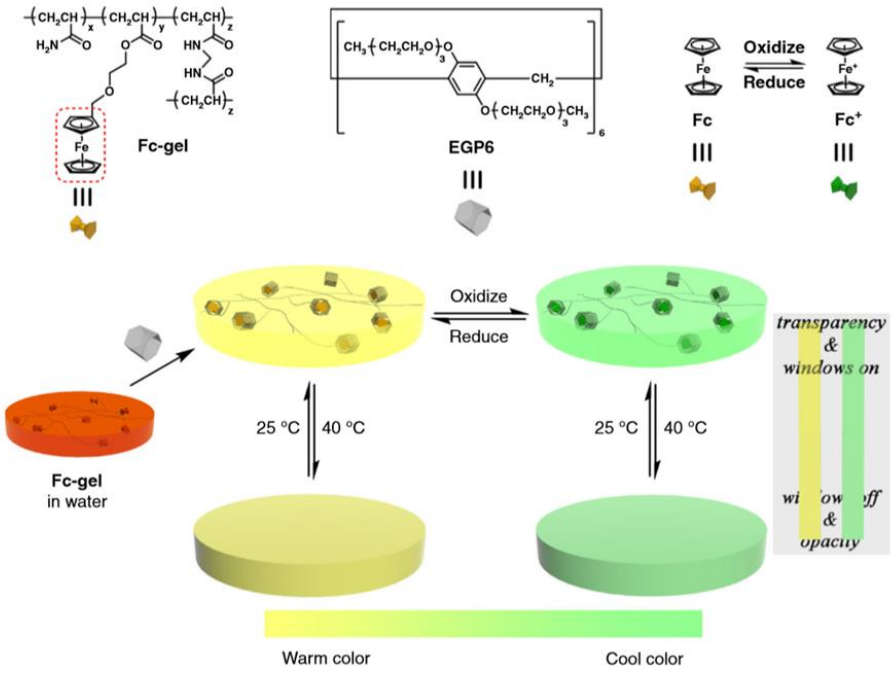

Figure 1.24. Chemical structures of the Fc-gel, EGP6 and the redox responsive ferrocene and schematic illustration of the warm/cool tone switchable thermochromic smart window. Reprinted from ref.[189] Copyright 2019 Springer Nature.

Finally our group demonstrated that BB-complexes are also good candidates to thermally control the expansion or contraction of chemically crosslinked hydrogels. In this example the exchange of BB between a non thermoresponsive poly(*N,N*-dimethylacrylamide) hydrogel functionalized with DNP guest units (NaphtGel) and a LCST-sensitive PNIPAm polymer end-functionalized with TTF moieties (TTF-PNIPAm) allows to indirectly control the water uptake of the hydrogel (Figure 1.25).

Owing to the higher binding affinity of TTF towards BB compared to DNP, at lower temperatures (8°C) the solution of this three component system will color green which is characteristic for the formation of the TTF-BB complexes. This means that at lower temperatures the BB will selectively form pseudorotaxanes with the TTF-PNIPAm present in the system. Upon heating, the TTF-PNIPAm polymers will collapse into insoluble aggregates as a result of their LCST behavior, dethreading the BB and leading to the disappearance of the green color. The free BB can subsequently penetrate the NaphtGel to form donor-acceptor complexes with the embedded DNP moieties which is accompanied with the color change of the hydrogel from yellowish to the characteristic purple color of the DNP-BB complex. Beside the color change also an expansion of the hydrogels is noticeable as upon complexation the electrostatic contribution of the ionic BB molecules and their counterions results in

an increased water uptake of the NaphtGel.BB hydrogel. Cooling the system back to 8 °C will allow the resolubilization of the TTF-PNIPAm, forcing the BB out of the hydrogel to form the stronger TTF-BB complex. This transfer can be visually detected by both the contraction of the NaphtGel and the color change of the NaphtGel and aqueous solution to yellow and green, respectively. In conclusion, this three component system can induce a less reported positive thermoresponsive behavior in which the hydrogel undergoes strong swelling upon mild heating.[190]

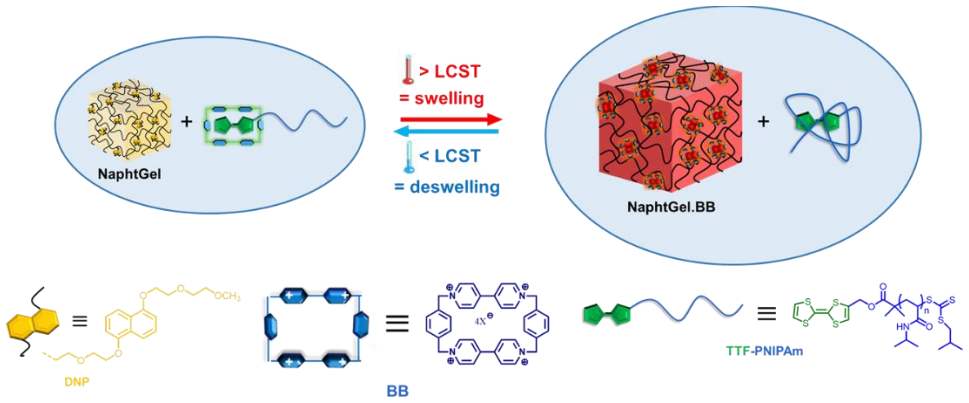

Figure 1.25. Schematic illustration of the UCST behavior of the three component system: NaphtGel, BB and TTF-PNIPAm.[190]

4 Conclusions

This chapter discusses the recent developments reported for the synthesis of stimuli-responsive polymeric systems in water mediated by host-guest complexes such as hydrogels and nanostructure composed of supra-amphiphiles which are very promising for life and material science applications, including drug delivery, tissue engineering and energy absorbing materials. These host–guest complexes have emerged as a powerful tool for the creation of these responsive materials due to their dynamic and adaptive character towards external stimuli e.g. temperature, pH and chemicals. Currently, cucurbit[n]urils (CB), cyclodextrins (CD) and pillar[n]arenes are most commonly used as host molecules for the synthesis of these water soluble stimuli-responsive polymeric materials. However, most of these host-molecules are difficult to include in aqueous-based sensor systems due to high hydrophobicity and resulting low water solubility, lack of a visual read-out signal upon complexation and complex synthesis. Therefore, continuous investigation towards other host molecules is required to improve the intended polymeric systems and introduce new and adaptable properties.

In this thesis, the less widely explored cyclophane-based host molecules cyclobis(paraquat-*p*-phenylene), also called blue box (BB) and cyclobis(paraquat-4,4'-biphenylene), commonly referred to as big blue box (BBB) are investigated for the use in aqueous smart materials. These cyclophanes can form strong 1:1 or 1:2 complexes, for BB and BBB respectively, with different-electron rich guest molecules such as naphthalene derivatives, tetrathiafulvalene and hydroquinone resulting in highly

colored complexes. These are mainly established by charge transfer interactions with the pyridinium moiety of the host molecules making it possible to easily detect and follow the complexation, but can also be used as a direct visual output in sensing applications. By careful selection of the guest molecule, the resulting 1:1 BB-guest complex can be controlled by many different stimuli including pH, redox potential and the concentration of competitive guest. In addition, the reversible formation of the 1:2 BBB-guest complexes allows them to be used as structural component of multi-responsive polymeric materials. Furthermore, the solubility of these macrocyclic host molecules can be easily controlled by changing the counter ions, allowing their use in different solvents including acetonitrile and water. Finally, the ionic character of BBB and BB will have a major influence on the hydrophilicity of the polymer systems upon complexation and can induce an increased uptake of water of the hydrogels functionalized with compatible guest molecules. These advantages make BB and BBB ideal candidates for novel aqueous-based smart sensor materials.

The goal of this thesis is therefore to characterize the association behavior of BBB with common guest molecules in water and highlight the applicability of the cylcophanes in smart materials by combining BB with a thermoresponsive hydrogel. By incorporating the guest molecules into the hydrogel, the subsequent complexation with BB will allow the control over the hydrophilicity of the hydrogel and therefore the swelling behavior. The decomplexation rate can thereby be controlled by either the stimuli-responsivity of the host-guest complex or by the temperature-induced contraction of the hydrogel. This has led to the first generation of reported polymeric sensors that contains a time-memory towards heating. Finally, an alternative pathway for the fabrication of smart materials by the incorporation of guest and/or host moieties on the material surface using a radical approach, expands the range of substrates including also conventional, high-volume plastics such as polyethylene and polypropylene.

5 References

1. Lehn, J. *Proc. Natl. Acad. Sci. USA* **2002**, *99*, 4763.
2. Lehn, J. M. *Chem. Soc. Rev.* **2007**, *36*, 151.
3. Kumar, D.; Sharma, D.; Singh, G.; Singh, M.; Rathore, M. S. *ISRN Pharm.* **2012**, *2012*, 1.
4. Ariga, K. In *Biomaterials Nanoarchitectonics*; Elsevier Inc., **2016**; pp 25.
5. J. M. Lehn *Angew. Chem. Int. Ed.* **1985**, *24*, 799.
6. Liu, J.; Scherman, O. A. *Adv. Funct. Mater.* **2018**, *28*, 1.
7. Ten Brinke, G.; Ikkala, O. *Chem. Rec.* **2004**, *4*, 219.
8. Yan, X.; Wang, F.; Zheng, B.; Huang, F. *Chem. Soc. Rev.* **2012**, *41*, 6042.
9. Bae, Y.; Fukushima, S.; Harada, A.; Kataoka, K. *Angew. Chem. Int. Ed.* **2003**, *42*, 4640.
10. Zhang, J.; Ma, P. X. *Adv. Drug Deliv. Rev.* **2013**, *65*, 1215.
11. Wang, L.; Lin, C.; Pan, Y.; Xiao, T.; Hu, X.; Li, Y.; Duan, Q.; Cao, Y. *J. Am. Chem. Soc.* **2013**, *135*, 10542.
12. Alvarez-Pérez, M.; Goldup, S. M.; Leigh, D. A.; Slawin, A. M. Z. *J. Am. Chem. Soc.* **2008**, *130*, 1836.
13. Kay, E. R.; Leigh, D. A. *Pure Appl. Chem.* **2008**, *80*, 17.
14. Wang, Y.; Frasconi, M.; Stoddart, J. F. *ACS Cent. Sci.* **2017**, *3*, 927.
15. Erbas-Cakmak, S.; Fielden, S. D. P.; Karaca, U.; Leigh, D. A.; McTernan, C. T.; Tetlow, D. J.; Wilson, M. R. *Science.* **2017**, *358*, 340.
16. Ikejiri, S.; Takashima, Y.; Osaki, M.; Yamaguchi, H.; Harada, A. *J. Am. Chem. Soc.* **2018**, *140*, 17308.
17. Gillam, P. Enzymes: Grade 9 Understanding for IGCSE Biology 2.10 2.11 2.13. https://pmgbiology.com/2014/12/03/enzymes-a-understanding-for-igcse-biology/ (last accessed Oct. 1, 2019).
18. Hemoglobine. https://biologielessen.nl/index.php/a-3/1993-hemoglobine (last accessed Oct. 1, 2019).
19. Sadava, D.; Heller, H. G.; Orians, G. H.; Purves, W. K.; Hillis, D. M. *Life: The science of biology*; 8th ed.; Sinauer associates, Inc. and W.H. Freeman & Co, **2008**.
20. Bhalla, V. *Resonance* **2018**, *23*, 277.
21. Ariga, K.; Kunitake, T. In *Supramolecular Chemistry — Fundamentals and Applications*; Springer, **2006**; pp 7.
22. Yamashoji, Y.; Tanaka, M.; Shono, T. *Chem. Lett.* **1990**, *19*, 945.
23. Szejtli, J. *Starch/Staerke* **2003**, *55*, 191.
24. Lo Nostro, P.; Fratoni, L.; Baglioni, P. In *Journal of Inclusion Phenomena and Macrocyclic Chemistry*; **2002**; Vol. 44, pp 423.
25. Buschmann, H. J.; Knittel, D.; Schollmeyer, E. *J. Incl. Phenom. Macrocycl. Chem.* **2001**, *40*, 169.
26. Singh, M.; Sharma, R.; Banerjee, U. C. *Biotechnol. Adv.* **2002**, *20*, 341.
27. Gatos, K. G. *Cyclodextrins-based nanocomplexes for encapsulation of bioactive compounds in food, com smetics and pharmaceutical products: principles of supramolecular complexes formation, their influence on the antioxidative properties of target chemicals, and recent* ; Elsevier Inc., **2016**.
28. Fernandes, P. In *Reference Module in Food Science*; Elsevier, **2018**; pp 1.

29. Sobel, R.; Gundlach, M.; Su, C. In *Microencapsulation in the Food Industry*; Elsevier Inc., **2014**; pp 421.
30. Crini, G. *Chem. Rev.* **2014**, *114*, 10940.
31. Del Valle, E. M. M. *Process Biochem.* **2004**, *39*, 1033.
32. Hedges, A. *Cyclodextrins: Properties and Applications*; Elsevier Inc., **2009**.
33. Harada, A.; Takashima, Y.; Nakahata, M. *Acc. Chem. Res.* **2014**, *47*, 2128.
34. Qian, A.; Liu, K.; Chen, P.; Yao, Y.; Yan, J.; Li, W.; Zhang, X.; Zhang, A. *Macromolecules* **2019**, *52*, 3454.
35. Wang, D.; Zhao, W.; Wei, Q.; Zhao, C. *ChemPhotoChem* **2018**, *2*, 403.
36. Schönbeck, C. *J. Phys. Chem. B* **2018**, *122*, 4821.
37. Tran, D. N.; Colesnic, D.; Adam De Beaumais, S.; Pembouong, G.; Portier, F.; Queijo, Á. A.; Vázquez Tato, J.; Zhang, Y.; Ménand, M.; Bouteiller, L.; Sollogoub, M. *Org. Chem. Front.* **2014**, *1*, 703.
38. Casas-Solvas, J. M.; Ortiz-Salmerón, E.; Fernández, I.; García-Fuentes, L.; Santoyo-González, F.; Vargas-Berenguel, A. *Chem. - A Eur. J.* **2009**, *15*, 8146.
39. Zhao, L.; Hao, S.; Zhai, Q.; Guo, H.; Xu, B.; Fan, H. *Soft Matter* **2017**, *13*, 3099.
40. Zhou, W.; Chen, Y.; Yu, Q.; Li, P.; Chen, X.; Liu, Y. *Chem. Sci.* **1999**, *144*, 263.
41. Zhou, W.; Chen, Y.; Yu, Q.; Li, P.; Chen, X.; Liu, Y. *Chem. Sci.* **2019**, *10*, 3346.
42. Behrend, R.; Meyer, E.; Rusche, F. *Justus Liebigs Ann. Chem.* **1905**, *339*, 1.
43. Masson, E.; Ling, X.; Joseph, R.; Kyeremeh-Mensah, L.; Lu, X. *RSC Adv.* **2012**, *2*, 1213.
44. Barrow, S. J.; Kasera, S.; Rowland, M. J.; Del Barrio, J.; Scherman, O. A. *Chem. Rev.* **2015**, *115*, 12320.
45. Burton, D. J.; Naae, D. G.; Flynn, R. M. *J. Org. Chem.* **1983**, *48*, 3618.
46. Zhao, N.; Liu, L.; Biedermann, F.; Scherman, O. A. *Chem. - An Asian J.* **2010**, *5*, 530.
47. Zhao, N.; Lloyd, G. O.; Scherman, O. A. *Chem. Commun.* **2012**, *48*, 3070.
48. Jiao, D.; Biedermann, F.; Scherman, O. A. *Org. Lett.* **2011**, *13*, 3044.
49. Samanta, K.; Sicking, W.; Schmuck, C. *Eur. J. Org. Chem.* **2018**, *2018*, 6515.
50. Kasera, S.; Walsh, Z.; Del Barrio, J.; Scherman, O. A. In *Supramolecular Chemistry*; **2014**; Vol. 26, pp 280.
51. Yang, H.; Chen, H.; Tan, Y. *RSC Adv.* **2013**, *3*, 3031.
52. Biedermann, F.; Scherman, O. A. *J. Phys. Chem. B* **2012**, *116*, 2842.
53. Appel, E. A.; Biedermann, F.; Hoogland, D.; Del Barrio, J.; Driscoll, M. D.; Hay, S.; Wales, D. J.; Scherman, O. A. *J. Am. Chem. Soc.* **2017**, *139*, 12985.
54. Appel, E. A.; Forster, R. A.; Koutsioubas, A.; Toprakcioglu, C.; Scherman, O. A. *Angew. Chem. Int. Ed.* **2014**, *53*, 10038.
55. Appel, E. A.; Forster, R. A.; Rowland, M. J.; Scherman, O. A. *Biomaterials* **2014**, *35*, 9897.
56. Biedermann, F.; Rauwald, U.; Zayed, J. M.; Scherman, O. A. *Chem. Sci.* **2011**, *2*, 279.
57. Uhlenheuer, D. A.; Young, J. F.; Nguyen, H. D.; Scheepstra, M.; Brunsveld, L. *Chem. Commun.* **2011**, *47*, 6798.
58. Hou, C.; Huang, Z.; Fang, Y.; Liu, J. *Org. Biomol. Chem.* **2017**, *15*, 4272.
59. Zou, H.; Liu, J.; Li, Y.; Li, X.; Wang, X. *Small* **2018**, *14*, 1.
60. Appel, E. A.; Dyson, J.; Delbarrio, J.; Walsh, Z.; Scherman, O. A. *Angew. Chem. Int. Ed.* **2012**, *51*, 4185.

61. Chang, D.; Han, D.; Yan, W.; Yuan, Z.; Wang, Q.; Zou, L. *RSC Adv.* **2018**, *8*, 13722.

62. Appel, E. A.; Biedermann, F.; Rauwald, U.; Jones, S. T.; Zayed, J. M.; Scherman, O. A. *J. Am. Chem. Soc.* **2010**, *132*, 14251.

63. Ogoshi, T.; Kanai, S.; Fujinami, S.; Yamagishi, T.; Nakamoto, Y. *J. Am. Chem. Soc.* **2008**, *130*, 5022.

64. Ogoshi, T.; Yamagishi, T. A.; Nakamoto, Y. *Chem. Rev.* **2016**, *116*, 7937.

65. Yang, K.; Pei, Y.; Wen, J.; Pei, Z. *Chem. Commun.* **2016**, *52*, 9316.

66. Song, N.; Kakuta, T.; Yamagishi, T.; Yang, Y.; Ogoshi, T. *Chem* **2018**, *4*, 2029.

67. Ogoshi, T.; Kakuta, T.; Yamagishi, T. In *Encyclopedia of Polymer Science and Technology*; **2016**; pp 1.

68. Han, C.; Ma, F.; Zhang, Z.; Xia, B.; Yu, Y.; Huang, F. *Org. Lett.* **2010**, *12*, 4360.

69. Guo, F.; Sun, Y.; Xi, B.; Diao, G. *Supramol. Chem.* **2018**, *30*, 81.

70. Song, N.; Kakuta, T.; Yamagishi, T. aki; Yang, Y. W.; Ogoshi, T. *Chem* **2018**, *4*, 2029.

71. Barboiu, M. *Angew. Chem. Int. Ed.* **2012**, *51*, 11674.

72. Guo, S.; Song, Y.; He, Y.; Hu, X. Y.; Wang, L. *Angew. Chem. Int. Ed.* **2018**, *57*, 3163.

73. Zhou, J.; Hua, B.; Shao, L.; Feng, H.; Yu, G. *Chem. Commun.* **2016**, *52*, 5749.

74. Tan, L. L.; Li, H.; Tao, Y.; Zhang, S. X. A.; Wang, B.; Yang, Y. W. *Adv. Mater.* **2014**, *26*, 7027.

75. Tian, M. M.; Chen, D. X.; Sun, Y. L.; Yang, Y. W.; Jia, Q. *RSC Adv.* **2013**, *3*, 22111.

76. Yu, G.; Tang, G.; Huang, F. *J. Mater. Chem. C* **2014**, *2*, 6609.

77. Wang, S.; Xu, Z.; Wang, T.; Xiao, T.; Hu, X.; Shen, Y.; Wang, L. *Nat. Commun.* 1.

78. Odell, B.; Reddington, M. V.; Slawin, A. M. Z.; Spencer, N.; Stoddart, J. F.; Williams, D. J. *Angew. Chem. Int. Ed.* **1988**, *27*, 1547.

79. Gong, H. Y.; Rambo, B. M.; Karnas, E.; Lynch, V. M.; Sessler, J. L. *Nat. Chem.* **2010**, *2*, 406.

80. Asakawa, M.; Ashton, P. R.; Menzer, S.; Raymo, F. M.; Stoddart, J. F.; White, A. J. P.; Williams, D. J. *Chem. - A Eur. J.* **1996**, *2*, 877.

81. Dale, E. J.; Vermeulen, N. A.; Thomas, A. A.; Barnes, J. C.; Juríček, M.; Blackburn, A. K.; Strutt, N. L.; Sarjeant, A. A.; Stern, C. L.; Denmark, S. E.; Stoddart, J. F. *J. Am. Chem. Soc.* **2014**, *136*, 10669.

82. Barnes, J. C.; Juríček, M.; Strutt, N. L.; Frasconi, M.; Sampath, S.; Giesener, M. A.; McGrier, P. L.; Bruns, C. J.; Stern, C. L.; Sarjeant, A. A.; Stoddart, J. F. *J. Am. Chem. Soc.* **2013**, *135*, 183.

83. Sun, J.; Frasconi, M.; Liu, Z.; Barnes, J. C.; Wang, Y.; Chen, D.; Stern, C. L.; Fraser Stoddart, J. *Chem. Commun.* **2015**, *51*, 1432.

84. Ashton, P. R.; Menzer, S.; Raymo, F. M.; Shimizu, G. K. H.; Stoddart, J. F.; Williamsb, D. J. *Chem. Commun.* **1996**, 487.

85. Juríček, M.; Barnes, J. C.; Strutt, N. L.; Vermeulen, N. A.; Ghooray, K. C.; Dale, E. J.; McGonigal, P. R.; Blackburn, A. K.; Avestro, A. J.; Stoddart, J. F. *Chem. Sci.* **2014**, *5*, 2724.

86. Cheng, J.; Deming, T. J. *Artificial Molecular Motors and Machines: Design Principles and Prototype Systems*; **2005**; Vol. 262.

87. Goodnow, T. T.; Reddington, M. V.; Stoddart, J. F.; Kaifer, A. E. *J. Am. Chem. Soc.* **1991**, *113*, 4335.

88. Nakagawa, M.; Rikukawa, M.; Sanui, K.; Ogata, N. *Synth. Met.* **1997**, *86*, 1873.

89. Frasconi, M.; Fernando, I. R.; Wu, Y.; Liu, Z.; Liu, W. G.; Dyar, S. M.; Barin, G.; Wasielewski, M. R.; Goddard, W. A.; Stoddart, J. F. *J. Am. Chem. Soc.* **2015**, *137*, 11057.

90. Grunder, S.; McGrier, P. L.; Whalley, A. C.; Boyle, M. M.; Stern, C.; Stoddart, J. F. *J. Am. Chem. Soc.* **2013**, *135*, 17691.

91. Sun, J.; Wu, Y.; Wang, Y.; Liu, Z.; Cheng, C.; Hartlieb, K. J.; Wasielewski, M. R.; Stoddart, J. F. *J. Am. Chem. Soc.* **2015**, *137*, 13484.

92. Miljanić, O. Š.; Dichtel, W. R.; Mortezaei, S.; Stoddart, J. F. *Org. Lett.* **2006**, *8*, 4835.

93. Spruell, J. M.; Coskun, A.; Friedman, D. C.; Forgan, R. S.; Sarjeant, A. A.; Trabolsi, A.; Fahrenbach, A. C.; Barin, G.; Paxton, W. F.; Dey, S. K.; Olson, M. A.; Benítez, D.; Tkatchouk, E.; Colvin, M. T.; Carmielli, R.; Caldwell, S. T.; Rosair, G. M.; Hewage, S. G.; Duclairoir, F.; Seymour, J. L.; Slawin, A. M. Z.; Goddard, W. A.; Wasielewski, M. R.; Cooke, G.; Stoddart, J. F. *Nat. Chem.* **2010**, *2*, 870.

94. Houk, K. N.; Menzer, S.; Newton, S. P.; Raymo, F. M.; Stoddart, J. F.; Williams, D. J. *J. Am. Chem. Soc.* **1999**, *121*, 1479.

95. Liu, Y.; Flood, A. H.; Bonvallet, P. A.; Vignon, S. A.; Northrop, B. H.; Tseng, H. R.; Jeppesen, J. O.; Huang, T. J.; Brough, B.; Baller, M.; Magonov, S.; Solares, S. D.; Goddard, W. A.; Ho, C. M.; Fraser Stoddart, J. *J. Am. Chem. Soc.* **2005**, *127*, 9745.

96. Amabilino, D. B.; Ashton, P. R.; Brown, C. L.; Newton, S. P.; Pietraszkiewicz, M.; Philp, D.; Raymo, F. M.; Reder, A. S.; Rutland, M. T.; Spencer, N.; Stoddart, J. F.; Córdova, E.; Godínez, L. A.; Goodnow, T. T.; Kaifer, A. E.; Slawin, A. M. Z.; Williams, D. J. *J. Am. Chem. Soc.* **1995**, *117*, 1271.

97. Bruns, C. J.; Frasconi, M.; Iehl, J.; Hartlieb, K. J.; Schneebeli, S. T.; Cheng, C.; Stupp, S. I.; Stoddart, J. F. *J. Am. Chem. Soc.* **2014**, *136*, 4714.

98. Lipke, M. C.; Wu, Y.; Roy, I.; Wang, Y.; Wasielewski, M. R.; Stoddart, J. F. *ACS Cent. Sci.* **2018**, *4*, 362.

99. McNaught, A. D.; Wilkinson, A.; Nic, M.; Jirat, J.; Kosata, B. In *IUPAC Compendium of Chemical Terminology*; **2014**.

100. Schneiderman, D. K.; Hillmyer, M. A. *Macromolecules* **2017**, *50*, 3733.

101. Lecommandoux, S.; Klok, H. A.; Zhong, Z.; Deming, T. J. *Biomacromolecules* **2019**, *20*, 1.

102. Braunecker, W. A.; Matyjaszewski, K. *Prog. Polym. Sci.* **2007**, *32*, 93.

103. Masuelli, M. A. *J. Polym. Biopolym. Phys. Chem.* **2014**, *2*, 37.

104. Moad, G.; Rizzardo, E.; Thang, S. H. *Aust. J. Chem.* **2005**, *58*, 379.

105. Matyjaszewski, K. Preparation of Functional Materials. https://www.cmu.edu/maty/materials/ (last accessed Oct. 1, 2019).

106. Odian, G. In *Principles of Polymerization*; Wiley-interscience, **2004**; pp 40.

107. Chain-growth versus step-growth polymerization. https://polymerdatabase.com/polymer chemistry/Chain versus Step Growth.html (last accessed Oct. 1, 2019).

108. Aplan, M. P.; Gomez, E. D. *Ind. Eng. Chem. Res.* **2017**, *56*, 7888.

109. Stille, J. K. *J. Chem. Educ.* **1981**, *58*, 862.

110. Semsarilar, M.; Perrier, S. *Nat. Chem.* **2010**, *2*, 811.

111. Webster, O. W. *Science (80-.).* **1991**, *251*, 887.

112. Nesvadba, P. In *Encyclopedia of Radicals in Chemistry, Biology and Materials*; John Wiley & Sons, Ltd: Chichester, UK, **2012**.

113. Szwarc, M. *Nature* **1956**, *178*, 1168.

114. Matyjaszewski, K. **2015**, *1187*, 769.

115. Matyjaszewski, K.; Xia, J. *Chem. Rev.* **2001**, *101*, 2921.

116. Nicolas, J.; Guillaneuf, Y.; Lefay, C.; Bertin, D.; Gigmes, D.; Charleux, B. *Prog. Polym. Sci.* **2013**, *38*, 63.

117. Guo, X.; Choi, B.; Feng, A.; Thang, S. H. *Macromol. Rapid Commun.* **2018**, *39*, 1.

118. Matyjaszewski, K. Features of Controlled/"living" Radical polymerizations. https://www.cmu.edu/maty/crp/features.html (last accessed Oct. 1, 2019).

119. Purkait, M. K.; Sinha, M. K.; Mondal, P.; Singh, R. In *Stimuli Responsive Polymeric Membranes*; Elsevier B.V., **2018**; pp 39.

120. Moad, G.; Rizzardo, E.; Thang, S. H. In *Fundamentals of Controlled/Living Radical Polymerization*; Tsarevsky, N. V.; Sumerlin, B. S., Eds.; the Royal Society of Chemistry, **2013**; pp 205.

121. Moad, G. *Polym. Chem.* **2017**, *8*, 177.

122. Hu, L.; Zhang, Q.; Li, X.; Serpe, M. J. *Mater. Horizons* **2019**.

123. Rosa, V. R. De; Woisel, P.; Hoogenboom, R. *Mater. Today* **2016**, *19*, 44.

124. Lopez, D.; Tocquard, K.; Venisse, J.-S.; Legue, V.; Roeckel-Drevet, P. *Front. Plant Sci.* **2014**, *5*, 1.

125. Wei, M.; Gao, Y.; Li, X.; Serpe, M. J. *Polym. Chem.* **2017**, *8*, 127.

126. Bawa, P.; Pillay, V.; Choonara, Y. E.; Du Toit, L. C. *Biomed. Mater.* **2009**, *4*.

127. Flores, J. D.; Abel, B. A.; Smith, D.; McCormick, C. L. In *Monitoring Polymerization Reactions: From Fundamentals to Applications*; Reed, W. F.; Alb, A. M., Eds.; **2013**; Vol. 1, pp 45.

128. Smith, A. E.; Xu, X.; McCormick, C. L. Stimuli-responsive amphiphilic (co)polymers via RAFT polymerization. *Prog. Polym. Sci.* **2010**, *35*, 45–93.

129. Moad, G. *Polym. Chem.* **2017**, *8*, 177.

130. Kizhakkedathu, J. N.; Norris-Jones, R.; Brooks, D. E. *Macromolecules* **2004**, *37*, 734.

131. Clark, E. A.; Lipson, J. E. G. *Polymer.* **2012**, *53*, 536.

132. Halperin, A.; Kröger, M.; Winnik, F. M. *Angew. Chem. Int. Ed.* **2015**, *54*, 15342.

133. Yu, G.; Zhou, J.; Chi, X. *Macromol. Rapid Commun.* **2014**, *36*, 23.

134. Sambe, L.; Delarosa, V. R.; Belal, K.; Stoffelbach, F.; Lyskawa, J.; Delattre, F.; Bria, M.; Cooke, G.; Hoogenboom, R.; Woisel, P. *Angew. Chem. Int. Ed.* **2014**, *53*, 5044.

135. Wei, P.; Götz, S.; Schubert, S.; Brendel, J. C.; Schubert, U. S. *Polym. Chem.* **2018**, *9*, 2634.

136. Yeniad, B.; Ryskulova, K.; Fournier, D.; Lyskawa, J.; Cooke, G.; Woisel, P.; Hoogenboom, R. *Polym. Chem.* **2016**, *7*, 3681.

137. Burkhart, A.; Ritter, H. *Beilstein J. Org. Chem.* **2014**, *10*, 1951.

138. Kim, J. H.; Koo, E.; Ju, S. Y.; Jang, W. D. *Macromolecules* **2015**, *48*, 4951.

139. Wang, L.; Li, X.; Zhang, Q.; Luo, Z.; Deng, Y.; Yang, W.; Dong, S.; Wang, Q. A.; Han, C. *New J. Chem.* **2018**, *42*, 8330.

140. Nandi, M.; Maiti, B.; Srikanth, K.; De, P. *Langmuir* **2017**, *33*, 10588.

141. Jia, Y. G.; Zhu, X. X. *Langmuir* **2014**, *30*, 11770.

142. Hao, J.; Gao, Y.; Li, Y.; Yan, Q.; Hu, J.; Ju, Y. *Chem. - An Asian J.* **2017**, *12*, 2231.

143. De La Rosa, V. R.; Nau, W. M.; Hoogenboom, R. *Org. Biomol. Chem.* **2015**, *13*, 3048.

144. Chi, X.; Ji, X.; Xia, D.; Huang, F. *J. Am. Chem. Soc.* **2015**, *137*, 1440.

145. Schmidt, B. V. K. J.; Barner-Kowollik, C. *Angew. Chem. Int. Ed.* **2017**, *56*, 8350.

146. Feng, A.; Yan, Q.; Zhang, H.; Peng, L.; Yuan, J. *Chem. Commun.* **2014**, *50*, 4740.

147. Yan, Q.; Xin, Y.; Zhou, R.; Yin, Y.; Yuan, J. *Chem. Commun.* **2011**, *47*, 9594.

148. Zhang, H.; Tian, W.; Suo, R.; Yue, Y.; Fan, X.; Yang, Z.; Li, H.; Zhang, W.; Bai, Y. *J. Mater. Chem. B* **2015**, *3*, 8528.

149. Liu, B. W.; Zhou, H.; Zhou, S. T.; Zhang, H. J.; Feng, A. C.; Jian, C. M.; Hu, J.; Gao, W. P.; Yuan, J. Y. *Macromolecules* **2014**, *47*, 2938.

150. Hu, X. Y.; Jia, K.; Cao, Y.; Li, Y.; Qin, S.; Zhou, F.; Lin, C.; Zhang, D.; Wang, L. *Chem. - A Eur. J.* **2015**, *21*, 1208.

151. Yu, G.; Yu, W.; Shao, L.; Zhang, Z.; Chi, X.; Mao, Z.; Gao, C.; Huang, F. *Adv. Funct. Mater.* **2016**, *26*, 8999.

152. Duan, Q.; Cao, Y.; Li, Y.; Hu, X.; Xiao, T.; Lin, C.; Pan, Y.; Wang, L. *J. Am. Chem. Soc.* **2013**, *135*, 10542.

153. Zhang, H.; Liu, Z.; Zhao, Y. *Chem. Soc. Rev.* **2018**, *47*, 5491.

154. Feng, W.; Jin, M.; Yang, K.; Pei, Y.; Pei, Z. *Chem. Commun.* **2018**, *54*, 13626.

155. Wang, S.; Yao, C.; Ni, M.; Xu, Z.; Cheng, M.; Hu, X. Y.; Shen, Y. Z.; Lin, C.; Wang, L.; Jia, D. *Polym. Chem.* **2017**, *8*, 682.

156. Wang, Y.; Li, D.; Wang, H.; Chen, Y.; Han, H.; Jin, Q.; Ji, J. *Chem. Commun.* **2014**, *50*, 9390.

157. Jiao, D.; Geng, J.; Loh, X. J.; Das, D.; Lee, T. C.; Scherman, O. A. *Angew. Chem. Int. Ed.* **2012**, *51*, 9633.

158. Loh, X. J.; Del Barrio, J.; Toh, P. P. C.; Lee, T. C.; Jiao, D.; Rauwald, U.; Appel, E. A.; Scherman, O. A. *Biomacromolecules* **2012**, *13*, 84.

159. Mahinroosta, M.; Jomeh Farsangi, Z.; Allahverdi, A.; Shakoori, Z. *Mater. Today Chem.* **2018**, *8*, 42.

160. Ahmed, E. M. *J. Adv. Res.* **2015**, *6*, 105.

161. Shapiro, Y. E. *Prog. Polym. Sci.* **2011**, *36*, 1184.

162. Okay, O. *Hydrogel Sensors and Actuators* **2010**, *6*, 1.

163. Caló, E.; Khutoryanskiy, V. V. *Eur. Polym. J.* **2015**, *65*, 252.

164. Mantooth, S. M.; Munoz-Robles, B. G.; Webber, M. J. *Macromol. Biosci.* **2019**, *19*, 1.

165. Jin, J.; Cai, L.; Jia, Y. G.; Liu, S.; Chen, Y.; Ren, L. *J. Mater. Chem. B* **2019**, *7*, 1637.

166. Hoque, J.; Sangaj, N.; Varghese, S. *Macromol. Biosci.* **2019**, *19*, 1.

167. Li, F.; He, J.; Zhang, M.; Tam, K. C.; Ni, P. *RSC Adv.* **2015**, *5*, 54658.

168. Chen, L.; Zhao, X.; Lin, Y.; Su, Z.; Wang, Q. *Polym. Chem.* **2014**, *5*, 6754.

169. Xiao, T.; Xu, L.; Zhou, L.; Sun, X. Q.; Lin, C.; Wang, L. *J. Mater. Chem. B* **2019**, *7*, 1526.

170. Ni, M.; Zhang, N.; Xia, W.; Wu, X.; Yao, C.; Liu, X.; Hu, X. Y.; Lin, C.; Wang, L. *J. Am. Chem. Soc.* **2016**, *138*, 6643.

171. Nomimura, S.; Osaki, M.; Park, J.; Ikura, R.; Takashima, Y.; Yamaguchi, H.; Harada, A. *Macromolecules* **2019**, *52*, 2659.

172. Liu, J.; Tan, C. S. Y.; Yu, Z.; Li, N.; Abell, C.; Scherman, O. A. *Adv. Mater.* **2017**, *29*, 1.

173. Zheng, Y.; Hashidzume, A.; Takashima, Y.; Yamaguchi, H.; Harada, A. *Nat. Commun.* **2012**, *3*, 831.

174. Takashima, Y.; Sawa, Y.; Iwaso, K.; Nakahata, M.; Yamaguchi, H.; Harada, A. *Macromolecules* **2017**, *50*, 3254.

175. Miyamae, K.; Nakahata, M.; Takashima, Y.; Harada, A. *Angew. Chem. Int. Ed.* **2015**, *54*, 8984.

176. Nakahata, M.; Takashima, Y.; Yamaguchi, H.; Harada, A. *Nat. Commun.* **2011**, *2*, 511.

177. Takashima, Y.; Hatanaka, S.; Otsubo, M.; Nakahata, M.; Kakuta, T.; Hashidzume, A.; Yamaguchi, H.; Harada, A. *Nat. Commun.* **2012**, *3*, 1270.

178. Park, K. M.; Yang, J. A.; Jung, H.; Yeom, J.; Park, J. S.; Park, K. H.; Hoffman, A. S.; Hahn, S. K.; Kim, K. *ACS Nano* **2012**, *6*, 2960.

179. Li, C.; Rowland, M. J.; Shao, Y.; Cao, T.; Chen, C.; Jia, H.; Zhou, X.; Yang, Z.; Scherman, O. A.; Liu, D. *Adv. Mater.* **2015**, *27*, 3298.

180. Appel, E. A.; Biedermann, F.; Rauwald, U.; Jones, S. T.; Zayed, J. M.; Scherman, O. A. *J. Am. Chem. Soc.* **2010**, *132*, 14251.

181. Xu, W.; Song, Q.; Xu, J. F.; Serpe, M. J.; Zhang, X. *ACS Appl. Mater. Interfaces* **2017**, *9*, 11368.

182. Appel, E. A.; Loh, X. J.; Jones, S. T.; Biedermann, F.; Dreiss, C. A.; Scherman, O. A. *J. Am. Chem. Soc.* **2012**, *134*, 11767.

183. Wang, S.; Xu, Z.; Wang, T.; Liu, X.; Lin, Y.; Shen, Y.-Z.; Lin, C.; Wang, L. *J. Photochem. Photobiol. A Chem.* **2018**, *355*, 60.

184. Zhang, X.; Xu, J.; Lang, C.; Qiao, S.; An, G.; Fan, X.; Zhao, L.; Hou, C.; Liu, J. *Biomacromolecules* **2017**, *18*, 1885.

185. Chen, J. F.; Lin, Q.; Yao, H.; Zhang, Y. M.; Wei, T. B. *Mater. Chem. Front.* **2018**, *2*, 999.

186. Chen, J.-F.; Chen, P. *ACS Appl. Polym. Mater.* **2019**, *1*, 2224.

187. Yan, D.; Liu, S.; Jia, Y.; Mo, L.; Qi, D.; Wang, J.; Chen, Y.; Ren, L. *Macromol. Chem. Phys.* **2019**, *220*, 1.

188. Zheng, Y.; Hashidzume, A.; Takashima, Y.; Yamaguchi, H.; Harada, A. *ACS Macro Lett.* **2012**, *1*, 1083.

189. Wang, S.; Xu, Z.; Wang, T.; Xiao, T.; Hu, X. Y.; Shen, Y. Z.; Wang, L. *Nat. Commun.* **2018**, *9*, 1.

190. Belal, K.; Stoffelbach, F.; Lyskawa, J.; Fumagalli, M.; Hourdet, D.; Marcellan, A.; Smet, L. De; de la Rosa, V. R.; Cooke, G.; Hoogenboom, R.; Woisel, P. *Angew. Chem. Int. Ed.* **2016**, *55*, 13974.

Chapter 2. Complexation of cyclobis(paraquat-4,4'-biphenylene) (BBB) in water

Abstract

The macrocylic host molecule cyclobis(paraquat-4,4'-biphenylene), also referred to as 'big blue box' (BBB) was here for the first time characterized in aqueous media. BBB is able to form strong and colorful 2:1 complexes with different electron-rich guest molecules, including dihydroxynaphthalene (Napht) and tetrathiafulvalene (TTF). As BBB can be highly soluble in water depending on the counter ions, its host-guest complexation in aqueous solution opens up a variety of new applications, including materials with a high water content like hydrogels. To enhance the aqueous solubility of the hydrophobic, electron-rich guest molecules TTF and Napht, as required for complexation with BBB in water, reversible addition–fragmentation chain transfer (RAFT) polymerization was employed to synthesize short, water-soluble poly(*N,N*-dimethylacrylamide) chains, end-functionalized through the use of a chain transfer agent bearing either a Napht or TTF moiety. After characterizing these RAFT polymerizations and demonstrating the high level of control over chain length and chain end fidelity, well-defined, end-functionalized PDMAc polymers with low Đ and similar molecular weight were created to study the complexation of both Napht and TTF with BBB in aqueous solution using UV-VIS and NMR spectroscopic titrations, Isothermal calorimetry titration (ITC) and diffusion ordered NMR spectroscopy (DOSY). In a final step the potential thermo-responsiveness of the Napht-PDMAc complex with BBB was highlighted. The obtained association constants of the 1:2 BBB complexes in water combined with their stimuli-responsivity towards pH, competitive guest molecules, temperature and redox potential opens up the potential to use this macrocyclic host molecule for the creation of highly adaptable and sophisticated smart materials with an inherent visual output signal resulting from (de)complexation.

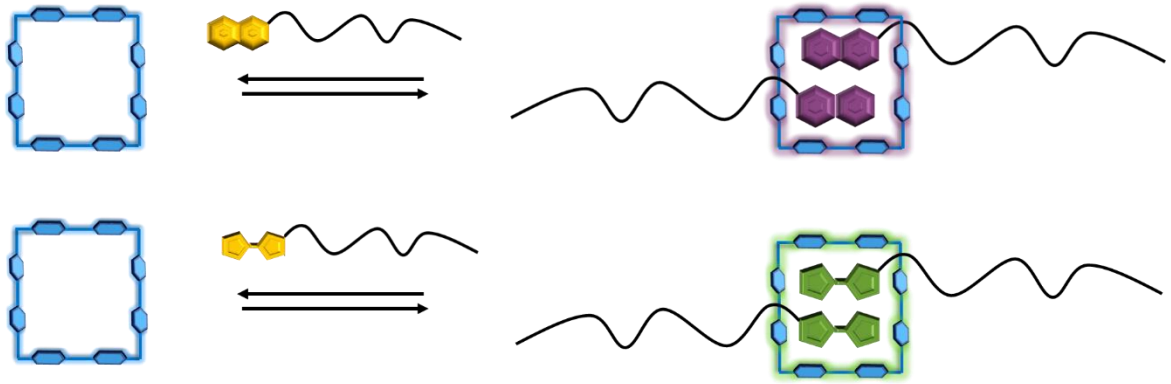

Parts of this chapter will be published as:

L. De Smet, A. Malfait, P. Standford, J. Potier, J. lyskawa, R. Hoogenboom and P. woisel. Complexation of cyclobis(paraquat-4,4'-biphenylene) in water and application in the preparation of smart polymeric materials. 2019 Manuscript in preparation.

1 Introduction

Supramolecular chemistry studies the assembly of molecular systems based on weak but reversible non-covalent interactions, such as metal coordination, hydrogen bonding, π-π stacking, hydrophobic association and van der Waals forces between two or more building blocks.[1–5] An important category of supramolecular chemistry is the formation of inclusion complexes consisting of a macrocyclic host molecule that interacts in a highly controlled and cooperative manner with one or more smaller entities called guest molecules, via both non-covalent interactions and specific three-dimensional spatial arrangements. The integration of these supramolecular assemblies into conventional polymer chemistry has emerged as a powerful tool for the fabrication of smart polymeric materials due to their dynamic, reversible and adaptive nature towards external stimuli.[6–10] Furthermore, this strategy of incorporating interchangeable host-guest complexes into a polymer matrix also enables the straightforward fabrication of smart materials with unique responses by allowing the introduction of multiple guest molecules. Currently, pillar[n]arenes, cyclodextrins, cucurbit[n]urils and crown ethers are the most commonly used macrocyclic host molecules to develop smart materials with the ability to respond to changes in temperature, pH, light, solvent, redox potential and the presence of competing molecules/ions.[11–18] The stimuli-responsive character of these supramolecular materials can be a combination of both the polymeric scaffold through the use of a stimuli-responsive polymer matrix and/or the host-guest binding motifs.[9,19–23]

An interesting example of a material incorporating stimuli-responsive behavior resulting from host-guest interactions has been reported by Kim *et al.* who utilized the high-affinity host-guest assembly to achieve strong and reversible underwater adhesion of two substrates.[24] In this approach, the silicon surfaces were functionalized either with the host molecule CB[7] or with the complementary guest molecule amminomethylferrocene to form a supramolecular velcro as shown in Figure 2.1. It was reported that both surfaces could easily be glued together in aqueous solutions without the addition of any curing agents. These material are also highly responsive to oxidative stress due to the redox-sensitive nature of the ferrocene guest molecule allowing for the reversal of the adhesion process and the reuse of the separated materials.

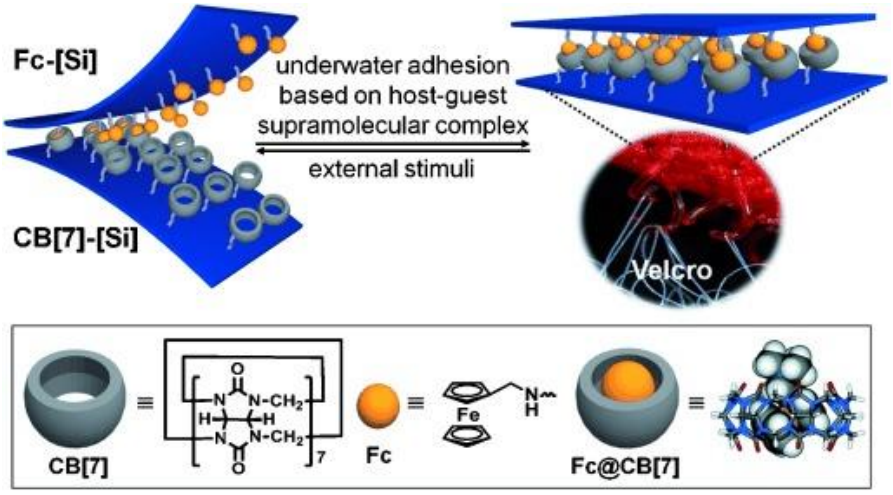

Figure 2.1. The supramolecular velcro approach for the efficient adhesion of two substrates in water based on amminomethylferrocene (Fc) and CB[7]-based silicon substrates. This adhesion process was controlled by the redox-responsive behavior of the Fc:CB[7] complex. Reprinted from ref.[24] Copyright 2019 John Wiley and Sons.

Another example from Wang *et al*. combines both a stimuli-responsive matrix and host-guest complexation to create a multi-sensitive supramolecular hydrogel. This triple responsive hydrogel was synthesized using a poly(*N*-isopropylacrylamide) (PNIPAM) functionalized with azobenzene-groups which could be crosslinked using cyclodextrin (CD) dimers connected via disulfide bonds. The sol-gel transition could thereby be induced via either the thermo-responsive behavior of the PNIPAM polymer chain, by the redox labile bond of the disulfide bridge in the CD dimer and by the light-sensitive switching of the azobenzene guest from trans to cis disrupting the host-guest assembly (Figure 2.2).[25]

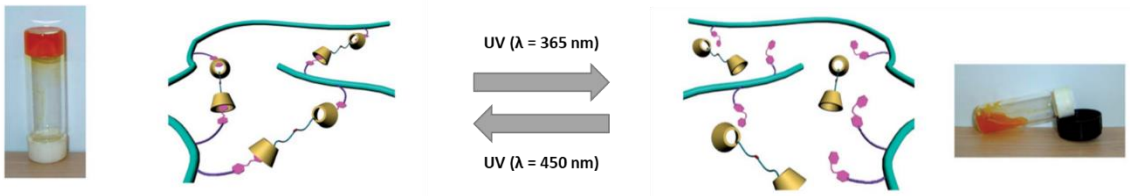

Figure 2.2. The reversible sol-gel transition of the PNIPAm polymer chains functionalized with azobenzene groups and CD controlled by UV (365 nm) and visible light (450 nm) irradiation. Adapted from reference.[25] Copyright 2019 John Wiley and Sons

During my research, the less exploited cyclobis(paraquat-4,4'-biphenylene), also called big blue box (BBB), was investigated for its potential use as macrocyclic host molecule for the creation of similar stimuli-responsive materials in water. This cyclophane macromolecule consists of two electron-deficient viologen groups that are ideally separated to strongly interact simultaneously with two planar electron-rich aromatic guest molecules.[26–28] The formed complexes are well known for their redox-sensitivity and strong color depending on the used guest molecules.[29,30] These features would allow for highly adaptable and sophisticated smart materials with an inherent visual output signal. To date, the complexation of BBB with electron rich guest molecules including tetrathiafulvalene (TTF) and dihydroxynaphthalene (Napht) has been thoroughly studied in polar organic solutions for the synthesis

of mechanically interlocked molecules (MIM) such as rotaxanes and cantenanes and artificial molecular machines (AMM) and molecular devices, including switches, pumps and muscles.[28,30–32] The state-of-the-art regarding the host-guest complexation of BBB uses organic solvents to investigate the reversible assembly and to fabricate the responsive materials due to their low boiling point and the mainly hydrophobic guest molecules. However, the tetracationic character of the cyclophane makes it possible to gain control over the solubility of both the host and its inclusion complexes by careful selection of the counterions allowing the use of BBB in various solvent, including water. Currently, no studies have been reported that describe the complexation behavior of BBB in aqueous solution. This could however open up the potential use of these responsive ternary complexes for the synthesis of supramolecular polymers and higher polymeric structures in water which are not possible with the smaller conventional BB. For example, as BBB can form strong 1:2 inclusion complexes with planar electron-rich aromatic guest molecules, this highly water soluble host may be used for the creation of physical hydrogels possessing interesting features like self-healability and shape memory function but also for the synthesis of smart supramolecular nanostructures which can be used for sensor systems as colored complexes are formed. Furthermore, the reversible formation of the BBB-guest complexation can be controlled using many different stimuli including pH, redox potential, competitive guest, depending on the used guest molecule allowing them to be used for the creation of multi-responsive polymeric materials. Additionally, the ionic character of BBB can be used to mask the hydrophobic nature of most compatible guest molecules upon complexation, resulting in an increased solubility of these molecules in aqueous solution. Finally, this cyclophane box like structure can form multi-sensitive, colored complexes with different guest molecules including naphthalene (Napht), tetrathiafulvalene (TTF) and hydroquinone making them the perfect candidates for sensor applications as the unambiguous output signal is immediately visible to the naked eye.

In this chapter the complex properties of BBB in aqueous media are investigated to further broaden the scope of this host molecule and its potential use in the fabrication of stimuli-responsive polymeric structures in water. In a first step, the complex formation of the BBB host molecule with electron-rich guest molecules including Napht and TTF was investigated in aqueous solution. Therefore, the solubility of these hydrophobic guest molecules was increased by incorporating these moieties as α-chain-end on a short, water-soluble poly(*N,N*-dimethylacrylamide) (PDMAc) through RAFT polymerization. The formation and association constant of the formed, colored donor-acceptor complexes between BBB and these water soluble polymeric guest molecules were investigated using NMR spectroscopy, UV-VIS spectroscopy and isothermal titration calorimetry (ITC). Finally, the temperature responsive behavior of the Napht-BBB complex in aqueous solution was highlighted as potential visual output signal.

2 Results and discussion

2.1 Synthesis of the building blocks

This chapter will start with a detailed description of the synthesis of BBB and the Napht- and TTF end-functionalized PDMAc polymers.

2.1.1 Synthesis of BBB

The first part of this chapter focusses on the synthesis of the host molecule BBB, which was based on the method reported by Venturi, M. *et al*.[33] In this two-step procedure, a disalt precursor was first prepared via the SN_2-substitution reaction of two 4,4'-bipyridine" with 4,4'-bis(bromomethyl)biphenyl followed by the subsequent cyclization reaction of this precursor with another 4,4'-bis(bromomethyl)biphenyl molecule as shown in Figure 2.3. To increase the yield of the second ring closure reaction significantly, a ferrocene template modified with glycol units was prepared and added to the reaction mixture. The electron-rich cyclopentadienyl rings can form π-π donor-acceptor interactions with the electron-deficient bipyridinium units of the forming BBB. By using glycol ferrocene as a template during the synthesis, the disalt and the 4,4'-bis(bromomethyl)biphenyl can be pre-organized in a box-like structure favoring the cyclisation reaction over the oligomerization, which increased the yield from 2% up to 32%.[26,33,34] The pure product was then obtained as a greenish solid through silica column chromatography with DMF/MeOH/2M $NH_4^+Cl^-$ 5/3/2 as eluent. In a final step, the counterions of this macrocyclic host molecule were exchanged from PF_6^- to chlorine ions to enhance its solubility in aqueous media. The structure of this macrocyclic host molecule was confirmed via ^{1}H-NMR spectroscopy as displayed in Figure 2.4.

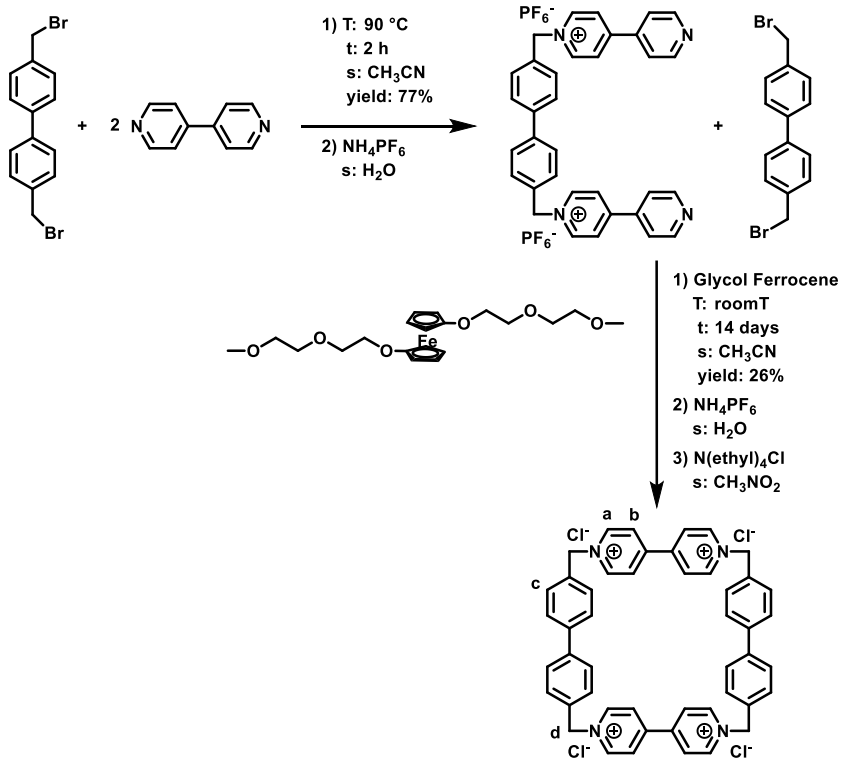

Figure 2.3. The schematic illustration of the synthesis route for BBB.

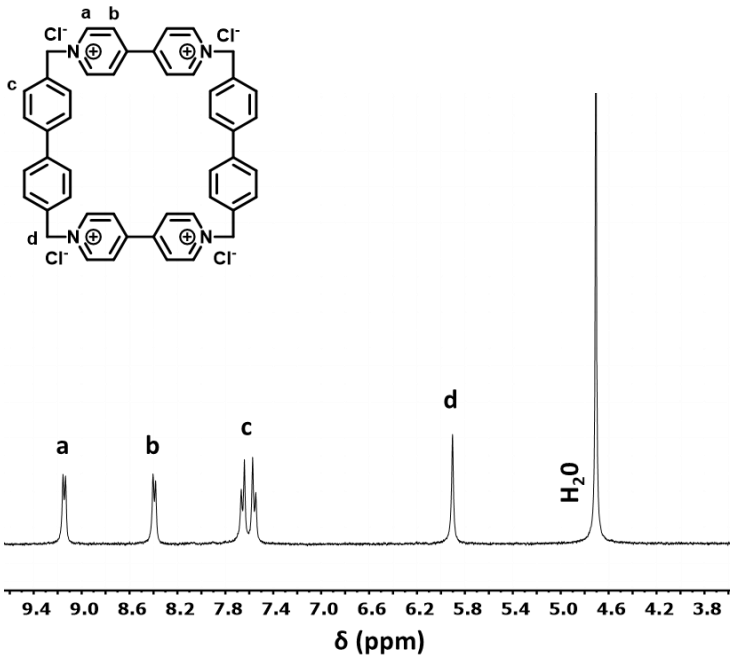

Figure 2.4. Partial ^{1}H NMR spectrum of BBB.4Cl^- recorded in D_20 at 300 MHz.

2.1.2 Synthesis of Napt-PDMAc

Owing to the poor water solubility of the guest molecules TTF and Napht, hydrophilic PDMAc polymers bearing an TTF or Napht moiety as end group were synthesized in order to properly investigate the complexation of these guest molecules with BBB in water. This was done via RAFT-polymerization as this CRP technique provides good end-group fidelity, high control over both the molecular weight (Mn) and molar mass dispersity (Đ) and it is rather straightforward to modify the CTA-agent prior to polymerization, which is required for the creation of well-defined end-functionalized TTF and Napht-PDMAc polymers. In this work, we aimed for low molecular weight (DP = 45) of Napht- and TTF end-functionalized polymers, in order to study the interaction of the electron rich guest molecules with the BBB in aqueous solutions without the interference of the hydrophilic polymer chain.

To create the low molecular weight Napht end-functionalized PDMAc polymers, a naphthalene bearing CTA-agent (Napht-CTA) was prepared starting from the commercially available 1.5-dihydroxynaphthalene which was firstly modified with two glycol linkers on both alcohol groups. These incorporated glycol linkers on the Napht unit will probably provide further stability to the interaction with the BBB host molecule via an additional hydrogen bond with the acidic alfa-protons of the host molecule, as reported for the smaller cyclophane blue box.[34] Subsequently, one alcohol group on the glycol chains was asymmetrically modified through methylation using methyl iodide to yield 2-[2-[[5-[2-(2-methoxyethoxy)ethoxy]-1-naphthalenyl]oxy]ethoxy] (Napht-OMe). Finally, the Napht-CTA-agent was formed using an carbodiimide-promoted esterification reaction of 2-(1-isobutyl)sulfanylthiocarbonylsulfanyl-2-methylpropionic acid (CTA-COOH) and the free alcohol group of Napht-OMe (Figure 2.5).

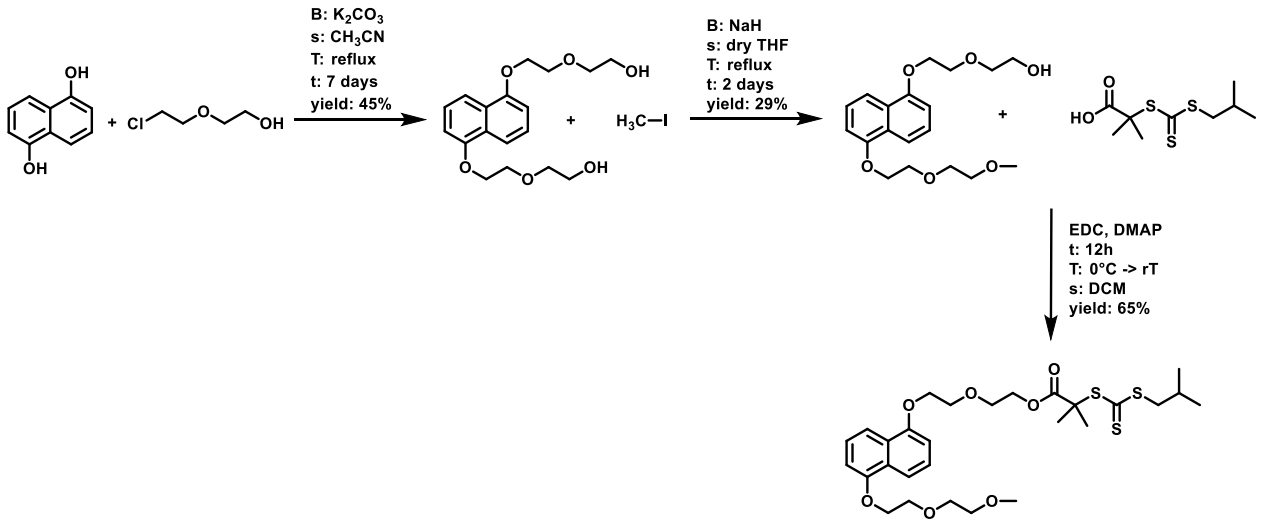

Figure 2.5. Reaction scheme for the synthesis of Napht-CTA.

The structure of the Napht-CTA was confirmed via ^{1}H-NMR spectroscopy revealing both the presence of the characteristic signals of the naphthalene unit (6.5 – 8.0 ppm) and the isobutyl group (< 3.2 ppm) as shown in Figure 2.6.[35,36]

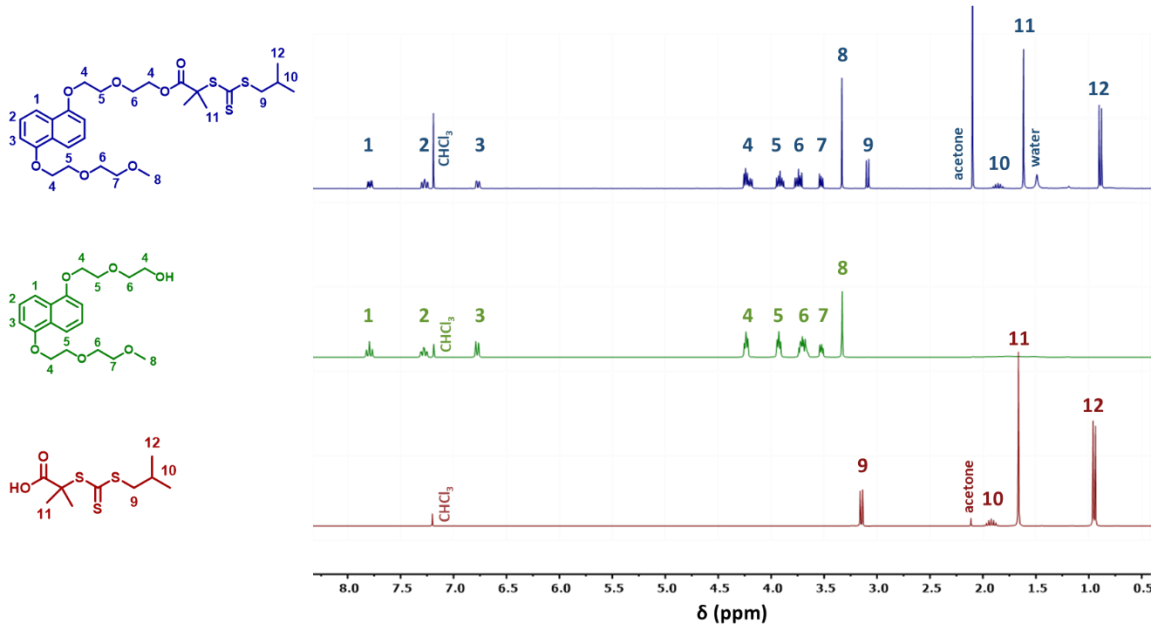

Figure 2.6. ^{1}H-NMR spectra of Napht-CTA (top), Napht-OMe (middle) and CTA-COOH (bottom) recorded in CD_3Cl at 300 MHz.

In the next step, the RAFT polymerization of *N,N*-dimethylacrylamide (DMAc) was carried out using the synthesized Napht-CTA as chain transfer agent and AIBN as radial initiator in DMF at 60°C for 80 min, with a molar ratio $[\text{Napht-CTA}]_0 : [\text{PDMAc}]_0 : [\text{AIBN}]_0$ of 1 : 70 : 0.3. The results of the kinetic study of the polymerization of DMAc with Napht-CTA are given in Figure 2.7 revealing not only a typical first order kinetic plot, but also the linear progression of the molecular weight (Mn) with monomer conversion and polydispersity values below 1.2, both characteristic for controlled RAFT polymerization. It should be noted that an inhibition period is visible, which commonly occurs in trithiocarbonate-mediated RAFT-polymerizations and is probably caused by a combination of different factors, including 1) the presence of some remaining oxygen in the reaction vessel, 2) the slow fragmentation of the initial RAFT agent under the polymerization conditions, 3) the slow fragmentation of the intermediate macroRAFT radical under the polymerization conditions and 4) the slower dissociation of the initiator at 60 °C.[37–40] In addition, it should be mentioned that these reported molecular weights are relative as they were determined using SEC against PMMA standards. Therefore, the calculated theoretical Mn are significantly different. The kinetic data was used to repeat the polymerization and synthesize a Napht-PDMAc with a DP as close to 45 as possible by terminating the polymerization after 61 min by cooling the mixture. The obtained polymer was isolated by precipitation in diethylether and characterized via SEC-LS determining the absolute molecular weight (Mn_{abs} = 5220 g/mol, dn/dc = 0.08) and the polydispersity (Đ = 1.1).

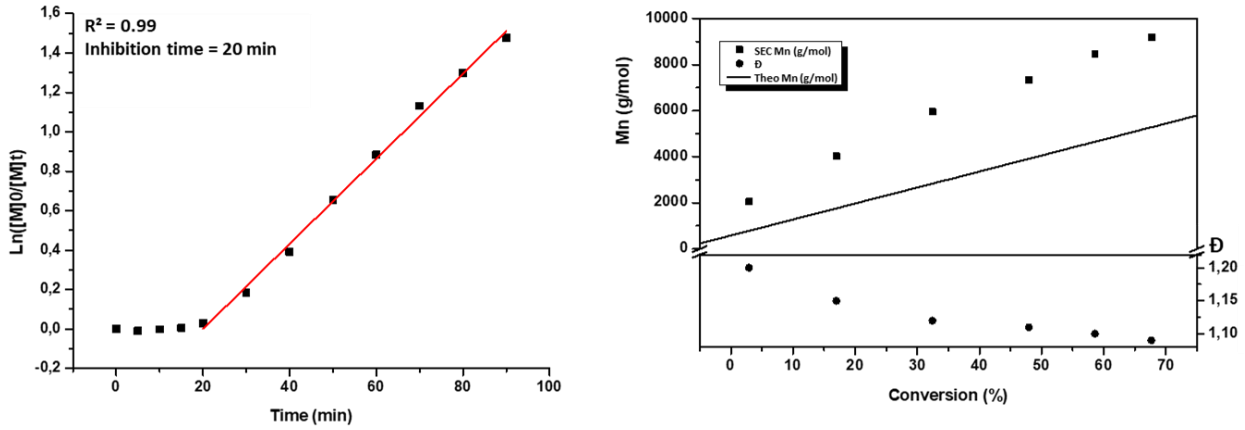

Figure 2.7. Kinetic study of the RAFT polymerization of DMAc with the Napht-CTA agent at 60°C in DMF. Left: First order kinetic plot. Right: Molecular weight evolution and Đ in function of conversion compared to theoretical Mn (full line).

The molecular weight of these short Napht-PDMAc polymers were determined via a second technique as the SEC-LS technique is not completely accurate for low molecular weight polymers as the hydrodynamic radius is too small for efficient light scattering. For this reason the molecular weight of the Napht-PDMAc polymers was also determined using UV-VIS spectroscopy as the Napht moiety has a characteristic absorbance band around 305 nm, as shown in Figure 2.8. Using the Lambert-Beer law, the extinction coefficient was calculated from the calibration curve using Napht-CTA solubilized in CH_3CN. Subsequently, the concentration of naphthalene moieties in a polymer stock solution can be determined with this extinction coefficient by measuring the absorbance at 305 nm. The Mn can afterwards be calculated by dividing the used mass of the Napht-PDMAc sample by the calculated moles of the Napht-CTA present in the solution. If we assume that every polymer chain contains one Napht unit, then the Mn of the Napht-PDMAc polymers is determined to be 4930 ± 153 g/mol using UV-VIS spectroscopy. This value is almost identical as the Mn determined via SEC-LS indicating that indeed every polymer chain presumably contains one Napht-unit proving the end group fidelity of the used RAFT polymerization. This is also represented graphically in Figure 2.8 displaying a similar intensity for the Napht CT-band of the Napht-CTA and Napht-PDMAc stock solution prepared with the same concentration of Napht end-groups.

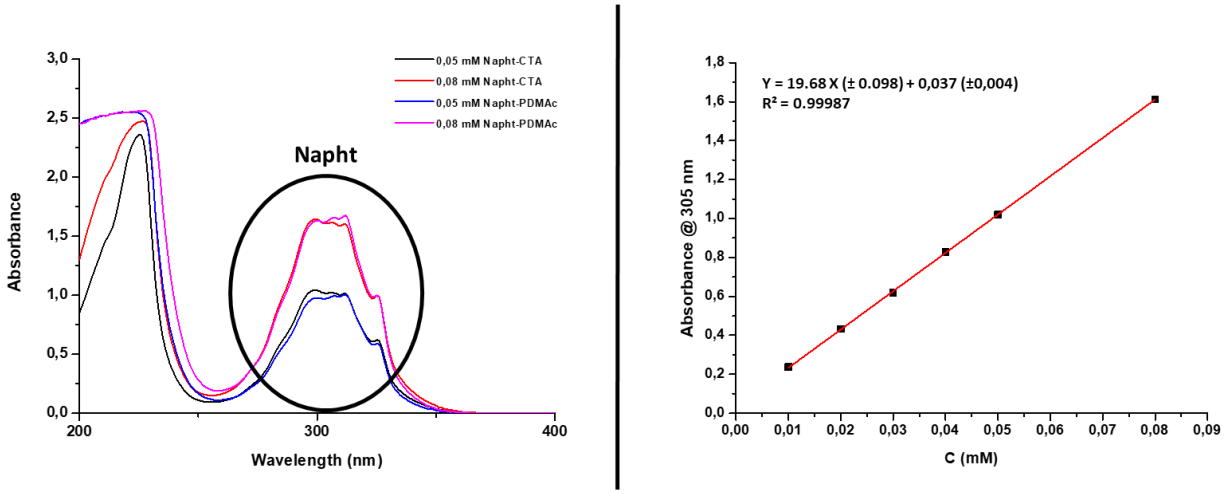

Figure 2.8. Left: Overlay of the absorbance spectra of Napht-PDMAc and Napht-CTA recorded in acetonitrile at 25°C at both 0.05 and 0.08 mM. Right: Calibration curve of Napht-CTA absorbance at 305 nm in CH_3CN.

2.1.3 Synthesis of TTF-PDMAc

A similar modification strategy was followed for the synthesis of well-defined TTF end-functionalized PDMAc polymers. First, a TTF decorated CTA-agent (TTF-CTA) was prepared by following a synthesis route reported by our group describing the Steglich esterification of 2-hydroxymethyltetrathiafulvalene and 2-(1-isobutyl)sulfanylthiocarbonylsulfanyl-2-methylpropionic acid.[41,42] The hydroxymethyltetrathiafulvalene was prepared starting from TTF which was first mono-functionalized with an aldehyde group via a nucleophilic acyl substitution reaction with *N*-methylformanilide followed by its reduction to an alcohol with sodium borohydride (Figure 2.9).

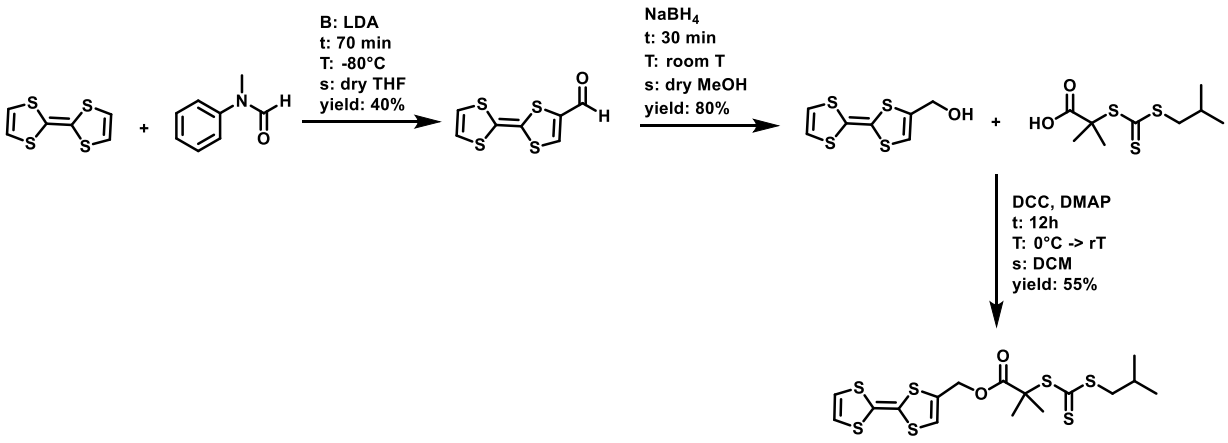

Figure 2.9. Reaction scheme for the synthesis of TTF-CTA

The structure of the TTF-CTA was confirmed via ^{1}H-NMR spectroscopy revealing the presence of characteristic signals of both the TTF unit (4.0 – 7.0 ppm) and the isobutyl group (< 3.2 ppm) as shown in Figure 2.10.

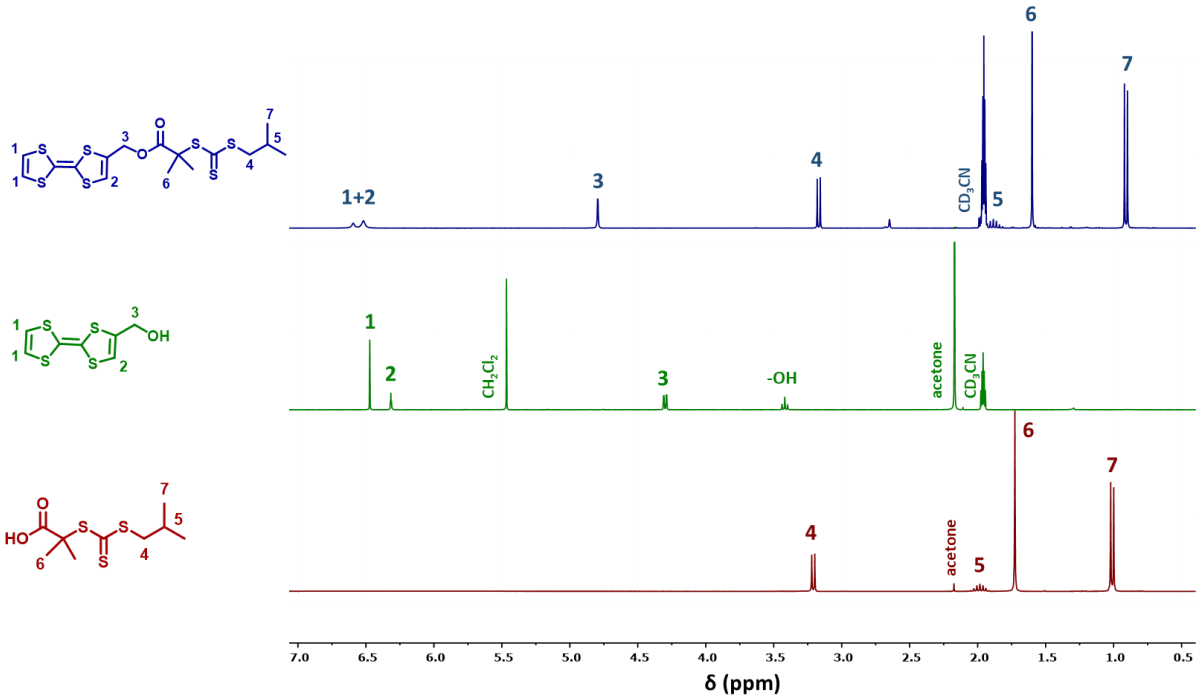

Figure 2.10. ^{1}H-NMR spectra of hydroxymethyltetrathiafulvalene (top), CTA-COOH (middle) and TTF-CTA (bottom) recorded in acetone or $CDCN_3$ at 300 MHz.

Afterwards the TTF-terminated PDMAc polymers were synthesized by performing a RAFT polymerization of DMAc in DMF at 70°C for 70 min using the TTF-CTA agent, initiated by AIBN with a molar ratio of $[TTF\text{-}CTA]_0$: $[PDMAc]_0$: $[AIBN]_0$ of 1 : 100 : 0.3. The results of the kinetic study of the polymerization controlled by the TTF-CTA is given in Figure 2.11. The kinetic plot shows a linear relationship which is characteristic for the first-order kinetics of CRP in general and RAFT specifically, proving minimal occurrence of any termination reactions. In comparison to the Napht-CTA, no inhibition period was observed as the reaction was performed at a higher temperature, indicating that enough radicals are formed during the first initiation step to immediately start the polymerization. In addition, a linear trend is also visible when the evolution of the Mn was plotted in function of the conversion, indicating a constant concentration of reactive polymer chains. Again, it should be mentioned that these molecular weights are relative and determined using SEC against PMMA standards. Therefore, the calculated theoretical Mn values are significantly different. In contrast to the results obtained for the Napht-PDMAc, it is noticed that the Mn values for the TTF-functionalized polymers are lower than the theorectical Mn values. This lower increase in molecular weight can be ascribed to the TTF moiety which will interfere with the radical CRP as it can be easily oxidized to its radical cation and dicationic states.[43,44] Similarly to the Napht-PDMAc, the obtained kinetics were used to synthesize a polymer with a DP of 45 by terminating the polymerization after 40% conversion by cooling down the polymerization. The polymer was purified by precipitation in diethylether and was

characterized via SEC-LS determining the absolute molecular weight (Mn_{abs} = 4840 g/mol, dn/dc = 0.09) and the polydispersity (Đ = 1.05).

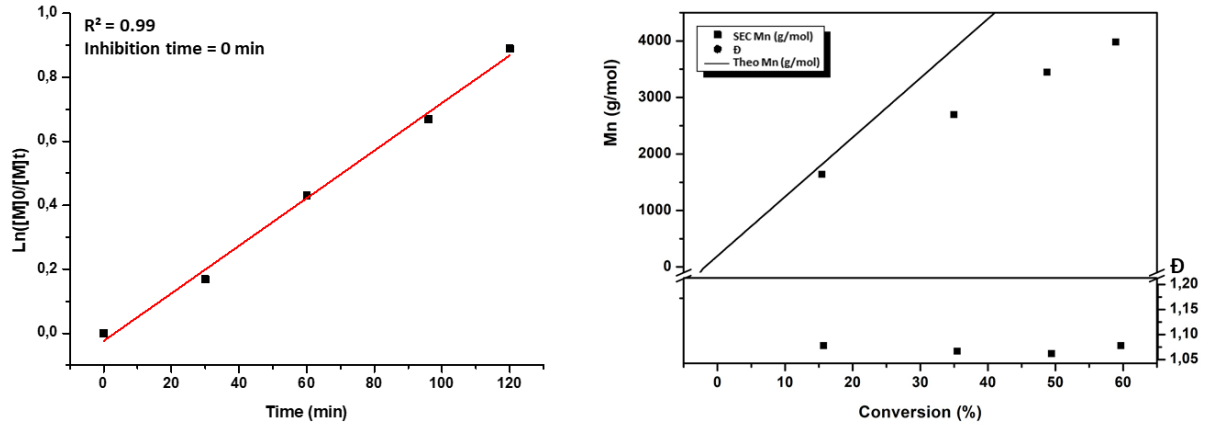

Figure 2.11. Kinetic study of the RAFT polymerization of DMAc with the TTF-CTA agent at 70°C in DMF. Left: First order kinetic plot. Right: Molecular weight evolution and Đ in function of conversion, compared to theoretical Mn (full line).

Similarly to Napht-PDMAc, the molecular weight of the TTF-PDMAc was determined via UV-VIS spectroscopy using the characteristic absorbance of TTF around 370 nm. The extinction coefficient of TTF-CTA was first determined and then used to estimate amount of TTF-units in the PDMAc polymer solution (Figure 2.12). Using different concentration of TTF-PDMAc solutions, the Mn of the polymer was determined to be 4780 ± 95 g/mol proving the high end group fidelity of the TTF-PDMAc polymers using RAFT polymerization.

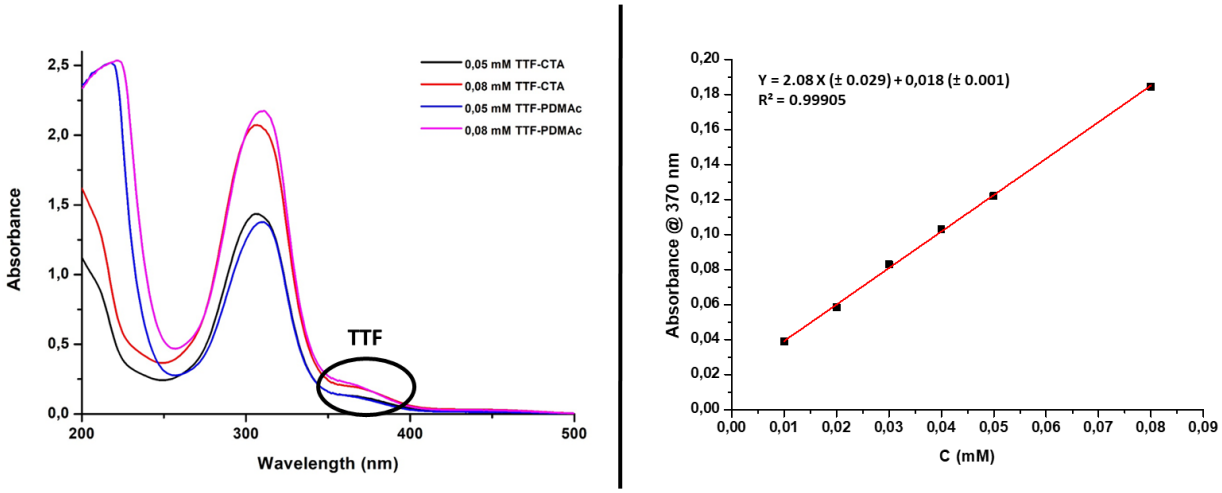

Figure 2.12. Left: Comparison of the absorbance spectra of TTF-CTA stock solution and TTF-PDMAc stock solution with a concentration of 0.05 mM and 0.08 mM in CH_3CN. Right: Calibration curve of TTF-CTA absorbance measured at 370 nm in CH_3CN.

2.2 The continuous variation method (Job plot)

As explained during the introduction, the size and shape of BBB allows to accommodate two planar electron-rich guest molecules inside the cavity. This 2:1 stoichiometry of BBB was investigated for both the Napht- and TTF-PDMAc polymers in water using the continuous variation approach or Job plots. These plots were prepared on the change of the NMR shift of the BBB peaks upon complexation with one of the guest molecules. The Job plot is a popular method to determine the stoichiometry of a host-guest complex by plotting the concentration of the host-guest complex, measured via a physical property change, against the molar fraction of a building block. This leads to a parabolic curve that reaches a maximum when $[H]_0 : [G]_0$ is equal to stoichiometry of the host-guest assembly, in this case expected to be 1 : 2. In this work, the total concentration of the host-guest solution was kept constant at 2 mM, while the molar fractions of the building blocks were altered between 0:1 and 1:0. The measured ^{1}H-NMR spectra and the resulting Job plot are given in Figure 2.13 and Figure 2.14 for Napht-PDMAc and TTF-PDMAc, respectively. The maximum of the job plots for both Napht-PDMAc and TTF-PDMAc lies somewhere between 0.33 and 0.40, indicating that the stoichiometry of both host-guest complexes are somewhere between 1:2 and 1:1, i.e. that both HG and HG_2 are readily formed during these titration experiments. These results were confirmed by investigating the job plots of the other protons of BBB.

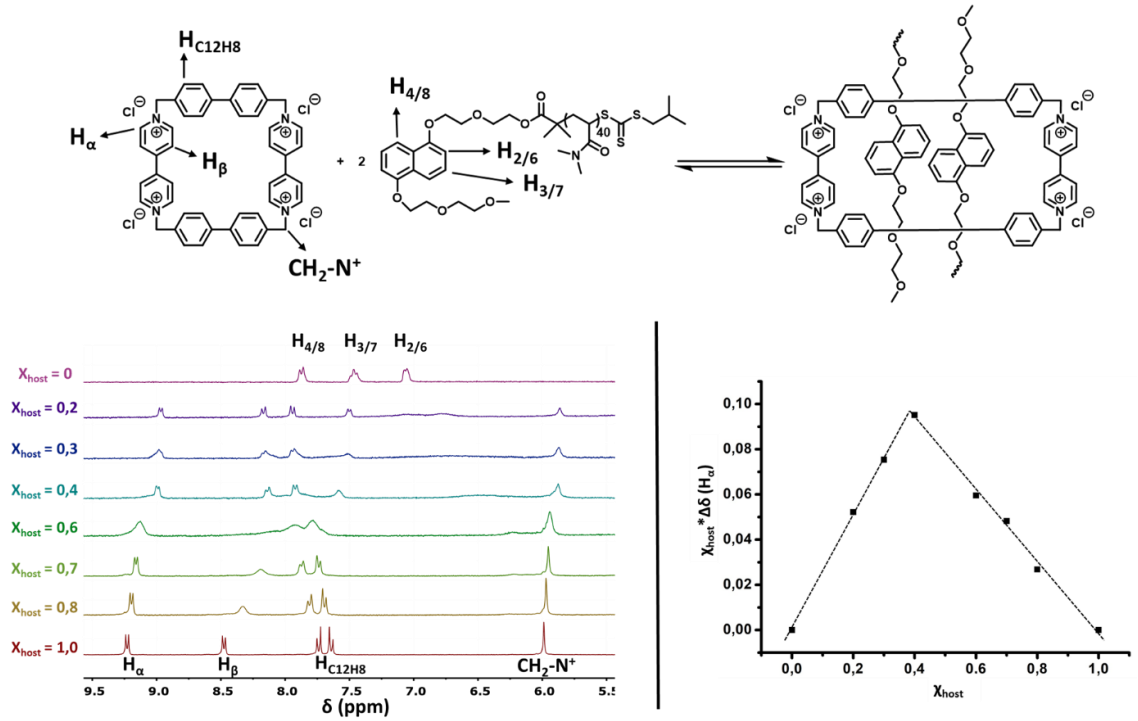

Figure 2.13.Top: Schematic representation of the complexation of BBB with 2 Napht-PDMAc with respective ^{1}H-NMR annotations. Bottom, left: The partial ^{1}H –NMR spectra of the BBB – Napht-PDMAc complex where the molar ratios of H:G are varied between 0:1 and 1:0 measured at 298 K in D_2O at 300 MHz. Right: The Job plot of BBB with Napht-PDMAc by following the difference in shift of the H_α signal of BBB.

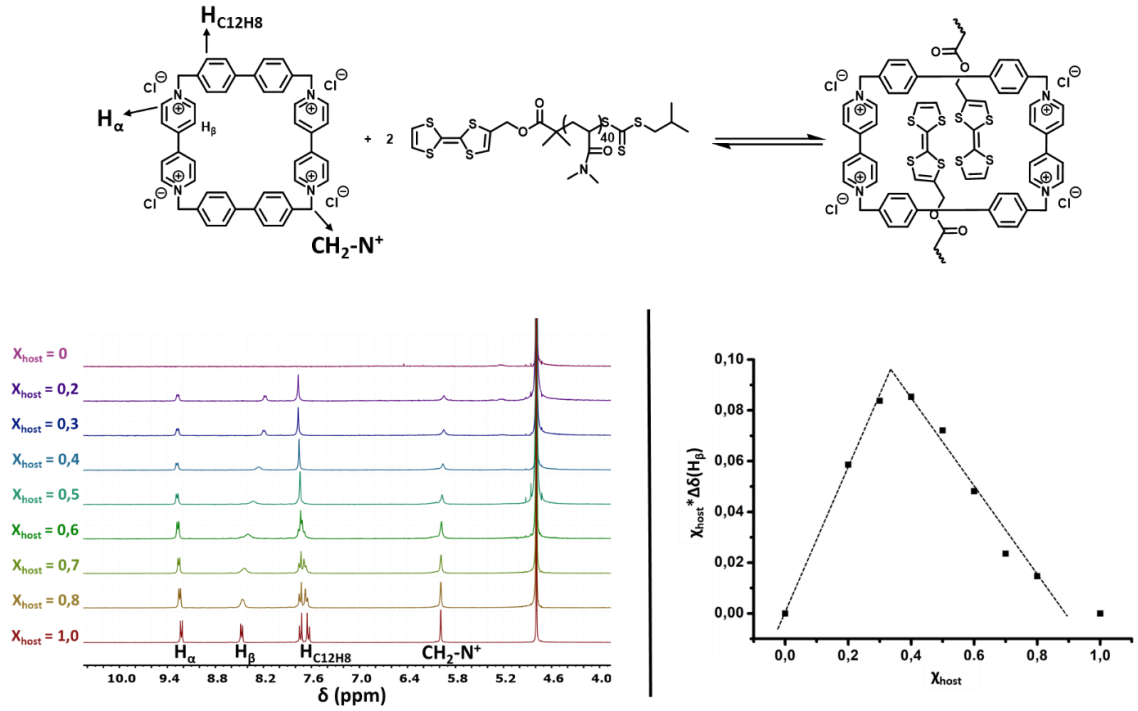

Figure 2.14. Top: Schematic representation of the complexation of BBB with 2 TTF-PDMAc with respective ^{1}H-NMR annotations. Bottom, left: Partial ^{1}H –NMR spectra of an aqueous solution of BBB and TTF-PDMAc where the molar ratios of H:G are varied between 0:1 and 1:0 measured at 298 K in D_2O at 300 MHz. Right: The Job plot of BBB with TTF-PDMAc by following the difference in shift of the CH_2-N^+ signal of BBB.

The measured ^{1}H-NMR spectra used to create the Job plots also provide further insight in the nature of the complexation of both TTF and Napht with BBB. Upon the addition of aliquots of either Napht-PDMAc (Figure 2.13, Left) or TTF-PDMAc (Figure 2.14, Left) to the aqueous solution of BBB, significant changes in chemical shifts were visible compared to the non-complexed species. More specifically for the signals corresponding to the Napht units, peak broadening and upfield shifting was observed starting from the addition of 0.2 mole fraction BBB and eventually these free Napht signals almost disappear with the addition of more BBB, indicating the fast kinetics of the complex by the gradual shifting of the signal. Additionally, for both Napht-PDMAc and TTF-PDMAc complexations, only one set of signals is observed confirming that the kinetics of the complexation is fast compared to the NMR time scale.

These trends were observed for both 1:1 and 1:2 complexes as displayed in Figure 2.15 for Napht-PDMAc and Figure 2.16 for TTF-PDMAc. Focusing on the Napht-PDMAc, the ^{1}H-NMR spectra displays significant changes in the chemical shifts of H_α ($\Delta\delta \approx 0.26$ ppm), H_β ($\Delta\delta \approx 0.54$ ppm), H_{C12H8} ($\Delta\delta \approx 0.37$ ppm) and CH_2-N^+ ($\Delta\delta \approx 0.13$ ppm) upon the addition of Napht-PDMAc and together with the broadening of the relevant peaks clearly confirms the formation of the molecular assembly. Similar to the complexation of the smaller cyclophane BB with a Napht-derivative, H_β is shifting upfield while the H_{C12H8} is shifting downfield when the concentration of complexes is increasing which results in the

typical switching or cross-over of both peaks in the ^{1}H-NMR spectrum (Figure 2.15).[45,46] While focusing on the TTF-PDMAc, the protons of TTF are undetectable in the ^{1}H-NMR spectra probably due to two factors: 1) the hydrophobic nature of the TTF leads to poor hydration as the TTF moieties are most likely inside the polymer globule and 2) the low mobility of the TTF-PDMAc chains. Nonethless, the formation of the supramolecular assembly between BBB and TTF-PDMAc was confirmed by the appearance of chemically shifted and broadened signals of BBB upon addition of aliquots of this host molecule. It was noticed that the difference in chemical signal, relative to the free BBB, was the highest for H_β ($\Delta\delta \approx 0.29$ ppm) compared to H_α ($\Delta\delta \approx 0.04$ ppm), H_{C12H8} ($\Delta\delta \approx 0.07$ ppm) and CH_2-N^+ ($\Delta\delta \approx 0.04$ ppm). Furthermore, a clear change in multiplicity was observed for the phenyl protons of the BBB, in which the doublets of H_{C12H8} are converging towards a singlet peak clearly showing that their electronical environment are becoming identical upon increasing the amount of TTF (Figure 2.16).

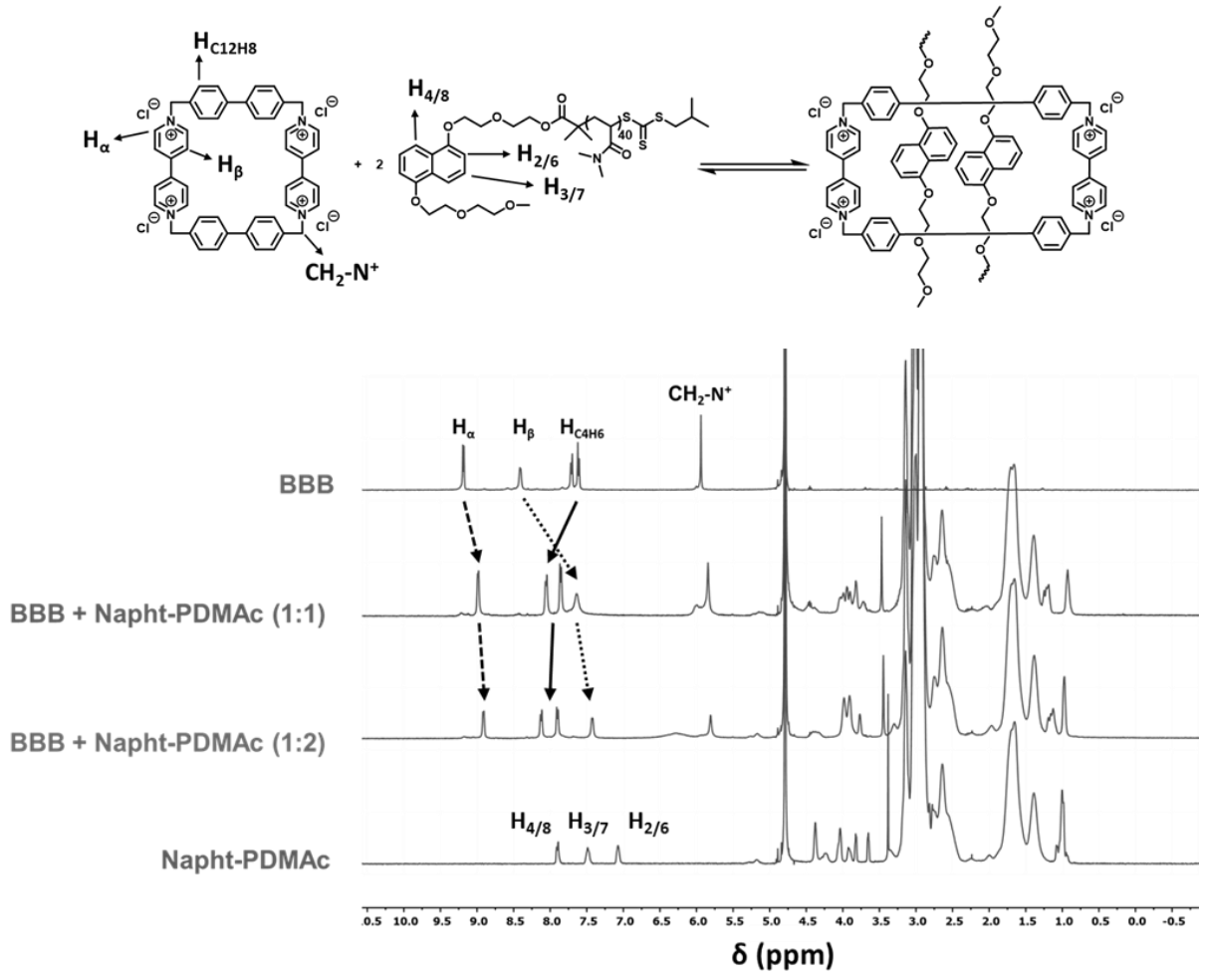

Figure 2.15. Top: Schematic representation of the complexation of BBB with 2 Napht-PDMAc with respective ^{1}H-NMR annotations. Bottom: The comparison of the ^{1}H-NMR spectra (400 MHz) of the separate building blocks BBB and TTF-PDMAc and upon the formation of the 1:1 and the 1:2 complex for BBB upon the addition of respectively 1 and 2 equivalents of TTF-PDMAc in D_2O at 298 K.

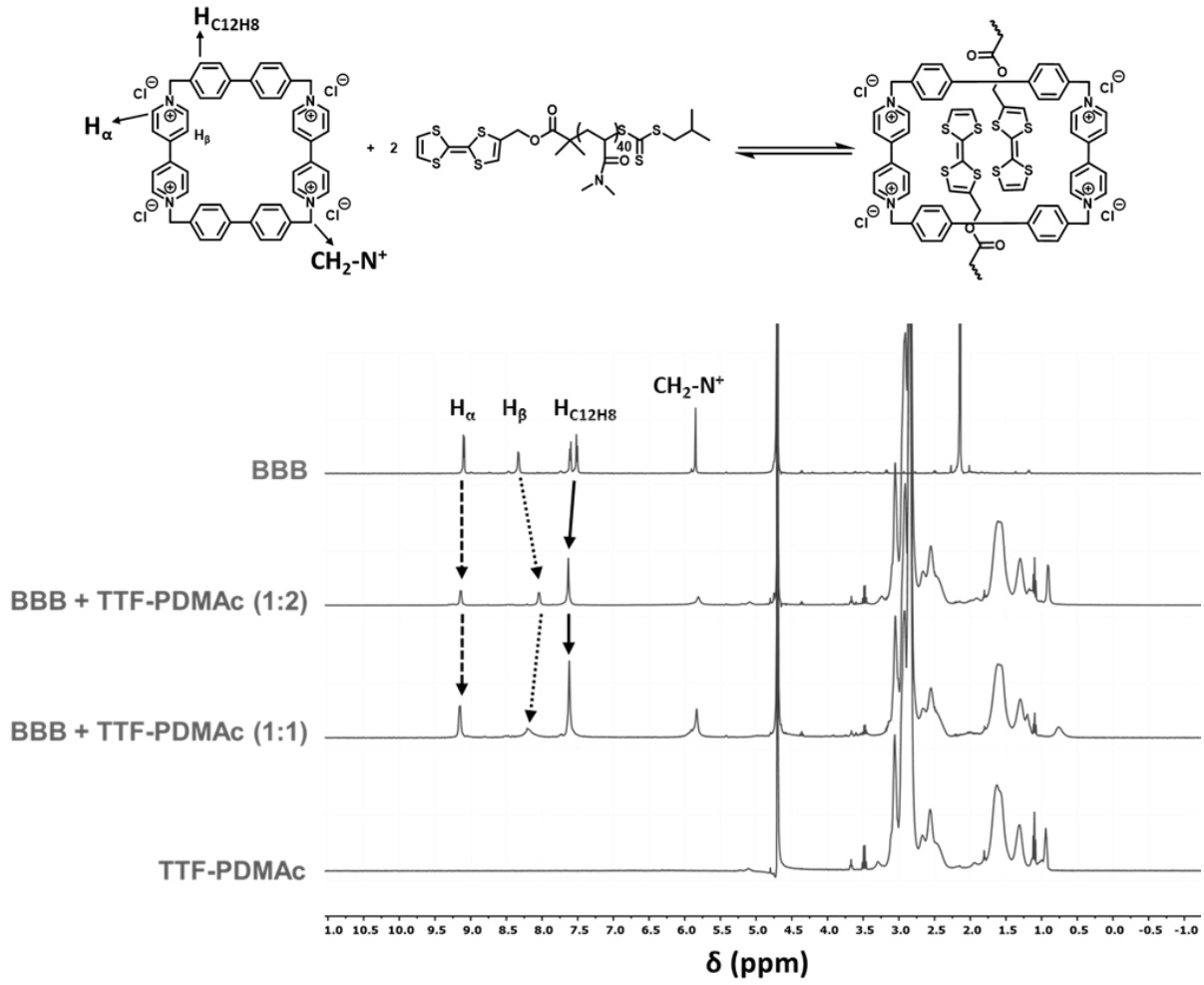

Figure 2.16. Top: Schematic representation of the complexation of BBB with 2 TTF-PDMAc with respective ^{1}H-NMR annotations. Bottom: The comparison of the ^{1}H-NMR spectra (400 MHz) of the separate building blocks BBB and TTF-PDMAc and upon the formation of the 1:1 and the 1:2 complex for BBB upon the addition of respectively 1 and 2 equivalents of TTF-PDMAc in D_2O at 298 K.

2.3 Complexation studies via diffusion-ordered NMR spectroscopy

The complex formation was furthermore confirmed via diffusion-ordered NMR spectroscopy (DOSY) which can be used to investigate the association and complexation behavior of the corresponding building blocks by measuring the diffusion coefficients via the Brownian motion. It was postulated that a change in diffusion coefficient would result from the complexation of TTF-PDMAc and Napht-PDMAc with BBB as the host-guest assembly has a different molar mass, especially if a ternary complex is formed, compared to its constituents for which the diffusion coefficients were measured to be 4.078 x 10^{-6} cm²/s and 2.163 x 10^{-6} cm²/s for BBB and Napht-PDMAc, respectively (Figure 2.17). Upon the addition of 1 eq of Napht-PDMAc to the BBB solution, it was noticed that the diffusion coefficient (2.176 x 10^{-6} cm²/s) of the measured species was now almost identical as for the Napht-PDMAc.

This indicates that the BBB is associated with the polymer and is now moving with the same speed through the solution as the polymer presumably as a 1:1 pseudorotaxane complex. A further decrease of the diffusion coefficient to 1.742 x 10^{-6} cm²/s was noticed upon addition of 2 eq of Napht-PDMAc to the BBB solution, ascribed to the formation of the larger 1:2 complex of BBB with Napht-PDMAc. These results were further confirmed by comparing the hydrodynamic radius of these species calculated from the Stokes-Einstein equation:

Equation 2.1: $$D = \frac{k_B T}{6\pi\eta R_H}$$

where k_B is the Boltzmann constant, T the absolute temperature, η the viscosity of the solution and R_H the hydrodynamic radius of the solute.[47] As observed for the diffusion constant, upon the addition of 1 eq of Napht-PDMAc to BBB the hydrodynamic radius increases from 6.0 Å to 11.3 Å showing that the formed species have the same hydrodynamic radius as the Napht-PDMAc polymer chains (11.3 Å) and thus confirming the formation of the pseudorotaxanes. Even though, upon the addition of 2 eq of Napht-PDMAc, the hydrodynamic radius of the formed species (14.1 Å) is only slightly higher than the R_H of the 1:1 complex (11.3 Å) this still proves that higher structures, presumably 1:2 complex, are formed. This small difference in R_H indicates that an average diffusion constant is presumably measured of the non-complexed molecules, the 1:1 complexes and the 1:2 complexes as a fast exchange was already noticed in the previous ^{1}H-NMR spectroscopy studies.

Sample	D x 10^{-10} (m^2 s^{-1})	R_H (Å)
BBB	4.078	6.0
Napht-PDMAc	2.163	11.3
BBB + 1 eq Napht-PDMAc	2.176	11.3
BBB + 2 eq Napht-PDMAc	1.742	14.1

Table 3.1. The diffusion coefficient (D) and Stokes-Einstein hydrodynamic radius (R_H) values for BBB, Napht-PDMAc, BBB with 1 eq of Napht-PDMAc and BBB with 2 eq of Napht-PDMAc in D_2O at room temperature (298 K).

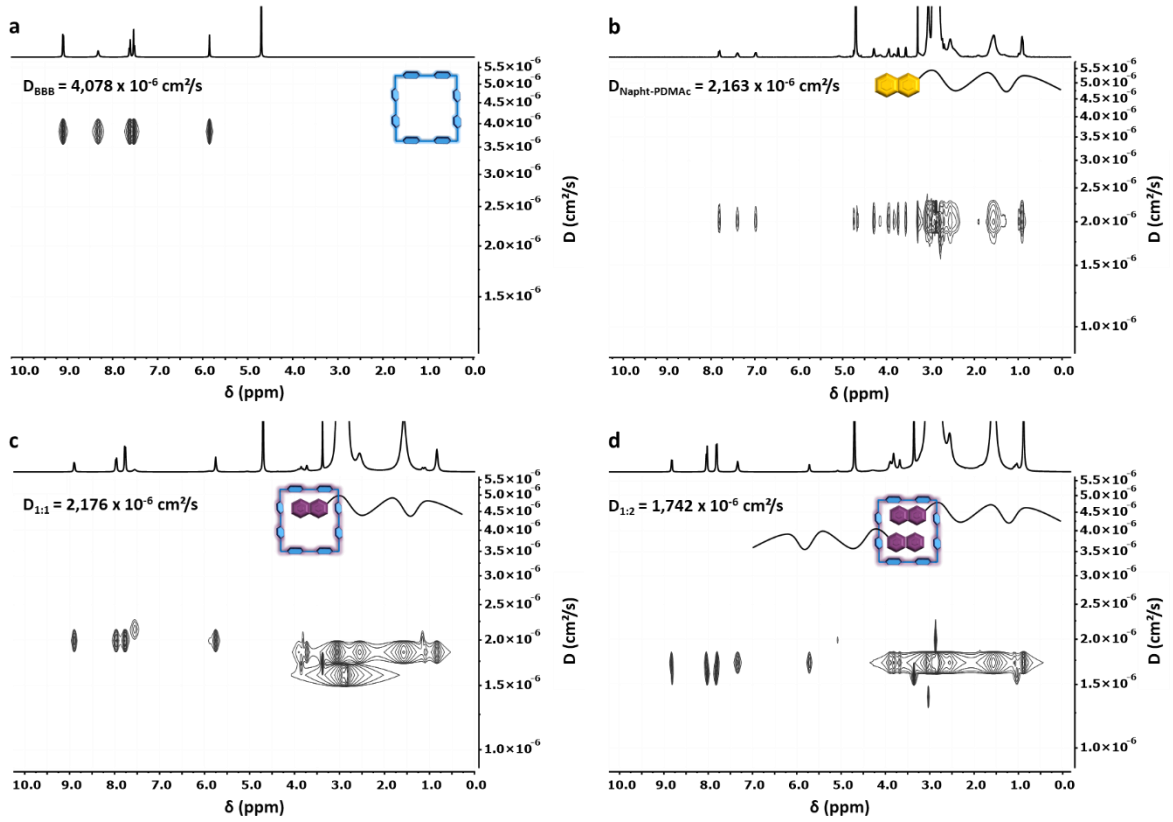

Figure 2.17. 2D DOSY-NMR spectra (400 MHz) of: a) 5 mM BBB solution, b) 5 mM Napht-PDMAc solution, c) 5 mM BBB and 5 mM Napht-PDMAc solution and d) 5 mM BBB and 10 mM Napht-PDMAc solution. All spectra were measured in D_2O at 298 K.

The same DOSY experiments were undertaken to confirm the complex formation between the TTF-PDMAc and BBB. The reference measurements revealed a similarly lower diffusion coefficient (2.008 x 10^{-6} cm^2/s) with higher R_H value (12.3 Å) for the TTF-PDMAc polymer, then for the BBB (D = 4.078 x 10^{-6} cm^2/s and R_H = 6.0 Å) (Figure 2.18, a and b, and Table 3.2.). For the 1:1 TTF-PDMAc-BBB complex it was noticed that the protons corresponding to BBB moved to a lower diffusion coefficient (2.628 x 10^{-6} cm^2/s) with higher hydrodynamic radius (11.9 Å) almost equal to the TTF bearing polymer (Figure 2.18, c and Table 3.2.). In addition, no cross-peaks were observed for the free BBB confirming the existence of the 1:1 assembly between both components. The same trend was visible upon the addition of 2 eq. of TTF-PDMAc, in which a further decrease of the diffusion coefficient is observed (1.846 x 10^{-6} cm^2/s) and a higher hydrodynamic radius of 13.3 Å as shown in Figure 2.18, d and Table 3.2, respectively. Again further increase of the R_H presumably indicates that an average diffusion coefficient is measured due to the fast exchange of the formed BBB-TTF complexes.

Sample	D x 10^{-10} (m^2 s^{-1})	R_H (Å)
BBB	4.078	6.0
TTF-PDMAc	2.002	12.3
BBB + 1 eq TTF-PDMAc	2.070	11.9
BBB + 2 eq TTF-PDMAc	1.846	13.3

Table 3.2. The Diffusion coefficient (D) and Stokes-Einstein hydrodynamic radius (R_H) values for BBB, Napht-PDMAc, BBB with 1 eq of TTF-PDMAc and BBB with 2 eq of TTF-PDMAc in D_2O at room temperature.

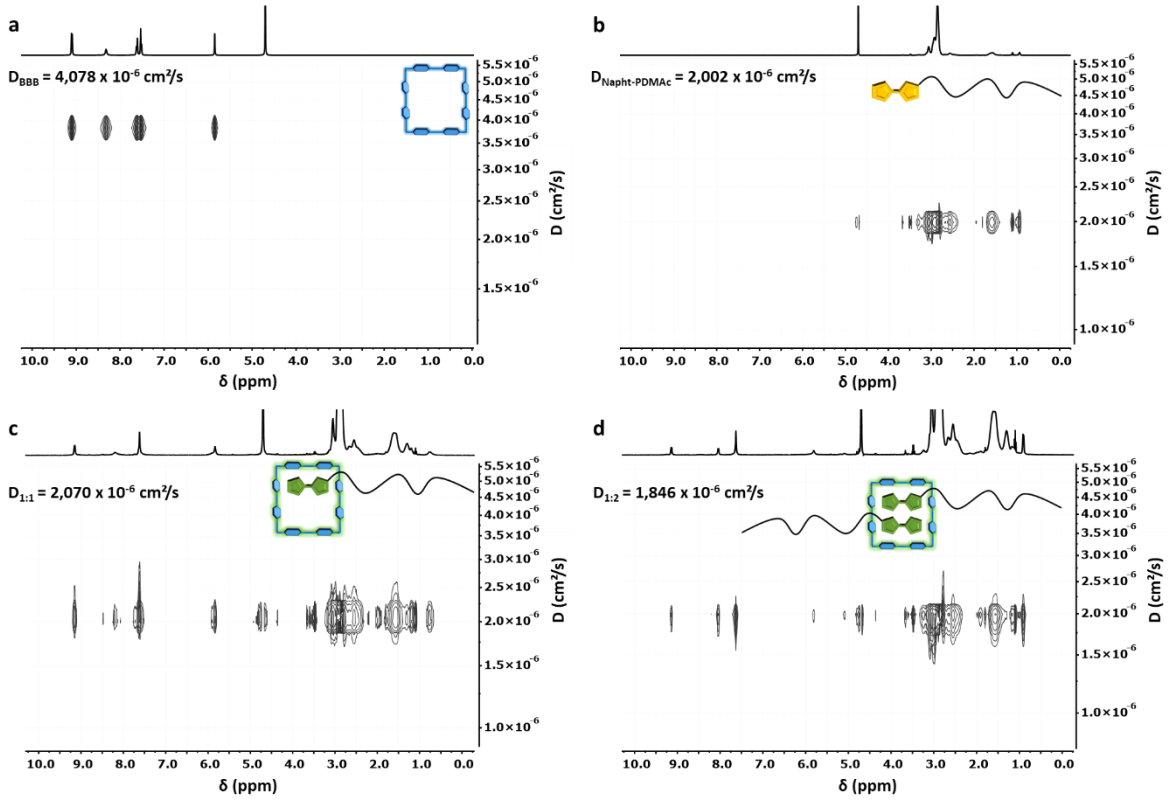

Figure 2.18. 2D DOSY-NMR spectra (400 MHz) of: a) 5 mM BBB solution, b) 5 mM TTF-PDMAc solution, c) 5 mM BBB and 5 mM TTF-PDMAc solution and d) 5 mM BBB and 10 mM TTF-PDMAc solution. All spectra were measured in D_2O at 298 K.

2.4 Complexation titrations via UV-VIS spectroscopy

After the first NMR spectroscopy results indicated that indeed 1:2 complexes can be formed in aqueous media, the strength and the nature of the complex was further investigated using UV-VIS spectroscopy. Here, the intensity of the absorption band of the complex was monitored while either host or the guest molecules are gradually added to an aqueous solution of the other building block.

2.4.1 UV-VIS titrations of BBB and Napht-PDMAc

During the first titration, a concentrated aqueous solution of BBB was added in steps of 0.1 eq to a dilute aqueous solution of Napht-PDMAc (Figure 2.19). Diluted Napht-PDMAc was also added to the concentrated BBB stock solution prior to titration to maintain a constant concentration of guests in the measured solution. Upon titration of the BBB to the Napht-PDMAc solution, the appearance of the characteristic purple color clearly indicated the formation of the complex as can be seen in Figure 2.19. The complexation can be monitored in the UV-VIS spectrum through the increase of the absorbance of the charge transfer (CT)-band at 550 nm. This absorbance peak becomes immediately visible upon addition of small aliquots of the BBB stock solution ascribed to the formation of 1:2-complexes as a large excess of Napht-PDMAc is present in the solution. Unfortunately, the main peak of BBB at 450-500 nm is much more intense than the formed CT-band and, therefore, it partially obscures the increase of the charge transfer absorbance peak upon further addition of BBB stock solution. When even more BBB is added to the solution, the amount of free BBB dominates the UV-VIS spectrum making the accurate quantification of the CT-band very difficult. Unfortunately, this interference prevents the calculation of the association constant through the monitoring of the absorbance increase of the CT-band.

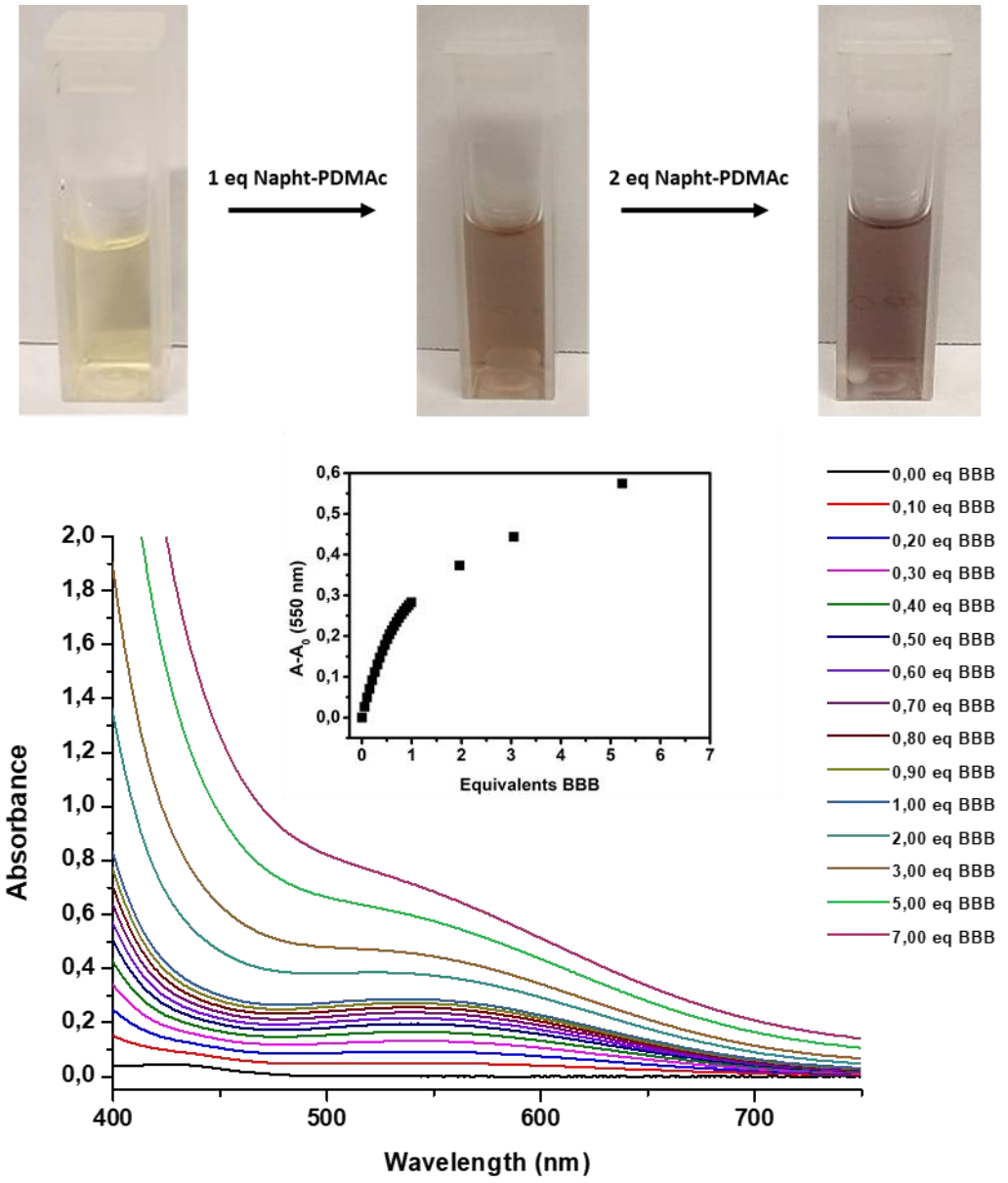

Figure 2.19. Top: The visualization of the color change upon complexation of BBB with 1 eq and 2 eq Napht-PDMAc ppolymer chains. Bottom: UV-VIS titration by adding a concentrated aqueous BBB solution (10.31 mM) to a diluted Napht-PDMAc (1.01 mM) solution in water at 25°C. Insert: The increase of absorbance at 550 nm versus equivalents BBB.

Due to the interference with the absorbance of free BBB, the opposite titration was also studied where a concentrated Napht-PDMAc solution was gradually added in steps of 0.1 eq to a BBB stock solution. In this way, the interference peak of the BBB is assumed to remain constant and when the initial absorbance of BBB was subtracted from the titration UV-VIS spectra, a slight blue shift in the CT-band of the complex was observed throughout the titration. This shift is highlighted in Figure 2.20 by plotting the wavelength at max. absorbance in the range of 500 – 600 nm in function of the equivalents of added Napht-PDMAc. At first, it can be noticed that the maximum of the CT-band is continuously progressing from approximately 528 nm to 550 nm upon the addition of approximately 0.8 eq Napht-PDMAc. Altough the specific cause of this shift could not be proven, this change can presumably be

ascribed to the possible shift in equilibrium from a 1:1 complex to a 1:2 complex as more Napht-derivatives are present in the solution forcing the equilibrium towards the 1:2 complexation. After that, the maximum of the CT-band remains constant at 550 nm and further addition of Napht-PDMAc will only cause an increment in the intensity of the absorbance band due to the formation of more 1:2 complexes. This observation that the 1:2 complex is already formed upon the addition of less than 1 eq of Napht-PDMAc could indicate the appearance of a strong cooperativity for the formation of the 1:2 complex. Surprisingly, the intensity of the complex bond is still rising with the addition of more than 2 eq Napht-PDMAc, which can be ascribed by the interference of the absorbance band of free Napht-PDMAc (250 nm – 350 nm) and/or a possible additional interaction of Napht-PDMAc with the viologen groups on the outside of the box like host molecule.

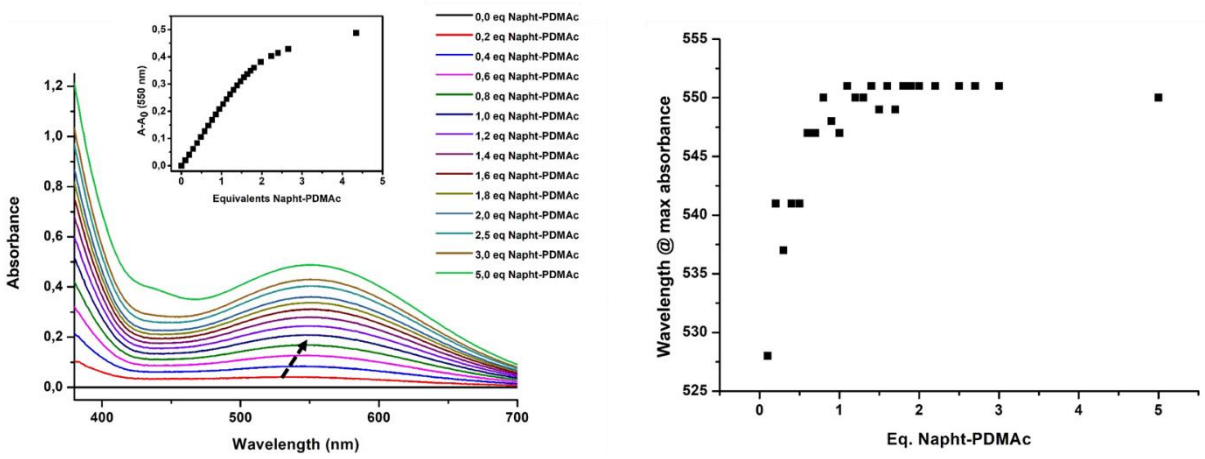

Figure 2.20: Left: UV-VIS titration by adding gradually a concentrated aqueous Napht-PDMAc solution (20.09 mM) to a diluted BBB (1.00 mM) stock solution. Insert: The increase of absorbance at 550 nm versus equivalents Napht-PDMAc. Right: Plot showing the wavelength at maximum absorbance in function of added eq Napht-PDMAc.

2.4.2 UV-VIS titrations of BBB and TTF-PDMAc

The same UV-VIS titration experiments were performed for TTF-PDMAc, to investigate its interaction with BBB by first performing a titration where a concentrated aqueous solution of BBB was added in steps of 0.1 eq to a dilute aqueous solution of TTF-PDMAc. Similarly to Napht-PDMAc, upon complexation the characteristic green color was immediately visible confirming the formation of the complex between the BBB and the TTF-derivative (Figure 2.21). In contrast to Napht-PDMAc, only a minor overlap with the free absorbance is noticed upon the addition of more than 1 equivalent of BBB as the CT-band of the complex is now located at a higher wavelength, namely at approximately 900 nm (Figure 2.21). This CT band is immediately visible upon the addition of aliquots of BBB and is increasing in intensity as more BBB is titrated into the solution. After the addition of 1 equivalent of BBB, the intensity of the CT-band of the complex remains constant as the added BBB can no longer form new complexes with TTF-PDMAc. Moreover, the presence of the free BBB is then visible by the

absorbance of a new peak in the region of 600 nm which partially overlaps with the CT-band of the complex. A red shift of the complex absorbance peak from 908 nm to 879nm was noticed upon the addition of more than 1 eq of BBB, which indicates that the equilibrium with an excess of BBB transfers from the initial formed 1:2 complex to the 1:1 complex.

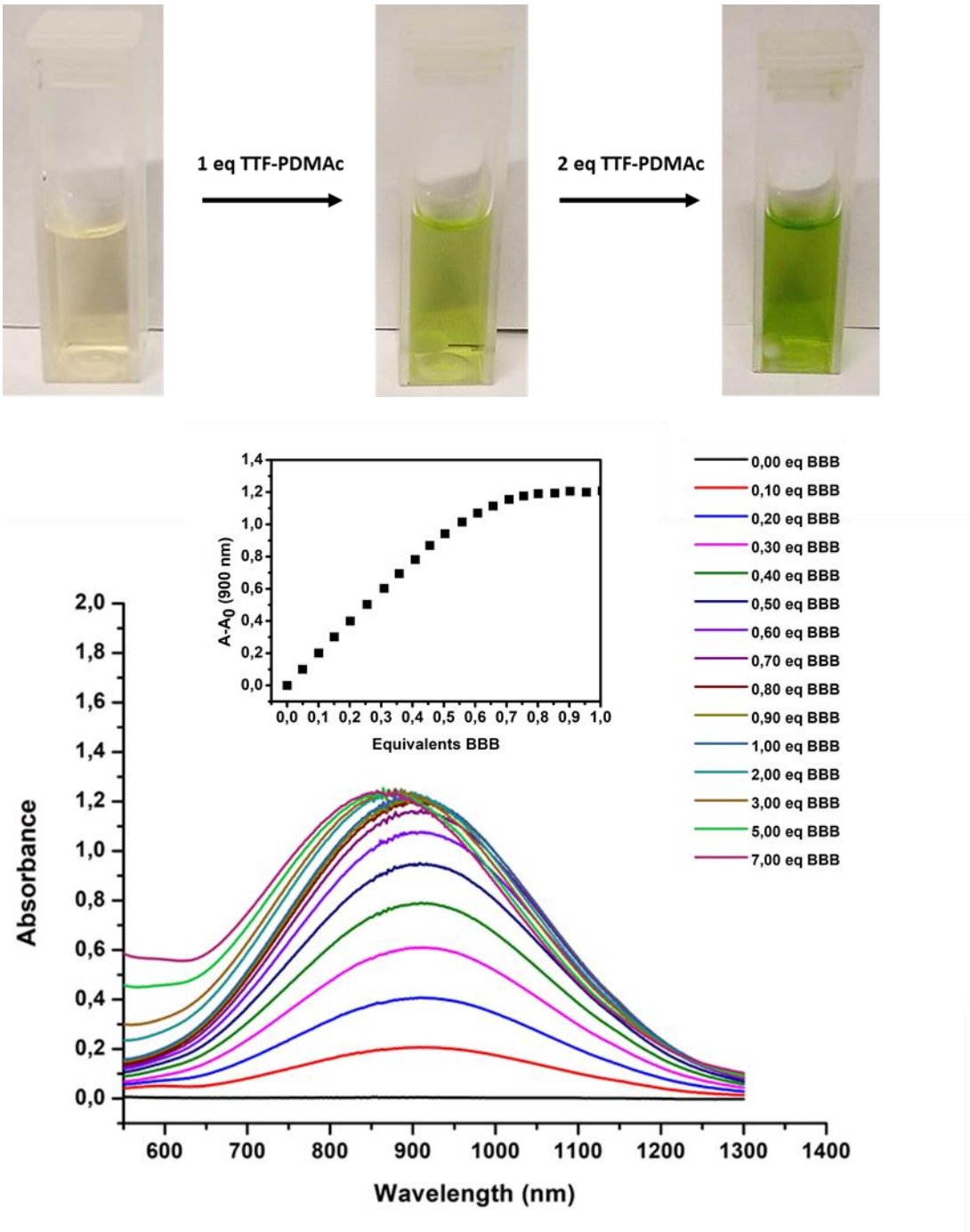

Figure 2.21. Top: The visualization of the color change upon complexation of BBB with 1 eq and 2 eq of TTF-PDMAc. Bottom: UV-VIS titration by adding a concentrated aqueous BBB solution (10.31 mM) to a diluted TTF-PDMAc (1.03 mM) solution at 25 °C. Insert: The increase of absorbance at 900 nm versus equivalents BBB.

The adverse effect is noticed when TTF-PDMAc is gradually added to a stock solution of BBB. Here, the gradual blue shift of the CT-band of the complex is observed from approximately 850 nm to approximately 909 nm when more than 1eq of TTF-PDMAc is added to an aqueous BBB solution, as highlighted in Figure 2.22. Similarly to Napht-PDMAc, this could also indicate that for TTF-PDMAc the equilibrium shift from the 1:1 complex to the 1:2 complex, is accompanied by a cooperative effect towards the formation of the ternary complex. However, the shift towards the formation of the ternary complex for TTF-PDMAc is less steep than the one for Napht-PDMAc (Figure 2.22, right) indicating that the 1:2 complex of Napht-PDMAc is more promptly formed compared to TTF-PDMAc displaying a possible higher cooperativity for the Napht-PDMAc-BBB complex.

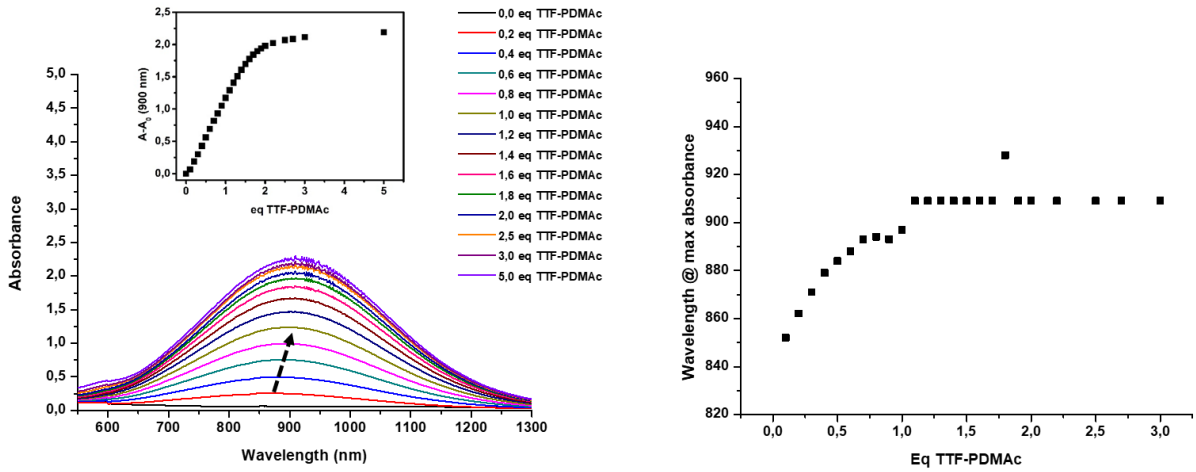

Figure 2.22. Left: UV-VIS titration by adding gradually concentrated aqueous TTF-PDMAc solution (20.43 mM) to a diluted BBB solution (1.00 mM). Insert: The increase of absorbance at 900 nm versus equivalents TTF-PDMAc. Right: plot showing the wavelength at maximum absorbance in function of equivalents added TTF-PDMAc polymer chains.

Normally, by plotting the difference in absorbance in function of the concentration of the gradually added building partner the value of the K_a can be estimated by fitting equation 2.3:

Equation 2.3:
$$\Delta A = \frac{\varepsilon_{HG}[H]_0 K_1[G] + \varepsilon_{HG2}[H]_0 K_1 K_2[G]^2}{1 + K_1[G] + K_1 K_2[G]^2}$$

With K_1 the association constant of the 1:1 complex ($K_1 = \frac{[HG]}{[H][G]}$) and K_2 the association constant of the 1:2 complex ($K_2 = \frac{[HG_2]}{[H][HG]}$), ε_{HG} and ε_{HG2} the absorbance coefficient of the 1:1 complex and the 1:2 complex respectively, $[H]_0$ the initial concentration of the host molecule and [G] the concentration of added guest molecule.[48] However, for our complexes the association constant cannot be calculated accurately from these UV-VIS titrations due to the interference of the absorbance of the building blocks together with the overlap of the CT-bands of the formed 1:1 and 1:2 complexes. To determine the association constant of the complex, isothermal titration calorimetry (ITC) measurements were performed and are discussed in the next paragraph.

2.5 Isothermal titration calorimetry (ITC) results

The association constants were investigated using isothermal titration calorimetry (ITC). In this method the interactions between two building blocks is measured by monitoring either the absorbed or released heat upon the formation of the complex, circumventing the interference problems with UV-VIS spectroscopy. ITC experiments are performed by adding gradually either the guest or the host molecule to a sample cell containing an aqueous or organic solution of the complementary building block and connecting this sample cell with a reference cell in an adiabatic circuit to carefully measure the heat changes. Afterwards these heat changes are plotted in function of the molar ratio of the added building block during the titration, providing a binding isotherm from which the association constant (K_a), the stoichiometry (n) and the binding enthalpy (ΔH) can be derived.

During these experiments the host molecule BBB was titrated into the sample cell containing an aqueous solution of the guest-derivative. The reverse titration, where the guest is titrated to the host, is not possible due to the exothermic dilution process of the concentrated PDMAc solutions, which interferes with the exothermic response of the complex formation.

The ITC binding isotherm derived from the addition of a concentrated BBB solution to a dilute aqueous solution of Napht-PDMAc showed exothermic responses indicating the formation of the host-guest complex. To our surprises the binding isotherm could only be fitted to the 1:1 binding model, revealing a K_a of 1.1 x 10^4 M^{-1} with a stoichiometry (n) of 0.62 (Figure 2.23). The best fit of the 1:1 model may be ascribed to the fact that when aliquots of BBB are added to an excess of Napht-PDMAc polymers, the 1:2 complex will preferably be formed in a one-step process. In addition, the stoichiometry of the complex lays in between the one for a 1:1 complex (n = 1) and for a 1:2 complex (n = 0.5), which could indicate that a mixture of both complexes is present during the titration which supports the conclusion drawn from the results of the UV-VIS titration.

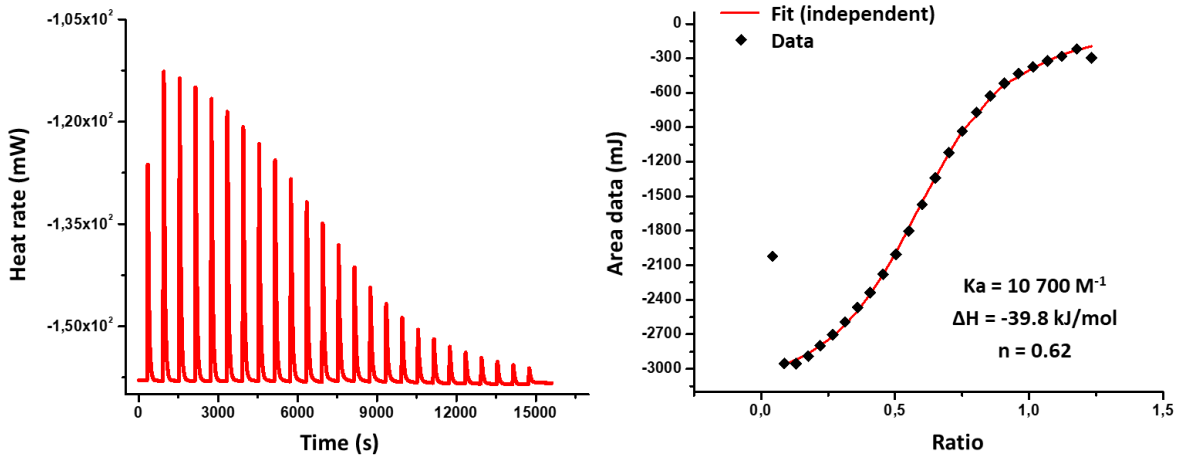

Figure 2.23. Isothermal titration calorimetry data for the addition of BBB to Napht-PDMAc recorded in Millli-Q water at 15°C

The same ITC experiment was performed using TTF-PDMAc and the fitting of the ITC isotherm revealed that a complex was formed with a stoichiometry of 0.71 and K_a of 2.7 x 10^4 M^{-1} (Figure 2.24). The binding affinity of TTF-PDMAc towards BBB is approximately 2.5 times higher than the one of Napht-PDMAc, indicating that the TTF-derivative interacts stronger with BBB presumably due to the stronger π-electron donor character of TTF compared to the Napht unit, which is also observed for the smaller tetracationic cyclophane BB.[49]

Similarly to the Napht-PDMAc, the stoichiometry of the BBB – TTF-PDMAc (n = 0.71) complex lays in between the 1:1 and 1:2 complex indicating that a mixture of both complexes is presumably present during titration supporting the UV-VIS data. However, this value leans more towards the stoichiometry of a 1:1 complex (n = 1.0), which could indicate that the difference in K_a for the 1:1 complex and the Ka of the 1:2 complex of the TTF-PDMAc with BBB is much smaller compared to the complex of BBB with Napht-PDMAc. This is in agreement with the observations from the UV-VIS titrations that showed a lower cooperativity for the formation of the BBB - TTF-PDMAc complex.

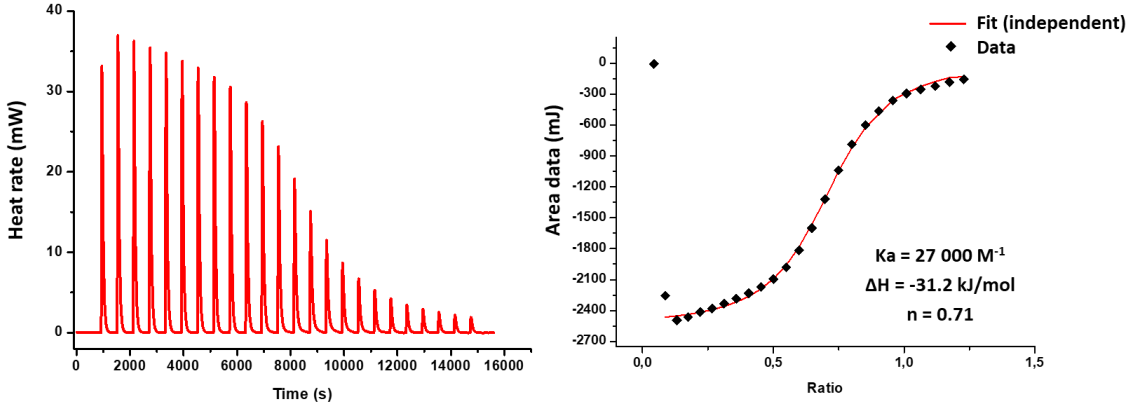

Figure 2.24. Isothermal titration calorimetry data for the addition of BBB to TTF-PDMAc recorded in Milli-Q water at 15°C

2.6 Temperature responsive complexation

The relative high K_a values, like the ones calculated for our Napht-PDMAc with BBB (K_a = 1.1 x 10^4 M^{-1}) and TTF-PDMAc with BBB (K_a = 2.7 x 10^4 M^{-1}), means that the host-guest equilibrium favors the associated state and is correlated with a negative change in Gibbs free energy, resulting in the formation of spontaneous assemblies as shown in previous sections. Due to the temperature dependence of this thermodynamic potential, the chemical equilibrium of the host-guest complex was hypothesized to depend on the surrounding temperature. In this last section, the temperature responsivity of the BBB - Napht-PDMAc complex in aqueous solution, selected based on its lower K_a compared to the TTF-PDMAc complex, was quickly, due to lack of time, investigated by heating a NMR sample of the complex in D_2O. Upon heating to 100°C, the decomplexation of the Napht-PDMAc and BBB assembly was immediately visible due to the disappearance of the characteristic purple color as

displayed in Figure 2.25. This process is completely reversible as the complexation was spontaneously restored upon cooling the solution back to 5°C as shown by the characteristics purple color of the solution. Further investigations towards this thermo-responsivity should be done in the future.

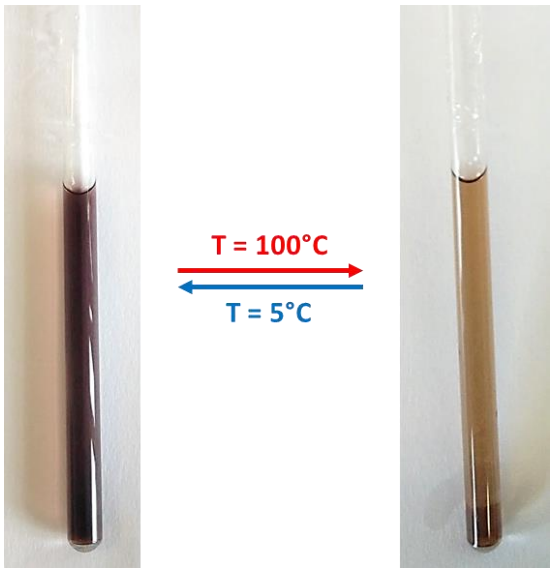

Figure 2.25. Disassembly of Napht-PDMAc and BBB by heating the solution to 100 °C and the reformation of the complex upon cooling to 5°C in D_2O.

3 Conclusions and outlook

In summary, we have explored the ability of the macrocyclic host molecule BBB to form strong inclusion complexes with different electron-rich guest molecules in aqueous media, which can play a significant role in the formation of the next-generation stimuli-responsive materials ranging from hydrogels to micelles and (multilayer) films. In a first step, the electron-rich guest molecules, Napht and TTF, were successfully functionalized with a CTA-agent group allowing the controlled synthesis of water-soluble, end-functionalized PDMAc polymers bearing either a TTF – or Napht moiety using RAFT-polymerization. The ability of these polymers to form supramolecular complexes with BBB was afterwards investigated using UV-VIS spectroscopy, NMR spectroscopy and ITC measurements revealing that colored 1:2 complexes are formed with a high association constant of 1.1 x 10^4 M^{-1} and 2.7 x 10^4 M^{-1} for Napht-PDMAc and TTF-PDMAc respectively. During the UV-VIS titration of both complexes a shift in the CT-band was observed, which can presumably be ascribed to the transfer of the 1:1 complex into the 1:2 complex and vice versa. These shifts were already noticed before 1 eq of Napht-PDMAc or TTF-PDMAc was added to the concentrated BBB solution favoring the formation of the 1:2 complex over the 1:1 complex. This cooperativity effect was more pronounced for the Napht-PDMAc complex than for the TTF-PDMAc complexes.

Finally, the reversible temperature dependence of the Napht-PDMAc complex was investigated showing a clear disruption of the complex when heated above 100°C and the quick reformation of the complex upon subsequent cooling below 5°C.

As a future follow-up study, the possible stimuli-responsivity of BBB-complexes could be expanded by using the reversible redox-responsive behavior of the TTF-PDMAc complex with BBB, which should lead to disruption of the complex when the TTF unit is electrochemically oxidized to its radical $TTF^{\cdot+}$ state followed by the reassembly of the complex by the subsequent reduction. The results presented in this chapter can now be used to incorporate the responsive BBB-guest complexes into multifunctional supramolecular materials through the use of both the host-guest responsivity and a stimuli-responsive polymer matrix which can lead to the creation of a variety of high-performance, smart materials ranging from actuators to shape memory and self-healing materials. Especially, the color change related with BBB complex formation opens up potential use of these smart materials for sensing purposes as the unambiguous output signal is immediately visible to the naked eye.

Secondly, an in depth comparison of the thermodynamics received with ITC of the polymer functionalized with the guest molecule with BBB and the their corresponding smaller molecules with BBB should be done in the future to enable more insight into the stoichiometry of both complexes. In addition, new investigations towards the influence of the polymer identity and chain length should be performed as the chemical nature of the polymer chain could have an influence on the stability of the formed end chain complex leading to a more accurate K_a value for the host-guest assembly.[50] Finally, in this manuscript mainly the head-to-tail conformation has been presented as the sterical hindrance of both polymer chains will then be reduced to a minimum. However, to fully confirm this, further studies should be performed.

4 Experimental details

4.1 Materials and instrumentation

All chemicals and solvents were commercially available and used as received unless otherwise stated with 2-(2-chloroethoxy)ethanol, 1.5-dihydroxynaphthalene, *p*-toluenesulfonyl chloride, 1,1'-ferrocenedimethanol, sodium hydride as a 60% dispersion in mineral oil (NaH), 2-methyl-1-propanethiol, aliquat 336, hydrochloride (HCl), *n*-butyllithium (n-BuLi), diisopropylamine, *N*-methylformaniline, sodium borohydride, methyliodide, *N,N'*-dimethylacrylamide (99%, contains 500 ppm monomethyl ether hydroquinone as inhibitor) (DMAc), azobisisobutyronitrile (AIBN), carbondisulfide, 4,4' bis(bromomethyl)bisphenyl, sodium hydroxide, tetraethylammonium chloride ($N(Et)_4^+Cl^-$) and ammonium hexafluorophosphate ($NH_4^+PF_6^-$) were purchased from Sigma Aldrich. DMAc

was purified by distillation and AIBN was recrystallized from MeOH before usage. Tetrathiafulvalene (TTF) was bought from Tokyo Chemical Industry (TCI), potassium carbonate, 4,4'-bipyridine and 4-dimethylaminopyridine (DMAP) from Acros organics and (3-dimethylaminopropyl)-*N'*-ethylcarbodiimide hydrochloride (EDC.HCl) from Iris Biotech GmbH. Finally anhydrous magnesium sulfate was supplied by Fisher Chemicals. All HPLC grade solvents were purchased from Acros (diethylether), Sigma Aldrich (Acetone, THF), Alfa Aesar (Nitromethane), Biosolve (DMF) and Fisher (ACN, MeOH, DCM, EtOH). All anhydrous solvents, were obtained by passing over aluminium oxide by means of a J.C. Meyer solvent purification system. All deuterated solvents were purchased from Cambridge Isotope Laboratories. Milli-Q Water (18.2 MΩ/cm) was generated using a Millipore Milli-Q academic water purification system

Nuclear magnetic resonance (NMR). ^{1}H-NMR spectra were recorded in CD_3CN, D_2O or $CDCl_3$ on a Bruker Advance 300 MHz or 500 MHz spectrometer at room temperature unless otherwise noted. Chemical shifts are reported as parts per million (ppm) downfield from the TMS resonance for the organic solvents CD_3CN and $CDCl_3$ and the solvent water peak for D_2O as internal standard.

Diffusion ordered spectroscopy (DOSY) NMR experiment. DOSY NMR experiments were performed on a 400 MHz Bruker Avance II spectrometer equipped with a broadband 1H decoupling probe (PABBO) using double stimulated echo, 2 spoil gradients and alternative phase cycle provided by Garreth Morris at a temperature of 298.2 K. Proton pulse lengths were determined to be 10.12 µs and bipolar gradient of δ = 2.5 ms length were incremented from G = 2.588 G/cm to 49.163 G/cm in 64 steps. 16 scans with 12 k complex data points were recorded for each increment with 16 dummy scans per experiment. The diffusion delay Δ was set to 1000 µs. Processing was achieved using TopSpin 3.2 with the Dynamic Center 2.0.4. After zero filling to 24 k points and apodization using an exponential window function with an additional linewidth of 0.1 Hz, 1D increment spectra were Fourier transformed and the signal decay due to gradients was fitted using MestReNova.

Size-exclusion chromatography (SEC). SEC was performed on an Agilent 1260-series HPLC system equipped with a 1260 online degasser, a 1260 ISO-pump, a 1260 automatic liquid sampler, a thermostatted column compartment at 50 °C equipped with two PLgel 5 µm mixed-D columns protected with a PLgel 5 µm guard column in series, a 1260 diode array detector (DAD) and a 1260 refractive index detector (RID). DMAc containing 50 mM of LiCl was used as eluent at a flow rate of 0.500 mL/min. The spectra were analyzed using the Agilent Chemstation software with the GPC add on using a PMMA calibration curve.

Size-exclusion chromatography with light scattering (LS) Light scattering (LS) measurements are performed on a 3-angle static light scattering (MALS) detector, i.e. miniDAWN TREOS, from Wyatt

Technology. The detector is coupled on-line to an Agilent 1260 infitiny HPLC system (vide DMA-SEC), and used to determine absolute molar mass of the analyzed polymer samples. The measurements are performed at ambient temperature, i.e. no temperature control unit is supplied/installed with the above mentioned LS detector. The refractive index (RI) increment (dn/dc) values are either used as reported for the certain polymer in *N,N*-dimethyl acetamide (DMA) or determined via online size-exclusion chromatography (SEC) equipped with an RI detector, which measures the RI increase for a 1-10 mg/mL concentration series of the mentioned polymers. The LS results are further analyzed with the provided Astra 7 software, also designed by Wyatt Technology.

Gas Chromatography (GC) was performed on 7890A from Agilent Technologies with an Agilent J&W Advanced Capillary GC column (30 m, 0.320 mm and 0.25 µm). Injections were performed with an Agilent Technologies 7693 auto sampler. Detection was done with a FID detector. Injector and detector temperatures were kept constant at 250 °C and 280 °C, respectively. The column was initially set at 50 °C, followed by two heating stages: from 50 °C to 100 °C with a rate of 20 °C/min and from 100 °C to 300 °C with a rate of 40 °C/min. and then held at this temperature for 0.5 minutes. Conversion was determined based on the integration of monomer peaks using DMF as internal standard

UV/VIS spectroscopy. UV/Vis spectra were recorded on a Varian Cary 300 Bio UV-VIS spectrophotometer equipped with a Cary temperature and stir control. Samples were measured in either quartz or disposable cuvettes with a path length of 1.0 cm in the wavelength range of 200 to 700 nm.

4.2 Synthesis of ferrocene template

4.2.1 Synthesis of 2-(2methoxyethoxy)-1-benzenesulfonate (TS-DGM)[51]

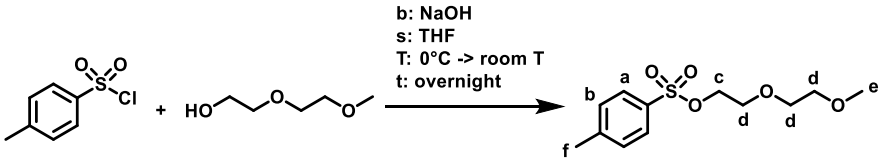

Figure 2.26. Reaction conditions for the synthesis of TS-DGM with respective ^{1}H-NMR annotations.

An aqueous solution of NaOH (2.50 g, 0.064 mol, 1.5 eq) in 25 mL water was added to a solution of 2-(2-methoxyethoxy)ethanol (5g, 0.0417mol, 1eq) dissolved in 40 ml THF, which was first cooled in an ice bath to 0°C. The resulting reaction mixture was left to stir for 2 h at 0 °C followed by the dropwise addition of a solution of *p*-toluenesulfonyl chloride (8.00 g, 0.042 mol, 1 eq) dissolved in 20 mL THF at 0 °C after which the reaction mixture was allowed to warm to room temperature and was subsequently stirred overnight. For the workup, the reaction was washed with brine for three times, dried over

anhydrous $MgSO_4$ and dried under reduced pressure to afford a clear oil. The crude product was used in the next reaction without further purification.

Yield: 8.10 g (70%).

^{1}H-NMR spectroscopy (300 MHz, $DCCl_3$) δ(ppm) 7.8 (d, *J* = 8.2 Hz, 2H, H_a), 7.34 (d, *J* = 8.0 Hz, 2H, H_b), 4.17 (t, *J* = 4.9, 2H, H_c), 4.72-3.44 (m, 6H, H_d), 3.35 (s, 3H, H_e), 2.45 (s, 3H, H_f)

4.2.2 Synthesis of 1,1-bis[[2-(2-methoxyethoxy)ethoxy]methylene]-ferrocene (ferrocene template)[33]

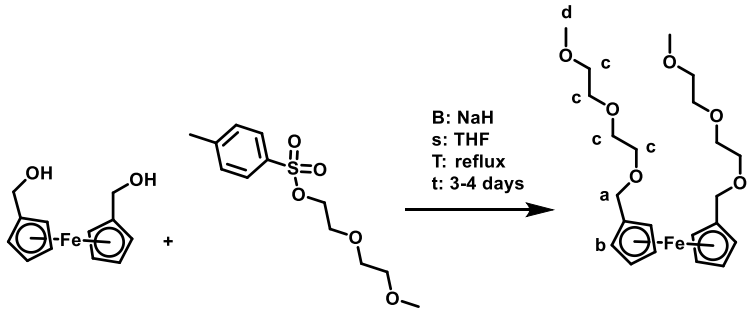

Figure 2.27. Reaction mechanism for the synthesis of the ferrocene template with respective ^{1}H-NMR annotations.

To a solution of 1,1'-ferrocenedimethanol (0.50 g, 1.97 mmol, 1 eq) and NaH (0.12 g, 5.00 mmol, 2.5 eq) in 175 mL dry THF under inert atmosphere, TS-DGM (5.43 g, 0.020 mol, 10 eq) dissolved in 175 mL dry THF was added dropwise. The reaction mixture was heated overnight under reflux after which another portion of NaH was added and heated again under reflux for 12 h. The reaction was followed on TLC (eluent: DCM/acetone 6/1) and depending on the presence of the starting product another portion of NaH was added to the mixture followed by overnight heating under reflux. This step was repeated until no more starting product is present in the reaction mixture. The reaction was stopped by diluting the reaction mixture with 300 mL water after cooling to room temperature. This aqueous phase was extracted with dichloromethane. The organic phases were collected, washed with water and dried over $MgSO_4$. The product was further purified using column chromatography (silica, DCM/Acetone 1/0->6/1) yielding the pure ferrocene template as a dark orange oil.

Yield: 0.76 g (84%).

^{1}H-NMR spectroscopy (300 MHz, CD_3CN) δ(ppm) 4.29 (s, 4H, H_a), 4.20 (d, *J* = 22.1 Hz, 1H, H_b), 3.55 (s, 16H, H_c), 3.32 (s, 6H, H_d)

4.3 Synthesis of cyclobis(paraquat-4,4'-biphenylene)

4.3.1 Synthesis of 1,1'-[4,4'-biphenylenedimethlyene]bis(4,4'-bipyridinium) bis(hexafluorophosphate) (Big disalt. $2PF_6^-$)[52]

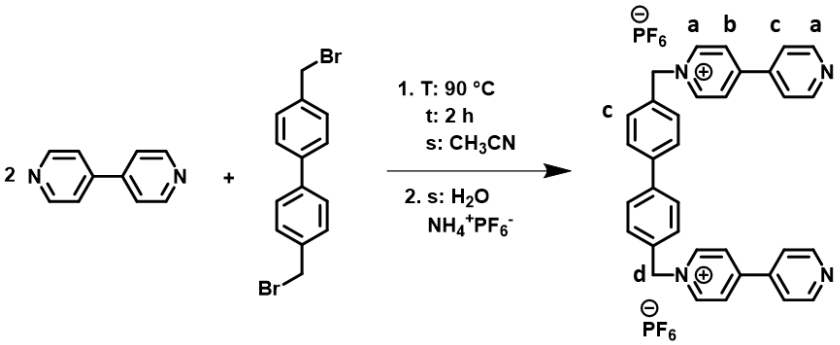

Figure 2.28. Synthetic scheme for the synthesis of big disalt.2PF6$^-$ with respective ^{1}H-NMR annotations.

A solution of 4,4' bis(bromomethyl)bisphenyl (23.12 g, 68.00 mmol, 2 eq) and 4,4'-bipyridine (5.00 g, 32.05 mmol, 1eq) dissolved in 250 mL dry CH_3CN was refluxed for 2 h. The bright green precipitation was filtered and washed with CH_3CN. Subsequently, the precipitated product was dissolved in a minimum of deionized water after which a saturated solution of $NH_4^+PF_6^-$ was added dropwise until all the big disalt.$2PF_6^-$ is precipitated out. The purification of this product was afterwards done via automatic flash column chromatography which started by rinsing the column for 5 column volumes (CV) with pure DCM, then the solvent was gradually changed to pure CH_3CN over 5 CV and was kept at 100% CH_3CN for 3 CV afterwards. Finally the elution solvent was changed to H_2O to remove all the by-products of the column. (15 µm Silica, 40 g, flow rate: 8 mL/min). All the fractions were collected and the solvent was evaporated under reduced pressure.

Yield: 1.15 g (77%)

^{1}H-NMR spectroscopy (300 MHz, CD_3CN) δ(ppm) 8.89 (m, 8H, H_a), 8.37 (d, *J* = 6.9 Hz, 4H, H_b), 7.81 (m, 8H, H_c), 7.60 (d, J = 8.4 Hz, 4H, H_c) 5.83 (s, 4H, H_d)

4.3.2 Synthesis of Cyclobis(paraquat-4,4'-biphenylene) tetrakis(hexafluorophosphate) (BBB)[33]

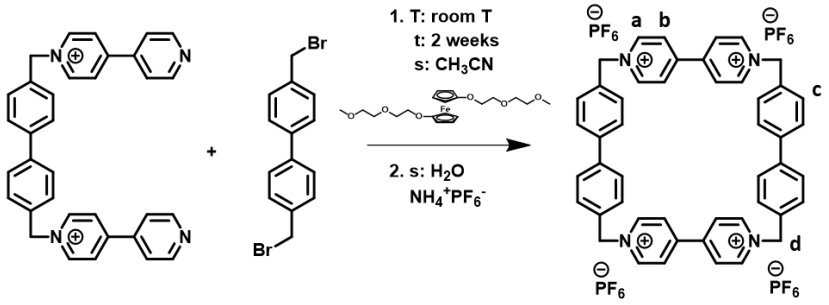

Figure 2.29. Reaction conditions for the synthesis of BBB with respective ^{1}H-NMR annotations.

A solution of 0.336 g big disalt.2PF_6^- (0.336 g, 0.527 mmol, 1 eq), 4,4'-bis(bromomethyl)biphenyl (0.1704 g, 0.501 mmol, 1 eq) and ferrocene template (0.3798 g, 0.846 mmol, 1.5 eq) in 100 mL dry CH_3CN was stirred at room temperature (20-25 °C). The reaction was monitored using TLC (silica, DMF/MeOH/2 M $NH_4^+Cl^-$ 5/3/2) and was stopped after 14 days. The solvent was evaporated under reduced pressure after which the resulting precipitate was washed with chloroform to remove the used Fc-template. The product was purified using column chromatography with the same conditions as used for TLC. The resulting product was then dissolved in a minimum of distilled water and was precipitated out by the addition of 1 eq NH_4PF_6.

Yield: 0.144g (26%)

^{1}H-NMR spectroscopy (300 MHz, CD_3CN) δ(ppm) 9.03 (d, *J* = 6.4 Hz, 8H, H_a), 8.33 (d, *J* = 6.4 Hz, 8H, H_b), 7.68 (d, *J* = 8 Hz, 8H, H_c), 7.58 (d, *J* = 8 Hz, 8H, H_c), 5.90 (s, 8H, H_d)

4.3.3 Ion exchange reaction of BBB from PF_6^- to Cl^-

In order to solubilize BBB in water, its counter ions needed to be exchanged from 4 PF_6^- to 4 Cl^- ions. This ion exchange reaction from PF_6^- to Cl^- was done by solubilizing the BBB.4PF_6^- in a minimum amount of nitromethane. Subsequently 6 eq of tetraethylammonium chloride were added yielding a greenish precipitate. This greenish precipitate was filtered, washed with MeOH and diethyl ether and dried under vacuum.

^{1}H-NMR spectroscopy (300 MHz, D_2O) δ(ppm) 9.15 (d, *J* = 6.4 Hz, 8H, H_a), 8.39 (d, *J* = 6.5 Hz, 8H, H_b), 7.65 (d, *J* = 29 Hz, 8 Hz, 8H, H_c), 7.56 (d, *J* = 8 Hz, 8H, H_c), 5.90 (s, 8H, H_d)

4.4 Synthesis of the TTF functionalized CTA-agent

4.4.1 Synthesis of 2-(1-isobutyl)sulfanylthiocarbonylsulfanyl-2-methylpropionic acid (TTF-CTA)[53,54]

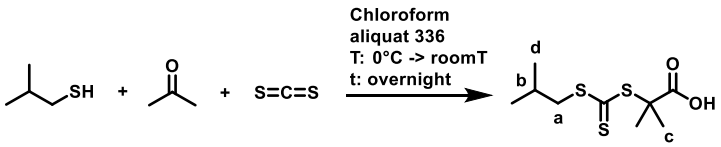

Figure 2.30. reaction conditions for the synthesis of CTA-COOH with respective ^{1}H-NMR annotations.

A mixture of 2-methyl-1-propanethiol (9.6 mL, 90 mmol, 1 eq) and aliquat 336 (1.6 mL) in 56 mL acetone was added to a 3-neck flask and was left to cool in an icebath under inert atmosphere. Subsequently, 8 mL of a 50 wt% NaOH solution was added dropwise after which the vigorous stirring was continued for another 20 min leading to the formation of white precipitates. In a next step, a solution containing carbondisulfide (5.6 mL, 93 mmol, 1 eq) was added slowly to the reaction during which the solution colors bright yellow and was left to stir for 30 min. After the stirring, chloroform (11.2 mL, 69 mmol, 0.76 eq) was added in one portion followed by the dropwise addition of 26 mL 50 wt% NaOH. Then the solution was allowed to heat up to room temperature and was stirred overnight. Afterwards, the solution was acidified to pH = 1-2 by adding 130 mL H_2O and 66 mL concentrated HCl solution. The acetone was removed by bubbling nitrogen into the reaction mixture to precipitate out the yellowish solid. The formed yellowish precipitate was removed via filtration and was washed with an excess of H_2O. The final product was further purified via recrystallization in a hexane/acetone mixture (1:20).

Yield: 11.20 g (55%)

^{1}H-NMR spectroscopy (300 MHz, $DCCl_3$) δ(ppm) 3.21 (d, *J* = 6.8 Hz, 2H, H_a), 1.98 (q, *J* = 6.7 Hz, 1H, H_b), 1.72 (s, 6H, H_c), 1.01 (d, *J* = 6.7 Hz, 6H, H_d)

4.4.2 Synthesis of 2-formyltetrathiafulvalene[55]

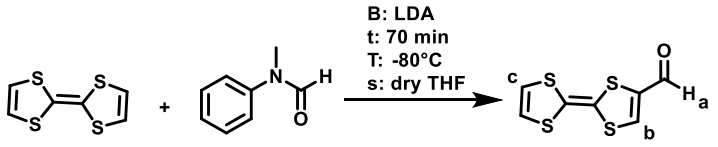

Figure 2.31. Synthetic scheme for the synthesis of 2-formyltetrathiafulvalene with respective ^{1}H-NMR annotations.

A LDA-solution, which was prepared by adding slowly n-BuLi (6.3 mL, 66.87 mmol, 7 eq) to a solution of diisopropylamine (1.8 mL, 12.8 mmol, 1.5 eq) in 40 mL THF, was added dropwise to a solution

containing tetrathiafulvalene (2 g, 9.79 mmol, 1 eq) in 200 mL diethylether/THF at -80 °C under inert atmosphere. The mixture was left for 40 min to stir at -80 °C and subsequently *N*-methylformanilide (2.6 mL, 21.1 mmol, 2eq) was added under the same conditions. The reaction was stirred for another 30 min at -80 °C after which the temperature was allowed to warm up to room temperature. After that, 200 mL of diethylether and 200 mL of a 10 % HCl-solution was added to acidify the aforementioned mixture. The organic phase was collected, washed 3 times with 10 % HCl-solution and dried over $MgSO_4$.The resulting reddish solid was further purified using column chromatography (Silica, eluent: dichloromethane/petroleum ether (50:50))

Yield: 0.89g (40%)

^{1}H-NMR spectroscopy (300 MHz, $DCCl_3$) δ(ppm) 9.50 (s, 1H, H_a), 7.79 (s, 1H, H_b), 6.53 (s, 2H, H_c)

4.4.3 Synthesis of 2-hydroxymethyltetrathiafulvalene[55]

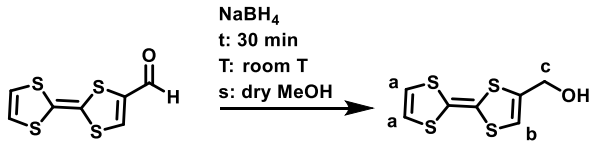

Figure 2.32. Synthetic conditions for the synthesis of 2-hydroxymethyltetrathiafulvalene with respective ^{1}H-NMR annotations.

Sodium borohydride (0.25 g, 6.61 mmol, 2 eq) was slowly added to a stirring solution of 2-formyltetrathiafulvalene (0.80 g, 3.07 mmol, 1 eq) dissolved in 15 mL dried MeOH. The mixture was subsequently stirred for 30 min coloring the solution bright yellow. Next, the mixture was diluted by adding 100 mL of DCM after which the organic phase was three times washed with 100 mL deionized water to remove residual sodium borohydride. The organic phases were collected, dried over $MgSO_4$ and concentrated by rotary evaporation. The resulting oil was purified using column chromatography (silica, eluent: dichloromethane) yielding a bright yellow solid.

Yield: 0.58 g (80%)

^{1}H-NMR spectroscopy (300 MHz, $DCCl_3$) δ(ppm) 6.47 (s, 2H, H_a), 6.32 (t, *J* = 1.3 Hz, 1H, H_b), 4.30 (dd, *J* = 1.2 Hz, 6.1 Hz, 2H, H_c), 3.42 (t, *J* = 6.2 Hz, -OH)

4.4.4 Synthesis of the TTF-CTA agent[56]

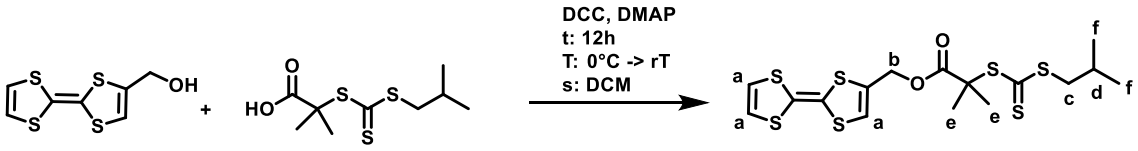

Figure 2.33. Reaction conditions for the synthesis of TTF-CTA with respective ^{1}H-NMR annotations.

A solution containing EDC.HCl (0.59 g, 3.06 mmol, 1.25 eq) and CTA-COOH (0.89 g, 3.53 mmol, 1.5 eq) in 60 mL dry DCM was added dropwise to a solution of TTF-OH in 40 mL dry DCM at 0 °C and under inert atmosphere. Afterwards, the mixture was allowed to warm to room temperature and was stirred overnight. The organic solution was washed with 0.1 M $NaHCO_3$ solution (2 x 100 mL) and brine solution (2 x 100 mL). The collected organic phases were subsequently dried over $MgSO_4$. The crude product was further purified via column chromatography (silica, eluent: DCM/PE (1:1)) affording an orange powder.

Yield: 0.60 g (55%)

^{1}H-NMR spectroscopy (300 MHz, $(CD_3)_2CO$) δ(ppm) 6.56 (m, 3H, H_a), 4.79 (d, *J* = 1.0 Hz, 2H, H_b), 3.17 (d, *J* = 6.8 Hz, 2H, H_c), 1.87 (m, 1H, H_d), 1.60 (s, 6H, H_e), 0.91 (d, *J* = 6.7 Hz, 6H, H_f)

4.5 *Synthesis of* 2-(2-((5-(2-(2-methoxyethoxy)ethoxy)naphthalen-1-yl)oxy)ethoxy)ethyl2-(((isobutylthio)carbonothioyl)-2-methylpropanoate (Napht-CTA)

4.5.1 Synthesis of 1.5-bis[2-(2-(2-hydroxyethoxy)ethoxy)ethoxy]naphthalene (NaphtOH)[57]

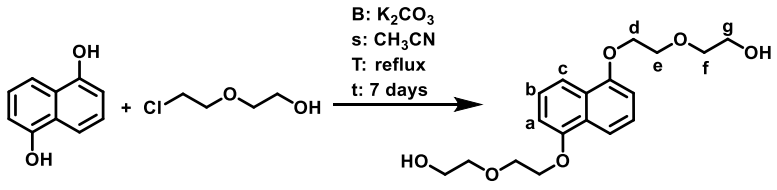

Figure 2.34. Reaction scheme for the synthesis of NaphtOH with respective ^{1}H-NMR annotations.

Potassium carbonate (36.53 g, 264.36 mmol, 4 eq) was added to a vigorously stirring solution of 1,5-dihydroxynaphthalene (10.58 g, 66.11 mmol, 1 eq) dissolved in 200 mL CH_3CN. This mixture was refluxed for 30 min under N_2. 2-(2-Chloroethoxy)ethanol (16.37 g, 132.03 mmol, 2 eq) in 100 mL CH_3CN was added dropwise to the mixture which was first allowed to cool down to room temperature. The reaction was refluxed for 7 days. The potassium carbonate was removed by filtration and washed with CH_3CN. The collected filtrate was evaporated under reduced pressure and the remaining residue was dissolved in DCM. The organic phase was then washed with a 10 % HCl aqueous solution, dried on $MgSO_4$ and purified via a recrystallization (overnight) in cold EtOH.

Yield: 9.00 g (45%).

^{1}H-NMR spectroscopy (300 MHz, $DCCl_3$) δ(ppm) 7.86 (d, *J* = 8.5 Hz, 2H, H_a), 7.35 (t, *J* = 8.5 Hz, 2H, H_b), 6.84 (d, *J* = 7.6 Hz, 2H, H_c), 4.27 (m , 4H, H_d), 3.96 (m, 4H, H_e), 3.73 (m, 8H, H_f+H_g)

4.5.2 Synthesis of 2-[2-[[5-[2-(2-methoxyethoxy)ethoxy]-1-naphthalenyl]oxy]ethoxy] (NaphtOMe)[45]

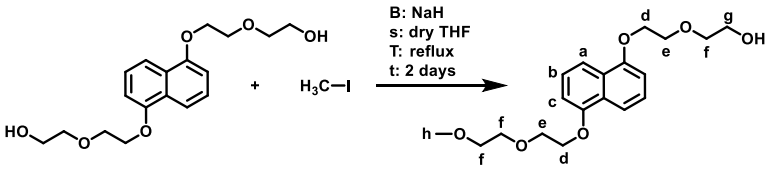

Figure 2.35. Synthetic scheme for the synthesis of NaphtOMe with respective ^{1}H-NMR annotations.

A solution of Napht-OH (9.20 g, 27.36 mmol, 1 eq) dissolved in 50 mL dry THF was added dropwise over a period of 30 min to a suspension of NaH (0.95 g, 0.04 mmol, 1.3 eq) in 50 mL dry THF. The resulting mixture was stirred and heated to reflux (80 °C) for 30 min under Ar_2. Afterwards, MeI (3.90 g, 27 mmol, 1 eq) dissolved in 30 ml THF was added dropwise at room temperature. The reaction was heated to reflux under Ar and was monitored via TLC (Silica, petroleum ether/acetone 7/3, Rf_{dubble}: 0.69, Rf_{mono}: 0.37 and $Rf_{reagent}$: 0.20), which showed nearly full conversion of Napht-OH after 2 days. Residual NaH was deactivated by the addition of 10 mL MeOH after which the solvent was evaporated under reduced pressure. The residue was dissolved in 100 mL CH_2Cl_2, washed with saturated Na_2CO_3 solution and water, dried with $MgSO_4$ and subsequently dried under vacuum. The resulting yellowish solid was further purified using a gradient column chromatography (silica, starting eluent: acetone/petroleum ether (30:70) to end with pure acetone).

Yield: 2.75 g (29%).

^{1}H-NMR spectroscopy (300 MHz, $DCCl_3$) δ(ppm) 7.79 (t, *J* = 8.0 Hz, 2H, H_a), 7.28 (td, *J* = 8.0 Hz, 2.4 Hz, 2H, H_b), 6.77 (d, *J* = 7.7 Hz, 2H, H_c), 4.23 (m , 4H, H_d), 3.92 (m, 4H, H_e), 3.64-3.73 (m, 6H, H_f), 3.52 (m, 2H, H_g), 3.33 (s, 3H, H_h)

4.5.3 Synthesis of Napht-CTA[46]

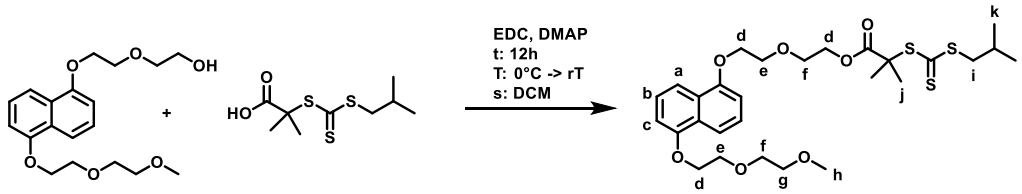

Figure 2.36. Reaction conditions for the synthesis of Napht-CTA with respective ^{1}H-NMR annotations.

A solution of EDC.HCl (0.8 g, 4.20 mmol, 1.5 eq), DMAP (0.5 g, 4.13 mmol, 1.5 eq) and CTA-COOH (0.72 g, 3.00 mmol, 1 eq) in 25 ml DCM was added dropwise to Napht-OMe (1.75 g, 3 mmol, 1 eq) dissolved in 25 mL DCM. The reaction was stirred for 12 h at 0 °C under inert atmosphere after which the mixture was allowed to heat up to room temperature. In a next step, the organic solution was washed with 0.1

M HCl, 0.1M $NaHCO_3$, water and was dried with $MgSO_4$. The remaining solvent was removed under vacuo after which the crude product was purified in a final step using column chromatography (SiO_2, acetone/petroleum ether (40:60) affording the pure product as a yellowish oil.

Yield: 1.14 g (65%)

^{1}H-NMR spectroscopy (300 MHz, $DCCl_3$) δ(ppm) 7.79 (dd, *J* = 8.6 Hz, 3.6 Hz, 2H, H_a), 7.26 (td, *J* = 8.3 Hz, 1.6 Hz, 2H, H_b), 6.76 (d, *J* = 8.0 Hz, 2H, H_c), 4.23 (m, 6H, H_d), 3.99 (m, 4H, He), 3.81 (m, 4H, H_f), 3.60 (m, 2H, H_g), 3.40 (s, 3H, H_h), 3.16 (d, *J* = 6.8 Hz, 2H, Hi), 1.69 (s, 6H, H_j), 0.96 (d, *J* = 6.7 Hz, 6H, H_k)

4.6 RAFT-polymerizations of Napht-CTA with DMAc

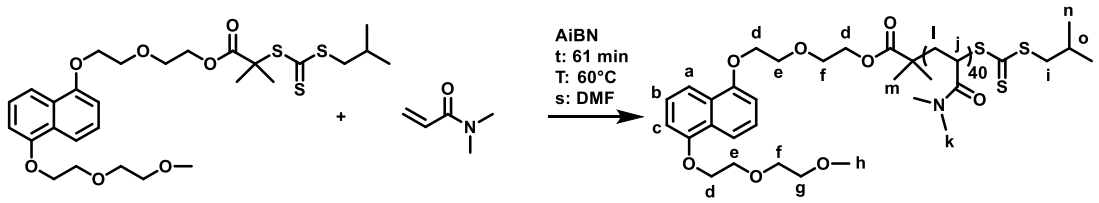

Figure 2.37. Synthesis conditions for the RAFT-polylmerization of DMAc using Napht-CTA with respective ^{1}H-NMR annotations.

DMAc (1.5 g, 15 mmol, 70 eq), Napht-CTA (0.125 g, 0.21 mmol, 1 eq) and AIBN (0.011 g, 0.064 mmol, 0.3 eq) were dissolved in 3.5 mL DMF. After dissolving and degassing during three consecutive freeze-pump-thaw cycles, the mixture was heated to 60 °C for 81 min. The polymerization was quenched by immersing the flask into an ice-bath allowing the reaction mixture to cool down to room temperature. In the next step, the polymer was diluted by adding 5-10 mL ethyl acetate and subsequently purified by precipitating the mixture into 100 mL ice-cold diethyl ether. The crude polymer was dissolved in 5 mL ethyl acetate and precipitated again in 100 mL ice-cold diethyl ether. This procedure was repeated for at least two times generating the pure polymer as a white fluffy powder.

Conversion: 60% (GC with DMF as internal standard), **SEC (DMA + 50 mM LiCl, PMMA-std)**: Mn = 5300 g/mol, Đ = 1.10

^{1}H-NMR spectroscopy (300 MHz, $CDCl_3$) δ(ppm) 7.85 (t, *J* = 7.6 Hz, 2H, H_a), 7.40-7.29 (m, 2H, H_b), 6.84 (d, *J* = 7.6 Hz, 2H, H_c), 4.38-4.12 (m, 6H, H_d), 4.08-3.91 (m, 4H, H_e), 3.90-3.71 (m, 4H, H_f), 3.66-3.56 (m, 2H, H_g), 3.40 (s, 3H, H_h), 3.27 (d, J = 6.7 Hz, 2H, H_i), 3.2-2.2 (broad, H_j+H_k), 1.9-1.4 (broad, H_i+H_m), 1.1-0.9 (broad, H_n+H_o)

4.7 RAFT-polymerization of TTF-CTA with DMAc

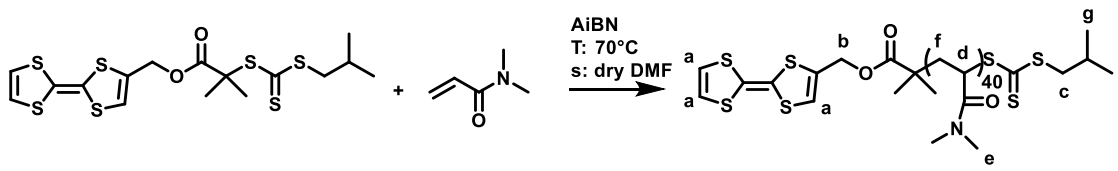

Figure 2.38. Reaction conditions for the RAFT-polymerizations of DMAc using TTF-CTA with respective ^{1}H-NMR annotations.

DMAc (3.05 g, 30.76 mmol, 100 eq), TTF-CTA (0.14 g, 0.305 mmol, 1 eq) and AIBN (0.043 g, 0.256 mmol, 0.3 eq) were dissolved in 3 mL DMF. After dissolving and degassing during three consecutive freeze-pump-thaw cycles, the mixture was heated to 70 °C for 70 min. The polymerization was quenched by immersing the flask into an ice-bath allowing the reaction mixture to cool down to room temperature. In the next step, the polymer was diluted by adding 5-10 mL ethyl acetate and subsequently purified by precipitating the mixture into 100 mL ice-cold diethyl ether. The crude polymer was dissolved in 5 mL ethyl acetate and precipitated again in 100 mL ice-cold diethyl ether. This procedure was repeated for at least two times generating the pure polymer as a white fluffy powder.

Conversion: 40% (^{1}H-NMR), **SEC (DMA + 50 mM LiCl, PMMA-std)**: Mn = 3000 g/mol, Đ = 1.05

^{1}H-NMR spectroscopy (300 MHz, CH_3CN) δ(ppm) 6.7-6.5 (broad, H_a), 4.9-4.7 (broad, H_b), 3.4-3.3 (broad, H_c), 3.2-2.2 (broad, H_d+H_e), 1.4-1.9 (broad, H_f), 1.4-1.1 (broad, H_g)

4.8 Procedure continuous variation method (Job Plot)

The stoichiometry of the host-guest complexation was determined using Job's method of continuous variation. A stock solution was prepared for each complementary recognitions motif dissolved in D_2O in a 10 mL vial. The appropriate amount from the stock solution was transferred to the NMR tube in which the total concentration of the recognition motifs was kept constant at 2 mM. The molar fraction of the host and guest was varied between 0 and 1. The changes in chemical shift (ppm) was multiplied by the molar fraction and plotted against the molar fraction to receive the Job plot.

4.9 Procedure Isothermal titration calorimetry (ITC) experiment

ITC experiments were performed at 15 °C using a nano-ITC titration calorimeter from TA Instruments with a standard sample cell volume of 1 mL, following standard procedures. A 250 µL injection syringe was used with stirring at 400 rpm. Host molecules were dissolved in Milli-Q water and the solutions were degassed gently under vacuum before use. Each titration comprised an initial 2 µL preinjection followed by 24 × 10 µL injections of BBB (8 mM) into Napht-PDMAc or TTF-PDMAc solutions (≈ 2 mM).

4.10 Procedure UV-VIS spectrophotometric titration experiment

UV-VIS titration was performed by adding via microliter pipettes solutions containing either the host (BBB) or the guest (Napht-PDMAc or TTF-PDMAc) to a solution of the complementary guest (Napht-PDMAc or TTF-PDMAc) or host in a 1 cm disposable cuvette. Deionized water was used as solvent for UV-VIS titration. UV-ViIS scanning conditions were as follows: Scanning rate = 300 nm/min, bandwidth = 0.5 nm, response time = 0.1 s, accumulations = 1 scan.

5 References

1. Steed, J. W.; Atwood, J. L. *Supramolecular Chemistry: Second Edition*; **2009**.
2. J. M. Lehn *Angew. Chem. Int. Ed.* **1985**, *24*, 799.
3. Oshovsky, G. V.; Reinhoudt, D. N.; Verboom, W. *Angew. Chem. Int. Ed.* **2007**, *46*, 2366.
4. Theato, P.; Klok, H. A. *Functional Polymers by Post-Polymerization Modification*; Theato, P.; Klok, H.-A., Eds.; Wiley-VCH Verlag GmbH & Co. KGaA: Weinheim, Germany, **2012**.
5. Scherman, O. A. *Nat. Chem.* **2009**, *1*, 524.
6. Lamping, S.; Stricker, L.; Ravoo, B. J. *Polym. Chem.* **2019**, *10*, 683.
7. Nakahata, M.; Takashima, Y.; Harada, A. *Macromol. Rapid Commun.* **2016**, *37*, 86.
8. Xiao, T.; Xu, L.; Zhou, L.; Sun, X. Q.; Lin, C.; Wang, L. *J. Mater. Chem. B* **2019**, *7*, 1526.
9. Mantooth, S. M.; Munoz-Robles, B. G.; Webber, M. J. *Macromol. Biosci.* **2019**, *19*, 1.
10. Ji, X.; Ahmed, M.; Long, L.; Khashab, N. M.; Huang, F.; Sessler, J. L. *Chem. Soc. Rev.* **2019**, *48*, 2682.
11. Nakahata, M.; Takashima, Y.; Yamaguchi, H.; Harada, A. *Nat. Commun.* **2011**, *2*.
12. Kakuta, T.; Takashima, Y.; Nakahata, M.; Otsubo, M.; Yamaguchi, H.; Harada, A. *Adv. Mater.* **2013**, *25*, 2849.
13. Wang, K.; Wang, C. Y.; Wang, Y.; Li, H.; Bao, C. Y.; Liu, J. Y.; Zhang, S. X. A.; Yang, Y. W. *Chem. Commun.* **2013**, *49*, 10528.
14. Li, H.; Yang, Y.; Xu, F.; Liang, T.; Wen, H.; Tian, W. *Chem. Commun.* **2019**, *55*, 271.
15. Ni, M.; Zhang, N.; Xia, W.; Wu, X.; Yao, C.; Liu, X.; Hu, X. Y.; Lin, C.; Wang, L. *J. Am. Chem. Soc.* **2016**, *138*, 6643.
16. Zheng, B.; Wang, F.; Dong, S.; Huang, F. *Chem. Soc. Rev.* **2012**, *41*, 1621.
17. Appel, E. A.; Loh, X. J.; Jones, S. T.; Biedermann, F.; Dreiss, C. A.; Scherman, O. A. *J. Am. Chem. Soc.* **2012**, *134*, 11767.
18. Das, D.; Scherman, O. A. *Isr. J. Chem.* **2011**, *51*, 537.
19. Hu, J.; Liu, S. *Acc. Chem. Res.* **2014**, *47*, 2084.
20. Rosa, V. R. De; Woisel, P.; Hoogenboom, R. *Mater. Today* **2016**, *19*, 44.
21. Xiao, T.; Xu, L.; Zhou, L.; Sun, X. Q.; Lin, C.; Wang, L. *J. Mater. Chem. B* **2019**, *7*, 1526.
22. Yan, X.; Wang, F.; Zheng, B.; Huang, F. *Chem. Soc. Rev.* **2012**, *41*, 6042.
23. Ji, X.; Chen, J.; Chi, X.; Huang, F. *ACS Macro Lett.* **2014**, *3*, 110.
24. Ahn, Y.; Jang, Y.; Selvapalam, N.; Yun, G.; Kim, K. *Angew. Chem. Int. Ed.* **2013**, *52*, 3140.
25. Guan, Y.; Zhao, H. B.; Yu, L. X.; Chen, S. C.; Wang, Y. Z. *RSC Adv.* **2014**, *4*, 4955.
26. Asakawa, M.; Ashton, P. R.; Menzer, S.; Raymo, F. M.; Stoddart, J. F.; White, A. J. P.; Williams, D. J. *Chem. - A Eur. J.* **1996**, *2*, 877.
27. Coskun, A.; Spruell, J. M.; Barin, G.; Fahrenbach, A. C.; Forgan, R. S.; Colvin, M. T.; Carmieli, R.;

Benítez, D.; Tkatchouk, E.; Friedman, D. C.; Sarjeant, A. A.; Wasielewski, M. R.; Goddard, W. A.; Stoddart, J. F. *J. Am. Chem. Soc.* **2011**, *133*, 4538.

28. Spruell, J. M.; Coskun, A.; Friedman, D. C.; Forgan, R. S.; Sarjeant, A. A.; Trabolsi, A.; Fahrenbach, A. C.; Barin, G.; Paxton, W. F.; Dey, S. K.; Olson, M. A.; Benítez, D.; Tkatchouk, E.; Colvin, M. T.; Carmielli, R.; Caldwell, S. T.; Rosair, G. M.; Hewage, S. G.; Duclairoir, F.; Seymour, J. L.; Slawin, A. M. Z.; Goddard, W. A.; Wasielewski, M. R.; Cooke, G.; Stoddart, J. F. *Nat. Chem.* **2010**, *2*, 870.

29. Frasconi, M.; Fernando, I. R.; Wu, Y.; Liu, Z.; Liu, W. G.; Dyar, S. M.; Barin, G.; Wasielewski, M. R.; Goddard, W. A.; Stoddart, J. F. *J. Am. Chem. Soc.* **2015**, *137*, 11057.

30. Lipke, M. C.; Cheng, T.; Wu, Y.; Arslan, H.; Xiao, H.; Wasielewski, M. R.; Goddard, W. A.; Stoddart, J. F. *J. Am. Chem. Soc.* **2017**, *139*, 3986.

31. Barin, G.; Coskun, A.; Friedman, D. C.; Olson, M. A.; Colvin, M. T.; Carmielli, R.; Dey, S. K.; Bozdemir, O. A.; Wasielewski, M. R.; Stoddart, J. F. *Chem. - A Eur. J.* **2011**, *17*, 213.

32. Sun, J.; Wu, Y.; Wang, Y.; Liu, Z.; Cheng, C.; Hartlieb, K. J.; Wasielewski, M. R.; Stoddart, J. F. *J. Am. Chem. Soc.* **2015**, *137*, 13484.

33. Balzani, V.; Becher, J.; Credi, A.; Nielsen, M. B.; Raymo, F. M.; Stoddart, J. F.; Talarico, A. M.; Venturi, M. *J. Org. Chem.* **2000**, *65*, 1947.

34. Ashton, P. R.; Menzer, S.; Raymo, F. M.; Shimizu, G. K. H.; Stoddart, J. F.; Williamsb, D. J. *Chem. Commun.* **1996**, 487.

35. Bigot, J.; Fournier, D.; Lyskawa, J.; Marmin, T.; Cazaux, F.; Cooke, G.; Woisel, P. *Polym. Chem.* **2010**, *1*, 1024.

36. Bigot, J.; Bria, M.; Caldwell, S. T.; Cazaux, F.; Cooper, A.; Charleux, B.; Cooke, G.; Fitzpatrick, B.; Fournier, D.; Lyskawa, J.; Nutley, M.; Stoffelbach, F.; Woisel, P. *Chem. Commun.* **2009**, 5266.

37. Moad, G.; Rizzardo, E.; Thang, S. H. In *Fundamentals of Controlled/Living Radical Polymerization*; Tsarevsky, N. V.; Sumerlin, B. S., Eds.; the Royal Society of Chemistry, **2013**; pp 205.

38. Moad, G.; Rizzardo, E.; Thong, S. *J. Am. Chem. Soc.* **2002**, *43*, 114.

39. Perrier, S.; Barner-Kowollik, C.; Quinn, J. F.; Vana, P.; Davis, T. P. *Macromolecules* **2002**, *35*, 8300.

40. Chong, B. Y. K.; Krstina, J.; Le, T. P. T.; Moad, G.; Postma, A.; Rizzardo, E.; Thang, S. H. *Macromolecules* **2003**, *36*, 2256.

41. Bigot, J.; Charleux, B.; Cooke, G.; Delattre, F.; Fournier, D.; Lyskawa, J.; Stoffelbach, F.; Woisel, P. *Macromolecules* **2010**, *43*, 82.

42. Bigot, J.; Charleux, B.; Cooke, G.; Delattre, F.; Fournier, D.; Lyskawa, J.; Sambe, L.; Stoffelbach, F.; Woisel, P. *J. Am. Chem. Soc.* **2010**, *132*, 10796.

43. Kaplan, M. L.; Haddon, R. C.; Wudl, F.; Feit, E. D. *J. Org. Chem.* **1978**, *43*, 4642.

44. Pittman, C. U.; Mitsuru, U.; Liang, Y. F. *J. Org. Chem.* **1979**, *44*, 3639.

45. Sambe, L.; Delarosa, V. R.; Belal, K.; Stoffelbach, F.; Lyskawa, J.; Delattre, F.; Bria, M.; Cooke, G.; Hoogenboom, R.; Woisel, P. *Angew. Chem. Int. Ed.* **2014**, *53*, 5044.

46. Malfait, A.; Coumes, F.; Fournier, D.; Cooke, G.; Woisel, P. *Eur. Polym. J.* **2015**, *69*, 552.

47. Ferrazza, R.; Rossi, B.; Guella, G. *J. Phys. Chem. B* **2014**, *118*, 7147.

48. Thordarson, P. *Chem. Soc. Rev.* **2011**, *40*, 1305.

49. Sambe, L.; Belal, K.; Stoffelbach, F.; Lyskawa, J.; Delattre, F.; Bria, M.; Sauvage, F. X.; Sliwa, M.; Humblot, V.; Charleux, B.; Cooke, G.; Woisel, P. *Polym. Chem.* **2014**, *5*, 1031.

50. Bigot, J.; Charleux, B.; Cooke, G.; Fournier, D.; Lyskawa, J.; Woisel, P. *Macromolecules* **2010**, *43*, 82.

51. Meng, B.; Song, H.; Chen, X.; Xie, Z.; Liu, J.; Wang, L. *Macromolecules* **2015**, *48*, 4357.

52. Amabilino, D. B.; Ashton, P. R.; Brown, C. L.; Newton, S. P.; Pietraszkiewicz, M.; Philp, D.; Raymo, F. M.; Reder, A. S.; Rutland, M. T.; Spencer, N.; Stoddart, J. F.; Córdova, E.; Godínez, L. A.; Goodnow, T. T.; Kaifer, A. E.; Slawin, A. M. Z.; Williams, D. J. *J. Am. Chem. Soc.* **1995**, *117*, 1271.

53. Wu, Y.; Liu, S.; Tao, Y.; Ma, C.; Zhang, Y.; Xu, J.; Wei, Y. *ACS Appl. Mater. Interfaces* **2014**, *6*, 1470.

54. Qiu, X. P.; Tanaka, F.; Winnik, F. M. *Macromolecules* **2007**, *40*, 7069.

55. Garin, J.; Orduna, J.; Uriel, S.; Moore, A. J.; Bryce, M. R.; Wegener, S.; Yufit, D. S.; Howard, J. A. K. *ChemInform* **2010**, *25*, no.

56. Bigot, J.; Charleux, B.; Cooke, G.; Delattre, F.; Fournier, D.; Lyskawa, J.; Stoffelbach, F.; Woisel, P. *Macromolecules* **2010**, *43*, 82.

57. Kieran, A. L.; Pascu, S. I.; Jarrosson, T.; Gunter, M. J.; Sanders, J. K. M. *Chem. Commun.* **2005**, 1842.

Chapter 3. Supramolecular hydrogels with time memory function

Abstract

This third chapter will focus on the creation of smart polymeric materials by incorporating blue box -naphthalene (BB-Napht) host-guest complexes in a more complex 3D-matrix, namely polymeric hydrogels. In order to create a hydrogel capable of programmable volume changes, a poly(*N*-isopropylacrylamide) hydrogel functionalized with naphthalene units (Napht-co-PNIPAM hydrogel) was synthesized by using free radical polymerization of *N*-isopropylacrylamide (NIPAm), Naphthalene functionalized with an acrylamide group (Napht.Ac) and *N,N'*-mehtylenebisacrylamide as cross-linker in various monomer ratios. The dynamic character of the BB-Napht assembly introduces a large hysteresis window of the thermo-responsive volume phase transition in the system which was thoroughly investigated via DSC and NMR spectroscopy. When heated above its volume phase transition temperature (VPTT), the collapse of the hydrogels causes disassembly of the complex, expelling the BB from the hydrogel. The rate of releasing the BB, i.e. diffusion out of the collapsed hydrogel, was found to be kinetically controlled by the solution temperature and heating time. It was demonstrated that this difference in release of BB influences the hydrophobicity of the resulting hydrogel inducing dimensional changes upon cooling. By careful monitoring of these variations, the system can report how long it was heated at a known temperature. To the best of our knowledge, this is the first reported polymeric sensor device that contains a time memory function.

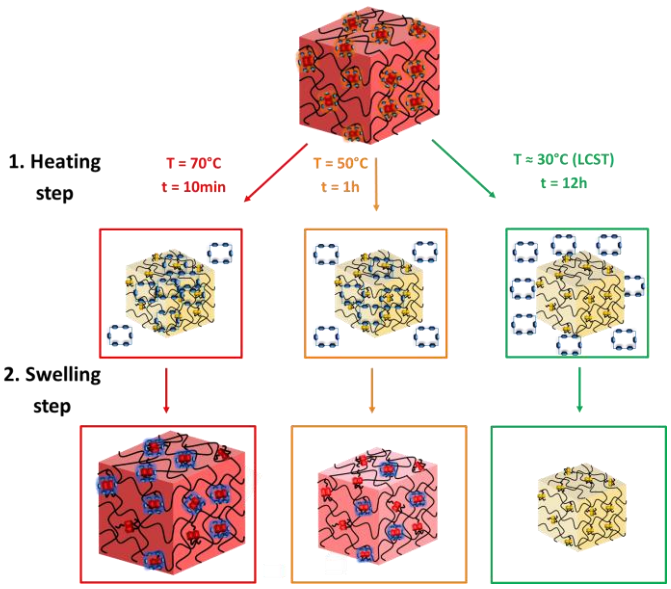

Contributing authors:

Khaled Belal for the synthesis of the different Napht-co-PNIPAm hydrogels with different mol% Napht together with their swelling tests and DSC measurements.

Parts of this chapter will be published as:

L. De Smet, K. Belal, J. Lyskawa, R. Hoogenboom and P. Woisel. Supramolecular hydrogels with time and temperature memory function**. 2019** *Manuscript in preparation.*

1 Introduction

Smart or stimuli-responsive materials that are capable of altering their properties and function in response to small external environmental changes such as fluctuations in temperature[1–4], pH[5–8], electric or magnetic fields[9–11], solvent[12] or chemicals[13,14] and light[15–19] have been the focus of research in several fields. A wide range of artificial multi-responsive polymeric structures have been reported, including star co-polymers[20–22] and nanoparticles[23,24], with hydrogels being the most prominent example. Hydrogels are three-dimensional networks of cross-linked macromolecules capable of entrapping a substantial amount of water. Responsive hydrogels can undergo reversible volume phase transitions, i.e. swelling and shrinking in aqueous solution, or sol-to-gel phase transitions when subjected to various stimuli. A popular thermo-responsive hydrogel is cross-linked poly(*N*-isopropylacylamide) (PNIPAm) and its derivatives. The LCST character of the PNIPAm introduces a shrinkage of the hydrogel when it is heated above the volume phase transition temperature (VPTT), caused by the expulsion of the water molecules from the hydrogel. Upon cooling, the hydrogen bonds between the water molecules and the PNIPAM side chains are reformed resulting in reswelling of the hydrogel. This temperature dependent volume change is used in many different applications ranging from biomedical applications[4,25,26] such as drug delivery systems and tissue engineering to sensors[27–29] and actuators[30,31].

An important parameter of thermo-responsive hydrogels is the hysteresis of the thermal phase transition, which can be defined as the difference between the shrinkage and reswelling temperatures. By changing the inter- or intramolecular interactions of the polymer chains, this difference between the VPTT of the heating and cooling cycles can be controlled.[32,33] Literature reports have shown that if this thermal hysteresis is very large, it can be used to allow the hydrogel to memorize changes in its environment, resulting in multiple swelling degrees of the hydrogel to be stable at room temperature.[34–37] Our group has reported one approach to improve or induce this large hysteresis window by introducing host-guest complexations in a linear soluble PNIPAm chain.[38,39] By functionalizing the polymer with naphthalene moieties and subsequently allowing the formation of donor-acceptor complexes with cyclobis(paraquat-*p*-phenylene), also called Blue Box (BB), a large hysteresis of the thermo-responsive LCST phase transition is introduced. Upon heating this system above its transition temperature, the polymer forms insoluble aggregates leading to disruption of the BB-Napht assembly and release of the BB making the polymer more hydrophobic. During subsequent cooling, the rehydration of these more hydrophobic uncomplexed polymer chains now becomes more difficult, significantly lowering the clearance point temperature. This means that depending on the assembly and disassembly of the incorporated host-guest complexation, the hydrophobicity of the

polymer chain can be altered leading to different collapse and redissolution temperatures with a large hysteresis window enabling a thermal sensor with a memory function.

This straightforward supramolecular strategy was here exploited for the creation of the next generation polymeric memory devices with potential time memory function. In this chapter, a PNIPAm hydrogel is designed containing naphthalene units that can form interactions with the tetracationic host molecule BB, inducing an additional uptake of water upon complexation. When heated at a temperature above its VPTT, the shrinking of the hydrogel induces the disassembly of the BB-Napht complexes, leading to a thermal hysteresis as described in our previous work for the soluble polymer system. However, depending on the exposure time at a known temperature, the hydrogel will expel free BB at different rates as it depends on the diffusion of free BB out of the hydrogel. The kinetically controlled amount of BB released and hence the time at a certain temperature, will control the swelling degree during rehydration of the hydrogel upon cooling as this is controlled by the amount of hydrophilic BB that is retained in the hydrogel. These changes could therefore be used to create a polymeric sensor with a potential erasable time memory function.

2 Results and discussion

2.1 Synthesis of the Napht-co-PNIPAm hydrogels

As a first step in this work, the naphthalene acrylamide monomer (Napht.Ac) was prepared starting from the commercially available 1.5-dihydroxynaphthalene (DNP) based on the synthesis route described by Lena Sambe et al.[38] In this synthesis route displayed in Figure 3.1, two glycol linkers where incorporated on both alcohol groups of DNP after which these alcohol groups were asymmetrically modified through consecutive methylation using methyl iodide and amination using a two-step procedure involving the generation and reduction of a phthalimide intermediate. Finally, the acrylamide was formed using acyl substitution with acryloyl chloride. The glycol linkers on the naphthalene monomer are incorporated for aqueous solubility and to further stabilize the [2]pseudorotaxane between the DNP and the BB host molecule. The oxygen atoms present in the glycol chain can interact with the acidic alfa-protons of the host molecule by forming a hydrogen bond providing an extra thermodynamic stability upon assembly.[40]

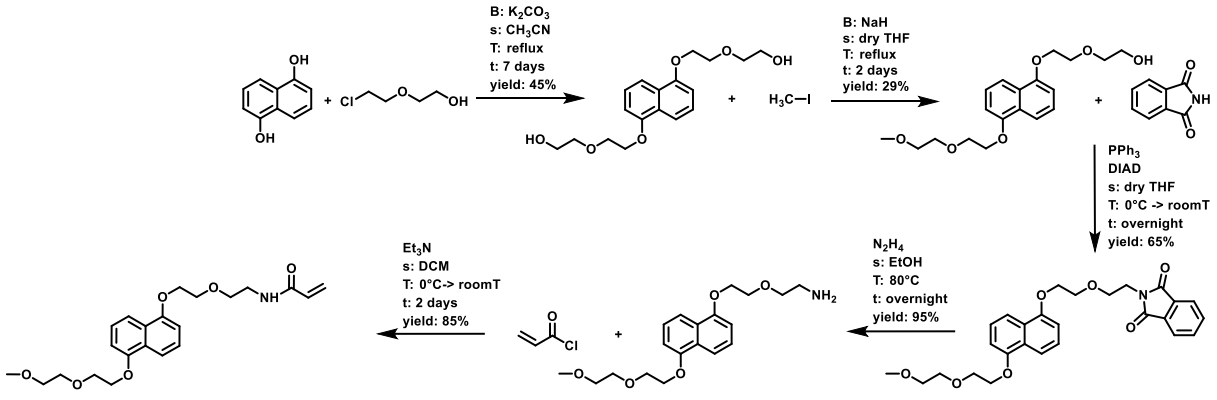

Figure 3.1. synthesis scheme of Napht.Ac.

The synthetic design of the Napht-co-PNIPAm hydrogel is depicted in Figure 3.2, which shows that the hydrogel system was prepared by free radical co-polymerization (FRP) of the Napht.Ac and *N*-isopropylacrylamide (NIPAm) in the presence of the cross-linker *N*,*N*'-methylene-bisacrylamide (MBA) initiated by potassium persulfate (KPS). Owing to the low aqueous solubility of the Napht-monomer, organogels were first synthesized in dimethyl sulfoxide (DMSO), subsequently washed in acetone, dried and allowed to swell in water to give the resulting Napht-co-PNIPAm hydrogel. The polymerization was done in a mold created by two rectangular shaped glass plates separated by teflon tubing with 4.0 mm diameter reinforced with copper wires. Hydrogels were synthesized with different amounts of Napht-Ac. to prepare hydrogels with 0, 1.5, 3, 6 and 12 mol% naphthalene units. The molar percentage of the initiator and cross-linking agent was kept constant at 1%.

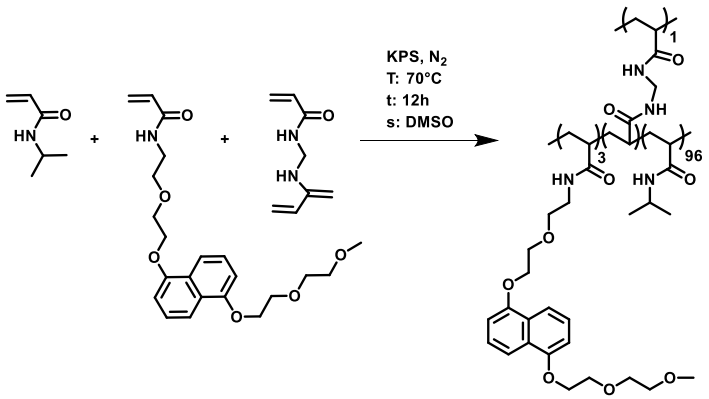

Figure 3.2. Synthetic scheme for the synthesis of the Napht-co-PNIPAm organogels.

It has been reported that gel-phase samples cause peak broadening in normal solution NMR spectroscopy as the polymer chains do not have sufficient internal mobility to average the direct polar coupling between nuclear spins.[41–43] Furthermore, the difference in magnetic susceptibility will induce variations in the magnetic field which also results in additional peak widening. However, these effects can be reduced by using high resolution magic angle spinning (HR-MAS) NMR spectroscopy. In this case the sample is rapidly rotated at an angle of 54.7° with respect to the static magnetic field, which

significantly decreases the line broadening for semi-solid samples making it possible to characterize our hydrogels via HR-MAS NMR spectroscopy.[44] A sample was prepared by soaking 3-4 mg of dried hydrogel in 40 µL deuterated DMSO for 24h before measuring. The spectrum that was recorded for 3% Napht-co-PNIPAm (3 mol% Napht.Ac feed) confirmed the presence of the characteristic signals attributed to the naphthalene moiety and the PNIPAm backbone as assigned in Figure 3.3.

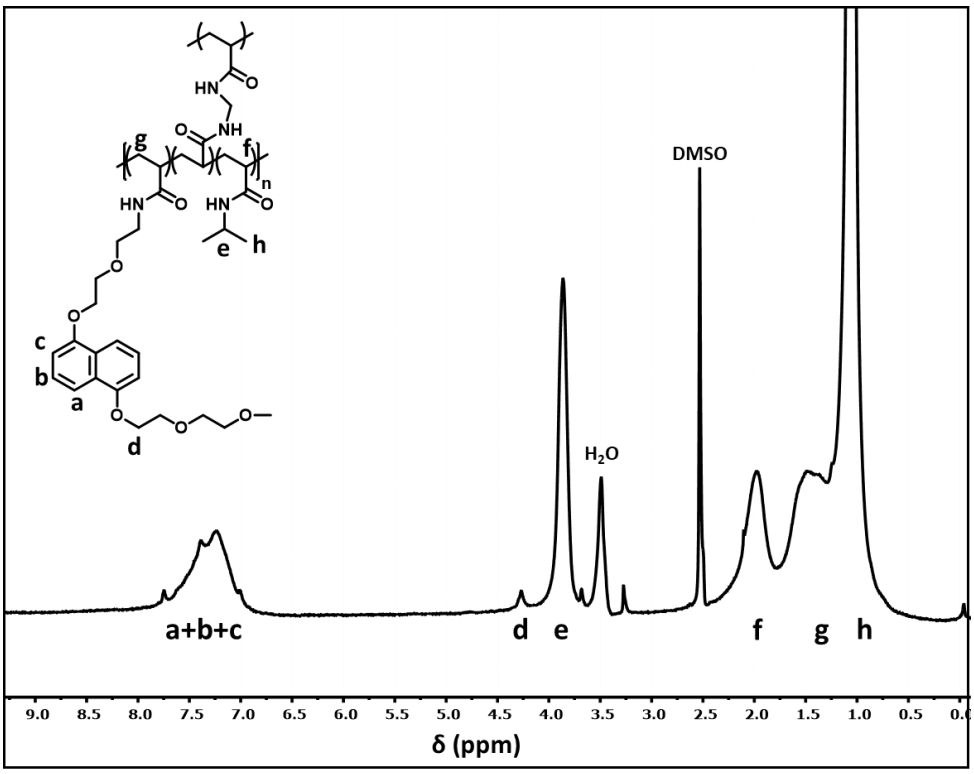

Figure 3.3. HR-MAS ^{1}H-NMR spectrum of an 3% Napht-co-PNIPAM hydrogel calibrated on solvent signal (DMSO-6d).

Although, the aromatic peaks corresponding with the naphthalene were overlapping with the NH-signal of the polymer sidechains, it was still possible to estimate the molar fraction of naphthalene (mol% $_{napht.Ac}$) inside the hydrogel by HR-MAS ^{1}H-NMR spectroscopy. For this calculation the more defined signals of the methylene (H_d) next to the dihydroxynaphthalene and H_e related to the C-H of the isopropyl group of PNIPAm were used in the following equation 3.1.

Equation 3.1

$$mol\%_{Napht.Ac} = \frac{U_{Napht.Ac}}{U_{Backbone}}$$

with:

$$U_{Backbone} = U_{Napht.Ac} + U_{NIPAm} = \frac{I_d}{4} + I_e$$

$$U_{Napht.Ac} = \frac{I_d}{4}$$

$U_{Napht.Ac}$ is the units Napht.Ac incorporated in the hydrogel and $U_{Backbone}$ the units of the hydrogel backbone which consist mainly out of PNIPAm and Napht.Ac. The concentration of the naphthtalene groups inside the 3% Napht-co-PNIPAm was estimated to be 2.55 ± 0.23% using this calculation. Although, this indicates that slightly lower amounts of Napht units are integrated than expected, the difference is rather small assuming that most added Napht.Ac monomer is incorporated during synthesis.

2.2 Complexation of the Napht-co-PNIPAm hydrogels with BB

From literature, it is well known that naphthalene can form inclusion donor-acceptor host-guest assemblies with BB.[45–49] Therefore, the ability of the Napht-co-PNIPAm hydrogels to form complexes with the BB was investigated as well as the influence of the complexation on the water uptake. These tests were performed on rectangular pieces (1.0 cm by 0.5 cm by 0.5 cm) of Napht-co-PNIPAm hydrogel to ensure a high surface/bulk ratio to facilitate the diffusion of BB into the hydrogel to complex with the embedded naphthalene. In a first step, a solution containing three equivalents of BB in a minimum amount of water (1 mL) was added to the hydrogel, which was left to complex for approximately 24 hours at 5 °C. The amount of BB was calculated using the weight percentage embedded naphthalene (wt% $_{Napht.Ac}$) which was estimated to be equal to 11% for the 3% Napht-co-PNIPAm hydrogel by using the following equation 3.2:

Equation 3.2
$$wt\%_{Napht.Ac} = \frac{mol\%_{Napht.Ac} * MW_{Napht.Ac}}{mol\%_{Napht.Ac} * MW_{Napht.Ac} + mol\%_{NIPAm} * MW_{NIPAm}}$$

with $MW_{Napht.Ac}$ and MW_{NIPAm} the molecular weight of the Napht.AC monomer (430.5 g/mol) and the NIPAM (99.13 g/mol), respectively. The molar percentage of Napht.Ac ($mol\%_{Napht.Ac}$) and NIPAM ($mol\%_{NIPAM}$) in the hydrogel was calculated using the results received from the HR-MAS ^{1}H-NMR spectrum discussed in section 2.1. By employing this value in the underlying equation 3.3, we were able to calculate the amount of BB needed for the complexation.

Equation 3.3
$$m_{BB} = MW_{BB} * Eq_{BB} \frac{m_{Dry} * wt\%_{Napht.Ac}}{MW_{Napht.AC}}$$

With MW_{BB} the molecular weight of BB (662.5 g/mol), Eq_{BB} the desired equivalents of BB added to the Napht-co-PNIPAm hydrogel (here three equivalents), m_{dry} the mass of the dried hydrogel piece, $wt\%_{Napht\text{-}monomer}$ the weight percentage of the incorporated naphthalene units (11%) and $MW_{Napht.Ac}$ the molecular weight of the naphthalene monomer (430.5 g/mol).

Upon the addition of the host molecule BB to the swollen 3% Napht-PDMAc, the typical purple color of the BB-napht donor-acceptor complex was immediately visible on the surface of the gel which diffused homogenously through the hydrogel with time as shown in Figure 3.4.

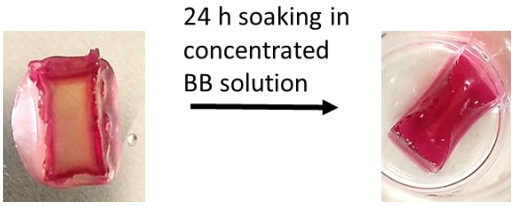

Figure 3.4. Pictures showing the homogenous diffusion of BB through the hydrogel by comparing a picture of the hydrogel submerged for several minutes in the concentrated BB solution (left) and soaked for 24h in the concentrated BB solution (right).

In a final step, an excess of water was added to the now fully complexed hydrogel, allowing it to swell until equilibrium swollen state (Figure 3.5). This two-step method ensures that the BB can easily interpenetrate the hydrogel to form complexes with the embedded naphthalene units. This is not only visible via the color change but also via the accompanied increase in swelling ratio meaning that the hydrogel now can take up more water (Figure 3.5). This enhanced swelling behavior is most likely due to the ionic contribution of the BB molecules and their counter ions, here Cl^- ions, which was already reported by our group.[50]

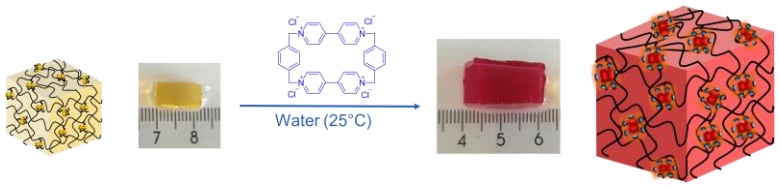

Figure 3.5. Schematic representation of the color change and the dimensional changes associated with the complexation of the Napht-co-PNIPAm hydrogel. The hydrogel was complexed via the two step procedure where the hydrogels was firstly exposed for 24 h to a concentrated BB solution and subsequently allowed to swell to equilibrium (24 h) upon the addition of an excess of water (9 mL). Pictures are of the 3% Napht-co-PNIPAm at equilibrium swelling.

This two-step complexation procedure was followed for 3% Napht-co-PNIPAm hydrogel by measuring the swelling ratio in time, Figure 3.6. Only 40% of the additional water uptake was gained during the first complexation step. This means that this step is only necessary to ensure the full complexation of the hydrogel while the second step is crucial to reach the swollen equilibrium state of the complexed hydrogel. This phenomenon that the hydrogel swells more when fresh water is added can be ascribed to a difference in osmotic pressure of the hydrogel with the surrounding environment. In step one, a concentrated solution of BB is taken up by the hydrogel leading to the complexation of the embedded Napht moieties while the concentration of BB inside and outside the hydrogel remains constant. Upon the addition of 9 mL water in step two the concentration of BB in the surrounding environment significantly decreases, which lowers the ionic strength of the solution and enhances the osmotic pressure and water uptake.

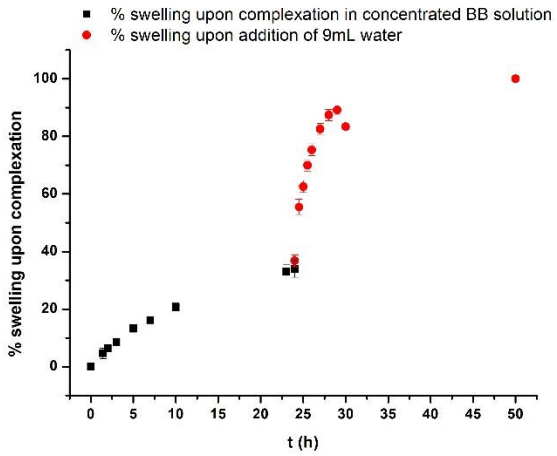

Figure 3.6. The percentage swelling upon complexation Q(t)/Q(eq), with Q(t) = the swelling ratio at swelling time t during the complexation and Q(eq) = the swelling ratio of the complexed 3% napht-co-PNIPAm at equilibrium in function of swelling time.

In a next step, this difference in swelling ratio of the non- and complexed 0%, 2%, 3%, 6% and 12% Napht-co-PNIPAm hydrogels (mol% Napht.Ac feed) was investigated by Dr. Khaled Belal at the university of Lille 1 and is given in Figure 3.7. As expected, for the non-complexed hydrogel it can be noticed that the swelling ratio at equilibrium is decreasing with higher incorporated amounts of hydrophobic naphthalene units (Figure 3.7, orange data points). Upon complexation with 3 eq of BB, an increase in swelling ratio at equilibrium can be seen with increasing amount of naphthalene moieties. This is due to the ionic contribution of the BB molecules and their counter ions. The increased swelling reaches a maximum in function of incorporated Napht-moieties at 3%, while further increase of the functionalization to 6% and 12% showed a steady decrease of water uptake. Even after soaking the 12% Napht-co-PNIPAm hydrogel for several days in the BB-solution, the complexation would only occur on the outside of the hydrogel piece as shown in Figure 3.7. This is probably caused by two events occurring simultaneously leading to a lower complexation and swelling ratio than expected. Firstly the amount of embedded naphthalene is too high for the hydrogel making it too hydrophobic for efficient water uptake and to allow the BB to diffuse inside. Secondly, the naphthalenes located on the outer sphere of the hydrogels will complex first with BB creating a high positive charge density on the surface which prevents the further diffusion of more BB molecules into the hydrogel via coulomb repulsion.

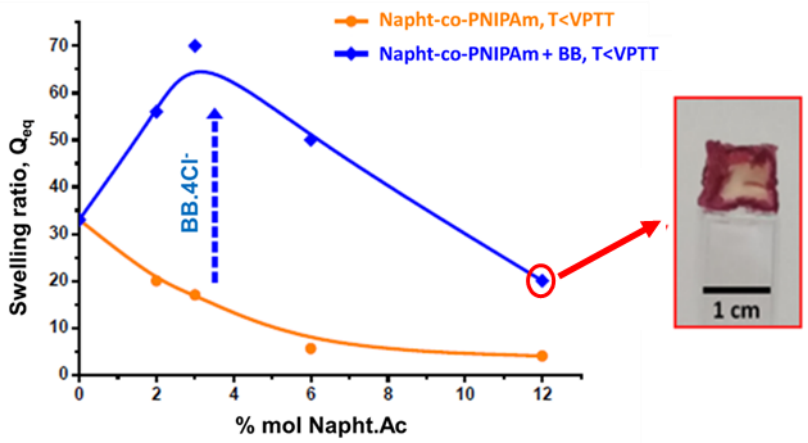

Figure 3.7. The calculated swelling ratio at equilibrium before (orange) and after (blue) the addition of BB to the Napht-co-PNIPAm hydrogels in function of the functionalization grade of Napht.Ac respectively 0%, 2%, 3%, 6% and 12%. The hydrogel pieces were soaked to equilibrium at a temperature below their VPTT (5 °C). Inset: A picture of a cut complexed the 12% Napht-co-PNIPAm piece displaying that only complexation upon the addition of BB is occurring on the outer sphere upon soaking for several days in concentrated BB solution. These results were obtained by Dr. Khaled Belal at University Lille 1.

As the 3% Napht-co-PNIPAm hydrogel revealed the largest increase in swelling degree upon complexation, this hydrogel was selected for further in depth studies. The complex formation of the 3% Napht-co-PNIPAM was investigated in more depth via 2D-NMR (COSY, NOESY) and via HR-MAS ^{1}H-NMR spectroscopy titration by increasing the amount of BB host molecule (Figure 3.8). With HR-MAS NMR spectroscopy, it is possible to record defined NMR spectra with more narrow signals allowing the characterisation of our complexation inside the hydrogel. Dried pieces of the hydrogel were swollen in deuterated water containing 0.2, 0.5, 0.7, 1.0 or 1.5 eq of BB relative to the embedded mol% Napht.Ac. During an overnight swelling step in the fridge (5 °C), i.e. below the VPTT, the polymer chains become more solvated gaining segmental motion which allows the BB to diffuse inside.

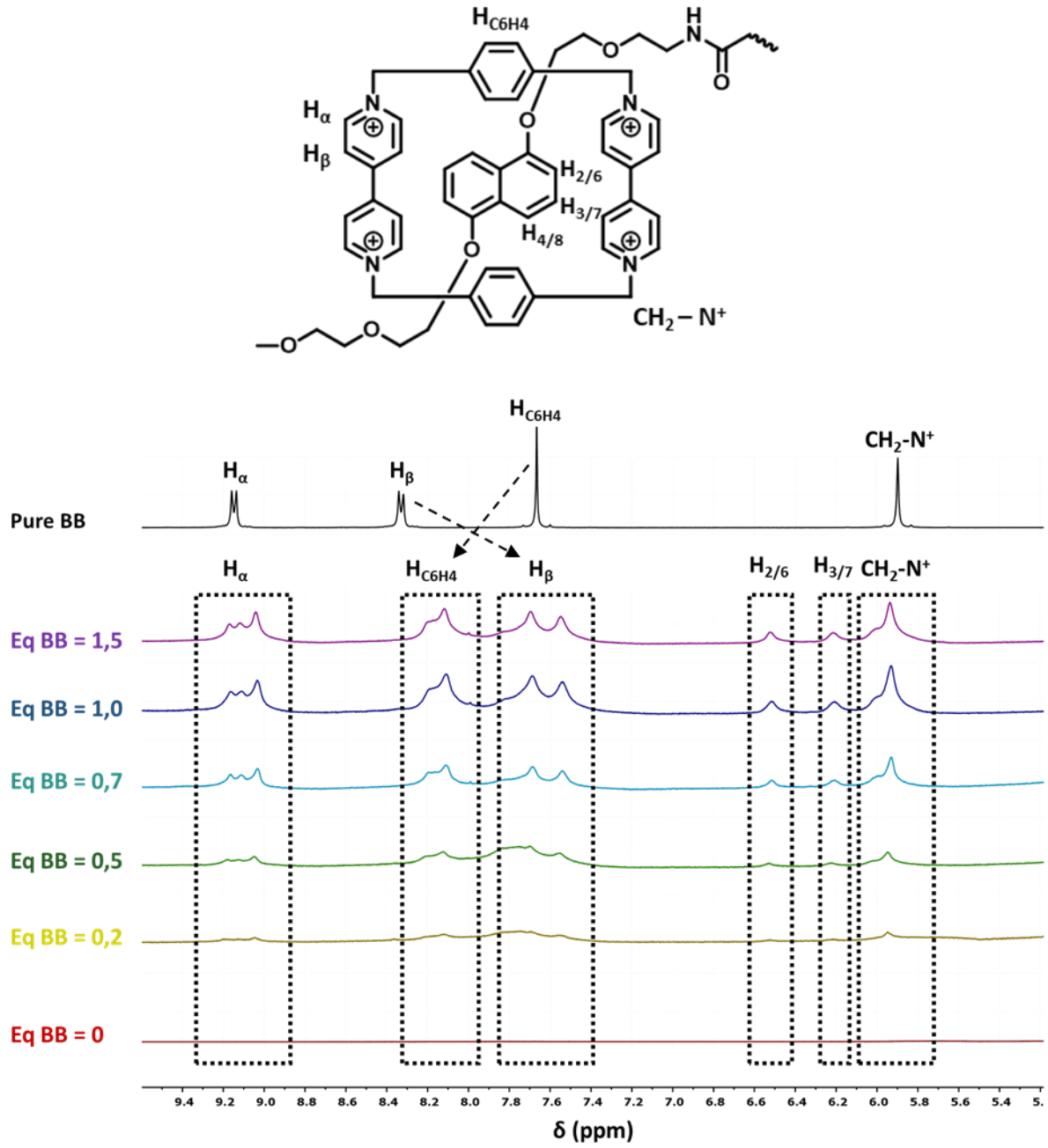

Figure 3.8. Top: Schematic illustration of the pseudorotaxane Napht.Ac-BB inside the hydrogel. Bottom: HR-MAS ^{1}H-NMR spectra of 3% Napht-co-PNIPAm hydrogel measured in D_2O upon the addition of 0, 0.2, 0.5, 0.7, 1.0 and 1.5 equivalents of BB. For comparison, the ^{1}H-NMR spectrum (300 MHz) of pure BB recorded in D_2O is also shown.

It can be noticed in Figure 3.8 that without the addition of BB, no peaks around the aromatic region (7-9 ppm) of the ^{1}H-NMR spectra of the 3% Napht-co-PNIPAm hydrogel are visible, which could be due to the hydrophobic nature of naphthalene leading to poor hydration. The addition of aliquots of BB to the supernatant of the hydrogel resulted in the appearance of the characteristic peaks of this inclusion complex, with the Napht signals appearing from 6.2 ppm to 6.6 ppm ($H_{2/6}$ and $H_{3/7}$) and BB signals around 7.6 ppm (H_{β}), 9.1 ppm (H_{α}) 8.1 ppm (H_{C6H4}) and 5.9 ppm ($H_{CH2\text{-}N+}$). These have almost identical multiplicity and shifts as reported for the complexation of BB with naphthtalene functionalized linear

PNIPAm chains.[38,51] As expected, the resonance peaks of the naphthalene moiety shifted upfield out of the aromatic region to 6.2-6.6 ppm due to the shielding of the BB, which is typical for the formation of the BB-Napht complexation. In addition, the formation of the BB-Napht charge-transfer complex is confirmed by the broadening of all relevant peaks and the typical cross-over shift of the H_β and H_{C6H4} peaks of the BB (Figure 3.8). The intensity of the peaks further increases as more equivalents of BB are added to the sample, indicating that more complexes are formed. Upon the addition of 1 equivalent of BB or more, the intensity stays approximately constant indicating that most of the Napht.Ac units inside the hydrogel are complexed.

The assignments of the peaks was confirmed via 2D-COSY NMR spectroscopy of the complexed hydrogel where a correlation was found between the neighbouring protons H_α - H_β in BB (Figure 3.9, left indicated in green) and $H_{3/7}$ - $H_{4/8}$ in Napht.Ac (Figure 3.9, left indicated in red). Additionally, the dipolar correlation between the H_{C6H4} and the naphthalene proton $H_{3/7}$ observed in the NOESY spectrum (Figure 3.9, right), proves that the pseudorotaxane architecture is formed inside the hydrogel.

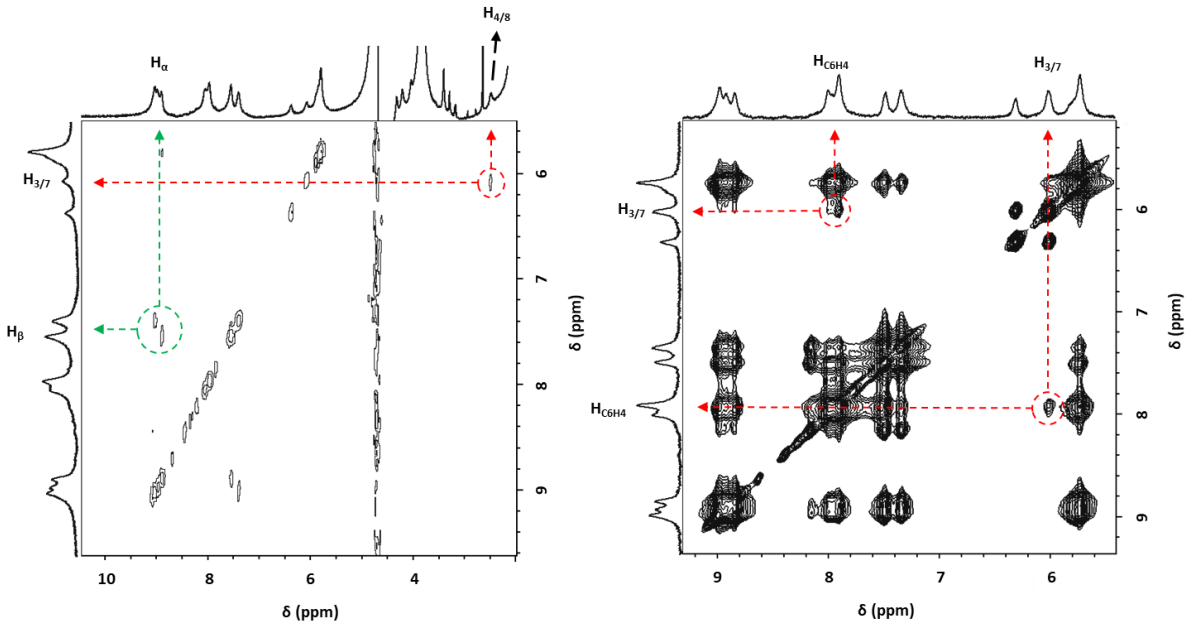

Figure 3.9. Left: Partial 2D-COSY NMR spectrum of the 3% Napht-co-PNIPAm hydrogel complexed with 1 eq BB recorded in D_2O. Right: Partial 2D-NOESY NMR spectrum of 3% Napht-co-PNIPAm hydrogel complexed with 1 eq BB in waterecorded in D_2O.

2.3 Degradation of the naphthalene units in the hydrogel

One problem we encountered during this research is that the color of the 3% Napht-co-PNIPAm hydrogels was changing in time from yellowish to dark brown indicating the degradation of the naphthalene moieties embedded in the water swollen hydrogels (Figure 3.10).

Figure 3.10. Pictures showing the color change of the 3% Napht-co-PNIPAm hydrogel after synthesis and after 3 months storage in water.

This degradation was investigated via ^{1}H-NMR spectroscopy revealing that the sharp naphthalene peaks corresponding to the aromatic part of the naphthalene (f+g+h) and the methylene next to the dihydroxynaphthalene (e) are disappearing over time (Figure 3.11).

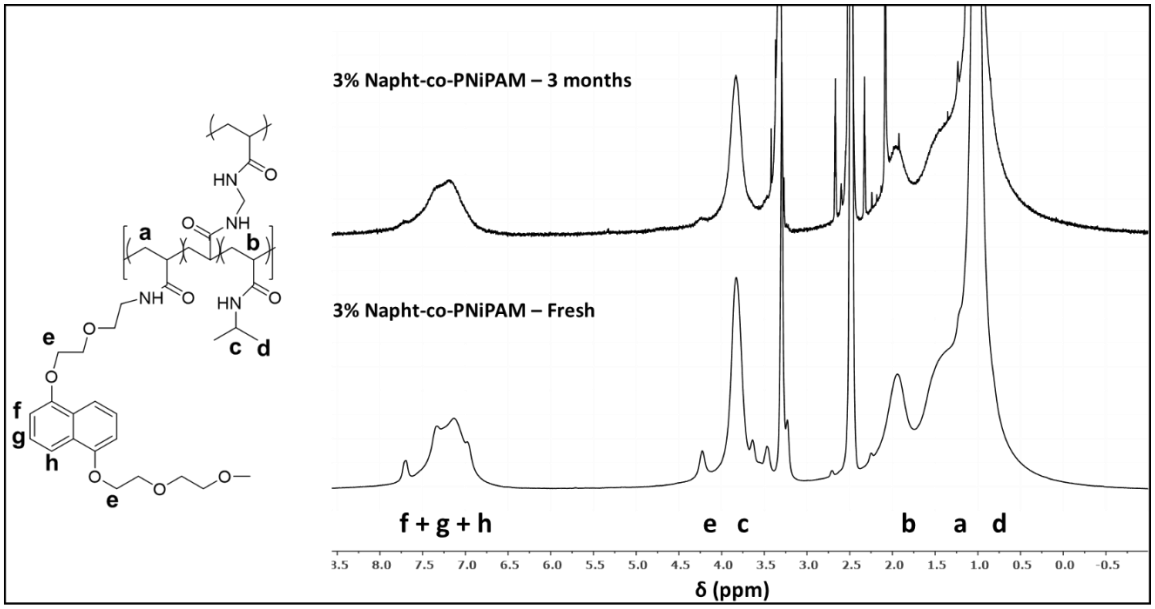

Figure 3.11. ^{1}H-NMR spectrum of the 3% Napht-co-PNIPAm hydrogel immediately after synthesis via FRP (below) and after soaking for 3 months in water at 5°C (above), measured in DMSO-d6. The assignment of the peaks was done using the structure of the hydrogel displayed on the left.

Not only was the coloration of the hydrogel visible to the naked eye but also the supernatant water in contact with the hydrogel showed a darker color with increasing soaking time indicating that the degradation products of naphthalene are diffusing out of the hydrogel. The supernatant was therefore investigated using liquid chromatography-mass spectrometry (LC-MS). The chromatogram (Figure 3.12, Left) showed several peaks and one of them could be identified as a phenyl-2-propenal derivative of our Napht.Ac which is in correlation with the research done by B. J. McConkey et al.[52] on the photo-

oxidation of polycyclic aromatic hydrocarbons, including naphthalene, under environmental lighting conditions. In this study an aqueous naphthalene solution was exposed to natural sunlight for 24 h. In a next step, the photo-oxidation products were separated on LC and analyzed, identifying 5 major constituents including phenyl-2-propenal which was also identified in the supernatant of our hydrogels. The proposed reaction scheme of the photo-degradation of naphthalene, as reported by McConkey is displayed in Figure 3.12, right.

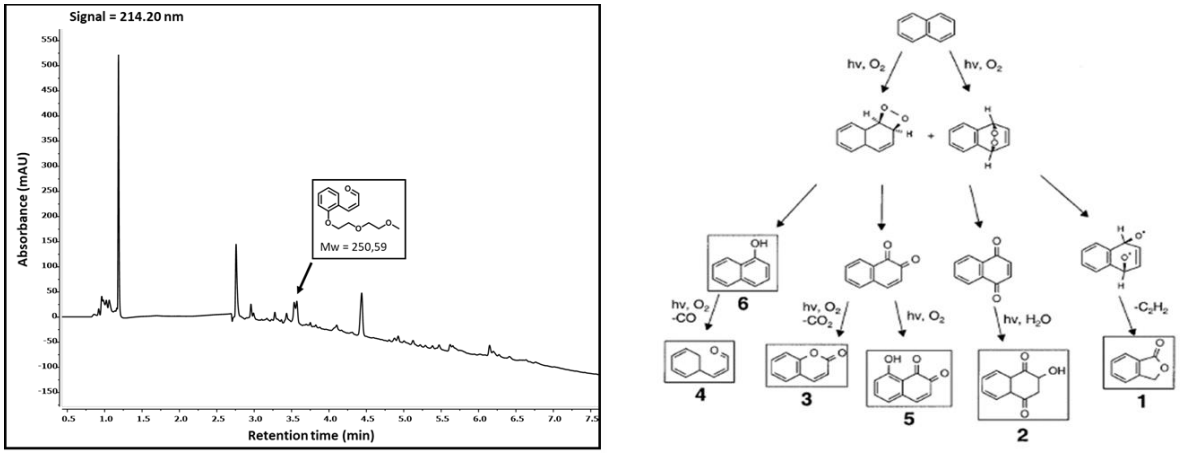

Figure 3.12. Left: LC-MS chromatogram of the supernatant of the degraded 3% Napht-co-PNIPAm hydrogel with UV-signal at 214.20 nm. Right: The proposed reaction scheme of the photo-degradation of naphthalene in water under sunlight. Reprinted from ref.[52] Copyright 2019 Springer Nature.

To further prove that the coloration of the hydrogel is due to the degradation of the Napht-moieties, the swelling ratio of the non-complexed and fully complexed Napht-co-PNIPAm was investigated in function of the storage time. The non-complexed 3%-Napht-co-PNIPAm hydrogel pieces were soaked for weeks in a beaker filled with water at 5°C covered with aluminium foil in order to block the hydrogels from the sunlight and prevent the photo-oxidation. After 0, 1, 2 and 3 weeks of soaking in water, the hydrogel pieces were removed and complexed following the same two-step procedure used in the previous swelling trials. The results are given in Figure 3.13 revealing a steady decrease in water uptake of the 3%-Napht-co-PNIPAm hydrogels for the pieces soaked for 0, 1, 2 and 3 weeks in water prior to complexation. Within a time span of only 3 weeks, a reduction in swelling ratio from 100% to 65% upon complexation was noticed indicating that the degradation of the naphthalene moieties occurs rapidly and is not only a result of photo-oxidation as the sunlight was blocked during the soaking steps. This reduction in swelling ratio could also result from the fact that electron rich species, such as dopamine and anthracene, can upon polymerization reactions easily form additional crosslinks in the hydrogel resulting in lower swelling ratios. However, this hypothesis should be further investigated in the future. In contrast, the fully complexed hydrogel showed no difference in swelling ratio in time indicating that the formation of the BB-Napht inclusion complexes might shield the naphthalene from degradation or possible crosslinking reactions. Although more investigation is required in order to fully

understand the mechanism of this non-photoinduced oxidation of the Napht-moieties, the Napht-co-PNIPAm hydrogels used in this chapter were immediately complexed after synthesis to avoid this encountered oxidation problem.

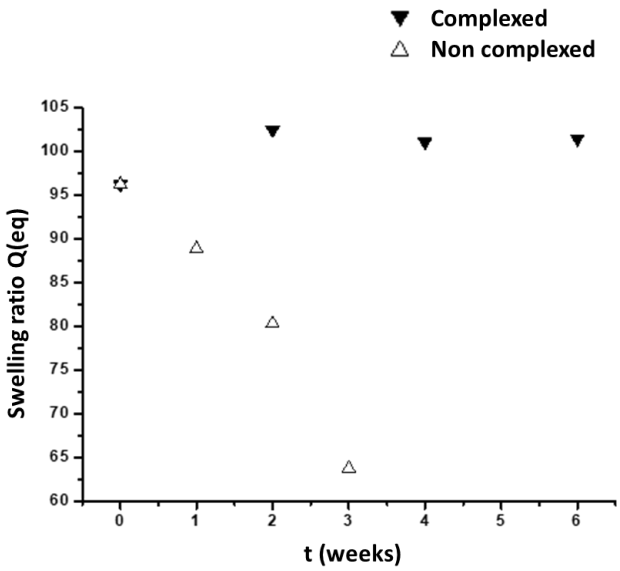

Figure 3.13. The swelling ratio upon complexing 3% Napht-co-PNIPAm hydrogel pieces soaking them for respectively 0, 1, 2 and 3 weeks in water at 5°C (hollow upward triangles). The swelling ratio for a complexed 3% Napth-co-PNIPAm hydrogel soaked for respectively 0, 1, 2 and 3 weeks (black downward triangles).

2.4 Temperature dependence of the Napht-co-PNIPAm hydrogel

In most literature reports, PNIPAm polymers have been employed for the preparation of thermo-responsive systems as it exhibits a sharp coil-globule phase transition upon heating above 32 °C, called the lower critical solution temperature (LCST).[53–55] An identical thermo-responsive phenomenon can be observed in the Napht-co-PNIPAm hydrogels as upon heating above a certain temperature the hydrogels will also display such an entropy driven phase separation where the polymer chains will be dehydrated upon heating. As the hydrogels consist of a 3D polymeric network the transition will induce a volume change going from a hydrated or swollen state to a dehydrated or collapsed state. This critical temperature where the reversible changes in water uptake of the hydrogel occurs is called the volume phase transition temperature (VPTT).[56,57] The VPTT of the Napht-co-PNIPAm hydrogels can be investigated via differential scanning calorimetry (DSC) as the transition temperature is correlated to an endothermic peak shown in the thermogram.[58] The endothermic nature of this transition is related to the breaking of polymer-solvent interactions, here hydrogen bonding between water and PNIPAm, and the release of the water molecules from the collapsing hydrogel.

The VPTT was determined via DSC for non-complexed and complexed 0%, 2%, 3%, 6% and 12% Napht-co-PNIPAm hydrogels (mol% Napht.Ac feed) and is depicted in Figure 3.14. During the experiments the

hydrogel pieces were heated from 0 °C to 70 °C with a rate of 2 °C/min for two consecutive heating cycles in order to check whether the volume changes were reversible.

The same trend as for the swelling ratio (Figure 3.7) was visible. The VPTT decreased with higher incorporation of naphthalene units as the introduction of more hydrophobic moieties lowers the VPTT of the Napht-co-PNIPAm hydrogel (Figure 3.14, gray). Initially upon complexation, higher VPTTs are achieved for hydrogels functionalized with higher amount of naphthalene moieties, again reaching a maximum at 3% functionalization (Figure 3.14, Blue). Further increase of the naphthalene units results in a decrease in the VPTT of the complexed hydrogel, although still higher than its non-complexed counterpart. This means that even though the hydrogel becomes too hydrophobic for the BB to diffuse inside, the complexation on the outer sphere of the hydrogel still induces a minor effect on the VPTT.

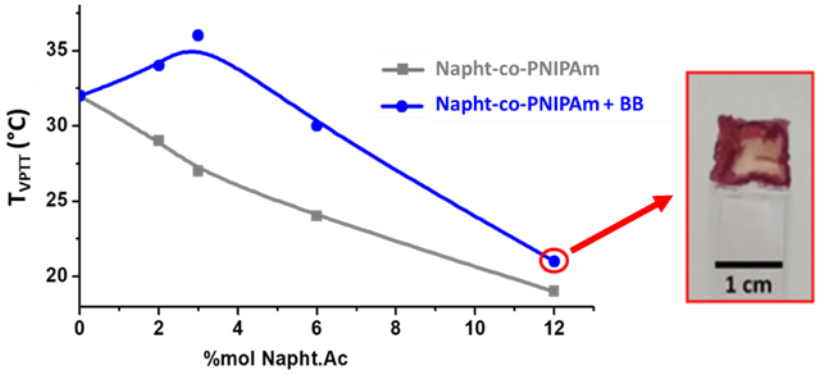

Figure 3.14. The VPTT of the non-complexed (grey) and complexed (blue) 0%, 2%, 3%, 6% and 12% Napht-co-PNIPAm hydrogels measured via DSC. In addition, a photo of a cut complexed the 12% Napht-co-PNIPAm piece illustrating that only complexation upon the addition of BB is occurring on the outer sphere. These results were obtained by Dr. Khaled Belal at University Lille 1.

The reversibility of the volume phase transition function of the complexed hydrogel is investigated by exposing hydrogel pieces to three consecutive heating (5 °C to 50 °C) – and cooling (50 °C to 5 °C) cycles in an aqueous solution of 3 eq of BB. The difference in swelling ratio was determined gravimetrically and the results are given in Figure 3.15 with the data points at 5 °C in blue and at 50 °C in grey. The 0 % Napht-co-PNIPAm hydrogel showed a decrease in swelling ratio of roughly 30% upon heating resulting from the LCST-behavior of PNIPAm. Incorporating Napht-BB complexes will affect this temperature-dependent volume change in two ways: 1) reduction of the swelling above VPTT due to increased hydrophobicity of the uncomplexed Napht units and 2) increase of the swelling below VPTT due to the additional ionic character resulting from the formation of Napht-BB complexes similarly to Figure 3.7. This results in a maximum contraction/expansion range for the complexed 3% Napht-NIPAm hydrogel and a decrease of this range with higher Napht content due to lower diffusion of BB into the hydrogel at T < VPTT as explained in section 2.2.

During heating, the swelling of the hydrogels is determined by the Napht-co-PNIPAm polymer chains complexed with the hydrophilic BB masking the hydrophobic contribution of the naphthalene units. Upon cooling, however, the rehydration of the polymer Napht-co-PNIPAm chains inside the hydrogel becomes more important as the donor-acceptor complex can only be formed when the naphthalene units go back into solution.[38] This reversible transition is also visually displayed in Figure 3.15, right. Here, the complexed 6% napht-co-PNIPAm hydrogel was heated for 5 min at a temperature above its VPTT (50°C) favouring the polymer-polymer interactions and causing it to shrink to a rigid opaque gel. Furthermore, exposing the complexed 6% Napht-co-PNIPAM hydrogels to a temperature above the VPTT revealed that the phase transition is accompanied by an almost complete disappearance of the purple color which was reappearing after cooling back to 5°C (< VPTT of the non-complexed 6% Napht-co-PNIPAm). This reversible color change displays the dynamic character of these complexes (Figure 3.15, Right). In the following experiments, we further explored this behaviour for the 3% Napht-co-PNIPAm hydrogels as it possessed the largest hysteresis window of around 10°C (Figure 3.14).

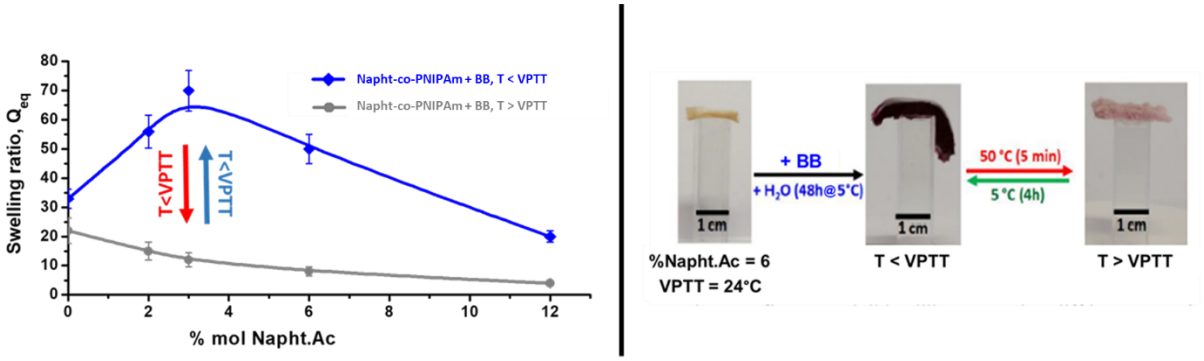

Figure 3.15. Left: the reversible volume phase transition function illustrated by giving the swelling ratio upon heating and cooling in function of the incorporated percentage naphthalene for 0%, 2%, 3%, 6% and 12% respectively. Right: the visualization of the disassembly of the donor-acceptor complex that is accompanied with the VPTT of the 6% Napht-co-PNIPAm hydrogel. These results were obtained by Dr. Khaled Belal at University Lille 1.

The continuous volume phase transition of the non-complexed and complexed 3% Napht-co-PNIPAm was studied more in detail by conducting 500 MHz NMR spectroscopy at different temperatures. The sample of the complexed 3% Napht-co-PNIPAm gel was prepared by adding 20 mg of dried hydrogel to a solution of 3 mg BB (1 eq) in 0.7 mL D_2O in a NMR tube. The sample for the non-complexed hydrogels was prepared in the same way without the addition of the BB. All gel pieces were left to swell to equilibrium overnight in the fridge. This allows full hydration of the polymer chains in the hydrogels, ensuring maximal segmental motion resulting in a decrease in line broadening of the NMR spectra. Full ^{1}H-NMR spectra were recorded over a temperature range from 20 °C to 45 °C in steps of 1 °C, with a 300 second incubation time prior to the measurement allowing the hydrogel to adjust to the changes in the surrounding temperature.

The overlay of the spectra clearly shows that the signals corresponding to the PNIPAm polymer chains (0 – 2.6 ppm) are diminishing with increasing temperature (Figure 3.16). This phenomenon can be ascribed to a decrease in chain mobility upon collapsing of the hydrogel which causes line broadening, significantly reducing the peak intensity. The reverse observation can be made for the peaks related to BB (5.5 – 10 ppm) as upon heating more defined peaks of the BB host molecule become visible proving the expulsion of BB from the hydrogel (Figure 3.16).

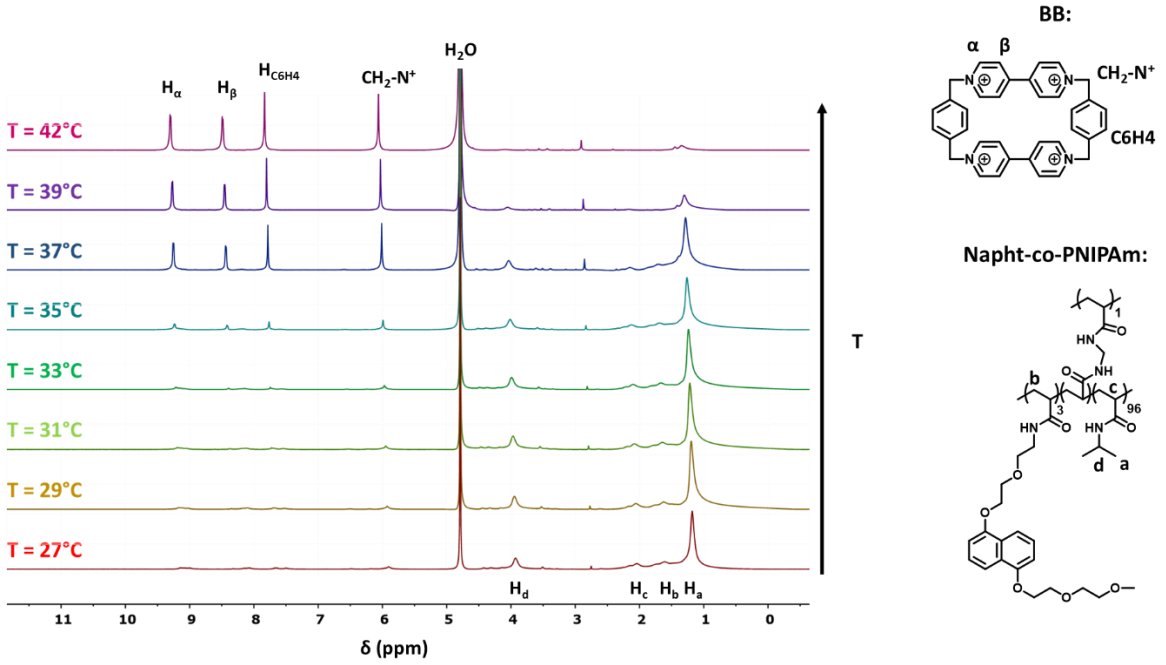

Figure 3.16. ^{1}H-NMR spectra of the 3% napht-co-PNIPAm complexed with 1 eq. BB measured at 27 °C, 29 °C, 31 °C, 33 °C, 35 °C, 37 °c, 39 °C and 42 °C.

Considering that the integrated intensities of the PNIPAm polymer are decreasing with the inverse of the absolute temperature (1/T) , the fraction of collapsed hydrogel can be determined via equation 3.4:

Equation 3.4

$$p(T) = 1 - \frac{I}{I_0(T_0/T)}$$

where I is the integrated intensity of the signal corresponding to the partly collapsed hydrogel at the absolute temperature T (K) and I_0 is the initial integrated intensity of the same polymer signal at temperature T_0 which is below the VPTT.[59] The fraction of collapsed hydrogel was determined by integrating the polymer region from 0 to 2.6 ppm and is given in function of temperature to evaluate the thermal behaviour of the non-complexed and complexed 3% Napht-co-PNIPAm hydrogel in Figure 3.17. A gradual transition for the non-complexed hydrogels was observed with the fraction of collapsed polymer going from ca. 0% to ca. 90% over a temperature range of 15 °C. A sharper transition, from ca. 0% to 100% collapsed polymer, was encountered for the complexed hydrogel in the range from 34

°C to 38 °C. The cloud point temperature (T_{cp}), at which half of the polymer chains have phase separated from the solvent, of the non-complexed hydrogel is around 28 °C while the T_{cp} of the complexed hydrogel is slight higher at 34 °C. This means that the 3% Napht-co-PNIPAm systems contains a hysteresis window of 7 °C which is in agreement with the results obtained in Figure 3.14.

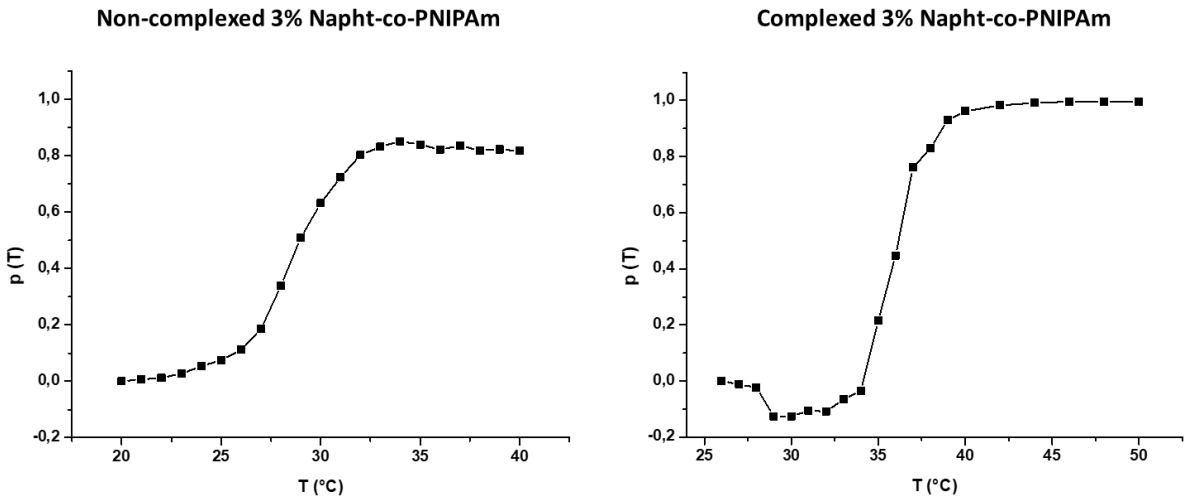

Figure 3.17. The collapsed fraction (p(T)) of the non-complexed and complexed 3% Napht-co-PNIPAm hydrogel in function of the temperature. The collapsed faction was determined via 500 MHz NMR spectroscopy.

Furthermore, these variable temperature ^{1}H-NMR spectroscopy experiments provided further insights on the VPTT mediated host-guest disassembly (Figure 3.18). As expected, the peaks corresponding to the donor-acceptor complex are diminishing with increasing temperature, especially from 33 °C to 37 °C, which is a direct proof of the dynamic nature of the BB-Napht complex during the volume phase transition.

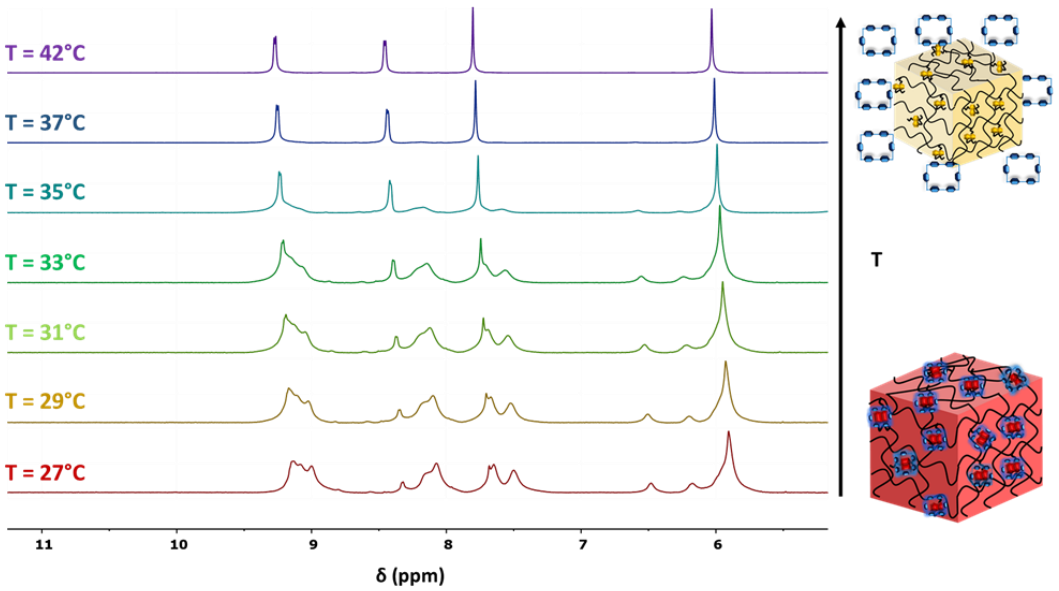

Figure 3.18. Partial ^{1}H-NMR spectra of the complexed 3%-Napht-co-PNIPAm hydrogels recorded at 27°C, 29°C, 31°C, 33°C, 35°C, 37°C and 42°C. The disassembly induced by the volume phase transition of the complexed hydrogel is given in an schematic illustration next to the ^{1}H-NMR spectra.

Simultaneously, the peaks corresponding to the free BB are becoming more prominent with increasing temperature, until at 37 °C only the signals from the free BB are visible in the spectrum. Furthermore, the ratios of the integrated intensities of the residual peaks in the spectrum at these higher temperatures correspond to BB, confirming the presence of free BB in solution (Figure 3.19).

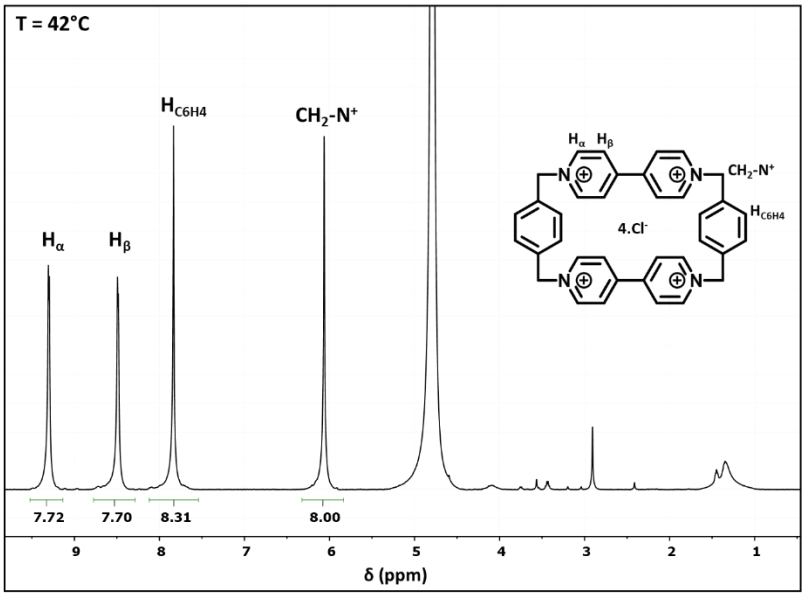

Figure 3.19. Integrals and assignment of the residual peaks measured via 500 Hz ^{1}H-NMR spectroscopy for the complexed 3% Napht-co-PNIPAm hydrogels heated at 42 °C.

2.5 Time memory function

In the previous section, we have described that incorporating the BB-Napht host-guest complexation into PNIPAm hydrogels introduces a hysteresis window resulting from the dynamic character of the Napht-BB complexes. A thermal hysteresis of approximately 7 °C in its volume phase transition was determined for the BB complexed 3% Napht-co-PNIPAm hydrogels, providing a potential memory function in dimensional changes. It was postulated that both temperature and exposure time will have an influence on the disassembly and BB diffusion rate, providing kinetic control over the amount of BB that is retained in the hydrogel. This will cause different volume changes upon reswelling of these heated hydrogels in fresh water. This difference in swelling ratio is further investigated as basis for a thermal memory function where the systems remembers how long it had been exposed to a certain temperature, thereby creating a time memory function.

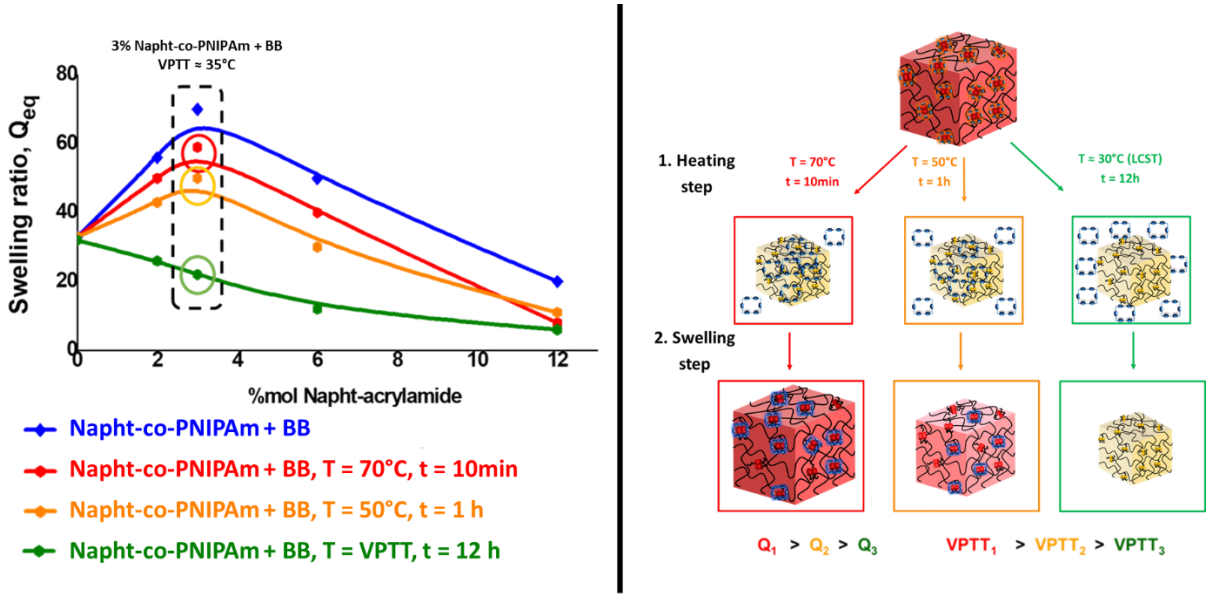

Figure 3.20. Left: The Napht-co-PNIPAm hydrogels modified with respectively 2%, 3%, 6% and 12% of naphthalene were exposed for 10 min at 70 °C, 1 h at 50 °C and 12 h at their corresponding VPTT. The swelling ratios after heating (Q) were determined by letting them soak to equilibrium in fresh demineralised water at 5 °C and the results are given in the graph in function of the naphthalene functionalisation degree. Right: Schematic illustration of the disassembly of the Napht-BB complex and the accompanied diffusion of the free BB out of the hydrogel upon heating and reswelling in the subsequent soaking step for 10 min at 70 °C, 1 h at 50 °C and 12 h at the VPTT of the hydrogel.

To demonstrate this effect, the 2%, 3%, 6% and 12% Napht-co-PNIPAm hydrogels were heated for 10 min at 70 °C, 1 h at 50 °C and 12 h at their VPTT (33 °C, 35 °C, 30 °C and 21 °C) respectively, after which the hydrogels were soaked to equilibrium in 20 mL fresh demineralised water at 5 °C (Figure 3.20). The decomplexation of Napht-BB and the accompanied decrease in swelling ratio upon heating as described in the previous section can be controlled by the heating temperature and exposure times as shown in Figure 3.20. To illustrate the importance of the exposure time, full decomplexation (i.e. at T = VPTT for 12h) was compared with samples that were heated at temperatures exceeding the VPTT for shorter exposure times. Surprisingly, the samples that were heated at 50°C and 70°C for only 1 h and 10 min of exposure time respectively, showed a higher reswelling ratio indicating lower decomplexation. It is proposed that at these elevated temperatures the hydrogel will collapse more briskly trapping the free BB inside the hydrogel. As a result, during the subsequent resoaking step more complexes are restored resulting in higher reswelling ratios compared to the samples that were heated at the VPTT for 12h. The higher amount of restored Napht-BB complexes of these samples is further confirmed by their higher intensity of the purple color and their higher VPTT after the reswelling step in fresh water (Figure 3.20).

This behaviour can be explained by the influence of both temperature and exposure time on the rate of contraction of the Napht-co-PNIPAm hydrogels. Both these factors will strongly influence the decomplexation- and diffusion speed of the BB out of the Napht-co-PNIPAm hydrogels, leading to different reswelling ratios afterwards. This difference in diffusion rate of the BB and the accompanied

variation in either reswelling ratios or VPTT of the hydrogel was hypothesized to be used in a memory system preserving information on the physical history, here the exposure time at a certain temperature.

This memory function, where the system remembers how long it had been heated to a certain temperature, was further explored for a 3% Napht-co-PNIPAm hydrogel by heating complexed pieces at different temperatures ranging from close to the phase transition temperature (VPTT = 35°C) up to 60°C for increasing periods of time of 1 h, 5 h, 10 h and 14 h. After heating, the hydrogels were allowed to reswell in fresh demineralised water below the VPTT of the hydrogels (T = 5 °C) up to 96 h after which the percentage of decomplexation was determined using the reswelling ratio (Figure 3.21). A first trend that was noticeable is that hydrogels that were heated at higher temperatures show lower decomplexation percentages during reswelling, which confirms the previously obtained results. This is most likely due to a quicker collapse and more efficient dehydration of the 3% Napht-co-PNIPAm hydrogel at higher temperatures compared to the VPTT, trapping the decomplexed BB inside the hydrogel leading to lower decomplexation values after the reswelling step. Secondly, all graphs show that the decomplexation percentage increases with longer reswelling times. This is probably due to the use of fresh demineralised water and therefore the achievement of a new concentration equilibrium of BB inside and outside the hydrogel during the relaxation of the collapsed polymer chains leading to loss of BB.

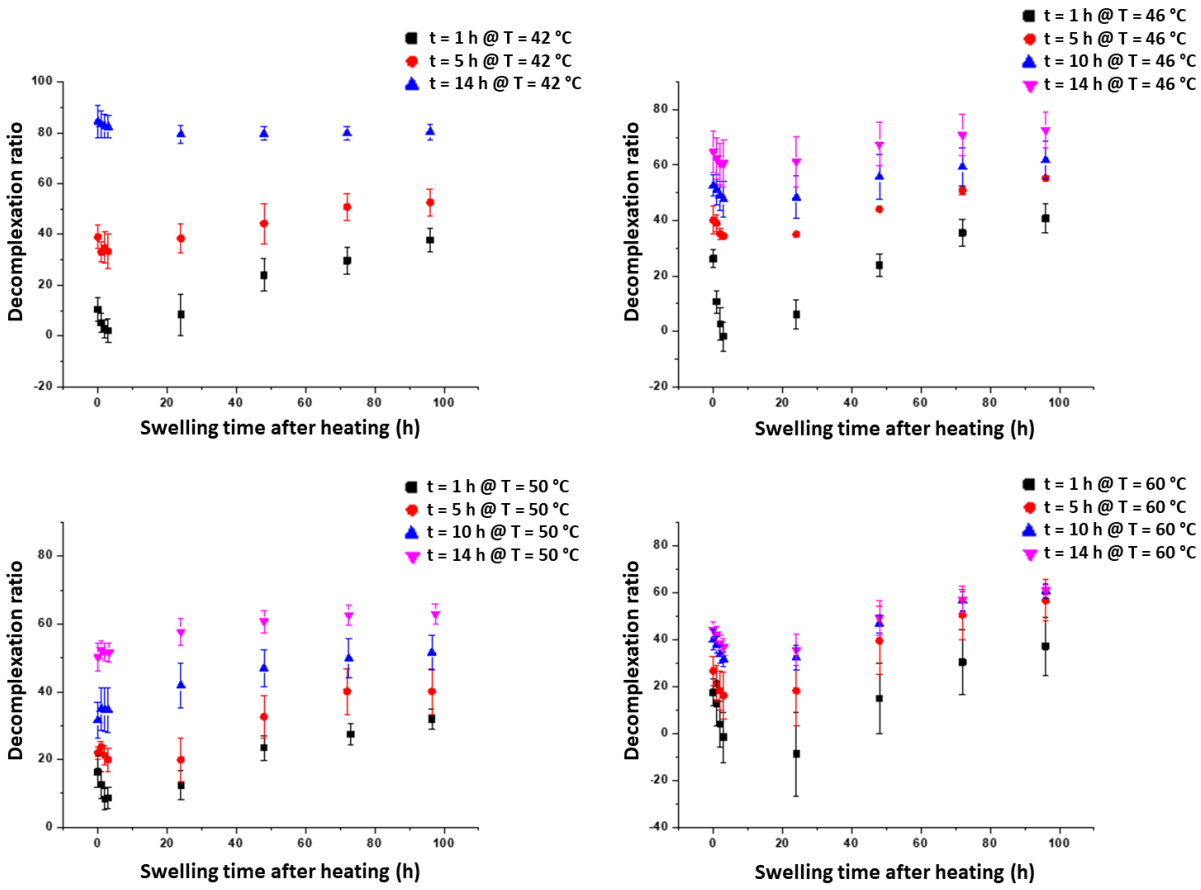

Figure 3.21. Decomplexation percentages of 3% Napht-co-PNIPAm hydrogels being exposed for 1 h (black squares), 5 h (red circles), 10 h (blue upward triangle) and 14 h (purple downward triangle) at 42°C, 46°C, 50°C and 60°C and subsequently being soaked in fresh demineralised water (20 mL) for 1 h, 2h, 3h, 24 h, 48 h, 72 h and 96 h. All tests were performed in triplicate.

To fully explain the influence of the heating temperature on the possible memory function, we will focus first on the hydrogel pieces that were heated near the VPTT (35°C), i.e. at 42 °C (upper left graph, Figure 3.21). If the complexed 3% Napht-co-PNIPAm hydrogels pieces were heated near the VPTT (35°C) at 42 °C then 80% of the BB-Napht complexes were disassembled and therefore only approximately 20% of the initial swelling ratio of the complexed hydrogel is restored after heating them for 14 h. With decreasing heating times, the decomplexation rate also decreases showing respectively 40% and 30% after 5 h and 1 h of heating, corresponding to a restored swelling ratio of 60% and 70% in the subsequent reswelling step. Thus lower reswelling ratios are achieved with longer heating times as most of the BB can diffuse out of the slowly collapsing hydrogel. Even after more than 96h of resoaking in fresh demineralised water, a clear difference in decomplexation ratio is observed after a new equilibrium is achieved, allowing to differentiate between the different exposure times. With increasing the heating temperature up to 46 °C and 50 °C, the time memory function window steadily decreases, however still significant differences in the restored swelling ratios is observed. Up to 24 h of reswelling, the heated samples clearly remember the exposure time as the difference in

decomplexation ratio for the different exposure times is reaching a maximum. With longer reswelling times up to 96 h, it is observed that the decomplexation ratios come more together losing their temperature-time memory function. Finally, almost no difference in decomplexation ratio is observed when the hydrogels are heated at 60°C or higher. It is theorized that this inability to differentiate between the exposure times at these high temperatures is due to the fast kinetic trapping of the BB in the collapsed hydrogel preventing the free diffusion of the BB outside of the hydrogel at elevated temperatures. This results in ambiguous decomplexation rates based on the subsequent reswelling step showing that the hydrogel collapses too rapidly for the time memory function to operate.

The above results show us that the system can report how long it was exposed to a certain temperature as the decomplexation and diffusion rate of BB has an exposure time and temperature dependence. As reswelling is rather fast and nearly complete after 2 h, a reswelling time of 2 h was chosen for further evaluation of the sensor. In Figure 3.22, the decomplexation of the samples is given in function of the exposure time at temperatures of 42 °C, 46 °C, 50 °C and 60 °C, respectively. It can be noticed that a higher difference in decomplexation is observed with increasing exposure times, which is related to the rather slow diffusion of BB from the collapsed hydrogels, even at the VPTT. Nonetheless, a first significant difference between 42 °C / 46 °C and 50 °C / 60 °C was already noticed after exposing the hydrogels for 5 h. With further increment of the exposure temperature to 14 h, a clear difference in decomplexation was observed for all temperatures indicating that the system can preserve information of the environmental temperature for a fixed exposure time or about the time for a fixed temperature. Future work will focus on time memory hydrogels that can measure shorter times, by introducing larger porosity into the hydrogels to facilitate and accelerate the diffusion of BB from the system.

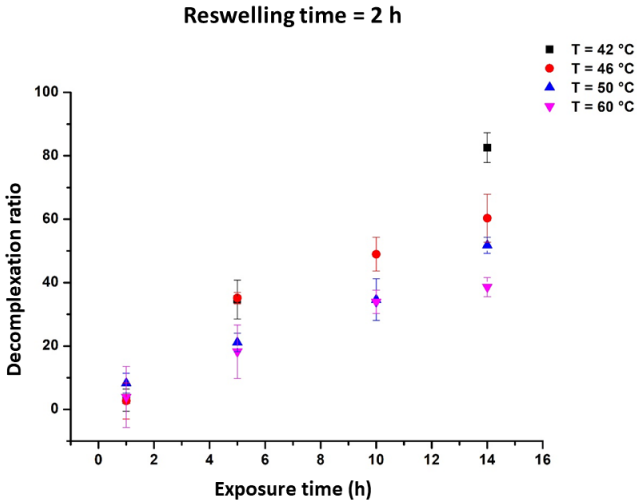

Figure 3.22. Decomplexation percentages of 3% Napht-co-PNIPAm hydrogels being exposed at different temperatures: 42 °C (black squares), 46 °C (red circles), 50 °C (blue upward triangles) and 60 °C (purple downward triangles) for 1 h, 5 h, 10 h and 14 h and subsequently being soaked in fresh demineralized water (20 mL) for 2 h respectively. All tests were performed in triplicate.

Besides the reswelling ratio, the visual changes in color and dimensions of the memory function of the 3% napht-co-PNIPAm hydrogel heated for 1 h, 5 h, 10 h and 14 h at 50 °C were also investigated, which are depicted in Figure 3.21. As expected, the hydrogels in the collapsed state immediately after heating show almost no color indicating fully decomplexation of the incorporated naphthalene moieties. After removing the samples from the heated solution, the color was restored after only 5 min in contact to air without the need of submerging them into water. This indicates that sufficient water is entrapped in the collapsed hydrogel to rehydrate the Napht-co-PNIPAm chains, allowing complexation with the BB that is still present in the hydrogel to occur immediately (Figure 3.23).

Upon restoring their swollen state after 24 h in 20 mL water, the slight dimensional change in shape of the hydrogel pieces persists, decreasing from 2 cm to approximately 1.5 cm when the exposure time increases from 1 h to 14 h, respectively. The lower uptake of water can be explained by the increased amount of expelled BB upon heating, resulting in lower recomplexation upon reswelling and ,thus, less efficient masking of the hydrophobicity of the embedded naphthalene moieties, which supports the findings in Figure 3.21.

Although the insignificant color change between the different sample upon resoaking prevents the use of these hydrogels as a visual sensor, the materials could possibly still be employed as a visual sensor through careful monitoring of the size changes, for example by using a smartphone camera capable of monitoring dimensional changes at pixel level.

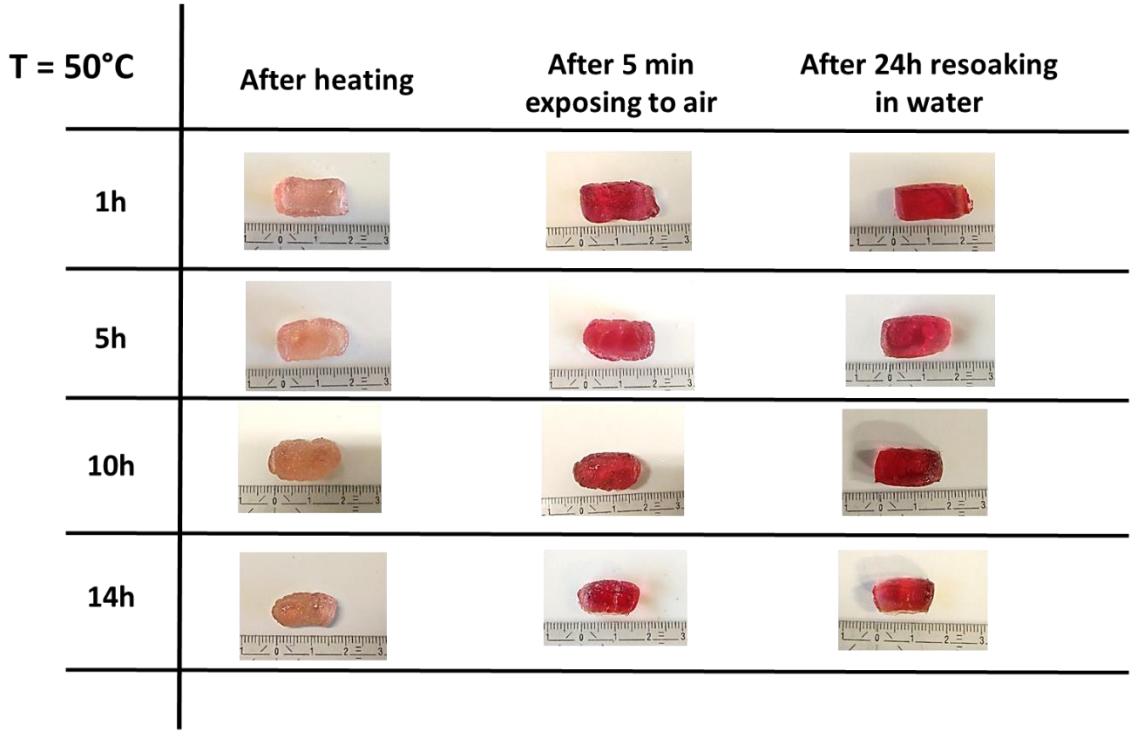

Figure 3.23. Visualisation of the dimensional and color changes of the 3% Napht-co-hydrogels samples immediately after heating for 1 h, 5 h, 10 h and 14 h at 50°C, after the exposure to the air for 5 min, and after reswelling them for 24 h in water.

3 Conclusions and outlook

In summary, a stimuli-responsive hydrogel was created that exhibits a time memory function in which the systems remembers information on how long it was exposed to a certain temperature. To achieve this, a thermally responsive hydrogels was synthesized via free radical co-polymerization of NIPAm with Napht.Ac in the presence of the cross-linking agent MBA. It was demonstrated that BB can easily penetrate the hydrogel functionalized with naphthalene moieties to form donor-acceptor complexes which is accompanied by a visible color change and with an increase in swelling ratio induced by the electrostatic contribution of the BB host molecule. The dynamic nature of these host-guest complexations made it possible to induce a large hysteresis window in the VPTT of these hydrogels as basis for a potential thermal memory. When heated above its VPTT, it was displayed that the disassembly of the complex is more important as the hydrophobic naphthalene units are masked by the ionic cyclic BB molecule ($VPTT_{complexed}$), while upon cooling the presence of the free naphthalene units significantly lowers the rehydration of the polymer chains ($VPTT_{non\text{-}complexed}$).

Finally, the time memory function and temperature memory function for 3% Napht-co-PNIPAm hydrogels was demonstrated. The time memory function was investigated by heating hydrogel pieces for a certain time period at a specific temperature above the VPTT, after which the heated pieces were transferred to fresh demineralized water to restore their swollen state. Both temperature and exposure time have an influence on the decomplextion- and diffusion speed of the BB from the Napht-co-PNIPAm hydrogels leading to different percentage of decomplexation and reswelling ratios afterwards. The same experiment was repeated keeping the reswelling time constant to demonstrate the time and temperature memory functions of the hydrogel. It was observed that the system preserves the information at which temperature it was heated only when the hydrogel was exposed for longer times as then a clear difference in BB diffusion and decomplexation was observed, ascribed to the slow diffusion of the release BB from the collapsed hydrogels.

In the future these memory functions should also be explored for the Napht-co-PNIPAm hydrogels functionalized with respectively 2% and 6% of naphthalene as these hydrogels also exhibit a large hysteresis window. This should give us more insights in the influence of the concentration of embedded Napht-BB assemblies on the influence of the time memory function and temperature memory function.

The current generation of time- and temperature memory hydrogel sensors as described in this chapter are sensitive towards several hours of exposure time, ideally 4 to 5 h or 14 h respectively. In order to decrease the possible exposure times, for the memory function a Napht-co-PNIPAm hydrogel can be prepared with macroscopic pores. We propose that BB can more easily diffuse out of such a

porous hydrogel during the heating cycle, which could induce a difference in reswelling ratios after being exposed for only several minutes at certain temperatures rather than several hours.

4 Experimental details

4.1 Materials and instruments

All chemicals and solvents were commercially available and used as received unless otherwise stated. All HPLC grade solvents were purchased from Acros (dry DMSO, diethylether), Sigma Aldrich (Acetone, THF), Alfa Aesar (Nitromethane), Biosolve (DMF) and Fisher (CH_3CN, MeOH, DCM, EtOH). All anhydrous solvents, expect for the dry DMSO, were obtained by passing over aluminium oxide by means of a J.C. Meyer solvent purification system. The used starting products Phthalimide, 4,4'-bipyridine and potassium persulfate (KPS) were purchased from Acros. Diisopropyl azodicarboxylate (DIAD), hydrazine monohydrate, *N*,*N*'-methylenebisacrylamide (MBA), acryloyl chloride, *N*-isopropylacrylamide (NIPAm), tetraethylammonium chloride ($N(Et)_4^+Cl^-$) and ammonium hexafluorophosphate ($NH_4^+PF_6^-$) were obtained from Sigma Aldrich. The NIPAm monomer was recrystallized from diethylether before usage. All deuterated solvents were purchased from Cambridge Isotope Laboratories.

Nuclear magnetic resonance (NMR). ^{1}H-NMR spectra were recorded in CD_3CN, D_2O or $CDCl_3$ on a Bruker Advance 300 MHz or 500 MHz spectrometer at room temperature unless otherwise noted. Chemical shifts are reported as parts per million (ppm) downfield from TMS resonance as internal standard for the ^{1}H-NMR spectroscopy. The hydrogel samples were prepared by swelling 20 mg of crushed hydrogels pieces in 0.7 mL D_2O overnight at 5°C in a NMR tube prior to measurement.

High Resolution Magic Angle Spinning (HR-MAS) NMR spectroscopy. 3-4 mg of small pieces of dried 3% Napht-co-PNIPAm hydrogel was added to a 4-mm zirconium MAS Rotor (50 µL). Afterwards 40 µL of BB in D_2O stock solution (200 µL) was added to introduce respectively 0.2, 0.5, 0.7, 1.0, 1.5 eq of BB in the HR-MAS probe. A Teflon coated cap was applied in order to seal the rotor. The sample was homogenized via manual stirring and subsequently the pieces were allowed to swell and complex overnight at 5 °C. Next, A bruker Avance II 700 MHz spectrometer device was used to record the HR-MAS ^{1}H-NMR spectra which was equipped with a ^{1}H, ^{13}C, ^{119}Sn and gradient channel. The spinning rate was kept at 6 kHz throughout the measurement.

Differential Scanning Calorimetry (DSC). DSC and MTDSC were performed on an Mettler-Toledo DSC1/700 equipped with a FRS5 sensor containing 56 thermocouples, an automatic sample robot and cooling using liquid nitrogen. Measurements were performed in 120 µL medium pressure sealed stainless steel crucibles with around 10 mg of swollen non-complexed and complexed 0 %, 2 %, 3 %, 6

% and 12 % Napht-co-PNIPAm hydrogels. The vessel was first allowed to stabilize 10 min at 0 °C prior to the initiation of the scanning experiment over a temperature range of 0 °C to 70 °C using a heating and cooling rate of 2 °C/min. Cooling the pans to initial conditions and a second measurement was done in order to check the reversibility of the volume phase transition. Absorbed and released heat was recorded relative to a reference vessel. Evaluation was done via the STARe software.

Liquid chromatography – mass spectrometry (LC-MS). Measurements were performed on an Agilent 1100 HPLC with quaternary pump and UV-DAD detection, coupled to an Agilent G1956B MSD with ESI (multimode) ionization source. 15 µL samples were injected onto a Phenomex-kinetic C18 (5 µm 150 X 4.6 mm) column with a flow rate of 1.5 mL/min at 35 °C. A 6 minute elution gradient from 0 → 100% acetonitrile in aqueous 5 mM ammonium acetate solution was applied. High resolution MS was performed on an Agilent 1100 HPLC with quaternary pump and UV-DAD detection, coupled to an Agilent 6220A TOF-MSD with ESI/APCI (multimode) ionization source.

Rheology. Measurements were conducted on an Anton Paar MCR 302 rheometer equipped with a CTD 180 oven. A normal force of 0.1 N was applied to maintain the contact with the hydrogel during the measurement. The swollen state of the hydrogels was preserved by using a solvent trap. The amplitude sweeps were performed at a constant angular frequency of 1 rad/s and with changing stain amplitude form 10^{-4} % to 10%.

4.2 Synthesis of 2-[2-[2-[[5-[2-(2-methoxyethoxy)ethoxy]-1-naphthalenyl]oxy]ethoxy] ethyl] (Napht-phtalimide)[38]

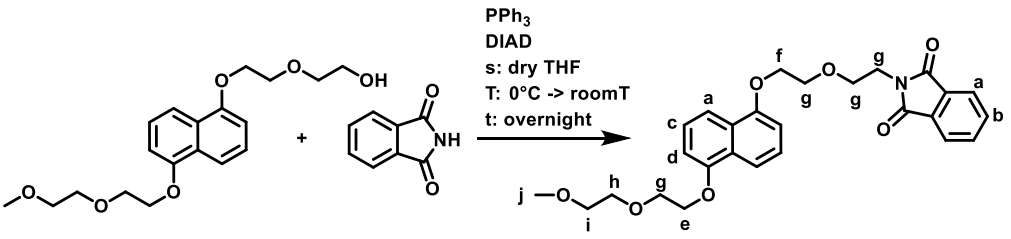

Figure 3.24. Reactions conditions for the synthesis of Napht-phthalimide with respective ^{1}H-NMR annotations.

Diisopropyl azodicarboxylate (DIAD) (1.76 g, 8.68 mmol) dissolved in 30 mL dry THF was added dropwise at 0 °C under nitrogen atmosphere to a solution of Napht-OMe (2.75 g, 7.85 mmol) containing phthalimide (1.31 g, 8.87 mmol) and triphenyl phosphine (PPh_3) (2.29 g, 8.76 mmol) in dry THF (90 ml). The mixture was stirred for 1 hour at 0 °C and overnight at room temperature. Subsequently the solvent was evaporated under reduced pressure and the residual orange colored oil was recrystallized from EtOH. The resulting shiny yellow solid was filtered and washed with cold EtOH.

Yield: 2.42 g (65%)

^{1}H-NMR spectroscopy (300 MHz, $DCCl_3$) δ(ppm) 7.9-7.7 (m, 4H, H_a), 7.63 (m, 2H, H_b), 7.28 (m, 2H, H_c), 6.79 (dd, *J* = 7.5 Hz, 2H, H_d), 4.30(m, 2H, H_e), 4.22 (m, 2H, H_f), 4.02-3.87 (m, 8H, H_g), 3.79 (q, *J* = 7.2 Hz, 2H, H_h), 3.60(m, 2H, H_i), 3.40(s, 3H, H_j)

4.3 Synthesis 2-[2-[[5-[2-(2-methoxyethoxy)ethoxy]-1-naphthalenyl]oxy]ethoxy]-ethanamine (Napht-NH_2)[38]

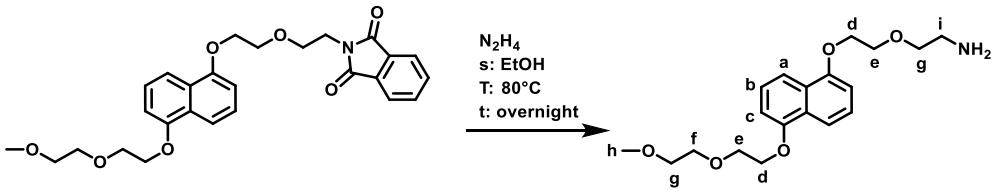

Figure 3.25. Synthetic scheme for the synthesis of Napht-NH_2 with respective ^{1}H-NMR annotations.

Hydrazine monohydrate (16.67 g, 32.94 mmol) was added dropwise under nitrogen atmosphere to a solution of Napht-phthalamide (2.42 g, 5.10 mmol) in EtOH (80 mL) after which the reaction was heated overnight under reflux. To ensure full conversion, another portion of hydrazine monohydrate (3 g, 5.93 mmol) was added to the mixture at room temperature and the mixture was allowed to reflux for another 12 h. The remaining residue after removing the solvent under reduced pressure was dissolved in chloroform and washed with brine. The organic phase was dried over $MgSO_4$, filtered and the solvent was evaporated to afford the pure compound as a shiny yellowish solid without any further purification.

Yield: 6.17 g (95%)

^{1}H-NMR spectroscopy (300 MHz, $DCCl_3$) δ(ppm) 7.87 (m, 2H, H_a), 7.33 (t, *J* = 8.0 Hz, 2H, H_b), 6.84 (d, *J* = 8.0 Hz, 2H, H_c), 4.29 (m, 2H, H_d), 3.97 (m, 2H, H_e), 3.77 (m, 1H, H_f), 3.62(m, 2H, H_g), 3.39 (s, 3H, H_h), 2.90 (t, *J* = 5.2 Hz, 2H, H_i), 1.42 (s, 2H, -NH_2)

4.4 Synthesis of N-[2-[2-[[5-[2-(2-methoxyethoxy)ethoxy]-1-naphthalenyl]oxy]ethoxy] ethyl]-2-Propenamide (Napht-Ac)[38]

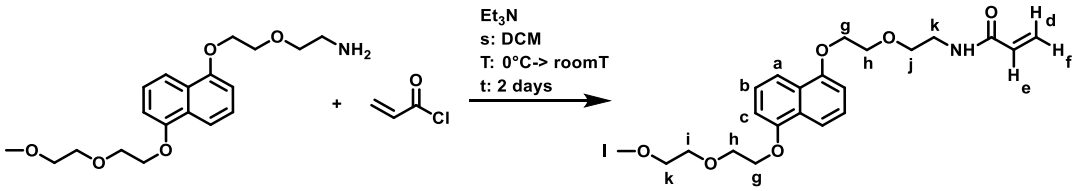

Figure 3.26. Reactions conditions for the synthesis of Napht.Ac with respective ^{1}H-NMR annotations.

Triethylamine (Et_3N) (2.15 g, 21.00 mmol) was added dropwise at 0 °C under nitrogen atmosphere to a solution of Napht-NH_2 (6.17 g, 18.00 mmol) dissolved in 120 mL DCM. Subsequently acryloyl chloride

(1.92 g, 21.00 mmol) was added dropwise under the same conditions after which the reaction mixture was allowed to heat up to room temperature and was stirred for 2 days. The compound was purified via 3 subsequent washing steps: 1) 10% NaOH, 2) brine and 3) H_2O. After drying of the organic phase with $MgSO_4$ the solvent was evaporated affording a brown-colored oil that was left to solidify in the fridge overnight. The resulting brown solid was filtered and washed with cold diethylether yielding the product as a yellowish solid.

Yield: 6.00 g (85%)

^{1}H-NMR spectroscopy (300 MHz, $DCCl_3$) δ(ppm) 7.86 (dd, *J* = 8.5 Hz, 2H, H_a), 7.35 (m, 2H, H_b), 6.87 (d, *J* = 7.8 Hz, 2H, H_c), 6.22 (dd, *J* = 17.0 Hz, 1.5 Hz, 2H, H_d), 5.93 (dd, *J* = 17.0 Hz, 10.4 Hz, 2H, H_e), 5.55 (dd, *J* = 10.3 Hz, 1.5 Hz, 1H, H_f), 4.31 (m, 4H, H_g), 3.98 (m, 4H, H_h), 3.80 (m, 2H, H_i), 3.71 (m, 2H, H_j), 3.58 (m, 4H, H_k), 3.40 (s, 3H, H_l)

4.5 Synthesis of 1,1'-(1,4-phenylenebis(methylene))bis(4,4'-pyridinium)bis(hexafluorophophate) (DS BB.2PF_6^-)[60]

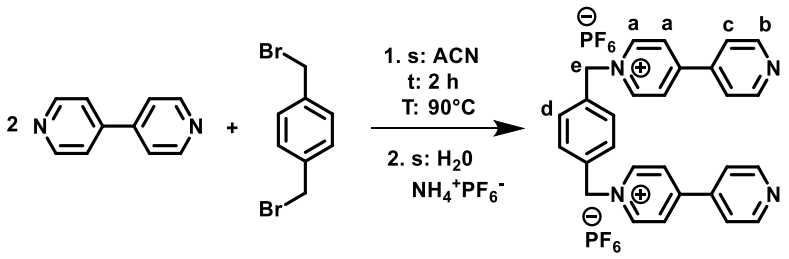

Figure 3.27. Reaction mechanism for the synthesis of DS BB.2PF_6^- with respective ^{1}H-NMR annotations.

α, α'-Dibromo-p-xylene (3.80 g, 14.00 mmol) and 4,4'-Bipyridine (8.90 g, 57.00 mmol) were dissolved in 120 mL of CH_3CN after which the solution was heated up to reflux for 2 h under inert atmosphere. The resulting bright yellow precipitation was filtered, dried under vacuum and further purified using a gradient column chromatography (silica, eluent: MeOH/2 M $NH_4^+Cl^-$ solution starting with an 8/2 ratio and ending with an 6/4 ratio). In a second step the counter ions of the end product were changed to PF_6^-. This was done by solubilizing the DS.2Cl^- in a minimum of water. Subsequently 3 eq of ammonium hexafluorophophate was added yielding a white precipitate. This white precipitate was filtered, washed with MeOH and diethyl ether and dried under vacuum.

Yield: 4.70 g (59%)

^{1}H-NMR spectroscopy (300 MHz, CD_3CN) δ(ppm) 9.17-8.67 (m, 8H, H_a), 8.56-8.24 (m, 4H, H_b), 8.02-7.70 (m, 4H, H_c), 7.59 (s, 4H, H_d), 5.81 (s, 4H, H_e)

4.6 Synthesis of cyclobis(paraquat-*p*-phenylene) (BB)[61]

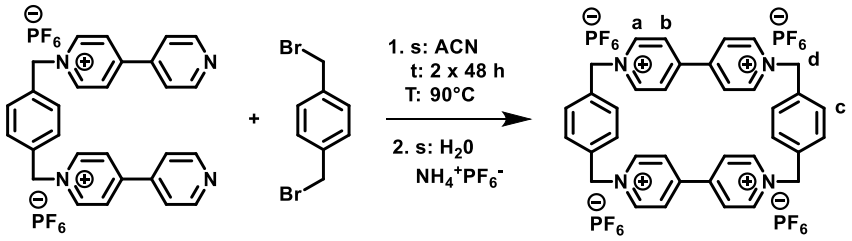

Figure 3.28. Synthetic scheme for the synthesis of BB with respective ^{1}H-NMR annotations.

A solution of DS.2PF_6^- (1.44 g, 2.50 mmol) and α, α'-dibromo-*p*-xylene (0.62 g, 2.30 mmol) in 200 mL CH_3CN was heated to reflux for 48 h after which another portion of α, α'-dibromo-p-xylene (0.46 g, 1.70 mmol) was added to the reaction mixture and was left to reflux for another 48 h. A bright yellow precipitate was formed upon reaction which was filtered, washed with CH_3CN and dried under vacuum. This crude product was purified via flash chromatography on 15 µm silica columns (40 g). The sample was prepared by mixing 1 g of silica with 1 g of crude product and introduced on the column via a solid loader. At first, this set-up was rinsed with 10 column volumes (CV) of MeOH, after which an eluent gradient was introduced of 50%-50% MeOH/H_2O over 10 CV. The fractions containing the pure product were collected and dried under reduced pressure.

In a final step the counter ions of the end product were changed to PF_6^-. This was done by solubilizing the purified BB product in a minimum of water. Subsequently, 3 eq of ammonium hexafluorophophate were added creating a white precipitate. This white precipitate was filtered, washed with MeOH and diethyl ether and dried under vacuum.

Yield: 0.25 g (10%)

^{1}H-NMR spectroscopy (300 MHz, CD_3CN) δ(ppm) 8.91(d, *J* = 6.3 Hz, 8H, H_a), 8.21 (d, *J* = 6.3 Hz, 8H, H_b), 7.58 (s, 8H, H_c), 5.79 (s, 8H, H_d)

4.7 Conditions to change counter ion BB to chlorine

In order to solubilize BB in water, its counter ions needed to be exchanged from 4 PF_6^- to 4 Cl^- ions. This ion exchange reaction from PF_6^- to Cl^- was done by solubilizing the BB.4$NH_4^+PF_6^-$ in a minimum amount of nitromethane. Subsequently 6 eq of tetraethylammonium chloride were added yielding a white precipitate. This white precipitate was filtered, washed with MeOH and diethyl ether and dried under vacuum.

^{1}H-NMR spectroscopy (300 MHz, D_2O) δ(ppm) 9.27 (d, *J* = 6.3 Hz, 8H, H_a), 8.46 (d, *J* = 6.4 Hz, 8H, H_b), 7.80 (s, 8H, H_c), 6.03 (s, 8H, H_d)

4.8 Synthesis of the Napht-co-PNIPAm hydrogel

The synthesis of the hydrogels using free radical polymerization will be illustrated using the synthesis of the 3% Napht-co-PNIPAm as representative example. NIPAm (0.71 g, 6.25 mmol) was dissolved together with MBA (0.01 g, 0.063 mmol) and Napht.Ac (0.077 g, 0.19 mmol) in 2.5 mL DMSO. An initiator stock solution was prepared containing KPS (0.18 g, 0.66 mmol) in 10 mL DMSO and both solutions were bubbled with argon for 5 minutes. After the deoxygenation, 1 mL of the initiator stock solution was transferred to the monomer solution, after which the mixture was stirred for another 10 seconds under inert atmosphere. Subsequently, the solution was injected into a mold, consisting of two glass plates (7 x 3 cm) separated by teflon tubing (4.0 mm diameter) reinforced by copper wire and was heated overnight at 70 °C under inert atmosphere. The formed hydrogel was afterwards released from the glass plates and soaked for two days in acetone to remove any unreacted monomers. Afterwards the hydrogel was dried at room temperature and swelled in water to equilibrium. For the synthesis of all my hydrogels a single Napht.Ac monomer batch was used. The purity was confirmed via NMR spectroscopy prior to polymer synthesis. These spectra and the consistent quality of the hydrogels gave an indication on the shelf life of the monomer as at least 6 months when stored under argon in the fridge.

4.9 Determination swelling ratio of the Napht-co-PNIPAm hydrogels

The Napht-co-PNIPAm hydrogel was cut in pieces of 1.0 cm x 1.0 cm x 0.5 cm that were immersed in a large beaker (100 mL) filled with deionized water. The hydrogel pieces were soaked for 3 days at 5 °C until equilibrium was reached. Afterwards these pieces were taken from the aqueous solution and weighted after removing the excess water on the surface of the hydrogel with paper. Subsequently, the swollen hydrogels were placed overnight in the oven at 60 °C to remove all water and were weighted to determine the mass of the dried hydrogel pieces. The swelling ratio at equilibrium was calculated using equation 3.5:

Equation 3.5

$$Swelling\ ratio = \frac{(W_{eq} - W_{dry})}{W_{dry}}$$

where W_{dry} is the weight of the dried Napht-co-PNIPAm hydrogel piece and W_{eq} is the mass of the swollen hydrogel piece at equilibrium.

4.10 Procedure for the complexation of the Napht-co-PNIPAm hydrogels

The complexation of the Napht-co-PNIPAm hydrogels will be illustrated using the synthesis of the 3% Napht-co-PNIPAm as representative example. Swollen rectangular pieces of 1.0 cm by 0.5 cm by 0.5 cm of Napht-co-PNIPAm were soaked for 24 h at 5 °C (fridge) in a 1 mL concentrated BB solution(≈ 13

mM). The exact amount of BB was determined using equation 3.3 and depends of the weight of the hydrogel piece:

Equation 3.3 $$m_{BB} = MW_{BB} * Eq_{BB} \frac{m_{Dry} * wt\%_{Napht.Ac}}{MW_{Napht.AC}}$$

with MW_{BB} the molecular weight of BB (662.5 g/mol), Eq_{BB} the desired equivalents of BB added to the Napht-co-PNIPAm hydrogel (here 3 equivalnets), m_{dry} the mass of the dried hydrogel piece, $wt\%_{Napht\text{-}monomer}$ the weight percentage of the incorporated naphthalene units (11%) and $MW_{Napht.Ac}$ the molecular weight of the naphthalene monomer (430.5 g/mol). To enhance the BB uptake and the complexation of the hydrogel, small vials of 10 mL were used ensuring the full coverage of the hydrogel when submerged into the 1 mL BB solution. After 24h, the solution was diluted by adding 9 mL of deionized water to the vial and the now fully complexed hydrogel. The hydrogel was left to swell until equilibrium for 2 days at 5 °C. The swelling ratio of the complexed hydrogels was again determined gravimetrically using equation 3.5.

4.11 Procedure for the memory experiments of 3 % Napht-co-PNIPAm

A large water bad was heated until the desired temperature stayed stable after which the complexed rectangular hydrogel pieces were submerged for either 1 h, 5 h, 10 h and 14 h. After the desired exposure time, the hydrogels were taken out of the heated aqueous solution, weighted after removing the excess of water with paper and submerged in 20 mL fresh deionized water. After the hydrogels were soaked for 1 h, 2 h, 3 h, 24 h, 48 h, 72 h and 96 h, the hydrogels were removed from the deionized water and their reswelling ratio was determined gravimetrically using equation 3.5. These reswelling ratios were then used to calculate the decomplexation rate using following equation 3.6:

Equation 3.6 $$\%\ Decomplexation = 100 - \left(\frac{Q_{reswollen\ x\ h} - Q_{eq,non-complexed}}{Q_{eq,complexed} - Q_{eq,non-complexed}}\right) x\ 100$$

with $Q_{reswollen\ x\ h}$ the swelling ratio of the heated hydrogel soaked for 1 h, 2 h, 3 h, 24 h, 48 h, 72 h and 96 h respectively in the 20 mL fresh deionized water, $Q_{eq,complexed}$ the swelling ratio of the complexed hydrogel at equilibrium, $Q_{eq,\ non\text{-}complexed}$ the swelling ratio of the non-complexed hydrogel piece at equilibrium. All heating experiments were performed in triplicate.

4.12 Reswelling ratios of the heated hydrogels

To indicate the swelling ratios and the effect of the decomplexation on the reswelling of the hydrogels, the data in Figure 3.21 was reworked to show the swelling ratio in function of the reswelling time for the different heating temperatures. The reswelling of the 3% Napht-co-PNIPAm hydrogels after the heating step at 42 °C, 46 °C, 50 °C and 60 °C with different heating times (1-5-10-14h) was followed in

function of the reswelling time in fresh demineralised water (Figure 3.29). The expected opposite trend was visible compared to previous Figure 3.21 because the decomplexation rate and reswelling ratio are inversely correlated, i.e. the more decomplexation has occurred, the less swelling is restored over time in fresh demineralised water. However, similar conclusions can be made with the samples heated at 42°C showing the largest temperature memory window between the different heating times, even after swelling up to 96 hours. This temperature memory window decreases when the hydrogel is heated at temperatures far greater than its VPTT due to the rapid collapse of the hydrogel preventing efficient diffusion of the BB outside of the hydrogel. The apparent decrease of the swelling ratio with increased swelling time in all samples is most likely related to the reformation of the new concentration equilibrium of BB between the heated hydrogel and the fresh demineralised water, resulting in diffusion of BB out of the swollen hydrogel.

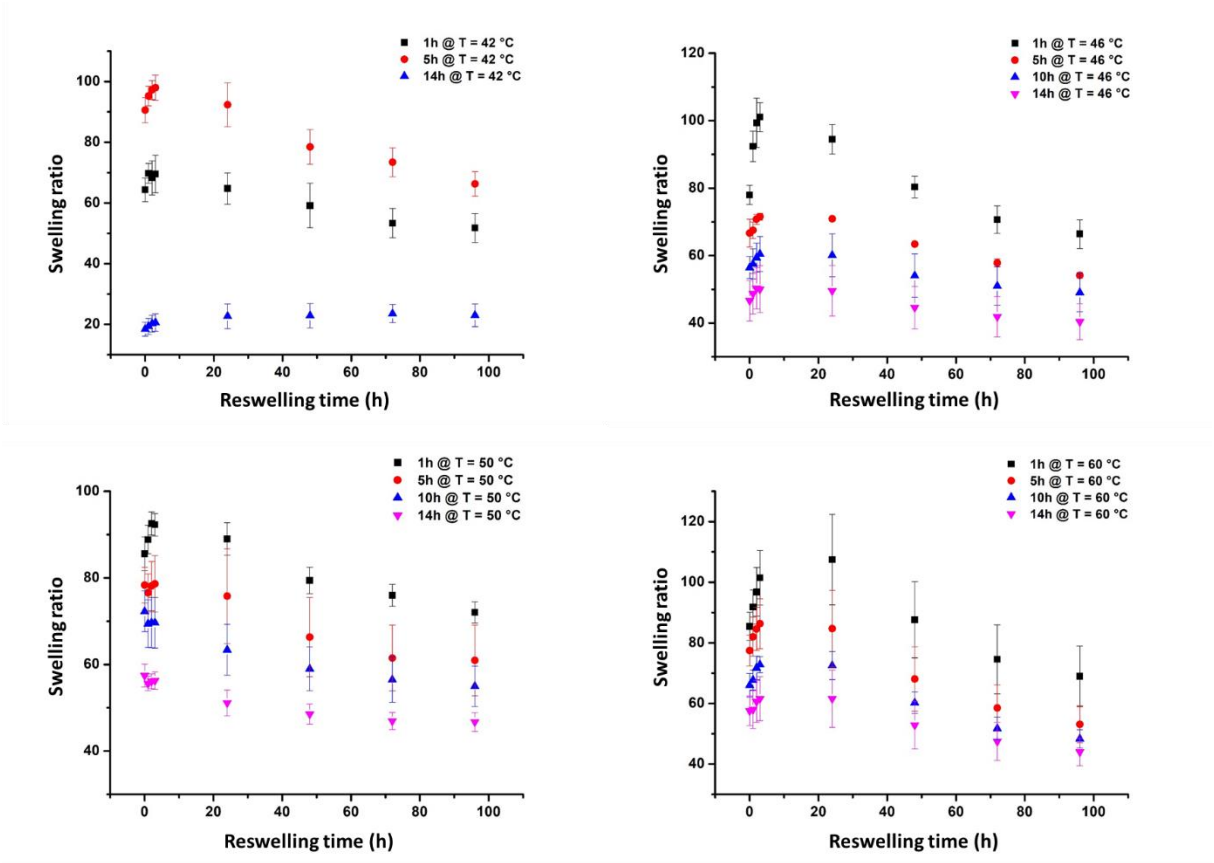

Figure 3.29. Reswelling ratios of 3% Napht-co-PNIPAm hydrogels being exposed for 1 h (black squares), 5 h (red circles), 10 h (blue upward triangle) and 14 h (purple downward triangle) at 42°C, 46°C, 50°C and 60°C and subsequently being soaked in fresh demineralised water (20 mL) for 1 h, 2h, 3h, 24 h, 48 h, 72 h and 96 h. All tests were performed in triplicate.

4.13 Mechanical properties of the 3% Napht-co-PNIPAm

The storage modulus was measured by performing an amplitude sweep with a normal force of 0.1 N covering strain amplitudes from 10^{-4} % to 10 %. It can be noticed that a linear viscoelastic range is present for both the non-complexed and the complexed hydrogels in the kPa range. From these results

it can be observed that complexation leads to weakening of the 3% Napht-co-PNIPAM hydrogels as indicated by the decrease of G' at lower strain rate as compared to the non-complexed hydrogel.

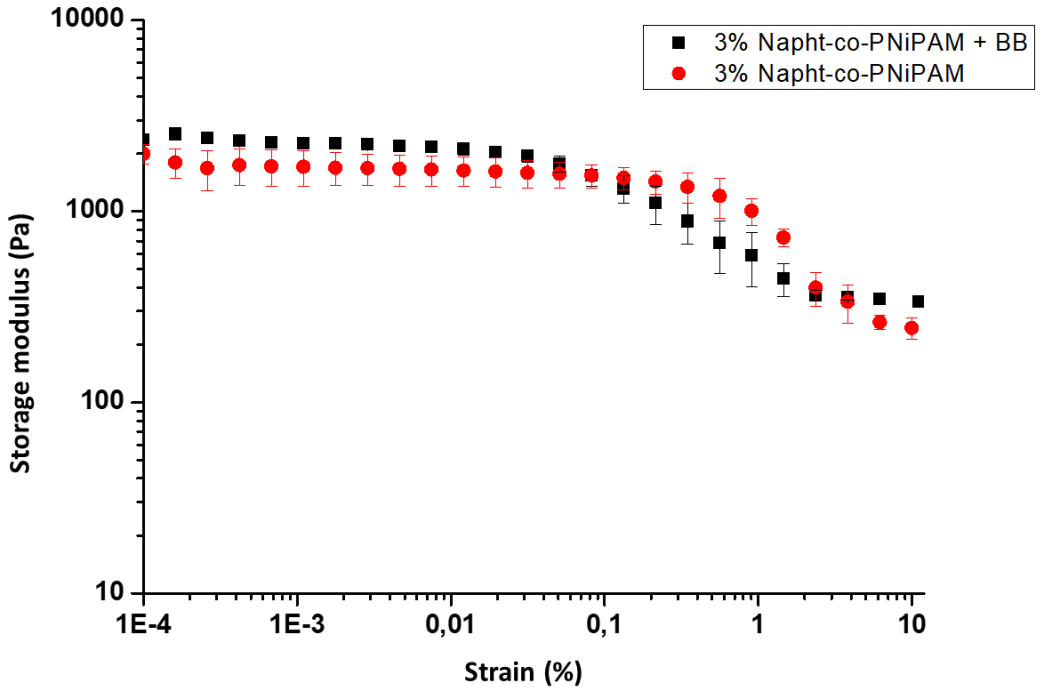

Figure 3.30. The amplitude sweeps of non-complexed and complexed 3% NApht-co –PNIPAm. The amplitude sweeps were performed at a constant angular frequency of 1 rad/s and with changing stain amplitude from 10^{-4} to 10%.

5 References

1. Sun, H.; Chen, J.; Han, X.; Liu, H. *Mater. Sci. Eng. C* **2018**, *82*, 284.
2. Chang, R.; Wang, X.; Li, X.; An, H.; Qin, J. *ACS Appl. Mater. Interfaces* **2016**, *8*, 25544.
3. Pietsch, C.; Mansfeld, U.; Guerrero-Sanchez, C.; Hoeppener, S.; Vollrath, A.; Wagner, M.; Hoogenboom, R.; Saubern, S.; Thang, S. H.; Becer, C. R.; Chiefari, J.; Schubert, U. S. *Macromolecules* **2012**, *45*, 9292.
4. Klouda, L.; Mikos, A. G. *Eur. J. Pharm. Biopharm.* **2008**, *68*, 34.
5. Wang, Y.; Wang, J.; Yuan, Z.; Han, H.; Li, T.; Li, L.; Guo, X. *Colloids Surfaces B Biointerfaces* **2017**, *152*, 252.
6. Chen, Y.; Liu, W.; Zeng, G.; Liu, Y. J. *J. Appl. Polym. Sci.* **2017**, *134*, 1.
7. Lu, L.; Tian, T.; Wu, S.; Xiang, T.; Zhou, S. *Polym. Chem.* **2019**, *10*, 1920.
8. Gulyuz, U.; Okay, O. *Macromolecules* **2014**, *47*, 6889.
9. Cantini, E.; Wang, X.; Koelsch, P.; Preece, J. A.; Ma, J.; Mendes, P. M. *Acc. Chem. Res.* **2016**, *49*, 1223.
10. Manouras, T.; Vamvakaki, M. *Polym. Chem.* **2017**, *8*, 74.
11. Thévenot, J.; Oliveira, H.; Sandre, O.; Lecommandoux, S. *Chem. Soc. Rev.* **2013**, *42*, 7099.
12. Dong, Y.; Wang, W.; Veiseh, O.; Appel, E. A.; Xue, K.; Webber, M. J.; Tang, B. C.; Yang, X. W.; Weir, G. C.; Langer, R.; Anderson, D. G. *Langmuir* **2016**, *32*, 8743.
13. Zhao, Q.; Dunlop, J. W. C.; Qiu, X.; Huang, F.; Zhang, Z.; Heyda, J.; Dzubiella, J.; Antonietti, M.; Yuan, J. *Nat. Commun.* **2014**, *5*, 1.
14. Qin, H.; Zhang, T.; Li, N.; Cong, H. P.; Yu, S. H. *Nat. Commun.* **2019**, *10*, 1.
15. Li, L.; Scheiger, J. M.; Levkin, P. A. *Adv. Mater.* **2019**, *1807333*.
16. Xu, Y.; Ghag, O.; Reimann, M.; Sitterle, P.; Chatterjee, P.; Nofen, E.; Yu, H.; Jiang, H.; Dai, L. L. *Soft Matter* **2017**, *14*, 151.
17. Liu, Q.; Liu, L. *Langmuir* **2019**, *35*, 1450.
18. Hauser, A. W.; Evans, A. A.; Na, J. H.; Hayward, R. C. *Angew. Chem. Int. Ed.* **2015**, *54*, 5434.
19. Kim, D.; Lee, H. S.; Yoon, J. *RSC Adv.* **2014**, *4*, 25379.
20. Tsitsilianis, C.; Gotzamanis, G.; Iatridi, Z. *Eur. Polym. J.* **2011**, *47*, 497.
21. Schmalz, A.; Schmalz, H.; Müller, A. H. E. *Soft Matter* **2012**, *8*, 9436.
22. Das, S.; Chatterjee, D. P.; Ghosh, R.; Das, P.; Nandi, A. K. *RSC Adv.* **2016**, *6*, 8773.
23. Du, J.; Choi, B.; Liu, Y.; Feng, A.; Thang, S. H. *Polym. Chem.* **2019**, *10*, 1291.
24. Yao, Y.; Saw, P. E.; Nie, Y.; Wong, P. P.; Jiang, L.; Ye, X.; Chen, J.; Ding, T.; Xu, L.; Yao, H.; Hu, H.; Xu, X. *J. Mater. Chem. B* **2019**, *7*, 576.
25. Ashraf, S.; Park, H. K.; Park, H.; Lee, S. H. *Macromol. Res.* **2016**, *24*, 297.
26. Sponchioni, M.; Capasso Palmiero, U.; Moscatelli, D. *Mater. Sci. Eng. C* **2019**, *102*, 589.

27. Hu, J.; Liu, S. *Macromolecules* **2010**, *43*, 8315.

28. Wang, F. W.; Hsu, C. W.; Hsieh, C. C. *ACS Appl. Mater. Interfaces* **2019**, *11*, 8591.

29. Körner, J.; Reiche, C. F.; Leu, H.-Y.; Farhoudi, N.; Magda, J.; Solzbacher, F. *Proceedings* **2018**, *2*, 1006.

30. Ionov, L. *Mater. Today* **2014**, *17*, 494.

31. Yuan, C.; Guo, J.; Yan, F. *Polymer.* **2014**, *55*, 3431.

32. Mori, T.; Beppu, S.; Berber, M. R.; Mori, H.; Makimura, T.; Tsukamoto, A.; Minagawa, K.; Hirano, T.; Tanaka, M.; Niidome, T.; Katayama, Y.; Hirano, T.; Maeda, Y. *Langmuir* **2010**, *26*, 9224.

33. Kim, D.; Kim, H.; Lee, E.; Jin, K. S.; Yoon, J. *Chem. Mater.* **2016**, *28*, 8807.

34. Zhang, K.; Feng, X.; Ye, C.; Hempenius, M. A.; Vancso, G. J. *J. Am. Chem. Soc.* **2017**, *139*, 10029.

35. Kiriya, D.; Chang, H. C.; Kitagawa, S. *J. Am. Chem. Soc.* **2008**, *130*, 5515.

36. Weidman, J. L.; Mulvenna, R. A.; Boudouris, B. W.; Phillip, W. A. *J. Am. Chem. Soc.* **2016**, *138*, 7030.

37. Wei, R.; Yang, F.; Gu, R.; Liu, Q.; Zhou, J.; Zhang, X.; Zhao, W.; Zhao, C. *ACS Appl. Mater. Interfaces* **2018**, *10*, 36443.

38. Sambe, L.; Delarosa, V. R.; Belal, K.; Stoffelbach, F.; Lyskawa, J.; Delattre, F.; Bria, M.; Cooke, G.; Hoogenboom, R.; Woisel, P. *Angew. Chem. Int. Ed.* **2014**, *53*, 5044.

39. De La Rosa, V. R.; Hoogenboom, R. *Chem. - A Eur. J.* **2015**, *21*, 1302.

40. Kristensen, R.; Andersen, S. S.; Olsen, G.; Jeppesen, J. O. *J. Org. Chem.* **2017**, *82*, 1371.

41. Van Vlierberghe, S.; Fritzinger, B.; Martins, J. C.; Dubruel, P. *Appl. Spectrosc.* **2010**, *64*, 1176.

42. Van Nieuwenhove, I.; Salamon, A.; Peters, K.; Graulus, G. J.; Martins, J. C.; Frankel, D.; Kersemans, K.; De Vos, F.; Van Vlierberghe, S.; Dubruel, P. *Carbohydr. Polym.* **2016**, *152*, 129.

43. Park, H. W.; Ro, Y. M.; Cho, Z. H. *Phys. Med. Biol.* **1988**, *33*, 339.

44. Ramadhar, T. R.; Amador, F.; Ditty, M. J. T.; Power, W. P. *Magn. Reson. Chem.* **2008**, *46*, 30.

45. Malfait, A.; Coumes, F.; Fournier, D.; Cooke, G.; Woisel, P. *Eur. Polym. J.* **2015**, *69*, 552.

46. Bria, M.; Cooke, G.; Cooper, A.; Garety, J. F.; Hewage, S. G.; Nutley, M.; Rabani, G.; Woisel, P. *Tetrahedron Lett.* **2007**, *48*, 301.

47. Yeniad, B.; Ryskulova, K.; Fournier, D.; Lyskawa, J.; Cooke, G.; Woisel, P.; Hoogenboom, R. *Polym. Chem.* **2016**, *7*, 3681.

48. Miljanić, O. Š.; Dichtel, W. R.; Mortezaei, S.; Stoddart, J. F. *Org. Lett.* **2006**, *8*, 4835.

49. Fumagalli, M.; Belal, K.; Guo, H.; Stoffelbach, F.; Cooke, G.; Marcellan, A.; Woisel, P.; Hourdet, D. *Soft Matter* **2017**, *13*, 5269.

50. Belal, K.; Stoffelbach, F.; Lyskawa, J.; Fumagalli, M.; Hourdet, D.; Marcellan, A.; Smet, L. De; de la Rosa, V. R.; Cooke, G.; Hoogenboom, R.; Woisel, P. *Angew. Chem. Int. Ed.* **2016**, *55*, 13974.

51. Malfait, A.; Coumes, F.; Fournier, D.; Cooke, G.; Woisel, P. *Eur. Polym. J.* **2015**, *69*, 552.

52. Mcconkey, B. J.; Hewitt, L. M.; Dixon, D. G.; Greenberg, B. M. *Water, Air, Soil Pollut.* **2002**, *136*,

347.

53. Teotia, A. K.; Sami, H.; Kumar, A. *Thermo-responsive polymers: Structure and design of smart materials*; Elsevier Ltd, **2015**.

54. Halperin, A.; Kröger, M.; Winnik, F. M. *Angew. Chem. Int. Ed.* **2015**, *54*, 15342.

55. Jain, K.; Vedarajan, R.; Watanabe, M.; Ishikiriyama, M.; Matsumi, N. *Polym. Chem.* **2015**, *6*, 6819.

56. Otake, K.; Inomata, H.; Konno, M.; Saito, S. *Macromolecules* **1990**, *23*, 283.

57. Haq, M. A.; Su, Y.; Wang, D. *Mater. Sci. Eng. C* **2017**, *70*, 842.

58. Schönhoff, M.; Larsson, A.; Welzel, P. B.; Kuckling, D. *J. Phys. Chem. B* **2002**, *106*, 7800.

59. Spěváček, J.; Hanyková, L. *Macromol. Symp.* **2016**, *359*, 111.

60. Naik, I. K.; Sarkar, R.; Madhu, V.; Bolligarla, R.; Kishore, R.; Das, S. K. *J. Phys. Chem. A* **2017**, *121*, 3274.

61. Odell, B.; Reddington, M. V.; Slawin, A. M. Z.; Spencer, N.; Stoddart, J. F.; Williams, D. J. *Angew. Chem. Int. Ed.* **1988**, *27*, 1547.

Chapter 4. Expansion of the Plasma dye coating (PDC) procedure towards the fabrication of smart supramolecular surfaces

Abstract

In this final chapter, the plasma dye coating (PDC) procedure was explored for the fabrication of stimuli-responsive materials and surfaces based on host-guest complexation. This PDC procedure was invented by our group for the creation of colored materials, significantly reducing dye leaching through covalent immobilization of the desired dye using plasma-generated radicals. This PDC procedure immobilizes a pre-adsorbed layer of polymerizable dye on the surface through radical addition during a short plasma treatment. The non-specific nature of the plasma-generated radicals allows for PDC for a wide variety of complex dyes, including azobenzenes and sulfonphthaleines, functionalized with radical sensitive groups to avoid significant dye degradation, to be combined with various polymeric materials including PP, PE, PA6, cellulose and PTFE. As part of this thesis, the work originally done in our group was first continued by the further characterization of the materials surface using SEM, contact angle measurements and XPS. Secondly, the dye application step was further optimized by developing a liquid spray technique to coat the materials with the desired dye prior to plasma treatment in order to allow lower dye consumption, the application of a specific design onto the surface and the use of more complex material surfaces. Finally, the applicability of this PDC technique was expanded towards the possible incorporation of other more complex molecules, such as host-guest assemblies on a variety of materials including more inert Teflon, PP and PE.

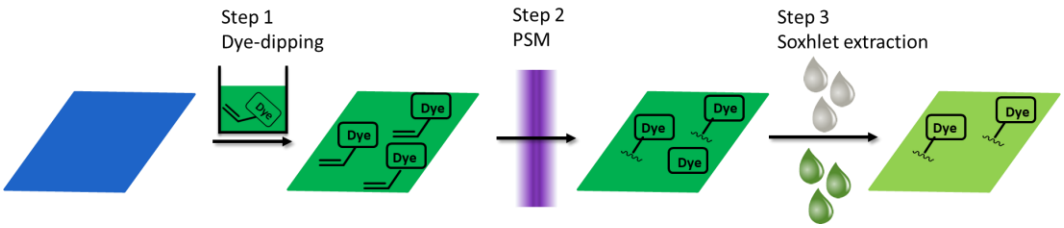

Contributing authors:

Ella Schoolaert for performing the SEM measurements, Elke Van De Walle for measuring the contact angles and Jan-Philip Zegwaart for performing the XPS measurements.

Parts of this chapter have been published in:

Lieselot De Smet*, Gertjan Vancoillie*, Peter Minshall, Kathleen Lava, Iline Steyaert, Ella Schoolaert, Elke Van De Walle, Peter Dubruel, Karen De Clerck and Richard Hoogenboom; Plasma Dye Coating: A Straightforward and Widely Applicable Procedure for Dye Immobilization on Common Polymeric Materials. **Nature communications**, 9, 1123, 2018. DOI: 10.1038/s41467-018-03583-4

1 Introduction

A very interesting use of supramolecular chemistry is to dynamically control the surface properties of polymeric materials without changing the bulk properties.[1–7] The use of stimuli-responsive host-guest assemblies by e.g. surface-bound rotaxanes has been developed for orthogonal adaptable surface properties such as the wettability, biocompatibility, antifouling and corrosion resistance. An example is shown in Figure 4.1 by Hu *et al.* who reported the creation of polymer brushes mediated by cucurbit[8]uril host-guest assemblies making the material surface properties highly responsive towards external stimuli including light, redox potential and the presence of competitive guest molecules. Compared to the traditional strategies to alter material surface properties including surface-initiated polymerization and layer-by-layer self-assembly, this supramolecular method uses a physical grafting-to strategy using host-guest assembly to immobilize well-defined polymers functionalized with a compatible guest molecule.[8]

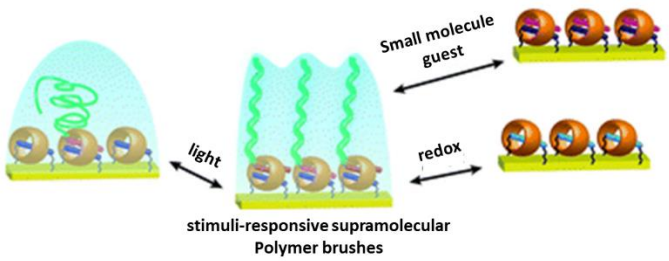

Figure 4.1. Schematic illustration of CB[8]-mediated supramolecular grating-to polymer brushes, orthogonally controlled by light, competitive guest molecules and redox potential. Reprinted from ref.[8] Copyright 2019 Royal Society of Chemistry.

Not only can supramolecular chemistry be used to modify surface properties but also to improve the adhesion between two substrates.[9–14] The strong and dynamic nature of the host-guest interactions in both organic and aqueous media has already led to the remarkable creation of reversible macroscopic adhesive systems based on nanoscale molecular interactions. For example, the Harada group has reported a series of stimuli-controlled, macroscopic assemblies by the adhesion of different hydrogels through host-guest interaction with cyclodextrin (CD).[15,16] Another famous example of such a supramolecular superglues was already discussed in Chapter 2, reported by Kim *et al.* who used a supramolecular Velcro to adhere two silicon surfaces, which could be regulated by the oxidation of the guest molecule (Figure 2.1).[9] A final example that will be highlighted here was reported by the group of Scherman, where porous (wood and bones) and nonporous (e.g. glass, aluminium) substrates were dynamically glued together by the creation of a supramolecular hydrogel based on CB[8] host molecules providing the necessary interfacial adhesive forces as displayed in Figure 4.2.[10] To create this interfacial supramolecular hydrogel, polymers functionalized with 1-benzyl-3-vinylimidazolium bromide were physically adsorbed onto the material surfaces prior to the addition of CB[8].

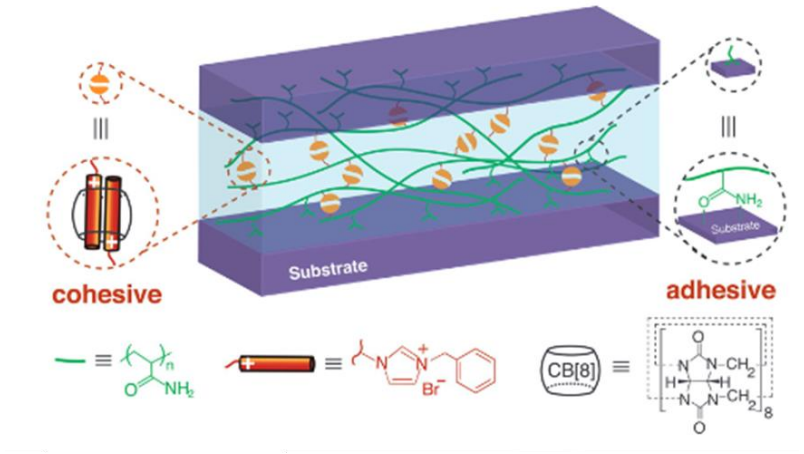

Figure 4.2. The creation of the supramolecular hydrogel using the ternary CB[8] complexes with 1-benzyl-3-vinylimidazolium bromide providing the interfacial adhesion of two substrates. Reprinted from ref.[10] Copyright 2019 John Wiley and Sons.

To date, the availability of guest or host molecules onto the surface of a material is generated by either incorporating the desired molecule into the 3D-network of the materials like the hydrogels reported by Harada *et al.* or through the post-polymerization modification with reactive surface groups as described by Kim *et al.* for the supramolecular Velcro between two rigid silicon materials. The latter approach is much more favorable as only a low amount of the desired host or guest is necessary to functionalize the surface of the materials. Mostly this chemical linkage between the surface and the host or guest molecule is achieved through the use of specific surface functionalities including amines and alcohols, allowing the immobilization through, respectively, amide or ester formation. Examples of this post-fabrication method are reported in literature by Takashima *et al.* by immobilizing acyl chloride containing derivatives of adamantane, ferrocene and azobenzene molecules onto a (3-aminopropyl)triethoxysilane (APTES) functionalized glass substrates creating a stable amide bond between both. After immobilization, it was observed that the glass plates could selectively adhere with CD host molecules and CD based hydrogels.[17] Similarly, Tian *et al.* reported the creation of a new hybrid magnetic material by the amidation of amine-functionalized Fe_3O_4 nanoparticles (Fe-NP) with carboxylatopillar[5]arene (CP[5]A) which can be employed for the sensing and detection of several herbicides in food safety control (Figure 4.2).[2]

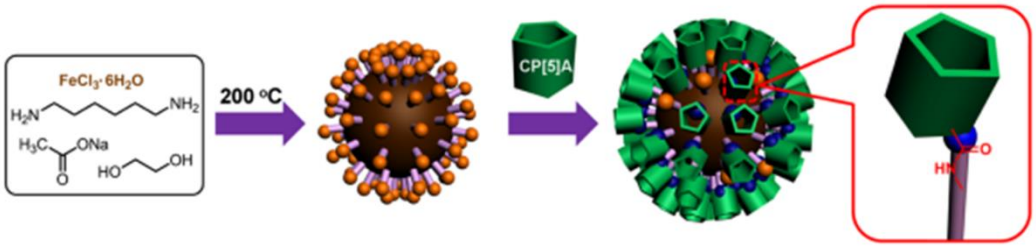

Figure 4.2. Synthesis route of the Fe-NP covalently functionalized with CP[5]A.[2]

However, these post fabrication methods are restricted to materials having a reactive surface or possessing surface functional groups, limiting the possible application of supramolecular adhesion and smart surfaces in common bulk plastics such as polypropylene (PP), polyethylene (PE) and polytetrafluoroethylene (PTFE). Additionally, the presence of residual reactive groups after the surface modification step could interfere with the supramolecular assembly and potentially its application.

An alternative method that bypasses the necessity of specific functional surface groups and thereby of the restriction on applicable polymeric materials, is based on the creation of surface radicals on the material using plasma surface modification (PSM) processes. Plasma is the fourth state of matter and consists of a gaseous mixture of highly energetic ionized atoms, radicals, electrons and neutral molecules which can create surface radicals through homolytic cleavage of the weakest bond or proton abstraction.[18–20] Commonly used gases include oxygen, argon and helium, which can be energized using for example extreme heat or by the application of an electrical field.[21] Thermal plasmas are often applied in molecular characterization methods like optical emission spectroscopy and mass spectroscopy, while cold or non-thermal plasmas can be used for the modification of material surfaces.[22] Khelifa *et.al* (2016), divided cold plasma techniques into two main categories: non-depositing and depositing techniques (Figure 4.3).[23] Non-depositing techniques, commonly known as plasma etching, employs plasma to clean material surfaces by removal of a few layers of atoms and possible surface contaminants.[21,24,25] Depositing techniques or plasma-enhanced chemical vapor deposition (PECVD) are used to introduce novel functionalities on the surface of the material by injecting various organic molecules into the plasma.[23,26] This provides control over surface properties like hydrophilicity, biocompatibility and adhesiveness but also surface chemistry by introducing reactive functionalities using simple molecules like amines (NH_3-plasma, 1,3-diaminopropane),[25,27] alcohols and epoxides (O_2-plasma)[20] and fluorine groups (C_2F_6-plasma).[28] These reactive surface groups can subsequently be used for immobilization of complex biomolecules such as biotin but also for surface-initiated 'grafting-from' polymerization.[29,30]

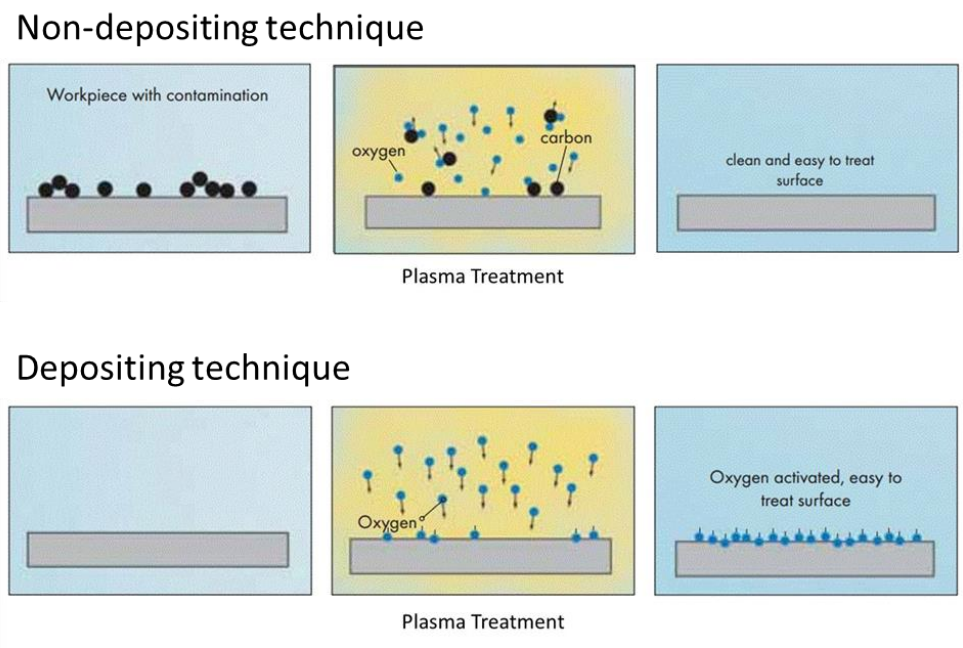

Figure 4.3. Illustration of the difference between a non-depositing cold plasma technique (top) and a depositing cold plasma technique (bottom) using oxygen gas.[18]

Another possibility to anchor complex aromatic molecules like dyes onto the surface of polymeric materials is by using the PDC method which was invented by our supramolecular chemistry group in Ghent as part of my master thesis.[31] This three step process, as illustrated in Figure 4.4, was initially investigated for the creation of colored and chromic materials by covalent immobilization of the desired reactive dye molecule using a short plasma depositing step which reduces significantly the dye leaching during their application. During the first step of this PDC procedure, the material is dipped for 1 minute into a 25 mg/mL solution of the desired reactive dye that is functionalized with a polymerizable group, in a volatile solvent allowing the homogenous adsorption of the dye onto the surface. The dye diffusion into the polymeric material could be suppressed by using a relative short dipping time in combination with a non-solvent for the used polymer material. In the next step, the stained material is exposed to the highly energetic and inert argon plasma creating surface radicals which can covalently immobilize the dye molecules via a radical addition reaction. In this optimized procedure the samples are plasma treated on both sides to ensure max dye immobilization onto the material. In the last and third step, unanchored dye molecules and byproducts generated by the plasma treatment step are removed using soxhlet extraction. During optimization, the plasma treatment time was identified as the most important parameter for the immobilized dye loading after PDC as it controls the balance between dye immobilization and dye/material degradation.

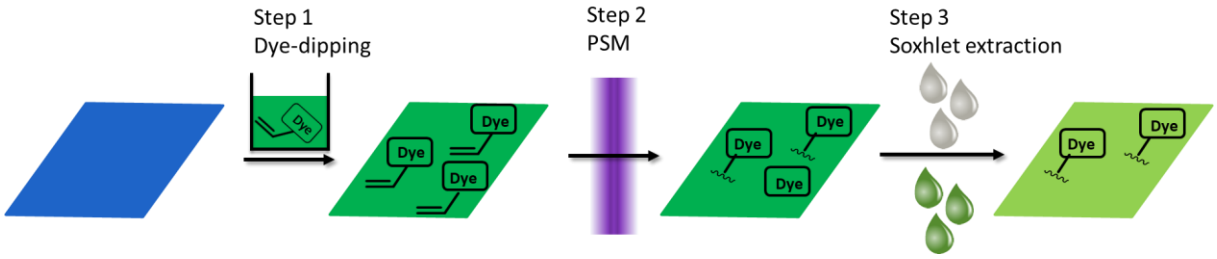

Figure 4.4. The schematic representation of the different steps used in the PDC procedure.

The importance of both the presence of a polymerizable reactive group in the desired dye molecules and the generation of the surface radicals through PSM in the PDC process was highlighted by performing reference experiments excluding these key-components. In comparison to the optimized PDC process depicted in the first row of Figure 4.5, no distinguishable dye immobilization was observed after soxhlet extraction in the two reference samples where either the polymerizable group or the plasma treatment step was eliminated confirming the necessity of these components. While the plasma treatment itself is critical for the generation of the necessary surface radicals, the polymerizable group is proposed to act as an antenna to react with the formed surface radicals and, thereby, to prevent the degradation of the complex aromatic molecules. The remaining color after extensive soxhlet extraction also serves as proof for the absence of dye leaching of the resulting materials using PDC.

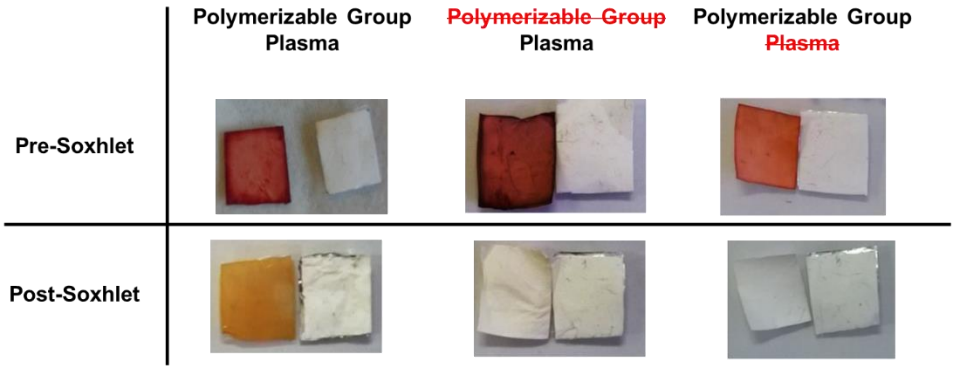

Figure 4.5. Proof-of-concept of the necessity of the two key-components: the PSM step and the polymerizable group onto the desired dye for the chemical modification using the PDC procedure to modify DR1-A onto PA6 substrates. All pictures are taken adjacent to an untreated piece of the used material. Reprinted from ref.[31] Copyright 2019 Springer Nature.

The wide applicability of this procedure is highlighted in Figure 4.6, where a wide variety of different dye/material combinations has been treated using the optimized PDC procedure. Although all dye/material combinations are colored after soxhlet extraction, the intensity of the treated materials differs significantly. The best results are obtained with DR1-A, which may be expected as the PDC procedure was optimized with this dye. This result indicates that the PDC process parameters, most importantly the PSM step, are possibly dependent on the dye, polymerizable group and material.

These should therefore be optimized for every new combination to ensure maximum dye immobilization.

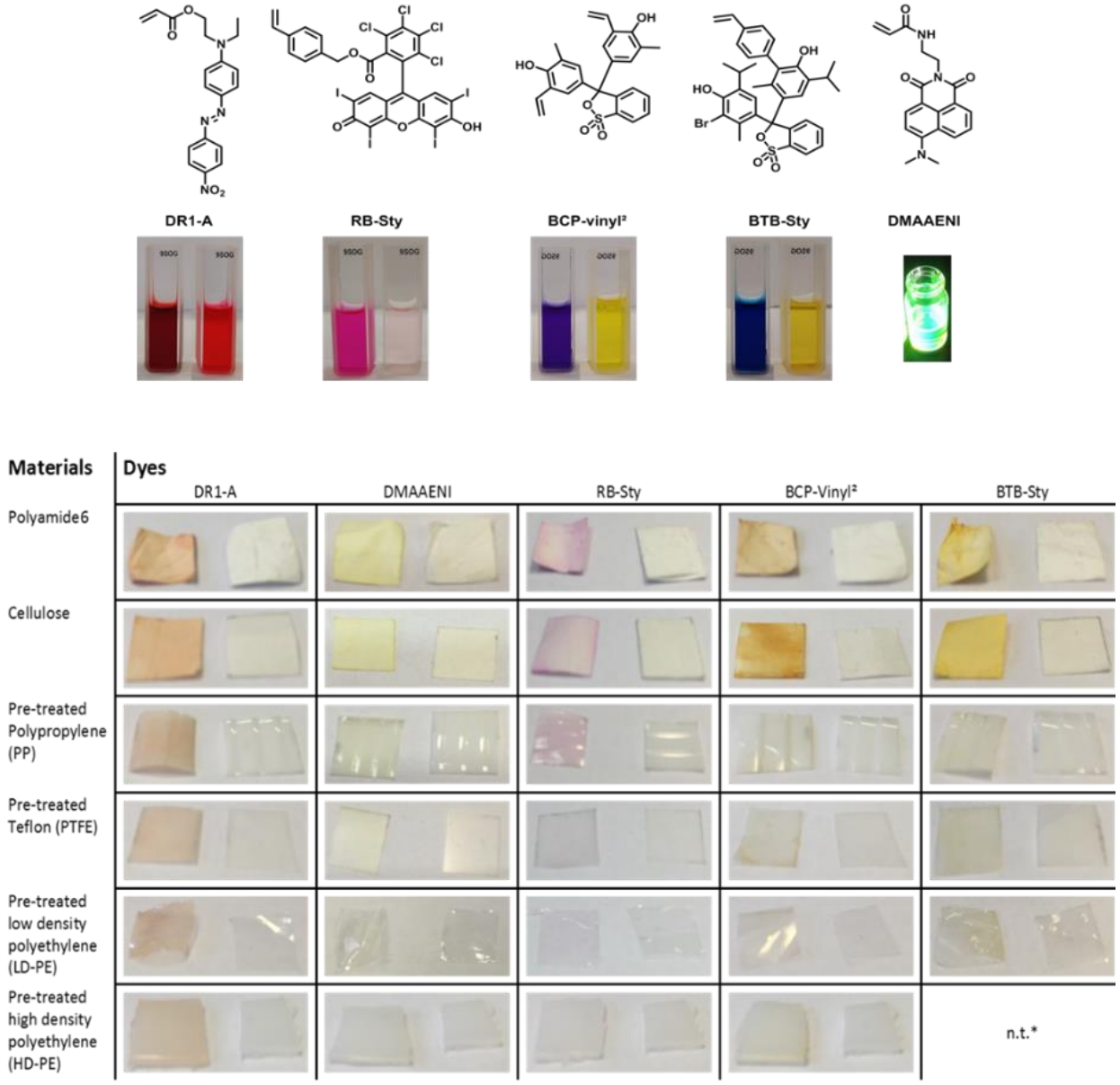

Figure 4.6. Top: Overview of the used halochromic dye molecules disperse red 1 modified with an acrylate group (DR1-A), Rose Bengal modified with a styrene group (RB-Sty), Bromocresol purple modified with two vinyl groups (BCP-vinyl²), bromothymol blue modified with a styrene moiety (BTB-Sty) and 4-N,N'-dimethylamino-1,8-acrylamidoethylnaphthilimide (DMAAENI) together with their pH-responsive behavior in organic solution. Bottom: Overview of the treated materials with the corresponding dye using the optimized PDC treatment. Each picture of the treated material after purification (left) is compared to an untreated reference sample (right). *not treated due to insufficient amount of dye. Reprinted from ref.[31] Copyright 2019 Springer Nature.

Furthermore, this PDC procedure can be used to introduce an additional responsivity onto the material surface by careful design of the used polymerizable dye, allowing the synthesis of various sensor materials. This was illustrated by the use of halochromic or pH-sensitive dye molecules with the PDC procedure after which their colorimetric response was investigated. It was noticed that the dye retains

its reversible halochromic behavior after the PDC immobilization which is illustrated in Figure 4.7 upon exposure to either acidic HCl saturated vapors or basic NH_3 saturated vapors.

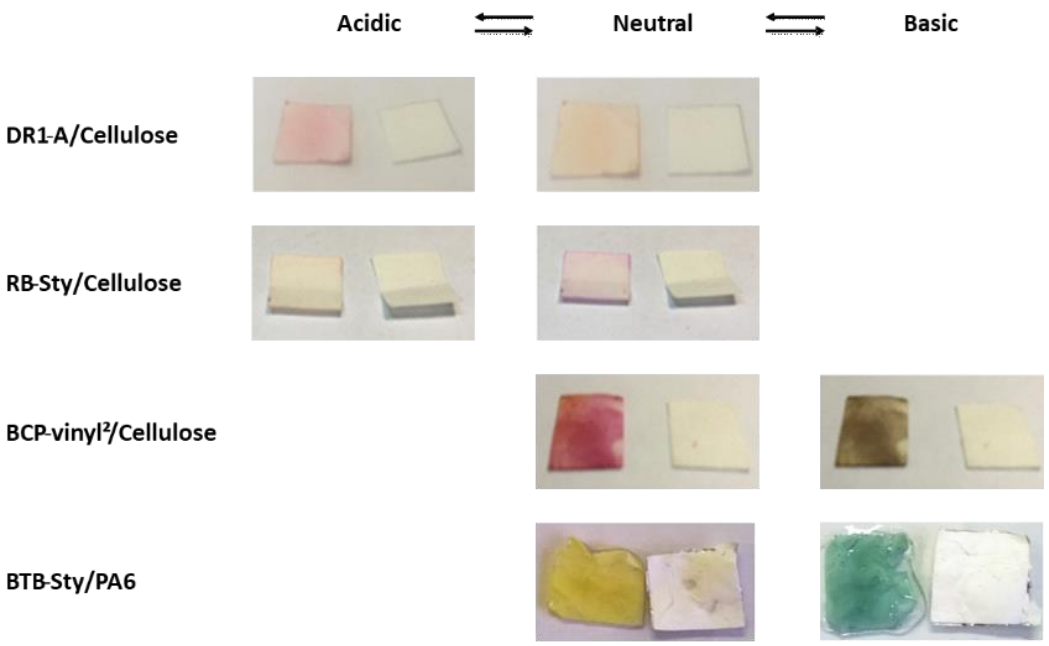

Figure 4.7. The halochromic behavior of plasma dye coated materials. The halochromic behavior of these materials treated with respectively DR1-A, RB-Sty and BCP-vinyl² is induced by the exposure to HCl and NH_3 saturated vapors or by the dipping into an acidic or basic aqueous solution in the case for BTB-Sty.Reprinted from ref.[31] Copyright 2019 Springer Nature.

The perseverance of the halochromic behavior after the PSM process clearly indicates the structural integrity of the selected dyes after PDC and the importance of the incorporation of a radical sensitive group into the desired dye which is required to avoid degradation of the electronic structure. Indeed, this radical active group will act as an antenna for the reaction with the surface radicals leaving the majority of the dye molecules intact during the plasma treatment step in the PDC procedure. This means that this procedure could potentially also be used to chemically immobilize other complex aromatic molecules onto surfaces including guest and host-molecules.

In this last chapter, the effect of the PDC procedure on the material surface was initially further investigated using scanning electron microscopy (SEM), contact angle measurements and X-ray photoelectron spectroscopy (XPS) to see if the PSM step influences the bulk properties of the material. Secondly, the expected material and dye dependence of the most important PDC parameter, namely the plasma treatment time, was further proven by optimizing the PDC procedure for the surface coating of PE with Rose Bengal functionalized with a styrene group, which yielded unsatisfactory results using the initially optimized settings. Thirdly, the dye deposition methodology was improved by incorporating a liquid spraying technique in order to allow lower dye consumption and modification of irregular material surfaces. Finally, the possible expansion of this PDC technique towards the

incorporation of host-guest assemblies onto polymeric materials was explored by introducing Napht-BB complexes onto a cellulose substrate.

2 Results and discussion

2.1 Surface composition of PDC treated samples

In the first part of this chapter, the effect of the highly energetic PSM step on the surface composition and characteristics of the substrate was investigated using scanning electron microscopy (SEM), contact angle measurements and X-ray photoelectron spectroscopy (XPS).

The difference in surface topology of all substrates before and after the PDC treatment with DR1-A using the previously optimized conditions (dipping concentration = 25 mg/mL, dipping time = 1 min and PSM time = 1 min) was investigated using SEM. The more inert materials including PTFE, PP and PE were pretreated with an additional plasma step (plasma time = 1 min) prior to the dip-coating. This additional plasma step will increase the surface energy of the more inert materials via post-plasma reactions with the exposed air introducing oxygen-containing functional groups allowing more efficient dye adsorption onto the surface.[32,33] The SEM images are depicted in Figure 4.8 showing no significant difference between both untreated (top) and PDC treated substrates (bottom) indicating that the PSM treatment step has no significant influence on the surface morphology. The straight lines on both LD-PE and HD-PE are mostly likely some tears or cuts from the manipulation of the material during the PDC procedure and SEM sample preparation as the PDC process should not lead to such artefacts.

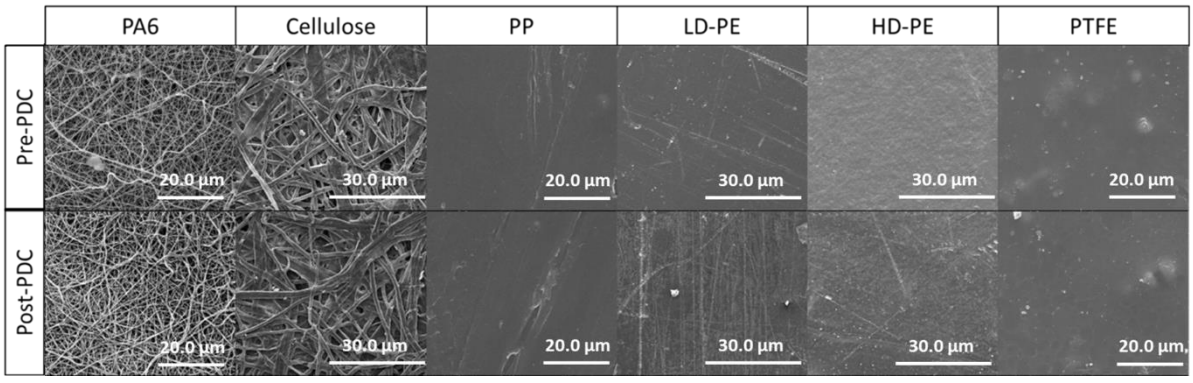

Figure 4.8. Overview of SEM images pre- and post PDC treatment with DR1-A as used dye molecule.

In a second test, the hydrophobicity of the PDC treated and untreated samples were compared using contact angle measurements. The contact angles for untreated surfaces were compared to substrates modified with either the more hydrophobic disperse red 1 functionalized with an acrylate group (DR1-A) or the hydrophilic Rose Bengal functionalized with a styrene group (RB-Sty) both using the same PDC procedure. All tests were performed in triplicate by placing a drop of MilliQ water on each surface after which the contact angle was determined after 5 sec. Averages are reported over five drops per

sample. The results shown in Figure 4.9 display that the PDC treated samples with both the hydrophobic and hydrophilic dyes for all materials are converging to the same value of approximately 70° indicating that the reactive dye molecule has little to no influence on the surface properties, but that the plasma treatment followed by exposure to air may lead to similar surface properties. Whereas no drastic change in contact angles ($\Delta < 10°$) is observed when untreated PP and HD-PE are compared with the corresponding PDC treated samples, a large difference of approximately 30°-40° is noticed for the LD-PE and PTFE samples. This means that the plasma treatment step causes mildly changes in the hydrophobicity depending on the used materials. This can be explained by the incorporation of oxygen species including alcohols and peroxide upon opening of the plasma chamber to the air after PDC treatment. In addition, the use of organic solvents or increased temperature of the soxhlet solvent could have influenced the surface properties as it clearly affects the density and rigidity of the LD-PE. The contact angles measurements are not included for the fibrous materials such as PA6 and cellulose as the water droplet was absorbed within 5 seconds into the materials for all measured samples making it impossible to correctly measure the contact angle.

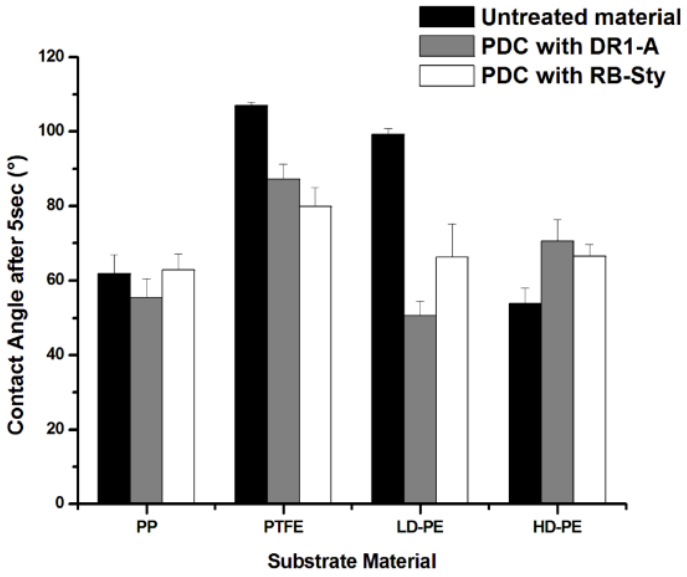

Figure 4.9. The contact angle measured for untreated material (black), PDC treated material with DR1-A (grey) and PDC treated material with RB-Sty (white). A drop of MilliQ water was placed on each surface after which the contact angle was determined after 5 sec, averaged over five drops per sample. The reproducibility of all samples was confirmed by measuring the contact angles on three PDC treated samples. Although LD-PE and HD-PE are made from the same material, a significant difference in their contact angle is observed. This is mainly due to the fact that daily used products, such as a solvent container for HD-PE and a small sealant bag for the LD-PE samples, were utilized which are presumably fabricated with different coatings depending on their application.

The significant difference in contact angle for LD-PE and HD-PE can be ascribed to the use of daily used products which can be

In a final test, the surface composition of PDC treated materials was investigated using XPS by comparing the atomic ratios of the untreated substrate with the PDC treated samples with varying plasma exposure times for PA6 and LD-PE or using the optimized PDC conditions with dipping

concentration = 25 mg/mL, dipping time = 1 min and plasma time = 1 min, for cellulose and UHMW-PE. XPS is a widely used surface analysis technique as it can be applied to a broad range of different materials providing quantitative information on the surface composition of the treated material with a typical analysis depth ranging from 1 nm to 10 nm. The XPS spectra are obtained by irradiating the substrate surface with a monochromatic X-ray beam while simultaneously measuring the kinetic energy and electrons emitted from the substrate surface (1-10 nm depth) using an electron energy analyzer which allows the determination of the elemental identity, chemical state and quantity of the detected elements. For this test all the substrates were treated with RB-Sty as the presence of the dye can be easily detected by the presence of Cl and I atoms allowing the comparison to a reference sample that underwent the same PDC procedure but without final plasma treatment. Important to note is that all inert materials such as LD-PE and UHMW-PE were pretreated with an additional plasma step before dip-coating to ensure enhanced adsorption of the RB-Sty dye molecule onto the surface.

To our surprise, no traces of the dye, displayed by the presence of I or Cl atoms, were observed by XPS indicating that the amount of incorporated RB molecules is lower than the detection limit of the XPS (Figure 4.10). Previous investigations using UV-VIS spectroscopy revealed only a dye loading in the range of nmol/cm² is incorporated onto the surface using PDC which is however, still sufficient to visualize the dye immobilization with the naked eye. Secondly, the XPS results show no noticeable difference in O/C ratio of the untreated and PDC treated samples indicating that the chemical composition of the surface layer is not significantly altered by the PDC process. Thirdly, in some samples silicon and fluorine atoms were measured which is probably due to potential contamination during the PDC treatment, sample preparation for XPS or interference of previous XPS measurements. Finally, a slight increase in the oxygen percentage is observed for PA6, UHMW-PE and LD-PE which is probably due to the exposure of the PDC treated materials to the air which is commonly noticed for plasma treatment of polymers and is in line with the contact angle results.[34,35]

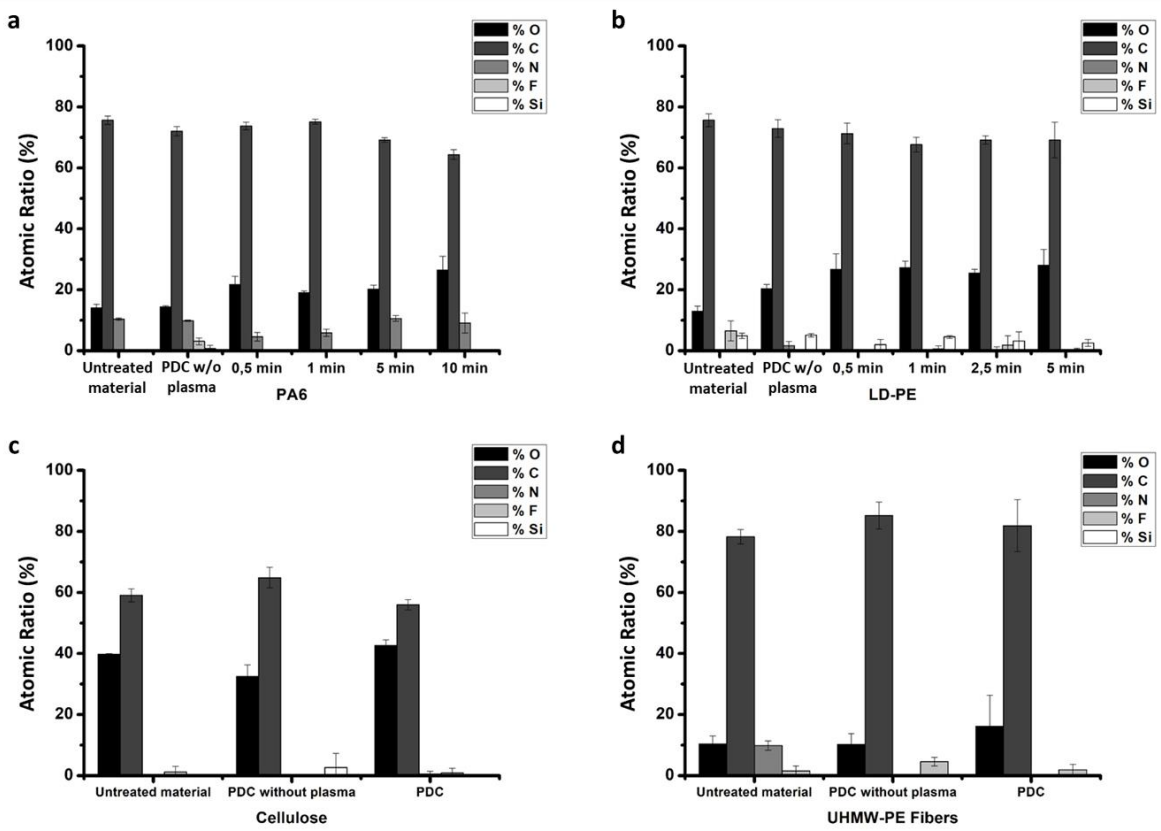

Figure 4.10. The surface atomic ratios of PA6 (a) and LD-PE (b) untreated (Untreated material), PDC without the plasma treatment step (PDC without (w/o) plasma) and the PDC treated sample with increasing plasma time. a) PA6: 0.5 min, 1 min, 5 min and 10 min respectively. b) LPDE: 0.5 min, 1 min, 2.5 min and 5 min. bottom: The surface atomic ratios of Cellulose (c) and UHMW-PE fibers (d): untreated (Untreated material), PDC without the plasma treatment step (PDC without plasma) and the PDC treated (PDC) sample. *The nitrogen content is probably a contaminant.

2.2 Material-molecule dependence of PDC parameters

Previous investigations clearly indicated a material-dye dependency of the PDC parameters, with the most important parameter being the plasma time. When using the parameter set optimized for the PA6/DR1-A combination, although all combination showed successful immobilization, the dye loading was significantly lower with different dyes, polymerizable groups and substrates (Figure 4.6). In order to validate this claim, a further optimization was performed for the PDC of RB-Sty onto LD-PE focusing on variation of the plasma time as this step controls the balance between dye immobilization and dye/material degradation. The optimized conditions for DR1-A/PA6 regarding a dipping time of 1 min and a dipping concentration of 25 mg/ml were kept constant and the plasma time was varied from 0.5 min, 1 min, 2.5 min and 5 min. Again, both coated sides of the samples were exposed to plasma treatment in two steps. The test indeed confirmed that a PSM step of 1 minute on each side as previously optimized for DR1-A/PA6 limits the dye loading on the RB-Sty/LD-PE as a further increase in color was visually noticeable with longer plasma times as shown in Figure 4.11. This trend was also confirmed using reflective UV-VIS showing that a maximum coloration and maximum absorbance is

reached after 2.5 min of plasma time. Although, these results confirm the wide applicability of the PDC procedure as a result of the non-specific nature of the immobilization process, it also indicates that a quick optimization of the PDC parameter is recommended when a new combination of reactive dye and polymer substrate is used.

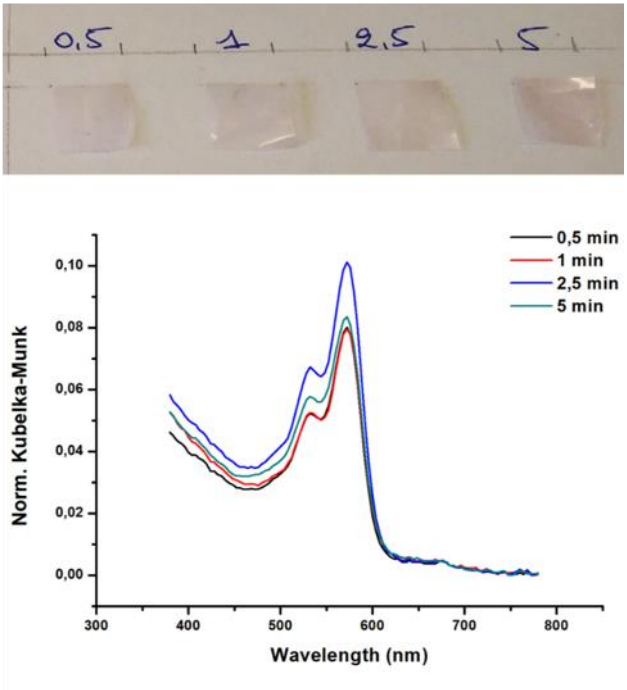

Figure 4.11. Top: Optimization of the plasma time on each side of the substrate for the RB-Sty/LD-PE combination. Bottom: Kubelka-Munk values normalized at max. reflection for LD-PE substrates treated with RB-Sty with respectively 0.5 min, 1 min, 2.5 min and 5 min plasma time.

2.3 Surface dependence of PDC treatment

In previous experiments, a higher dye loading was observed for fibrous materials such as cellulose filter paper and electrospun PA6 (Figure 4.6) than for the non-fibrous materials including PE, PP and PTFE when the same PDC conditions were used. This observation indicated that the drastic difference in surface area available for dye-immobilization may be important for the effectiveness of the PDC procedure. This hypothesis was further investigated by direct comparison of sheets and fibers of the same polymer material by using UHMW-PE fibers and flat LD-PE sheets. The inert UHMW-PE fibers were PDC treated according to the same method as the non-fibrous LD-PE, including the plasma pretreatment step to ensure a homogenous dye adsorption during the dipping deposition.

Firstly, the inert fibrous UHMW-PE material is compatible with the PDC procedure as can be visually observed in Figure 4.12 (right, bottom). Secondly, the same trend displaying higher dye immobilization with increased plasma time is observed in Figure 4.12 (left) for the UHMW-PE similarly to the RB/LD-PE combination shown in Figure 4.11. This observation emphasizes that the optimal PDC process

parameters are both material and dye specific but are less dependent on the surface area and shape of the substrate. Nonetheless, the higher surface area of the fibrous material results in deeper color of the PDC treated sample when compared to the non-fibrous LD-PE treated with a plasma time of 1 minute displayed in the insert of Figure 4.12 (right, top).

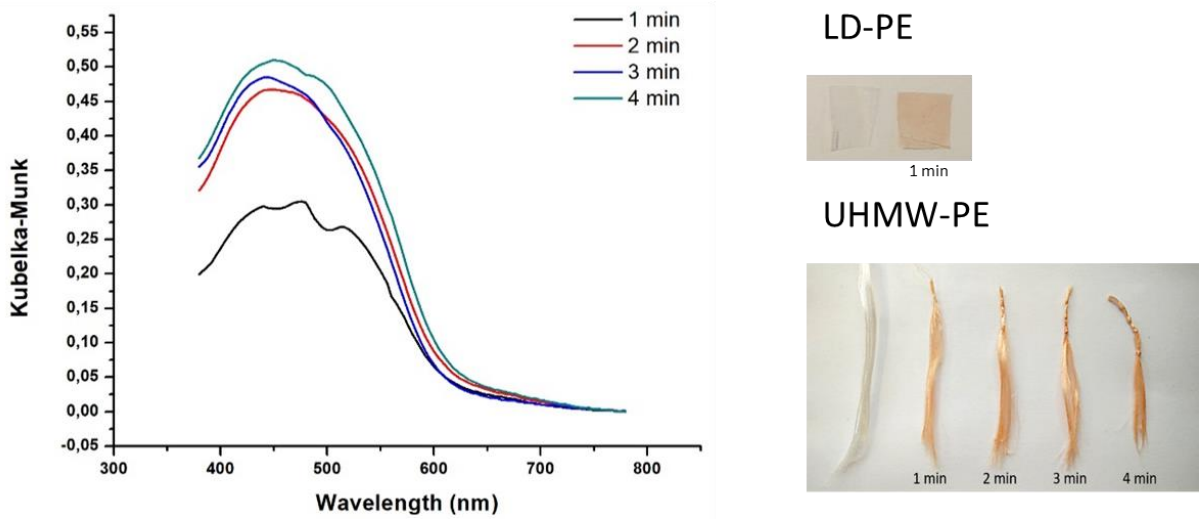

Figure 4.12. Left: Kubelka-Munk values, normalized at max reflection, for UHMW-PE/DR1-A treated respectively 1 min, 2 min, 3 min or 4 min plasma time. Right, top: LD-PE PDC treated with DR1-A under the optimized conditions with a dipping concentration = 25 mg/mL, dipping time = 1 min and plasma time = 1 min. Right, bottom: PDC treatment of UHMW-PE with DR1-A with a dipping concentration = 25 mg/mL, dipping time = 1 min and different plasma times of 1 min, 2 min, 3 min and 4 min respectively. the pictures of the treated fibrous PE substrates are taken after purification and compared to an untreated reference sample.

Finally, a quantitative analysis of the dye loading was accomplished using reflective UV-VIS spectroscopy (Figure 4.13). In both graphs, the increased absorbance around 450 – 500 nm can be noticed proving the presence of the red dye molecule on the surface of the material after PDC treatment and soxhlet extraction. Although the UV-VIS trace of the PDC treated fibrous UHMW-PE is less smooth due to enhanced scattering resulting from the uneven fiber surface, the increased absorbance of 0.31 at the maximum absorption wavelength of DR-1 compared to 0.26 for LD-PE indicates a higher dye loading for the fibrous material under identical procedural PDC parameters. This means that a higher dye loading is achieved for materials having a higher surface/bulk ratio, as anticipated. Finally, no distinction in intensity can be noticed between the PDC-without-plasma sample and the non-treated sample for non-fibrous and fibrous PE/DR1-A (Figure 4.13) showing again the necessity of the plasma step in the PDC procedure.

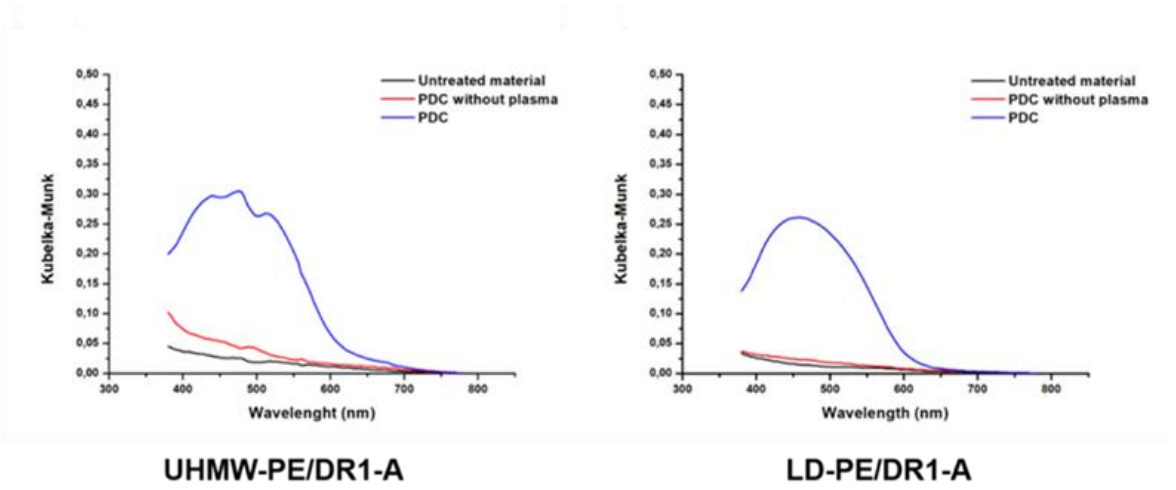

Figure 4.13. Left: The Kubelka-Munk, normalized at max. reflection, for non-treated (Untreated material), PDC without the plasma treatment step (PDC without plasma) and a PDC treated (PDC) sample of fibrous UHMW-PE/DR1-A, performed under following PDC conditions: plasma time: 1 min, dipping concentration: 25 mg/ml and dipping time: 1 min. Right: The Kubelka-Munk, normalized at max. reflection, are given for non-treated (Untreated material), PDC without the plasma treatment step (PDC without plasma) and a PDC treated (PDC) sample of non-fibrous LD-PE/DR1-A, performed under following PDC conditions: plasma time: 1 min, dipping concentration: 25 mg/ml and dipping time: 1 min. Insert: picture of measured LD-PE treated with DR1-A.

2.4 Development of PDC with spray-coating

As mentioned in the introduction (Figure 4.6), the intensity of functionalized DR1 onto the surface resulting from PDC is much lower for the more inert materials such as PTFE, PE and PP compared to e.g. PA6 and cellulose. This difference is partly due to the less efficient wetting of these more inert materials reducing the adsorption of the dye significantly during the dipping deposition step. Therefore, an additional plasma treatment of the substrate prior to the dipping step was used to increase the adsorption of the dye on the surface. This ensures a more homogenously adsorption of the desired dye molecule onto the surface, which significantly increased the intensity of the color after soxhlet extraction. Another way to overcome this problematic wetting and dye adsorption could be to use a liquid spraying technique to deposit the desired reactive dye onto the surface. Via this spraying technique, used commonly by painters and artists (air-brushing technique), a solution or suspension containing the desired dye can easily and homogenously be distributed over the substrate using compressed air. The spray is mostly generated by using a nozzle in combination with a compressor in which the high velocity of the compressed air will cause the atomization of the liquid. The breakup of the solution into droplets will increase the liquid surface area and thus enhance the evaporation of the organic solvent used for the dye solution or suspension. This makes a subsequent drying step to remove all residual solvent prior to the PSM step redundant. Other advantages of this spay-deposition technique is that full surface coverage can be obtained without the need to fully submerge the material into a dipping solution as well as the potential application of a specific design onto the surface.

Firstly, the influence of the dye concentration for the production of homogenously colored substrates using the spraying deposition method was investigated. The experiments were done using PTFE as a substrate and DR1-A as the reactive dye. The bright red colored dye has been used in the optimization of PDC before and is easily quantifiable and visible to the naked eye. The concentration of DR1-A dissolved in acetone was varied from 15 mg/mL to 35 mg/mL and was sprayed three times onto the substrate to generate a homogenous deposition of the dye prior to the plasma treatment. Simultaneously the influence of the plasma time was also investigated by increasing the plasma time from 0 min, 1 min, 3 min to 5 min as previous results have shown this to be the most important parameter. In contrast to the dipping method, only one side of the sample was spray-coated with the DR1-A and exposed to the plasma. The results are visually shown in Figure 4.14, it was immediately noticed that not all pieces were homogenously colored after the plasma treatment and soxhlet extraction. Another significant difference was visibly observed in the intensity of the red color of the PTFE substrates treated with a DR1-A concentration of 25 mg/mL compared to the samples treated with a DR1-A concentration of 15 mg/mL indicating that more dye molecules were immobilized onto the surface when a more concentrated solution is sprayed onto the material. Surprisingly, almost no dye-immobilization was visible to the naked eye with a further increment of the dye concentration to 35 mg/mL. In the latter situation, spraying the surface three times with that high concentration of dye probably results in a thick dye-molecule layer, preventing the creation of sufficient surface radicals that are required for dye immobilization.

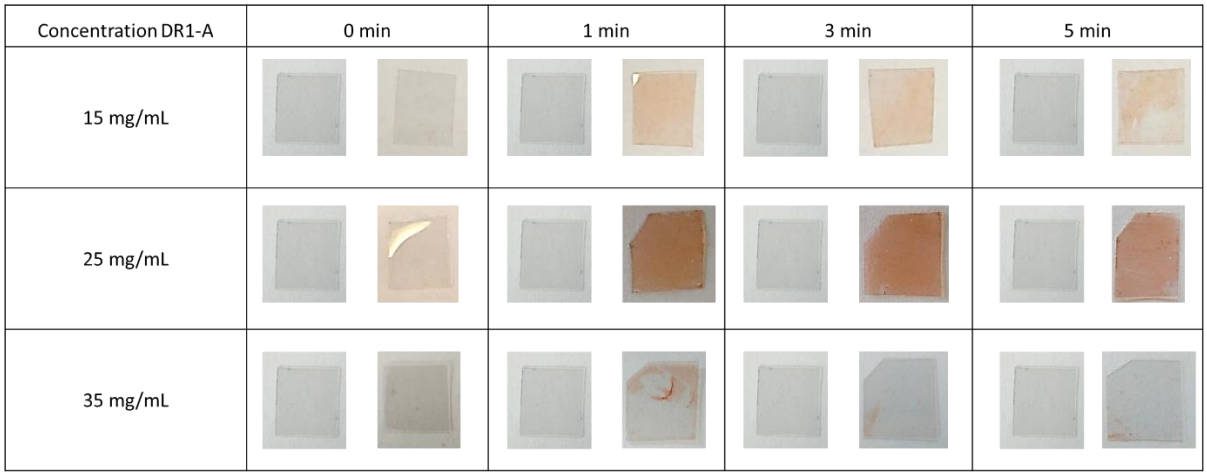

Figure 4.14. Pictures of the treated PTFE samples with a spraying concentration of respectively 15 mg/mL, 25 mg/mL and 35 mg/mL with a plasma time of 0 min, 1 min, 3 min and 5 min. The pictures are taken after soxhlet purification and compared to an untreated reference sample.

Using reflective UV-VIS, the color intensity of the treated substrate can be quantitatively compared as shown in Figure 4.15. In the graphs with a spraying concentration of 15 mg/mL and 25 mg/mL, an increased reflection around 450 – 500 nm is noticed proving the presence of DR1 after PDC treatment and soxhlet extraction. In agreement with the visual observations made in Figure 4.14, the highest dye-

immobilization was observed for the PTFE sprayed with a concentration of 25 mg/mL with a plasma treatment time between 1 and 3 min. Only a minor increase in absorbance was observed for the PTFE substrates treated with 35 mg/mL, confirming the visual observations.

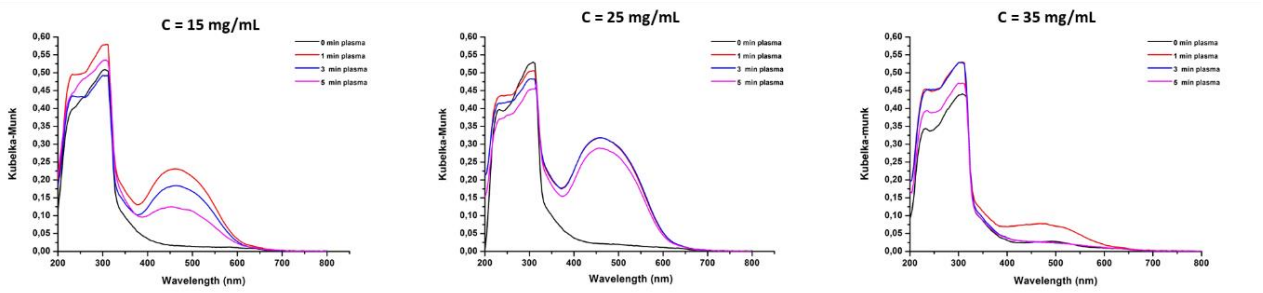

Figure 4.15. The Kubelka-Munk, normalized at max. reflection, for PTFE samples treated with a spraying concentration of 15 mg/mL (Left), 25 mg/mL (Center) and 35 mg/mL (Right) and different plasma times of 0 min, 1 min, 3 min and 5 min respectively.

The two depositions techniques, namely spraying and dipping, were also compared for fibrous cellulose and non-fibrous PTFE using reflective UV-VIS spectroscopy. The materials were colored with DR1-A under optimized conditions, namely with a dipping or spraying concentration of 25 mg/mL of DR1-A, three time spraying and a plasma treatment time of 1 min. The non-fibrous material had an additional plasma treatment step prior to the dipping method to enhance the surface wetting. Pictures of the treated samples are displayed in Figure 4.16, where an increased color intensity for the samples treated with the spraying deposition technique is visually observed. This indicates that dye-immobilization is presumably dependent on the deposition method and more investigation should be done towards other deposition techniques. It should be noted that for the non-fibrous materials the spraying deposition method has an advantage over the dipping method as the same intensity in coloration can be achieved without the need for an extra plasma treatment step.

	Cellulose	PTFE
Dip-coating		
Spray-coating		

Figure 4.16. The visual comparison in color intensity for PDC treated cellulose or PTFE with DR1-A using either the dip-coating or spray-coating as deposition technique.

To achieve an even higher dye loading and increased coloring of the substrates, we postulated that repeating the PDC cycle multiple times could lead to enhanced dye immobilization onto the surface until at a certain cycle the additional dye immobilization will be balanced or compensated by dye degradation. For this test, PTFE samples were treated with PDC up to 4 subsequent cycles using the

optimized conditions with a spraying concentration of 25 mg/mL of DR1-A in acetone, three times spraying and a plasma treatment time of 1 min. The pictures in Figure 4.17 clearly show that the intensity of the first cycle is the lowest (A_{DR1-A} = 0.10 – 0.15) after which it increases with each cycle up to a A_{DR1-A} of 0.40 for the last cycle, displaying a linear dependence in the absorbance of the CT-band (456 nm) with the number of used PDC cycles. This observation can also be visually confirmed and demonstrates that the dye loading can indeed be increased by using subsequent PDC cycles with the same dye and that with 4 cycles, the limit of the dye loading has not yet been reached (Figure 4.17, right). Important to note is that this test also shows that the current PDC setup still has its inconsistencies with a much lower dye loading as compared to previous results using the same combination and an unexpected inhomogeneous deposition of the dye, the latter becoming less problematic with increasing PDC cycles.

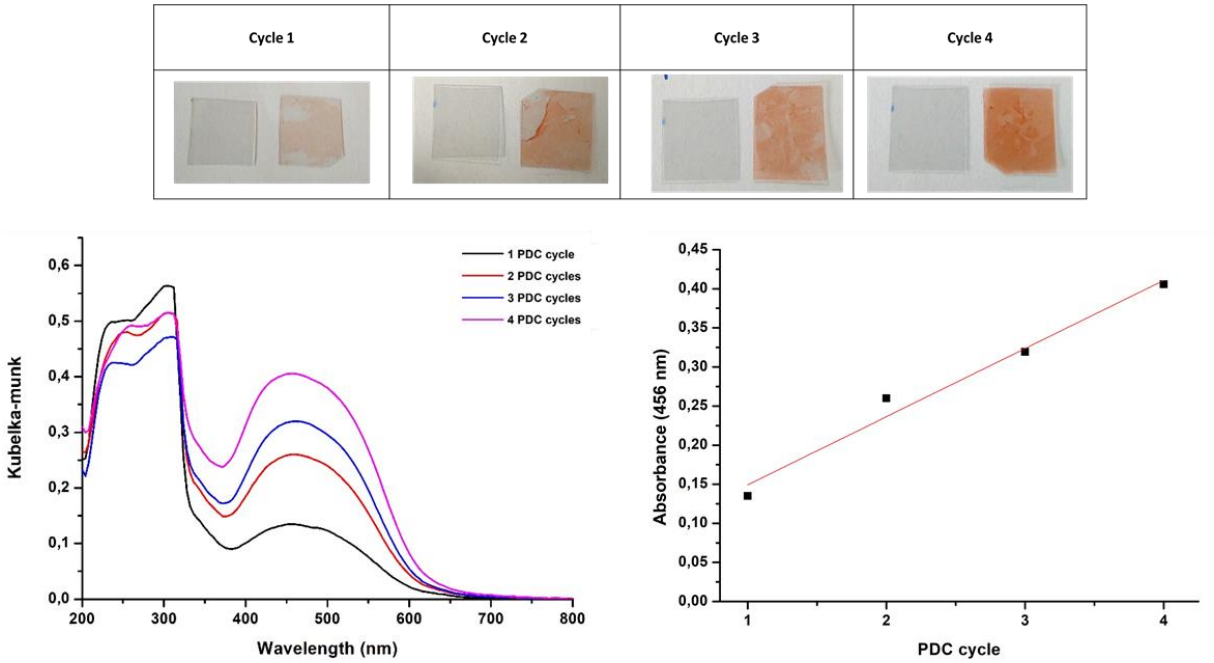

Figure 4.17. Top: Pictures showing the color intensity of PTFE samples PDC coated with DR1-A for 1, 2, 3 and 4 cycles performed under the following conditions: spraying concentration = 25 mg/mL and plasma time = 1 min. The pictures are taken after soxhlet purification and compared to an untreated reference sample. Bottom, left: The Kubelka-Munk spectra normalized at max. reflection for the PTFE substrates treated with respectively 1, 2, 3 and 4 cycles of PDC. Bottom, right: The absorbance at the max of the CT-band (456 nm) in function of the number of treated PDC cycles.

2.5 Combination of PDC with host-guest chemistry

Finally, the use of PDC for the introduction of host-guest chemistry onto a material surface was investigated. In order to evaluate if the PDC method could be used to covalently immobilize host-guest functionalities onto a polymeric substrate, a dihydroxynaphtalene functionalized with an acrylamide group (Napht.Ac), as described in Chapter 3, was used for PDC to immobilize this guest molecule onto a polymeric substrate. In this experiment a solution of 25 mg/ml Napht.Ac in acetone was sprayed

three times onto a fibrous cellulose substrate. Subsequently, the Napht.Ac coated cellulose piece was exposed to inert argon plasma for 1 min after which all the unreacted naphthalene monomers and the plasma byproducts were removed using soxhlet extraction. After the soxhlet extraction, most of the characteristic yellowish color from the Napht.Ac had disappeared from the cellulose substrate, visually showing no difference in color with the untreated cellulose. However, upon the addition of an aqueous BB solution (Figure 4.18), the cellulose piece colored bright pink resulting from the host-guest complexation indicating that the naphthalene units were successfully immobilized by the PDC treatment whereby their molecular structure stays intact enabling them to still form host-guest assemblies with BB.

Figure 4.18. Pictures of Napht.Ac/cellulose pieces after treatment with PDC and the color change from very light yellow (left) to bright pink (right).

Although no reflective UV-VIS spectroscopy measurements were carried out on the cellulose substrates functionalized with Napht.Ac due to lack of time, the absorbance band is expected to be present for the Napht units at 350-400 nm and a change in absorbance to approximately 520-550 nm, which is the CT-band of the Napht-BB complex, upon the addition of BB.

3 Conclusions and outlook

This chapter described the further investigation and optimization of the PDC procedure, which is a novel post-fabrication modification approach for the coloring of polymeric materials based on the radical, covalent coupling of a pre-adsorbed reactive dyes to the surface of a material through solvent-free plasma surface modification. First, the effect of the PDC procedure on the surface properties of the substrate was investigated using SEM, contact angle measurements and X-ray spectroscopy showing that the PSM treatment step has almost no influence on the surface topology, surface properties and composition indicating that most surface and bulk properties of the substrate are retained after PDC treatment. In a second test the dye and material dependence of this technique was confirmed indicating that a further optimization of the PDC parameters, especially the plasma treatment time, is recommended when a new polymerizable dye/material combination is used. Subsequently, the deposition step was also further improved by implementing a spray technique to coat the materials with the desired dye prior to plasma treatment in order to allow lower dye consumption, the application of a specific design onto the surface and the use of complex material

surfaces. Visually, an increased intensity in color was observed for the fibrous and non-fibrous materials PDC treated with spray-coating compared to the ones treated using the dip-coating deposition method. Additionally, spray-coating offers advantages for the scalability and made the plasma pretreatment step for inert surfaces redundant. Treating the substrate with more than 1 PDC cycle has been shown to effectively increase both the dye-loading and the homogenous incorporation of the desired dye. Furthermore, the pressure of the vacuum chamber and the used discharge power of the PDC procedure could also influence the dye loading significantly and should therefore be further optimized. In a later stage the use of atmospheric plasma generators should be evaluated to expand the use of this procedure to industry.

Finally, the applicability of the PDC procedure to covalently immobilize host-guest assemblies onto polymeric surfaces was successfully demonstrated by incorporating Napht.Ac onto a cellulose substrate preserving the chemical structure as the naphthalene could still interact with BB. These smart surfaces mediated by host-guest assemblies through the use of the PDC method could potentially be used to facilitate the purification process of the host molecule, in our case by filtering unpure BB over the cellulose filter modified with Napht units. Another application for the incorporation of host-guest complexes onto material surfaces is to provide strong and reversible supramolecular adhesion between two substrates including more inert substrates like PE, PP and PTFE by using the PDC procedure. For example, this can be done by linking the reactive guest molecule Napht.Ac onto different materials which can afterwards be glued together with the use of BBB forming 1:2 complexes in aqueous media as shown in Chapter 2.

4 Experimental details

4.1 Materials and instrumentation

All chemicals and solvents were commercially available and used as received unless otherwise stated. Disperse Red 1 (95%), acryloylchloride (97%, 200 ppm MEHQ as stabilizer), vinylbenzylchloride (90%) and phenothiazine (98%) were purchased from Sigma Aldrich and Rose Bengal (acid red 94, 95%) from TCI. Anhydrous magnesium sulfate was supplied by Fisher Chemicals. All solvents including dichloromethane, *N,N*-dimethylformamide, ethylacetate, triethylamine and methanol were HPLC-grade from Sigma-aldrich. All anhydrous solvents, were obtained by passing over aluminium oxide by means of a J.C. Meyer solvent purification system. All deuterated solvents were purchased from Cambridge Isotope Laboratories. The polyamide-6 support was fabricated in-house using electrospinning from acid solution according to a previously published protocol,[42] cellulose-based qualitative filter paper was purchased from VWR (Medium filtration rate), PTFE was obtained from

Holders Technology, samples of high-density polyethylene were cut out of a 2.5 L solvent container, low-density polyethylene was cut out of small sealant bag, polypropylene was cut out of a plastic cup and finally the UHMW-PE fibers, also known as Dyneema® fibers, were obtained from DSM. The synthesis of Napht.Ac and BB is described in chapter 3.

Plasma instrument. The instrument used for the creation of the plasma was a cylindrical dielectrical plasma discharge generator (Femot Model, Version 3, Diener Electronic, Germany). Argon was used as discharge gas at a pressure of 0.8 mBar and was activated by a rf-generator (100 W).

Nuclear magnetic resonance (NMR). ^{1}H-NMR spectra were recorded in DMSO or $CDCl_3$ on a Bruker Advance 300 MHz or 500 MHz spectrometer at room temperature unless otherwise noted. Chemical shifts are reported as parts per million (ppm) downfield from TMS resonance as internal standard.

Reflective UV/VIS spectroscopy. Reflective UV/VIS measurements were performed using a Perkin-Elmer Lambda 900 spectrophotometer, which is a double-beam UV-Vis spectrophotometer. For the reflection measurements on fabrics an integrated sphere (Spectralon Labsphere 150 mm) was used. The spectra were recorded from 380 nm to 780 nm with a data interval of 4 nm. Reflection is converted into Kubelka-Munk (K-M) since these values provide a correlation with dye concentration.

X-ray photoelectron spectroscopy (XPS). ESCA S-probe VG monochromatic spectrometer with an Al Kα X-ray source (1486 eV), recorded with a spot size of 250 µm by 1000 µm and analyzed using Casa XPS software package.

Contact angle measurements. The contact angle measurements were performed on a SCA 20 Instrument (Dataphysics), equipped with a light source and high speed video system with CCD cameras. To determine the static contact angles of the polymer surfaces, the sessile drop method was used. The static contact angle was determined 5 seconds after the first contact of the water droplet with the surface, using the circle fitting of the imaging software SCA20 (version 2.1.5).

Scanning electron microscopy (SEM). SEM images were obtained on an FEI Quanta 200F microscope. All samples were placed on a carbon tape and covered with gold layer using sputter coating prior to analysis.

4.2 Functionalization of Disperse red 1 through esterification

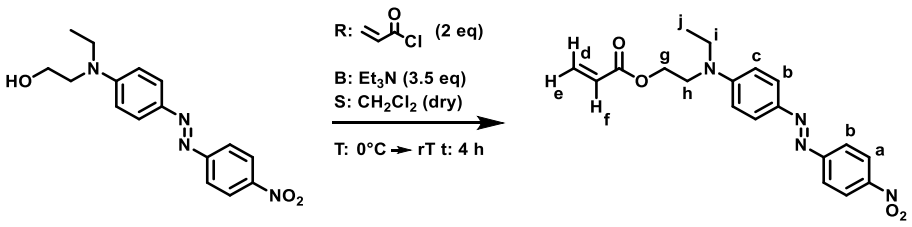

Figure 4.17. Reaction conditions for the synthesis of Disperse Red 1 – acrylate with respective ^{1}H-NMR annotations.

5.09 g of Disperse Red 1 (0.016 mol, 1 eq) was dissolved in anhydrous CH_2Cl_2 (250 mL) and Et_3N (7.7 mL, 0.055 mol, 3.4 eq) and cooled to 0 °C under inert atmosphere. 2.56 mL acryloyl chloride (0.032 mol, 2 eq) was added dropwise to the mixture under vigorous stirring after which the mixture was allowed to warm up to rT. The reaction was monitored using TLC (Silica, CH_2Cl_2/EtOAc 5/1, $Rf_{Reagent}$: 0.43, $Rf_{product}$: 0.89) and was stopped after 4 hours. The product was purified using column chromatography with the same conditions. After drying of the organic phase with $MgSO_4$ the solvent was evaporated, yielding DR1-A as a red powder.

Yield: 5.688 g (95 %).

^{1}H-NMR spectroscopy (300MHz, CD_2Cl_2) δ(ppm) 8.24 (2H, d, *J* = 9.33 Hz, H_a) 7.84 (4H, dd, *J* = 8.23 Hz, H_b) 6.76 (2H, d, *J* = 9.88 Hz, H_c) 6.31 (1H, dd, J = 17.56 Hz, *J* = 2.19 Hz, H_d) 6.05 (1H, dd, *J* = 18.66 Hz, *J* = 10.42 Hz, H_e) 5.78 (1H, dd, *J* = 10.42 Hz, J = 2.19 Hz, H_f) 4.30 (2H, tr, *J* = 5.49 Hz, H_g) 3.66 (1H, tr, *J* = 5.49 Hz, H_h) 3.47 (2H, quad, *J* = 7.58 Hz, H_i) 1.18 (3H, tr, J = 7.68 Hz, H_j)

4.3 Modification of Rose Bengal with a styrene group

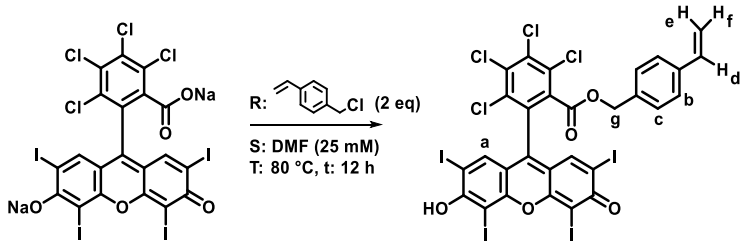

Figure 4.18. Reaction conditions for the synthesis of Rose Bengal – styrene (RB-Sty) with respective 1H-NMR annotations.

Rose Bengal (0.536 g, 0.53 mmol, 1 eq) and a spatula point of phenothiazine was dissolved in 20 mL of DMF (anhydrous) under Ar atmosphere. To this mixture, 0.16 mL of 4-chloromethylstyrene (1.14 mmol, 2.16 eq) was added after which the temperature was raised to 80 °C and stirred overnight. The reaction was followed using TLC (Silica, DCM/MeOH 95/5, Rf,RB = 0, Rf,RB-Sty = 0.1) and was purified by evaporating the DMF under reduced pressure and stirring the resulting solid in diethyl ether for 6 h. After filtration, the solid was purified using column chromatography (Silica, DCM/MeOH 95/5) yielding RB-Sty as a shiny, purple solid after evaporation.

Yield: 0.447 g (78 %).

^{1}H-NMR spectroscopy (300 MHz, DMSO-6d) δ(ppm) 7.54 (s, 2H, Ha), 7.23 (d, *J* = 8.2 Hz, 2H, Hb), 6.80 (d, *J* = 8.2 Hz, 2H, Hc), 6.68 (dd, *J* = 17.7, 10.9 Hz, 1H, Hd), 5.82 (dd, *J* = 17.7, 0.9 Hz, 1H, He), 5.27 (dd, *J* = 10.9, 0.9 Hz, 1H, Hf), 5.02 (s, 2H, Hg)

4.4 Plasma Dye Coating (PDC) procedure with dip-coating

The optimized PDC procedure conditions, done for the plasma dye coating process of disperse red 1 – acrylate (DR1-A) on PA6, is as follows: a 1 cm² piece of PA6 is dipped into a 25 mg/mL solution of DR1-A in THF for 1 min. The material is carefully removed while residual THF is collected and removed from the sides of the material using paper. The material is firstly dried to the air to ensure a homogenous dispersion of the dye after which the material is completely dried in a vacuum oven at 40 °C for 30 min. The material samples are then positioned in the plasma chamber on a glass surface and placed under 0.8 mBar of Ar pressure. After 1 min of plasma treatment, the chamber is opened to the air and the pieces are flipped over and treated again. The material is finally purified using soxhlet extraction using the same solvent as the dipping solution. For rose bengal – styryl (RB-Sty) the use of ethanol was required. Materials like cellulose and PA6 are sufficiently adsorbent to ensure a homogenous coverage of the polymer sample with the dye after dip-coating. PE, PP and PTFE were pretreated with plasma, under identical conditions as previously mentioned, before dip-coating to allow sufficient dye adsorption to the surface.

4.5 Plasma Dye Coating (PDC) procedure with spray-coating

DR1-A and Napht.Ac dissolved in acetone (mostly 25 mg/mL) was sprayed in three consecutive cycles onto the sample using a nozzle (diameter = 0.3 mm) in combination with a compressor at a pressure of 30 psi. During spray-coating, the sample is fixed in an upright position using double folded tape which also prevents the light-weighted sample from moving during spraying. The material is sprayed in a snake-like pattern with a flow rate of 33 mg/min from a distance of roughly 10 cm between the nozzle and the surface. The coated material is afterwards dried in a vacuum oven at 40 °C for 30 min. The material samples are then positioned in the plasma chamber on a glass surface and placed under 0.8 mBar of Ar pressure. After 1 min of plasma treatment of the dye-coated side of the sample, the chamber is opened to the air, after which the material is purified using soxhlet extraction with THF. The multiple treatments experiments were performed by repeating this entire procedure 2, 3 or 4 consecutive times.

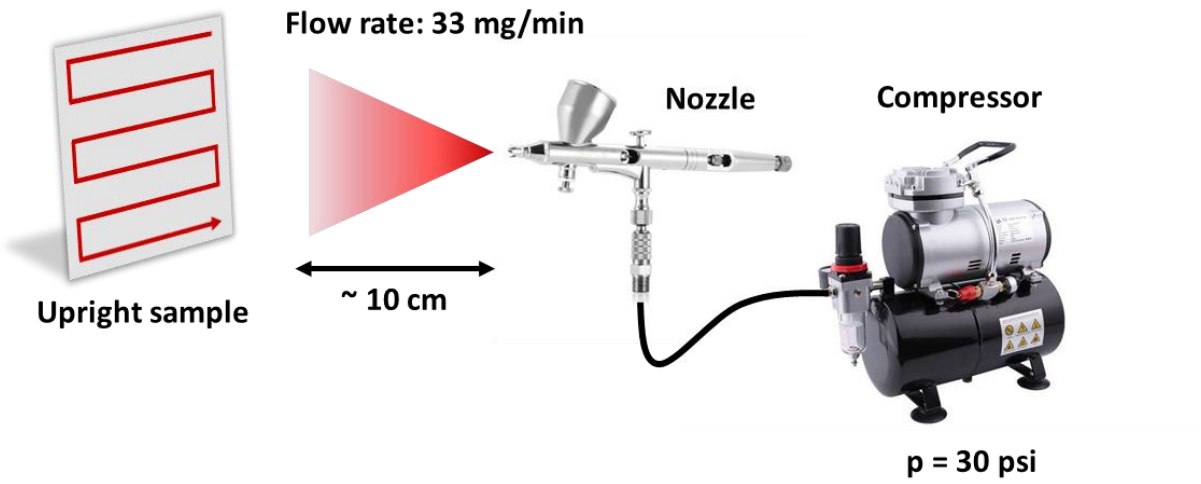

Figure 4.19. Visualization of the spray-coating setup displaying that the sample was sprayed with the dye in an upright position in a snakelike pattern (indicated by the red arrow). The nozzle was positioned around 10 cm from the sample and the pressure of the compressor was set at 30 psi to receive a flow rate of 33 mg/min.

5 References

1. Yang, Y. W.; Sun, Y. L.; Song, N. *Acc. Chem. Res.* **2014**, *47*, 1950.
2. Tian, M. M.; Chen, D. X.; Sun, Y. L.; Yang, Y. W.; Jia, Q. *RSC Adv.* **2013**, *3*, 22111.
3. Zhao, Y.; Huang, Y.; Zhu, H.; Zhu, Q.; Xia, Y. *J. Am. Chem. Soc.* **2016**, *138*, 16645.
4. Li, Q. L.; Sun, Y.; Ren, L.; Wang, X.; Wang, C.; Li, L.; Yang, Y. W.; Yu, X.; Yu, J. *ACS Appl. Mater. Interfaces* **2018**, *10*, 29314.
5. Li, H.; Chen, D. X.; Sun, Y. L.; Zheng, Y. B.; Tan, L. L.; Weiss, P. S.; Yang, Y. W. *J. Am. Chem. Soc.* **2013**, *135*, 1570.
6. Liu, Y.; Yang, Y. W.; Chen, Y. *Chem. Commun.* **2005**, *2*, 4208.
7. Li, H.; Yang, Y. W. *Chinese Chem. Lett.* **2013**, *24*, 545.
8. Hu, C.; Tian, F.; Zheng, Y.; Tan, C. S. Y.; West, K. R.; Scherman, O. A. *Chem. Sci.* **2015**, *6*, 5303.
9. Ahn, Y.; Jang, Y.; Selvapalam, N.; Yun, G.; Kim, K. *Angew. Chem. Int. Ed.* **2013**, *52*, 3140.
10. Liu, J.; Scherman, O. A. *Adv. Funct. Mater.* **2018**, *28*, 1.
11. Ju, G.; Zhang, Q.; Guo, F.; Xie, P.; Cheng, M.; Shi, F. *J. Mater. Chem. B* **2019**, *7*, 1684.
12. Ju, G.; Cheng, M.; Guo, F.; Zhang, Q.; Shi, F. *Angew. Chem. Int. Ed.* **2018**, *57*, 8963.
13. Ji, X.; Ahmed, M.; Long, L.; Khashab, N. M.; Huang, F.; Sessler, J. L. *Chem. Soc. Rev.* **2019**, *48*, 2682.
14. Liu, J.; Tan, C. S. Y.; Scherman, O. A. *Angew. Chem. Int. Ed.* **2018**, *130*, 8992.
15. Harada, A.; Kobayashi, R.; Takashima, Y.; Hashidzume, A.; Yamaguchi, H. *Nat. Chem.* **2011**, *3*, 34.
16. Nakahata, M.; Takashima, Y.; Harada, A. *Angew. Chem. Int. Ed.* **2014**, *53*, 3617.
17. Takashima, Y.; Sahara, T.; Sekine, T.; Kakuta, T.; Nakahata, M.; Otsubo, M.; Kobayashi, Y.; Harada, A. *Macromol. Rapid Commun.* **2014**, *35*, 1646.
18. *Plasma technology*; 1st ed.; Diener electronics: Germany, **2007**.
19. Hegemann, D.; Brunner, H.; Oehr, C. In *Nuclear Instruments and Methods in Physics Research, Section B: Beam Interactions with Materials and Atoms*; **2003**; Vol. 208, pp 281.
20. Oehr, C. In *Nuclear Instruments and Methods in Physics Research, Section B: Beam Interactions with Materials and Atoms*; **2003**; Vol. 208, pp 40.
21. Dai, L.; Griesser, H. J.; Mau, A. W. H. *J. Phys. Chem. B* **1997**, *101*, 9548.
22. Grace, J. M.; Gerenser, L. J. *J. Dispers. Sci. Technol.* **2003**, *24*, 305.
23. Khelifa, F.; Ershov, S.; Habibi, Y.; Snyders, R.; Dubois, P. *Chem. Rev.* **2016**, *116*, 3975.
24. De Geyter, N.; Dubruel, P.; Morent, R.; Leys, C. In *Low Temperature Plasma Technology: Methods and Applications*; Chu, P. K.; Lu, X., Eds.; CRC Press, **2013**; pp 401.
25. Chevallier, P.; Castonguay, M.; Turgeon, S.; Dubrulle, N.; Mantovani, D.; McBreen, P. H.; Wittmann, J. C.; Laroche, G. *J. Phys. Chem. B* **2001**, *105*, 12490.

26. Denes, F. S.; Manolache, S. *Prog. Polym. Sci.* **2004**, *29*, 815.

27. Alvarez-Blanco, S.; Manolache, S.; Denes, F. *Polym. Bull.* **2001**, *47*, 329.

28. Siow, K. S.; Britcher, L.; Kumar, S.; Griesser, H. J. *Plasma Process. Polym.* **2006**, *3*, 392.

29. Coad, B. R.; Styan, K. E.; Meagher, L. *ACS Appl. Mater. Interfaces* **2014**, *6*, 7782.

30. Denes, F.; Manolache, S.; Young, R. A. *J. Dispers. Sci. Technol.* **1999**, *12*, 27.

31. De Smet, L.; Vancoillie, G.; Minshall, P.; Lava, K.; Steyaert, I.; Schoolaert, E.; Van De Walle, E.; Dubruel, P.; De Clerck, K.; Hoogenboom, R. *Nat. Commun.* **2018**, *9*.

32. De Geyter, N.; Morent, R. In *Biomaterials for Bone Regeneration*; Elsevier, **2014**; pp 202.

33. Izdebska-Podsiadły, J. *Application of Plasma in Printed Surfaces and Print Quality*; Elsevier Inc., **2019**.

34. Barranco, a; Aparicio, F.; Yanguas-Gil, a; Groening, P.; Cotrino, J.; González-Elipe, a R. *Chem. Vap. Depos.* **2007**, *13*, 319.

35. Aparicio, F. J.; Alcaire, M.; Borras, A.; Gonzalez, J. C.; López-Arbeloa, F.; Blaszczyk-Lezak, I.; González-Elipe, A. R.; Barranco, A. *J. Mater. Chem. C* **2014**, *2*, 6561.

Chapter 5. Conclusions and outlook

The development of smart or intelligent polymeric materials has gained a lot of attention over the past decades. Smart materials are described as materials that are capable of altering their properties and functions in response to small external environmental changes such as fluctuations in temperature, pH, electric or magnetic fields, solvent or chemicals and light. Within this rapidly advancing field, supramolecular chemistry, including host-guest complexation, has emerged as a powerful tool for the creation of these responsive materials due to their dynamic, reversible and adaptive nature towards external stimuli. These host-guest inclusion complexes consist mostly of a macrocyclic host molecule which can interact in a highly controlled and selective manner with one or more smaller guest molecules, via both random non-covalent interactions and specific three-dimensional spatial arrangements. The integration of these dynamic supramolecular assemblies into conventional polymer chemistry through the incorporation of either the macrocyclic host or, mostly, the electron rich guest has allowed us to develop the next generation advanced materials in a less time-consuming way.

Nowadays cucurbit[n]urils (CB), cyclodextrins (CD) and pillar[n]arenes are most commonly used as host molecules for the synthesis of stimuli-responsive polymeric materials like hydrogels and nanostructures through macromolecular supra-amphiphiles in aqueous media which can be applied for different fields ranging from biomedical applications to nanotechnology and material science. In **Chapter 2**, a less widely explored macrocyclic host molecule cyclobis(paraquat-4,4'-biphenylene), also called big blue box (BBB), was investigated for the use in aqueous smart materials. BBB can form strong inclusion complexes with two planar electron-rich aromatic guest molecules simultaneously which provides opportunities for the creation of physical hydrogels possessing some interesting features like self-healability and shape memory function. Additionally, this macrocycle has the ability to introduce redox sensitive properties into polymeric systems as the host-guest interactions can be manipulated via the redox potential of its two bipyridinium units. Finally, complexes formed with BBB have an intense colour depending on the used guest molecules, which can be used as a direct visual output in sensing applications. In a first step, the complexation of BBB with the electron rich guest molecules dialkoxynaphthalene (Napht) and tetrathiafulvalene (TTF) in water was characterized using a combination of UV-VIS spectrophotometric titration, ITC and ^{1}H-NMR spectroscopy. However, due to the poor water solubility of the guest molecules Napht and TTF, short water-soluble polymers were synthesized with either TTF or Napht α-chain ends through RAFT polymerization with functionalized CTA-agents. These water-soluble TTF and Napht derivatives were shown to form colored 1:2 complexes in water with a relative high association constant of 1.1×10^4 M^{-1} and 2.7×10^4 M^{-1} for Napht-PDMAc and TTF-PDMAc, respectively. Finally, the inherent, reversible temperature dependence of the

Napht-PDMAc complex was highlighted showing a clear disruption of the complex when heated to 100 °C and the quick reformation of the complex upon subsequent cooling below 5 °C. These results indicate that these complexes provide a promising use for the creation of multi-stimuli responsive materials, including hydrogels and supramolecular nanostructures that can both be used for visual sensor systems as colored complexes are formed. For example, this reversible redox-responsive behavior of TTF-unit could be used to implement the complex as a sensor for oxidative stress. More research could also be done to investigate the influence of PDMAc chain on the host-guest complexation by investigating the effect of polymer chain length on the association constant in water to allow the more accurate determination of the strength of the specific host-guest complexation in water.

By embedding the dynamic nature of the microscopic host-guest complexes into hydrophilic polymeric networks, also called hydrogels, has allowed us to reversibly control the macroscopic shrinking and swelling of these materials. **Chapter 3** focusses on the use of cyclobis(paraquat-*p*-phenylene) or blue box (BB) complexes with Napht as guest molecule to gain control over the volume phase transition temperature (VPTT) of thermo-responsive PNIPAm hydrogels. The induced decomplexation upon temperature increase allowed to incorporate a time memory function in which the system reports information on how long it was exposed to a certain temperature. The hydrogel was synthesized using the free radical co-polymerization of *N*-isopropylacrylamide together with Napht functionalized with an acrylamide group in the presence of the cross-linking agent *N*,*N*'-methylenebisacrylamide. Upon the addition of BB to the environment of the hydrogel, a color change combined with a drastic increase in swelling ratio was visible demonstrating that BB can penetrate the hydrogel to form donor-acceptor interactions with the incorporated Napht units. The dynamic character of the host-guest complexes made it possible to introduce a large hysteresis window in the VPTT, which depends not only on the heating temperature but also on the heating time, forming the basis of the time memory function. The hysteresis window results from the disassembly of the host-guest complex and subsequent (limited) diffusion of BB from the hydrogel. Upon cooling, the presence of the released hydrophobic naphthalene units inside the hydrogel significantly lowers the rehydration of the hydrogel matrix, making the reswelling ratio a reporter event of this first generation of heating time sensor. Future generations of this smart material could potentially focus on different guest molecules to include different stimuli including redox potential, temperature, pH and competitive guests, to allow supramolecular communications between different individual hydrogels functionalized with either Napht units, TTF units or hydroquinone units.

In a last step, the incorporated time-memory function was further investigated for the NIPAm hydrogels functionalized with 3% of Napht moieties which gave the most promising results in the

preliminary screening. It was found that both the temperature and exposure time have an influence on the decomplexation and diffusion speed of the BB from the Napht-co-PNIPAm hydrogels resulting in different swelling ratios of the hydrogels due to the removal of the hydrophilic BB units and released hydrophobic Napht units. This difference in diffusion rate of the BB and the accompanied volume changes can be used as reporting event in a memory system preserving information on the exposure time at a certain temperature. The current generation of the developed time-memory hydrogel sensors can be considered medium length time-memory of several hours of heating, ideally 4 to 5 h. For the development of short length time-memory, hypersensitive Napht-co-PNIPAm hydrogels can be prepared by incorporating pores into polymeric structure significantly increasing the diffusion rate of the BB upon temperature increasing. Additionally, since the decomplexation and diffusion is mainly controlled by the temperature induced shrinkage of the hydrogel material, the temperature sensing window could be controlled by the chosen temperature responsive polymer matrix. Finally, the interaction of the Napht-co-PNIPAm hydrogel with BBB could also be studied as the formation of additional supramolecular cross-links can be used to control and enhance the mechanical properties and the energy dissipation of the hydrogel e.g. improving the toughness allowing its use as actuators or energy absorbing materials.

Chapter 4 describes a novel technique for the covalent incorporation of adaptable host-guest complexes on the surface of polymeric materials allowing control of the surface properties such as wettability, biocompatibility and corrosion resistance through the reversible host-guest complexation. For this the plasma dye coating (PDC) procedure was used which was initially invented by the University of Ghent for the coloration of materials with significantly reduced dye leaching during its application. In this post-fabrication functionalization method a solvent-free plasma surface modification step is used for the covalent immobilization of dye molecules onto a polymeric substrate. The novelty of this process is the incorporation of a radical sensitive group in the form of a double bond onto the dye structure which acts as an antenna for the reactive species generated by plasma, leaving the majority of the electron-rich dye-structure intact during the PDC process. Firstly, the effect of this PDC procedure on the properties of the treated materials was investigated using scanning electron microscope, contact angle measurements and X-ray spectroscopy showing almost no influence of PDC on the surface topology, surface properties and composition indicating that most surface and bulk properties of the substrate are retained after PDC treatment. Secondly, through further optimization of this procedure it was noticed that the parameters of the central plasma treatment step has a polymerizable dye/material dependence and optimization of at least the plasma treatment time is recommended for every new dye/material combination for an optimal dye loading and coloring. In addition, a different dye deposition technique based on solvent spraying was found to

be compatible with the used procedure. By spraying a solution of the desired polymerizable dye directly onto the material surface instead of dip-coating allows for a lower dye consumption, the application of a specific design onto the surface, the use of complex 3D printed material surfaces and a more simple incorporation into a continuous industrial process for the coloration of materials. Finally, the range of the immobilized molecule was further expanded by covalently immobilizing naphthalene units as representative guest molecules onto a fibrous cellulose matrix preserving the chemical structure as it could still interact with BB. This enables to create multi-responsive smart surfaces sensitive towards redox potential, competitive guests, pH and temperature mediated by surface bond pseudo-rotaxanes with either BB and BBB onto more conventional inert plastics including PE, PP and PTFE. Additionally also more complex materials could be used to create multifunctional materials with selective supramolecular adhesion based on host-guest complexation in a less time-consuming manner. The above results also provide further opportunities to immobilize different complex molecules onto the surface without changing their structural integrity including other different guest molecules, including TTF, but also host molecules such as cyclodextrins or cucurbit[n]urils as well as gelatin onto conventional plastics. The latter already gave some first promising results for the modification of gelatin on PTFE which can potentially be used in biomedical applications.

Nederlandstalige samenvatting

De ontwikkeling van slimme of intelligente polymeermaterialen heeft de afgelopen tien jaar veel aandacht gekregen. Slimme materialen worden beschreven als materialen die in staat zijn hun eigenschappen en functies te veranderen als reactie op kleine externe veranderingen in de omgeving, zoals temperatuurschommelingen, pH, elektrische of magnetische velden, oplosmiddelen of chemicaliën en licht. Binnen dit snel evoluerende domein is supramoleculaire chemie, inclusief gastheer-gast complexatie, naar voren gekomen als een krachtig instrument voor het creëren van responsieve materialen vanwege hun dynamische, omkeerbare en adaptieve aard als gevolg van veranderingen in externe stimuli. Deze gastheer-gast insluitingscomplexen bestaan meestal uit een macrocyclische gastheer molecule die op een sterk gecontroleerde en selectieve manier kan interageren met een of meerdere kleinere gastmoleculen. Dit gebeurt via zowel willekeurige niet-covalente interacties als specifieke driedimensionale ruimtelijke interacties. De integratie van deze dynamische supramoleculaire complexen in conventionele polymeersystemen heeft ons in staat gesteld om de volgende generatie geavanceerde materialen op een minder tijdrovende manier te ontwikkelen.

Tegenwoordig worden cucurbit[n]uril (CB), cyclodextrines (CD) en pillar[n]arenes het meest gebruikt als gastheermoleculen voor de synthese van intelligente polymeermaterialen zoals hydrogelen en nanostructuren door middel van supramoleculaire amfifiele macromoleculen in waterige media. Deze kunnen dan toegepast worden voor verschillende toepassingsgebieden, variërend van biomedische toepassingen tot nanotechnologie en materiaalkunde. In **hoofdstuk 2** werd een minder vaak onderzochte macrocyclische gastheermolecule cyclobis(paraquat-4,4'-bifenyleen), ook wel big blue box (BBB) genoemd, onderzocht voor gebruik in slimme materialen. BBB kan sterke inclusiecomplexen vormen met twee vlakke elektron-rijke aromatische gastmoleculen tegelijkertijd. Deze 1:2 complexen zouden gebruikt kunnen worden voor de creatie van fysische hydrogelen met enkele interessante eigenschappen zoals zelfhelend vermogen en vormgeheugenfunctie. Bovendien heeft deze macrocyclische gastheermolecule de mogelijkheid om redox-gevoelige eigenschappen in de polymeer-systemen te incorporeren, aangezien de gastheer-gast interactie kan gemanipuleerd worden via de redoxpotentiaal van zijn twee bipyridinium groepen. Ten slotte hebben complexen gevormd met BBB, afhankelijk van de gebruikte gastmoleculen, een intense kleur die als een directe visuele output in detectietoepassingen kan worden toegepast. In een eerste stap werd de complexatie van BBB met de elektronenrijke gastmoleculen dialkoxynaftaleen (Naft) en tetrathiafulvaleen (TTF) in water onderzocht met behulp van UV-VIS spectrometrische titratie, ITC en NMR spectroscopie. Door de slechte wateroplosbaarheid van de gastmoleculen Naft en TTF, werden echter korte in water

oplosbare polymeren gesynthetiseerd en gefunctionaliseerd met respectievelijk TTF of Napht molecules aan de uiteinden door middel van RAFT-polymerisatie. BBB vormde samen met de in water oplosbare TTF- en Napht-derivaten gekleurde 1:2 complexen in water met een hoge associatieconstante van 1.1 x 10^4 M^{-1} en 2.7 x 10^4 M^{-1} voor respectievelijk Naft-PDMAc en TTF-PDMAc. Tot slot werd de inherente, omkeerbare temperatuurafhankelijkheid van het Naft-PDMAc-complex met BBB aangetoond door een duidelijke visuele verstoring van het complex bij verhitting tot 100 °C met vervolgens de snelle hervorming van het complex bij opeenvolgende afkoeling onder 5 °C. Deze resultaten geven aan dat waterige complexen met BBB kunnen toegepast worden voor het creëren van multi-stimuli responsieve materialen, waaronder hydrogelen en supramoleculaire nanostructuren die kunnen gebruikt worden voor sensorsystemen aangezien gekleurde complexen worden gevormd. Het omkeerbaar redox-responsief gedrag van de TTF-eenheid zou bijvoorbeeld ook kunnen gebruikt worden om het complex te implementeren als een sensor voor oxidatieve stress. Meer onderzoek kan ook worden gedaan naar de invloed van de PDMAc keten op de gastheer-gast complexatie door het effect van de polymeerketenlengte op de associatieconstante in water te onderzoeken om zo de sterkte van de specifieke gastheer-gast complexatie in water nauwkeuriger te kunnen bepalen.

Door de dynamische aard van de gastheer-gast complexen te incorporeren in hydrofiele polymeernetwerken, ook wel hydrogelen genoemd, kunnen we de macroscopische krimping en zwelling van deze materialen omkeerbaar controleren. **Hoofdstuk 3** richt zich daarom op het gebruik van cyclobis(paraquat-*p*-phenyleen) of blue box (BB) complexen met naft als gastmolecuul om controle te krijgen over de volume fase overgangstemperatuur (VFOT) van thermo-responsieve hydrogelen. De geïnduceerde decomplexatie bij temperatuurstijging liet toe om een tijdgeheugenfunctie op te nemen waarin het systeem informatie rapporteert over hoe lang het werd blootgesteld aan een bepaalde temperatuur. De hydrogel werd gesynthetiseerd met behulp van vrije radicalaire co-polymerisatie van *N*-isopropylacrylamide samen met de Naft gastmolecule gefunctionaliseerd met een acrylamide groep in aanwezigheid van de crosslinker *N,N'*-methyleenbisacrylamide. Bij de toevoeging van BB aan de hydrogel werd een kleurverandering in combinatie met een drastische verhoging van de zwellingsgraad opgemerkt. Hieruit blijkt dat BB in de hydrogel kan dringen om donor-acceptor interacties te vormen met de geïntegreerde Naft groepen. Het dynamische karakter van de gastheer-gast complexen maakte het mogelijk om een groot hysterese venster in de VFOT in te voeren dat niet alleen afhankelijk is van de verwarmingstemperatuur, maar ook van de opwarmtijd, wat de basis vormt van de voorgenoemde tijdsgeheugenfunctie. Het hysterese venster is het resultaat van het opbreken van de gastheer-gast interacties en de daaropvolgende (beperkte) uitstoting van BB uit de hydrogel. Bij afkoeling verlaagt de rehydratie temperatuur van de hydrogelmatrix aanzienlijk door de aanwezigheid van de vrijgekomen hydrofobe naftaleeneenheden in de hydrogel. Dit leidt tot

verschillende zwellingsgraden van de hydrogel na opwarmen en dit verschil in water opname kan dan gebruikt worden als output voor de eerste generatie verwarmingstijdsensoren. In de toekomst kan zelfs communicatie, ofwel de uitwisseling van BB tussen verschillende hydrogelen gefunctionaliseerd met verschillende gastmolecule zoals Naft, TTF of hydroquinone molecule gerealiseerd worden door deze gevoelig te maken aan verschillende stimuli zoals redoxpotentiaal, temperatuur, pH en competitieve gasten.

In een laatste stap werd de ingebouwde tijdgeheugenfunctie verder onderzocht voor de NIPAm-hydrogelen die gefunctionaliseerd werden met 3% Naft groepen, welke de meest veelbelovende resultaten opleverde in de voorlopige screening. Het bleek dat zowel de temperatuur als de blootstellingstijd een invloed hebben op het uiteenvallen van het complex en de diffusiesnelheid van de BB uit de Naft-co-PNIPAm hydrogelen. Dit resulteert in een verschil in zwellingsgraad van de hydrogelen na verwarmen als gevolg van het verwijderen van de hydrofiele BB-eenheden en de vrijgekomen hydrofobe Naft-eenheden in de matrix. Het verschil in diffusiesnelheid van de BB en de daarmee gepaard gaande volumeveranderingen kunnen worden gebruikt als rapportage gebeurtenis in een geheugensysteem dat informatie over de blootstellingstijd bij een bepaalde temperatuur bewaart. De huidige generatie van de ontwikkelde tijdsgeheugen hydrogel sensoren kan verschillen van enkele uren verwarming, idealiter 4 tot 5 uur, onthouden en onderscheiden. Voor de ontwikkeling van kortere tijdsgeheugen die blootstellingstijden kunnen onthouden van enkele uren of minuten, kan een hypergevoelige Naft-co-PNIPAm-hydrogel verwezenlijkt worden door poriën in de polymeerstructuur te integreren, waardoor de diffusiesnelheid van de BB bij toenemende temperatuur aanzienlijk zal stijgen. Bovendien, aangezien het openbreken van het complex en diffusie van BB voornamelijk wordt gecontroleerd door de temperatuur geïnduceerde inkrimping van het hydrogelmateriaal, kan het temperatuursensorvenster aangepast worden door de gekozen temperatuur-responsieve polymeermatrix. Ten slotte kan de interactie van de Naft-co-PNIPAm hydrogel met BBB ook bestudeerd worden, aangezien de vorming van extra supramoleculaire crosslinks kan gebruikt worden om de mechanische eigenschappen en de energie dissipatie van de hydrogel te controleren en te verbeteren, bv. het verbeteren van de taaiheid van de hydrogel waardoor het gebruik ervan als robuuste actuatoren mogelijk wordt of als energie-absorberende materiaal.

Hoofdstuk 4 beschrijft een nieuwe techniek voor de covalente incorporatie van dynamische gastheer-gast complexen op het oppervlak van polymeermaterialen, die het mogelijk maakt de oppervlakte-eigenschappen zoals bevochtigbaarheid, biocompatibiliteit en corrosiebestendigheid reversibel te controleren. Hiervoor werd de '*plasma dye coating*' (PDC) procedure gebruikt die in eerste instantie werd ontwikkeld door de Universiteit van Gent voor de kleuring van materialen met significant

verminderde kleurstofuitloging tijdens de toepassing ervan. In deze post-fabricage methode worden oppervlakte radicalen, gecreëerd door een oplosmiddelvrije plasmaoppervlakte modificatiestap, gebruikt voor de covalente immobilisatie van kleurstofmoleculen op een polymeersubstraat. Het innoverende van dit proces is de functionalisatie van een radicaal-gevoelige groep in de vorm van een dubbele binding op de kleurstofstructuur die fungeert als antenne voor de reactieve radicalen die door plasma worden gegenereerd. Hierdoor blijft het grootste deel van de elektronenrijke kleurstofstructuur intact tijdens het PDC-proces. Ten eerste werd het effect van deze PDC procedure op de eigenschappen van de behandelde materialen onderzocht met behulp van rasterelektronenmicroscoop, contacthoekmetingen en X-straal fotoelektronische spectometer (XPS) waaruit blijkt dat PDC bijna geen invloed heeft op de oppervlaktetopologie, oppervlakte-eigenschappen en samenstelling van het substraat is waargenomen. Dit wil zeggen dat de meeste oppervlakte- en bulkeigenschappen van het substraat na de PDC-behandeling worden behouden. Ten tweede, door verdere optimalisatie van deze procedure werd opgemerkt dat de parameters van deze plasmabehandelingsproces een polymeriseerbare kleurstof/materiaalafhankelijkheid heeft en een optimalisatie van ten minste de plasmabehandelingstijd wordt aanbevolen voor elke nieuwe kleurstof/materiaalcombinatie voor een optimale kleuring. Bovendien werd een andere verfdepositietechniek op basis van solvent spuiten compatibel bevonden met de gebruikte procedure. Door een oplossing van de gewenste polymeriseerbare kleurstof direct op het materiaaloppervlak te spuiten in plaats van te dompelen, wordt een lager kleurstofverbruik, de toepassing van een specifiek ontwerp op het oppervlak, het gebruik van complexe 3D geprinte materiaaloppervlakken en een eenvoudigere integratie in een continu industrieel proces voor de kleuring van materialen mogelijk. Tot slot werd het bereik van de geïmmobiliseerde molecule verder uitgebreid door Naft-eenheden als representatieve gastmoleculen covalent te immobiliseren op een vezelachtige cellulosematrix. De geïncorporeerde Naft groepen behouden hun chemische structuur waardoor die nog steeds met BB kan interageren. Dit laat toe om multi-responsieve oppervlakken te creëren op meer conventionele inerte kunststoffen zoals PE, PP en PTFE die gevoelig zijn voor redoxpotentiaal, competitieve gasten, pH en temperatuur, door gebruik te maken van oppervlakte gebonden pseudo-rotaxanen met BB en BBB. Daarnaast kunnen ook deze inerte en/of complexere materialen gebruikt worden om multifunctionele materialen met selectieve supramoleculaire hechting op basis van gastheer-gast interacties gecreëerd worden en dit op een minder tijdrovende manier vergeleken met de conventionele manier. De bovenstaande resultaten bieden ook verdere mogelijkheden om verschillende complexe moleculen op het oppervlak te immobiliseren zonder hun structurele integriteit te veranderen, inclusief andere verschillende gastmoleculen, waaronder TTF, maar ook gastheermoleculen zoals cyclodextrine of cucurbit[n]uril alsook gelatine op conventionele

kunststoffen. Dit laatste gaf al eerste veelbelovende resultaten voor de modificatie van gelatine op PTFE die mogelijks gebruikt kan worden in biomedische toepassingen.

Résumé français

Le développement de matériaux polymères intelligents a suscité un intérêt croissant au cours de la dernière décennie. Les matériaux dits intelligents sont décrits comme des matériaux capables de modifier leurs propriétés et leurs fonctions en réponse à de faibles changements environnementaux externes comme des fluctuations de température, de pH, de champs électriques ou magnétiques, de solvants ou d'environnement chimiques, ou encore de lumière. Dans ce domaine en rapide évolution, la chimie supramoléculaire, notamment celle faisant appel à des complexes hôte-invité, est apparue comme un outil puissant pour la création de matériaux réactifs en raison de sa nature dynamique, réversible et adaptative aux stimulus externes. Ces complexes d'inclusion hôte-invité sont basés sur l'interaction sélective voire spécifique d'une molécule hôte macrocyclique avec une ou plusieurs molécules invitées plus petites, à la fois par des interactions non covalentes et par des arrangements spatiaux tridimensionnels spécifiques. L'intégration de ces assemblages supramoléculaires dynamiques dans des structures macromoléculaires, par incorporation dans le polymère soit de l'hôte macrocyclique ou de l'invité, a permis de développer une nouvelle génération de matériaux intelligents stimulables.

De nos jours, les cucurbit[n]uriles (CB), les cyclodextrines (CD) et les pillar[n]arènes sont les molécules hôtes les plus utilisées pour la conception de matériaux polymères stimulables tels que des hydrogels et des nanostructures auto-assemblées (micelles, vésicules, etc…). En milieu aqueux, ces systèmes supramoléculaires amphiphiles peuvent être utilisés pour différentes applications dans les domaines biomédical, nanotechnologique et de la science des matériaux. Dans le **chapitre 2**, une molécule hôte macrocyclique, le cyclobis (paraquat-4,4'-biphénylène), également appelée Big Blue Box (BBB), a été étudiée en vue de développer des assemblages macromoléculaires intelligents. Le BBB peut former de forts complexes d'inclusion avec deux molécules invitées aromatiques planaires riches en électrons, complexes qui pourraient potentiellement être utilisés pour la création d'hydrogels physiques possédant des propriétés intéressantes, comme l'auto-réparation ou la mémoire de forme. De plus, ce macrocycle permettrait de conférer des propriétés redox dans les systèmes polymères, offrant ainsi la possibilité de contrôler les interactions hôte-invité en réduisant la BBB. Enfin, les complexes formés avec la BBB ont une couleur intense et spécifique des molécules invitées, et peuvent donc être utilisés comme signal visuel direct pour des applications dans le domaine des senseurs. Dans un premier temps, la complexation dans l'eau de la BBB avec des entités hôtes riches en électrons, le dialkoxynaphtalène (Napht) et le tétrathiafulvalène (TTF) a été étudiée en utilisant différentes techniques de titration (UV-VIS, ITC, RMN). En raison de la faible solubilité dans l'eau des motifs Napht et TTF, des polymères hydrosolubles courts ont été synthétisés par polymérisation RAFT à partir

d'agents CTA intégrant les motifs hydrophobes, TTF ou Napht. Il a été démontré que ces dérivés hydrosolubles de TTF et de Napht pouvaient former des complexes colorés 1:2 avec la BBB dans l'eau, avec des constantes d'association élevées de 1.1 x 10^4 M^{-1} pour le dérivé Napht-PDMAc et 2.7 x 10^4 M^{-1} pour le dérivé TTF-PDMAc. Enfin, la dépendance thermique de la stabilité du complexe Napht-PDMAc :BBB a été étudiée. Cette étude a mis en évidence la réversibilité du complexe lorsqu'il est chauffé à plus de 100°C, et sa reformation rapide lorsqu'il est refroidi en dessous de 5°C. Ces premiers résultats mettent en avant le potentiel de ces complexes pour la création de matériaux sensibles, tels que des hydrogels ou des nanostructures supramoléculaires. Par exemple, le comportement redox réversible de l'unité TTF pourrait être utilisé pour mettre au point un capteur de stress oxydatif.

Le **chapitre 3** porte sur l'incorporation de complexes hôte-invité dynamiques à base de cyclobis(paraquat-p-phénylène), appelé Blue Box (BB), et de dérivés dialkoxynaphtalènes (Napht) comme molécules invitées dans des réseaux polymères hydrophiles, également appelés hydrogels, pour contrôler leur température de transition de phase volumique (TTPV) et leur propriété de gonflement, et ceci de manière réversible. La décomplexation induite par l'augmentation de la température a permis d'incorporer une fonction de mémoire de temps au système qui donne des informations sur la durée de son exposition à une certaine température. D'un point de vue pratique, l'hydrogel a été synthétisé par copolymérisation radicalaire du *N*-isopropylacrylamide et d'un acrylamide fonctionnalisé avec le groupement Napht, en présence d'un agent de réticulation, le *N,N'*-méthylène-bisacrylamide. En contact avec la BB, l'hydrogel change de couleur et gonfle de manière drastique, du fait de la formation de complexes d'inclusion au sein du matériau. L'étude détaillée de la thermosensibilité des hydrogels complexés a permis de mettre en exergue un large phénomène d' hystérèse, qui dépend non seulement de la température du chauffage mais aussi de sa durée d'application qui constitue la base de la fonction de mémoire en temps. L'hystérèse résulte de la dissociation du complexe hôte-invité puis de l'expulsion du BB à l'extérieur de l'hydrogel. Lors du refroidissement, la présence des unités Napht hydrophobes à l'intérieur de la matrice hydrogel diminue significativement sa réhydratation, ce qui impacte donc son taux de gonflement qui devient alors un indicateur de la durée d'exposition du matériau à une température donnée.

Dans ce mémoire, la fonction de mémoire en temps a été étudiée plus en détail pour des hydrogels PNIPAm fonctionnalisés avec 3% de Napht. Il a été notamment constaté que la température et le temps d'exposition ont une forte influence sur la décomplexation et la vitesse de diffusion de la BB des hydrogels Napht-*co*-PNIPAm, conduisant à des taux de gonflement différents des hydrogels après réhydratation. Cette différence de vitesse de diffusion du BB et les variations de volume associées est à l'origine de la mémoire temporel du vécu thermique des matériaux. La génération de matériaux développés au cours de ce travail de thèse est capable de mémoriser des temps de chauffage de 4-5

heures. Pour le développement d'hydrogels capables de mémoriser des temps plus courts de chauffage, il serait nécessaire de concevoir des hydrogels permettant une diffusion plus rapide des molécules de BB vers l'extérieur des matériaux lors de traitements thermiques. Sur le même principe, d'autres matériaux intelligents doués de fonctions mémoire redox ou pH devraient voir le jour très prochainement. Enfin, il pourrait être intéressant d'exploiter la possibilité de faire des complexes d'inclusion de stœchiométrie 2 :1 entre des hydrogels Napht-co-PNIPAm et la BBB pour contrôler et améliorer les propriétés mécaniques (dissipation d'énergie, résistance) des matériaux et envisager leur utilisation en tant qu'actionneurs.

Le **chapitre 4** décrit une nouvelle technique de greffage covalent de complexes hôte-invité sur des surfaces de matériaux afin d'en contrôler les propriétés de surface, telles que la mouillabilité, la biocompatibilité et la résistance à la corrosion. Pour ce faire, nous avons utilisé le procédé de Plasma Dye Coating (PDC), qui a été initialement inventé par des chercheurs de l'Université de Gand, pour la coloration efficace des matériaux avec une réduction significative de perte du colorant lors de son utilisation. Dans ce procédé, une approche basée sur la génération de radicaux en surface des matériaux, en utilisant une étape préliminaire de modification de surface par traitement plasma sans solvant, a été utilisée pour l'immobilisation covalente de molécules de colorant sur un substrat polymère. La nouveauté du procédé développé dans ce chapitre réside dans l'incorporation d'une double liaison C=C sensible aux radicaux à la structure du colorant, qui agit alors comme une antenne pour les espèces réactives générées par le plasma tout en laissant intacte la structure du colorant riche en électrons pendant le procédé PDC. Tout d'abord, l'effet de cette procédure de PDC sur les propriétés des matériaux traités a été étudié par Microscopie électronique à balayage, par spectrométrie photoélectronique X et en mesurant l'angle de contact. Les analyses ont montré que le procédé plasma n'avait pratiquement aucune influence sur la topologie, la composition et les propriétés de surface, indiquant ainsi que la plupart des propriétés du substrat sont conservées après traitement PDC. Deuxièmement, lors de l'optimisation de la procédure, il a été constaté que les paramètres clefs du traitement au plasma dépendaient du ratio colorant polymérisable / matériaux, et qu'une optimisation du temps de traitement au plasma était nécessaire pour chaque nouvelle combinaison colorant / matériaux pour obtenir une coloration optimale. En outre, une autre technique de dépôt de colorant par pulvérisation de solvant, compatible avec le procédé plasma, a été mis au point. En pulvérisant une solution du colorant polymérisable directement sur la surface du matériau au lieu de le tremper dans une solution de colorant, il est possible de réduire la consommation de colorant, d'appliquer un dessin spécifique sur la surface, d'utiliser des surfaces complexes de matériau imprimé en 3D, et donc d'intégrer plus facilement la technique dans un processus industriel continu pour la coloration des matériaux. Enfin, la gamme de molécules immobilisables a été étendue à l'unité de reconnaissance

moléculaire Napht afin d'élaborer une surface (matrice fibreuse de cellulose), capable d'interagir de manière supramoléculaire avec la BB, l'objectif à moyen terme étant de créer des plastiques (PE, PP et le PTFE), à la base inertes, intelligents, sensibles au potentiel redox, à la présence d'invités compétitifs, au pH et à la température en présence de BB. Cette approche pourrait également être utilisée pour créer des plastiques multifonctionnels plus complexes dotés de propriétés d'adhésion supramoléculaire sélective par formation de complexes hôte-invité à base de BB ou de BBB en surface. D'autres systèmes de reconnaissance moléculaire (cyclodextrines, cucurbit[n]uriles, gélatines) pourraient être également immobilisés sur des plastiques classiques sans modifier leur intégrité structurelle et leur conférer des propriétés intéressantes.

Publication list

1 Publications included in this thesis

- **L. De Smet***, G. Vancoillie*, P. Minshall, K. Lava, I. Steyaert, E. Schoolaert, E. Van De Walle, P. Dubruel, K. De Clerck and R. Hoogenboom; Plasma Dye Coating: A Straightforward and Widely Applicable Procedure for Dye Immobilization on Common Polymeric Materials. *Nature communications*, 9, 1123, 2018. DOI: 10.1038/s41467-018-03583-4
- **L. De Smet**, K. Belal, J. Lyskawa, R. hoogenboom and P. Woisel; Supramolecular hydrogels mediated by cyclobis(paraquat-p-phenylene) possessing a time and temperature memory function. 2019 *Manuscript in preparation*.
- **L. De Smet**, A. Malfait, P. Sandford, J. Potier, J. Lyskawa, R. Hoogenboom and P. Woisel; Complexation of cyclobis(paraquat-4,4'-biphenylene) in water and application in the preparation of smart polymeric materials. 2019 *Manuscript in preparation*.

2 Publications not discussed in this thesis

- H. Guo, D. Hourdet, A. Marcellan, F. Stoffelbach, J. Lyskawa, **L. De Smet**, A. Vebr, R. Hoogenboom, P. Woisel; Dual Responsive Regulation of Host-Guest Complexation in Aqueous Media to Control Partial Release of the Host, *Chemistry – A European Journal*, Accepted paper, October 2019. DOI: 10.1002/chem.201904287
- K. Belal, F. Stoffelbach, J. Lyskawa, M. Fumagalli, D. Hourdet, A. Marcellan, **L. De Smet**, V. R. De la rosa, G. Cooke, R. Hoogenboom, P. Woisel; Recognition-Mediated Hydrogel Swelling Controlled by Interaction with a Negative Thermoresponsive LCST Polymer, *Angewandte Chemie International Edition*, 55, 13974–13978, 2016. DOI: 10.1002/anie.201605630

Acknowledgments

With the submission of this thesis an important chapter in my life comes to an end and this journey would not have been possible without the supervision and trust of my two promotors Prof. Richard Hoogenboom and Prof. Patrice Woisel. I would like to thank the two of you for the opportunity to pursue a PhD research at both your groups, the SC-group in Ghent University and the UMET group in University of Lille. Both giving me the needed freedom during my PhD to follow some of my own ideas which has developed me to not only become a better researcher, but also to be more confident about myself and to grow as a person. I'm also very grateful for giving me numerous opportunities to present and share my research to the scientific community around the world allowing me to develop soft skills which I will employ in my future career. I would also take the opportunity to thank the members of my examination committee Prof. Oren Scherman, Prof. Pol Besenius, Prof. Rachel Auzely, Prof. Loïc Jierry, Prof. Filip Du Prez and Prof. Sandra Van Vlierberghe for taking the time to join my defense, to proof-read and advise some very useful suggestions for this manuscript.

Next, I would like to thank my colleagues with whom I have worked with during my PhD journey in both Ghent University and University of Lille. Firstly, I want to thank the entire UMET group in the university of Lille as I spend the first 1,5 year of my PhD in their labs. I want to gratefully thank some former and current co-workers Marie, Nérimel, Fanny, Aurélie, Benoit, William, David, Joël and Jonathan for helping me developing more lab experience on host-guest complexation with blue box and hydrogels but also for warmly welcoming me into the group. Special thanks goes also to Aurélien, without whom I would not have been able to survive the French administration system.

For the completion of my PhD, I came back to work with the SC-group. As most people I knew were already graduated by that time, the group was then packed with new faces but I couldn't have wished for better colleagues/friends for life! I have really enjoyed our kicker breaks and all our precious 'unofficial' hallway meetings. I will miss you all! To Ronald, Jente, Ali and Ine, I will miss all our ''HDG'' and ''shmebulock'' moments in the lab. Luckily, with our special made SC-group playlist I can always carry our memories with me to my next career adventure. To the other members of the group: Joachim, Suzan, Tim, Ella, Michal, Ondreij, Master Bera, Yann, Victor J., Adriana, Annelore, Valentin, Noémie, Xiaowen, Jana, Metwally, Martin and Glenn thank you for the legendary drinks/parties, but also for the in depth chemistry discussions and the detailed explanations. I should also not forget the master and internships students I have guided throughout my PhD. So thank you Pamela, Isabel, Florian, Wouter, Sander, Pieter and Emiel. Although, their research did not contribute to this work, I really enjoyed the challenge of these projects which have led to the further expansion of my knowledge

about polymer and supramolecular chemistry. I hope that I have helped you all to become better chemists and researchers.

From outside our research group, I would definitely like to thank the other research groups of Prof. Du Prez, Prof. Winne, Prof. Dubruel, Prof. Martins and Prof. Van Der Eycken for the lovely conversations throughout the years. Especially, Tim and Dieter to help me with all my NMR problems and to measure my samples. Besides these people I want to thank Veerle, Queenie, Paul and Jos for their help with ordering and delivering lab supplies.

In this final part, I want to thank all my family and friends who have supported me during the past four years. First and foremost, I would like to thank my parents for their constant support, love and patience throughout my academic carrier path. But also my other family members, my sister Charlot, godchild Damien, Kevin and grandmother 'meme zwevegem' for always believing in me, even when I lost all hope. I hope I made you all very proud.

I also want to thank Gertjan his family, namely Christine, Frank, Tante Mieke, Mieke, Hannes, Eline, Justine and grandfather André for listening and taking care of me even when I could not participate at the family parties by giving some left over cake along with Gertjan for me. The awesome front cover of this thesis was created by Hannes Willaert, please do remember this famous name! Special thanks to Magalie & Max; Shana; Leen, Maarten M. & Julien; Justine & Jonas; Debbie, Olivier, Marie & Lotte; Ayano & Joachim & Rei; Loortje & Bart; Boris & Luciana; Annelore & Maarten V. ; Maxime; Mien & Bram; Kristina & Mathijs; Ronald & Raven for both their sincere interest in my research and the lovely and also distracting dinner parties over the years. My gym/kickboxing partners in crime Angelique, Aurelie and Tom for the intensive trainings allowing me to let some steam off and releasing all my writing frustrations.

Last, but definitely not least, I want to thank my boyfriend Gertjan, aka 'totaalpakketje / total package'! Thank you for always believing in me and to help me through the struggles of the PhD life, especially the writing part. For buying me chocolate when I needed it and to put me back together after the millionth breakdown. I'm looking forward to share my future life with you in our new love nest! Without you this work would not have been possible!

Goodbye to my awesome PhD life and hello to my new industry career life!

Lieselot